Wissenschaftszentrum Weihenstephan für Ernährung, Landnutzung und Umwelt

Lehrstuhl für Experimentelle Genetik

The Epoxyeicosatrienoic Acid Pathway Enhances Hepatic Insulin Signaling and Is Repressed In High Fat Diet Induced Hepatic Insulin Resistance
A Proteomic Study

Alexander Schäfer

Vollständiger Abdruck der von der Fakultät Wissenschaftszentrum Weihenstephan für Ernährung, Landnutzung und Umwelt der Technischen Universität München zur Erlangung des akademischen Grades eines

Doktors der Naturwissenschaften

genehmigten Dissertation.

Vorsitzender: Univ.-Prof. Dr. H.-W. Mewes
Prüfer der Dissertation:

1. apl. Prof. Dr. J. Adamski
2. Univ.-Prof. Dr. B. Küster
3. Univ.-Prof. Dr. M. Ueffing
   (Eberhard-Karls-Universität Tübingen)

Die Dissertation wurde am 07.01.2015 bei der Technischen Universität München eingereicht und durch die Fakultät Wissenschaftszentrum Weihenstephan für Ernährung, Landnutzung und Umwelt am 30.03.2015 angenommen.

Table of Contents

Table of Contents

II

Table of Contents

IV

Summary

Type 2 diabetes mellitus (T2D) is a complex disease influenced by genetic as well as environmental factors, most notably increased body fat mass in adiposity. T2D develops over many years in patients and affects multiple organ systems at different stages in the disease progression. The hallmark of the early stages of the disease is impaired insulin sensitivity of the primary insulin target tissues: liver, muscle and white adipose tissue (WAT). Studies of the early stages of T2D are complicated considerably by the fact that patients are often unaware of their impaired insulin sensitivity. Therefore, the transition of individual organs to an insulin resistant state is not studied as well as other aspects of T2D.

In this thesis I present the results of a proteomic study of the transition of insulin sensitive to insulin resistant liver in a high fat diet (HFD) mouse model of T2D. My aims were to describe which biochemical pathways were affected by HFD feeding before and after the onset of hepatic insulin resistance and to find at least one new pathway which had a functional impact on insulin signaling. To this end, I monitored protein expression using state of the art LC-MS/MS based proteomics, employing discovery as well as targeted strategies. As a result, I was able to perform accurate quantification of hundreds of proteins in a total of 68 mice, by using customized and optimized proteomic workflows.

Peripheral and hepatic insulin sensitivity was tightly monitored through the application of the hyperinsulinemic-euglycemic clamp technique over the course of the feeding experiment by my collaboration partners. They could show that HFD feeding specifically induced hepatic insulin resistance after two weeks of HFD feeding.

By combining this extensive characterization of insulin sensitivity with proteomic profiling, expression changes could be correlated with hepatic insulin resistance. Pathway enrichment analysis enabled me to identify multiple metabolic pathways underlying differential protein expression. The most promising candidate pathways were the synthesis of polyunsaturated fatty acids (PUFA) pathway, and the epoxyeicosatrienoic acids (EET) eicosanoid synthesis pathway.

The expression profiles showed a biphasic response of these two interconnected pathways. Induction of PUFA synthesis enzymes was transient and peaked before the onset of hepatic insulin resistance. In contrast, the decline of EET synthesis enzymes coincided with hepatic insulin resistance. Therefore, I hypothesized that

Summary

EETs may be positive modulators of insulin signaling in hepatocytes and tested this hypothesis in primary hepatocytes as well as hepatocyte cell lines.

Subsequently, I could show for the first time that EETs indeed enhance insulin signaling at the level of Akt, the central protein kinase in downstream insulin signaling. The activation was not associated with changes in insulin receptor (IR) or insulin receptor substrate-1 (IRS-1) phosphorylation through EETs. Furthermore, I could show that this effect is exclusive to the eicosanoids as overexpression of the EET synthesizing or inactivating enzymes in absence of arachidonic acid had no impact on insulin signaling.

Based on the downregulation of the EET pathway in insulin resistant liver and the demonstration that EET enhance insulin signaling, a model can be proposed in which HFD feeding represses the synthesis of positive modulators of insulin signaling, thereby contributing to hepatic insulin resistance.

Zusammenfassung

Typ 2 Diabetes mellitus (T2D) ist eine komplexe Erkrankung die sowohl von genetischen als auch von umweltbedingten Faktoren, besonders erhöhte Körperfettmasse und Adipositas, beeinflusst wird. T2D entwickelt sich über viele Jahre in Patienten, wobei mehrere Organe in den unterschiedlichen Stadien der Krankheit in unterschiedlichem Ausmaß betroffen sind. Insulinresistenz der primären insulinabhängigen Organe Leber, Skelettmuskel und weißes Fettgewebe ist charakteristisch für die frühen Stadien von T2D. Die Erforschung dieser frühen T2D Stadien ist durch die Tatsache erschwert, dass die eingeschränkten Insulinwirkung in Patienten oft inapparent bleibt. Daher ist der Übergang einzelner Organe zum insulinresistenten Zustand weitaus weniger gut untersucht als andere Aspekte von T2D.

In dieser Arbeit präsentiere ich die Ergebnisse einer proteomischen Studie des Übergangs von insulinsensitiver zu insulinresistenter Leber in einem Hochfettdiät T2D Mausmodel. Meine Ziele waren zu beschreiben welche Stoffwechselwege vor und während der Manifestation der hepatischen Insulinresistenz durch die Diät beeinflusst wurden und wenigstens einen Stoffwechselweg zu identifizieren der einen funktionellen Effekt auf die Signaltransduktion des Insulins hat.

Ich setze dies um, indem ich Proteinexpression mittels modernster LC-MS/MS basierter Proteomik über den Verlauf der Diätstudie untersuchte, wobei sowohl shotgun als auch gezielte proteomische Strategien verwendet wurden. Durch diesen Ansatz, kombiniert mit dem Einsatz von optimierten Probenvorbereitungsverfahren, konnte ich hunderte von Proteinen in insgesamt 68 Mäusen mit hoher Genauigkeit quantifizieren.

Während des Fütterungsversuches konnten meine Kollaborationspartner periphere sowie hepatische Insulinsensitivität mittels der euglykämischen-hyperinsulinämischen clamp Technik nachverfolgen. Sie konnten dabei zeigen, dass die Hochfettdiät spezifisch hepatische Insulinresistenz nach zwei Wochen Fütterung hervorrief.

Durch die Kombination dieser umfassenden Charakterisierung der Insulinsensitivität mit den proteomischen Profilen konnten Proteinexpressionsänderungen mit hepatischer Insulinresistenz korreliert werden. Pathway enrichment Analyse erlaubte mir die differenziell exprimierten Proteine mehreren Stoffwechselwegen zuzuordnen. Die vielversprechendsten Kandidaten waren hierbei der Syntheseweg der mehrfach ungesättigten Fettsäuren und der

Zusammenfassung

Syntheseweg der Epoxyeikosatriensäuren (EETs), einer Unterfamilie der Eikosanoide.

Die Expressionsprofile zeigten eine biphasische Beeinflussung dieser beiden miteinander verbunden Stoffwechselwege durch die Diät. Die Induktion der Enzyme, welche mehrfach ungesättigte Fettsäuren synthetisieren, war transient und am stärksten direkt vor Erscheinen der hepatischen Insulinresistenz ausgeprägt. In Gegensatz dazu fiel die Repression des EET Syntheseweges zeitlich mit der hepatischen Insulinresistenz zusammen. Daher formulierte ich die Arbeitshypothese, dass EETs positive Modulatoren des Insulinsignalings sein könnten und testete dies in primären Hepatozyten und Hepatozyten Zelllinien.

In Folgenden konnte ich zum ersten Mal zeigen, dass EETs tatsächlich das Insulinsignal auf der Stufe von Akt, der zentralen Kinase des Insulinsignalweges, verstärken. Im Gegensatz dazu hatten die EETs allerdings weder einen Einfluss auf die Aktivierung des Insulinrezeptor (IR) noch IR Substrat 1 (IRS-1) durch Insulin. Weiterhin konnte ich zeigen dass dieser Effekt nur durch die Eikosanoide selbst hervorgerufen wurde, da Überexpression der EET synthetisierenden oder inaktivierenden Enzyme keinen Einfluss auf den Insulinsignalweg hatte.

Zusammenfassend lässt sich, basierend auf der Repression des EET Syntheseweges in insulinresistenter Leber und des Nachweises, dass EETs das Insulinsignal verstärken, ein Modell postulieren in dem die Hochfettdiät die Synthese positiver Modulatoren des Insulinsignalweges unterdrückt und auf diese Art zur hepatischen Insulinresistenz beiträgt.

4

1. Introduction

1.1 Type 2 diabetes mellitus

Type 2 diabetes mellitus (T2D) differs from type 1 diabetes mellitus (T1D) in its etiology and the requirement of patients for insulin. T1D is an autoimmune disease that leads to destruction of the insulin producing islets of Langerhans early in life (childhood or puberty) [1]. Consequently, T1D is a disease with absolute insulin deficiency and requires lifelong insulin treatment. In contrast, T2D and its pre-stages are characterized by a relative insulin deficiency, defined by an inadequate adjustment of the primary insulin dependent tissues to increasing plasma levels of insulin. It usually manifests in patients much later in life than T1D and it can be coupled with increased, normal or reduced insulin secretion and or plasma levels. Insulin therapy is used only as a last resort in T2D and it is also called non-insulin dependent diabetes mellitus (NIDDM) to contrast it to T1D, which is also called insulin dependent diabetes mellitus (IDDM) [1, 2].

There are some rare monogenetic forms of T2D referred to as maturity onset of diabetes of the young (MODY). Being hereditary disorders, they occur in much younger patients than acquired T2D. Five gene defects causing MODY have been identified, comprising mutations in the enzyme glucokinase (MODY2) and the transcription factors HNF-4α (MODY1), HNF-1α (MODY3), IPF-1 (MODY4) and HNF-1β (MODY5). Other minor genetic forms of diabetes exist as well [1]. The common denominator of MODY mutations is that they compromise insulin secretion from pancreatic islets. Therefore the etiology of MODY is more similar to T1D than to T2D.

Environmental components, most notably obesity, are of crucial importance in T2D, exemplified by the fact that lifestyle changes and weight loss are highly effective in improving insulin and blood glucose levels [3]. However, genetic predisposition is now an accepted contributing factor to T2D. People with positive family history for T2D have a more than twofold higher risk to develop the disease and results from concordance studies with monozygotic twins confirm that genetic factors play a role in T2D [3] .

As of 2012, 346 million people worldwide have diabetes according to the world health organization (WHO), and prognoses predict further increase of its incidence in the future [4]. Among all cases of diabetes mellitus, 10% of cases

are accounted for by T1D while 90% are T2D, of which less than 10% are MODY [3].

The main diagnostic criterion for T2D is hyperglycemia. Fasting glucose concentration is used to classify normoglycemia (<6.1mM, 110mg/dl), impaired fasting glucose (6.1mM< and <7mM) and T2D (>7mM, 126mg/dl) according to the WHO. An oral glucose tolerance test (oGTT) is used to distinguish glucose intolerance (7.8mM< and <11.1mM) and T2D (>11.1mM) by assessing plasma glucose levels two hours after oral intake of 75 g glucose [5].

1.1.1 Pathophysiology of T2D

The hallmarks of T2D are insulin resistance of liver, muscle and white adipose tissue, paired with abnormal function of the endocrine pancreas. Insulin resistance describes a state where the metabolic adaptation of a tissue is too low for a given change in plasma insulin concentration. Alterations of the pancreas can manifest initially in a compensatory increase in insulin levels, but ends in a decompensated stadium with decreased β-cell mass and a secretory defect [6]. In order to understand these dysfunctions it is helpful to compare the physiological effects of insulin to the deregulations in T2D (Fig. 1). Counter regulation through glucagon and the autonomous nervous system will be omitted for simplicity. Insulin is the main regulator of substrate distribution and utilization. Under fasting conditions (postabsorbtive phase, Fig. 1, upper left panel) insulin secretion proceeds at a basal rate and blood glucose levels are held constant by hepatic glucose production (HGP) from the liver, mediated by increased glycogenolysis and gluconeogenesis. Additional substrates in the form of free fatty acids (FFA) are provided by lipolysis from triacylglycerides (TG) from WAT. Muscle and liver cooperate in consuming circulating FFAs. The concurrent output of glucose by the liver is crucial for providing energy to the central nervous system (CNS) which cannot utilize FFAs. In sum a state of substrate mobilization and utilization prevails.

Following a meal (postprandial phase, Fig. 1, upper right panel) gradually increasing glucose concentrations stimulate insulin release from the endocrine pancreas. Insulin represses HGP to almost zero by inhibiting gluconeogenesis and glycogenolysis while at the same time stimulating the diametrically opposed processes of glycolysis and glycogen synthesis. Lipogenesis in liver and WAT from excess carbohydrates is induced in conjunction with inhibition of lipolysis in WAT, resulting in lowered plasma FFA. TGs produced in the liver and absorbed
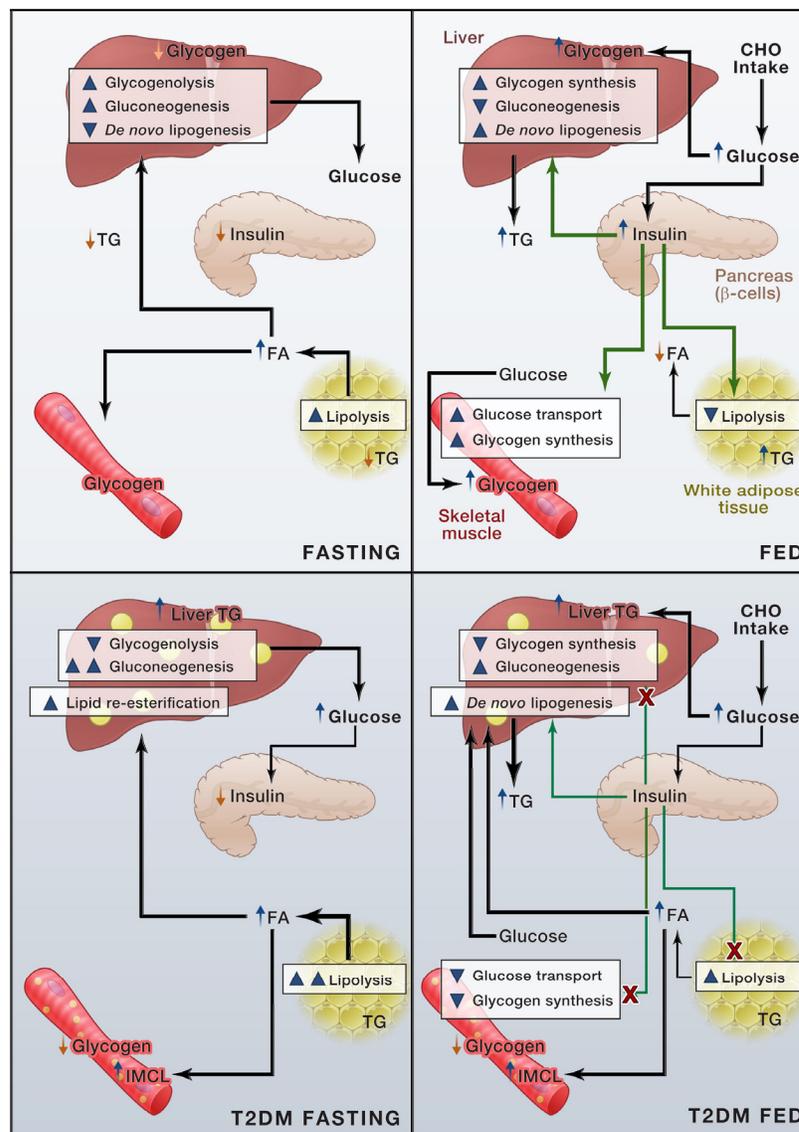
Figure 1. Pathophysiology of T2D.
The effect of insulin on liver, muscle and WAT is compared in the fasting (left) and fed (right) states under normal (upper panels) and T2D conditions (lower panels). Up- and downregulation of metabolic pathways is indicated by arrowheads, alterations in metabolites are indicated by arrows. Carbohydrates (CHO), triacylglycerides (TG) intramyocellular lipids (IMCL), fatty acids (FA). Reprinted with permission from [7] Elsevier.

from the intestine are gradually shipped to WAT for storage, elevating plasma TG levels (in the form of lipoproteins).

Insulin also greatly increases glucose uptake in muscle through translocation of GLUT4 and its storage in the form of glycogen. Approximately 25% of ingested glucose is taken up by liver and intestine, 50% is utilized by muscle and a small portion (4-5%) is also taken up by WAT [6]. The postprandial state is characterized by utilization of excess carbohydrates, conversion of carbohydrates to lipids and storage of synthesized as well as exogenous lipids in WAT.

Introduction

The fasting state in T2D (Fig. 1, left lower panel) is characterized by hyperglycemia. The main responsible organ is the liver, although reduced glucose uptake is a contributing factor. There is a tight correlation between the degree of fasting hyperglycemia and HGP [8]. It has been shown that HGP is mainly elevated due to increased gluconeogenesis, while glycogenolysis can even be slightly decreased [9, 10]. In accordance with this model, increased glucose-6-phasphatase activity has been found in microsomes of obese T2D patients in comparison to healthy obese subjects [11]. In addition, increased lipolysis in WAT leads to storage of FFA in the form of ectopic TG through re-esterification in muscle and liver.

When glucose levels rise in the postprandial phase in T2D (Fig. 1, lower right panel), insulin secretion can be increased, normal or decreased. The alteration of insulin secretion is associated with the severity of fasting hyperglycemia [12]. The present example assumes mid-stage T2D with pronounced insulin resistance. Note that gradual forms of insulin resistance without compensatory hyperinsulinemia exist. In either case the effect of insulin is blunted by resistance of its target tissues. HGP is not adequately repressed and endogenous glucose production persists in spite of exogenous glucose influx. This mechanism has been identified as one of the main factors contributing to postprandial hyperglycemia in T2D [13]. At the same time insulin stimulation of lipogenesis is still functional and acts together with insufficiently repressed lipolysis in WAT to increase FFA levels. In this way, ectopic lipid deposition is exacerbated. Glucose uptake and storage in the form of glycogen in muscle are defective as well, contributing to hyperglycemia. In the postprandial phase of T2D, hyperglycemia is maintained by insufficiently suppressed HGP coupled with insufficient utilization and storage of glucose by muscles. At the same time energy storage in the form of TG is still active but leads to deposition of TG in the wrong organs (liver and muscle).

As liver and muscle play different roles in the pathophysiology of T2D, insulin resistance is subdivided into hepatic insulin resistance (liver) and peripheral insulin resistance (muscle and WAT).

The current opinion as to the series of events leading to diabetes is that insulin resistance precedes hyperglycemia as well as an insulin secretory defect [6]. The finding that insulin resistance has been detected in people with normal fasting glucose levels and glucose tolerance is in line with this concept. These people could offset their insulin resistance by compensatory hyperinsulinemia [14].

Nevertheless, a secretory defect of the pancreas seems to be the primary defect in the pathogenesis of a subset of T2D cases [15, 16].

Results from tissue specific knock-out of the insulin receptor (IR) in mice provide a fascinating angle on the importance of specific organs in T2D. Liver and pancreatic β-cell specific knock-out causes severe glucose intolerance [17, 18], while WAT and muscle [19, 20] specific IR knock-outs have normal glucose tolerance.

1.1.2 Evaluation of insulin sensitivity and glucose tolerance.

The simplest test for glucose metabolism is the glucose tolerance test. A defined load of glucose is given after fasting and plasma glucose as well as insulin levels are monitored over time. Increased areas under the curve for glucose versus time indicate glucose intolerance. On the other hand, the area under the curve for insulin versus time gives information about increased or decreased glucose stimulated insulin secretion. In humans, the glucose load is given orally (oral glucose tolerance test (oGTT)), in mice it is most often administered intrapertioneally (ipGTT). Glucose can also be administered intravenously (ivGTT) but this produces an even less physiological scenario. The sensitivity to insulin can be assessed by an insulin tolerance test (ITT), which necessitates intravenous insulin application. The time course of the resulting decrease in plasma glucose levels is a measure of insulin action.

The gold standard to evaluate insulin action is the hyperinsulinemic-euglycemic clamp [21]. Here glucose and insulin levels are adjusted to constant target values (normal glucose, physiologically high insulin levels) by continuous infusion of both substances. The amount of glucose infused necessary to retain normoglycemia is the measure of insulin sensitivity. In addition to the cold glucose, a small amount of radiotracer ($3\text{-}^3\text{H}$-glucose) is infused, allowing the calculation of the total uptake of glucose in the body from blood samples taken throughout the clamp. Moreover, this enables the calculation of endogenous glucose production as the difference between whole body glucose uptake and amount of infused glucose. The organ mainly responsible for endogenous glucose production is the liver but kidneys can contribute as well. However, in the majority of clamp studies it is assumed that endogenous glucose production is identical to hepatic glucose production. The major advantage of the hyperinsulinemic-euglycemic clamp is that peripheral and hepatic insulin

sensitivity can be assessed simultaneously in the organism under physiological conditions.

Most mouse studies cited here used either HFD feeding or the genetic T2D mouse models *lep/lep* and *db/db* as well as the rat model *fa/fa*. These mice and rat are obese due to defects in either the hormone leptin (*lep/lep*, formerly *ob/ob*) or its receptor (*db/db* (mice), *fa/fa* (rats)). Leptin is an adipokine produced by WAT which inhibits food uptake by affecting neurons in the CNS. Therefore these mouse models are obese due to overfeeding, although leptin also exerts endocrine influence over the pancreas and insulin target tissues [22].

1.2 Insulin signaling pathway – Mechanism and function

Insulin causes pleiotropic effects in different cell types through profound influence of intracellular signaling (Fig. 2). The most important in the context of T2D are hepatocytes, myocytes and adipocytes. It is important to emphasize that the pathway depicted in Figure 2 is a union of processes that occur in these different cell types. Starting from a common core unit encompassing IR, IRS proteins, phosphatidylinositol-3-kinase (PI3K) and Akt (Fig. 2a, orange nodes), the pathway can be subdivided into different branches that mediate different functional outcomes. The most important branches in the context of T2D are those leading to GLUT4 translocation resulting in increased glucose uptake, particularly in muscle (Fig. 2b, light blue nodes) as well as those controlling metabolic enzymes through phosphorylation and expression changes (Fig. 2c-e, red nodes). In addition, insulin activates the mammalian target of rapamycin (mTOR) pathway regulating ribosomes and protein synthesis (Fig. 2f, yellow nodes) and the RAS/RAF cascade to transmit a mitogenic stimulus under some circumstances (Fig. 2g, green nodes).

1.2.1 Insulin signaling pathway core

The pathway core starts at the IR itself and its most important function is the activation of PI3K and Akt, the central kinases through which the different branches of the signaling pathway are regulated (Fig. 2a, orange nodes).

The insulin receptor is a tetrameric protein with $\alpha_2\beta_2$ structure. These subunits are bound covalently to each other by disulfide bridges [23]. The α subunits form the extracellular insulin binding domain, while the β subunits bridge the membrane with their transmembrane domains and contain the intracellular

kinase activity as well as phosphosites responsible for regulation and IRS docking [24]. The receptor pool is constantly replenished through internalization and recycling as well as through degradation and synthesis [23]. The IR is synthesized as a single pre-protein whose extracellular part is glycosylated before cleavage in α and β subunits in the Golgi apparatus [23]. Kinase activity of the β subunit is tightly regulated by a three tyrosine site in the cytoplasmatic C-terminal part of the receptor. These tyrosines (Y1175, Y1179, Y1180, inconsistent in the literature we use the Uniprot entry P15208 as reference) are autophosphorylated by the IR upon insulin binding. The number of phosphotyrosines in this motif of the IR correlates with its tyrosine kinase activity [24]. The activated IR phosphorylates itself on tyrosine residues in the juxtamembrane region, providing binding sites for IRS proteins, (e.g. Y960 [25]) and on tyrosine residues in the C-terminus. The active IR also phosphorylates tyrosines in IRS protein as well as in Cbl and Shp [26]. IRS proteins bind to the phosphotyrosines in the receptor facilitating their own phosphorylation. They may stay associated with the receptor as a cytoplasmatic extension or dissociate and continue to promote the signal. IR action is terminated by internalization and dissociation of insulin and dephosphorylation or IR by the phosphatase PTP1B [27].

IRS couple IR kinase activity to the main intracellular kinase cascades, most prominently the PI3K/Akt pathway. Six IRS proteins (IRS-1 - IRS-6) have been described today. The most important activators of downstream nodes and expressed in muscle and liver are IRS-1 and IRS-2. IRS-3 is expressed in adipose tissue along with IRS-1 [26]. While there is not much information about IRS-5 and -6, IRS-4 seems to be a negative regulator of insulin signaling based on the observation that IRS-4 overexpression inhibits IRS-1 and -2 mediated PI3K and Akt activation in cell culture systems [28].

All IRS proteins contain a pleckstrin homology (PH) domain facilitating plasma membrane recruitment through its binding to phosphatidylinositol-(3,4,5)-trisphosphate (PIP$_3$). They also contain a phosphotyrosine binding domain (PTB) for interaction with the IR [29]. IRS proteins are phosphorylated on multiple tyrosine resides by IR and almost all of these modulate their functions in signaling positively (Fig. 3). Upon binding to these phosphotyrosines PI3K and Grb2 are activated and influence their downstream targets accordingly (Fig. 2a). Activation of PI3K results from binding of its regulatory subunit p85 to phosphotyrosines on IR or IRS leading to relieve of inhibition of the catalytic
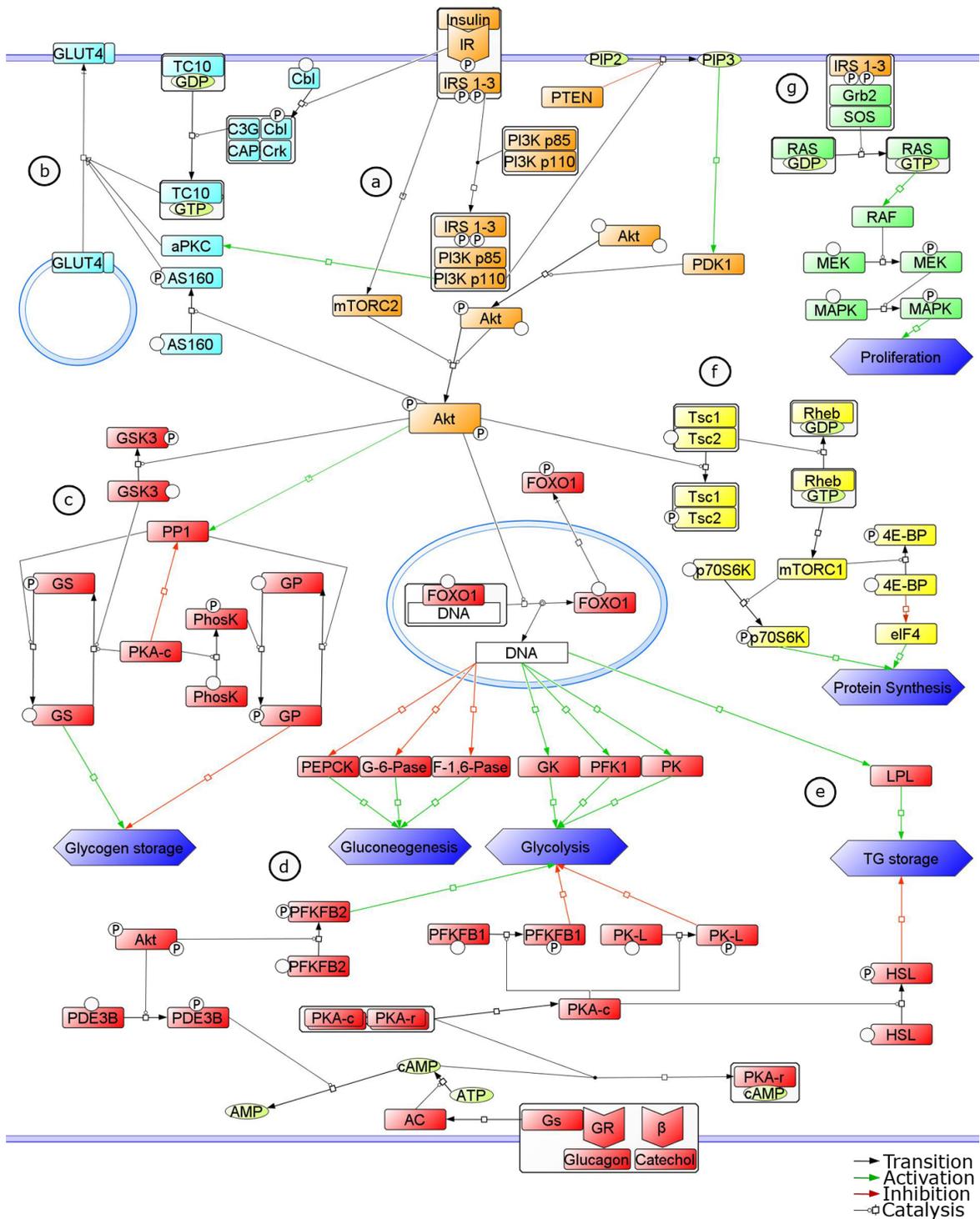
Figure 2. The insulin signaling network.
See text for details. Nodes belonging to the pathway core (**a**) are shown in orange, functional outcomes are drawn in dark blue. Proteins involved in GLUT4 translocation (**b**) are shown in light blue. Nodes belonging to the regulation of energy homeostasis are indicated by red shading illustrating the control of glycogen storage (**c**), glycolysis/gluconeogenesis (**d**) and TG metabolism (**e**). Nodes of the the mTOR pathway (**f**) and the RAS/RAF cascade (**g**) are shaded in yellow and green, respectively. Note that this schematic is a union of events occurring in hepatocytes, myocytes and adipocytes in response to insulin, glucagon and catecholamines. Redrawn based on [26, 27, 30-33].

subunit p110. Subsequently, PI3K phosphorylates phosphatidylinositol-(4,5)-bisphosphate (PIP_2) to PIP_3 in the plasma membrane. Both 3-phosphoinositide-dependent-kinase 1 (PDK-1) and Akt bind to PIP_3, facilitating phosphorylation of Akt by PDK-1 at Thr308. In order to be fully active, Akt also needs to be phosphorylated at Ser473 [34]. While Akt can autophosphorylate itself at Ser473 [35], mTOR was recently shown to facilitate this reaction. mTOR is the catalytic subunit of two complexes, called mTOR complex 1 and 2 (mTORC). Liver specific rictor$^{-/-}$ mice lack one of the key components of mTORC2. In these mice insulin stimulated Akt S473 phosphorylation was reduced while T308 phosphorylation was intact [36]. This defect led to a functional impairment of insulin signaling with insufficient repression of gluconeogenesis resulting in unsuppressed HGP in response to insulin and hyperglycemia as well as hyperinsulinemia [36]. With the full activation of Akt, the core of the insulin signaling pathway is complete and effects on the different branches ensue. The crucial role of Akt in insulin action can be deduced from its central position in the signaling network. Moreover, the severe phenotype of Akt2$^{-/-}$ mice (mammals have three Akt genes and Akt2 is the predominant form in liver and muscle [27]) underscores its importance for insulin. Akt2$^{-/-}$ mice develop diabetes with hyperglycemia and pronounced peripheral and hepatic insulin resistance [37]. Closer examination of the IRS node in the core part is in order, because impairment of IRS function, either by downregulation, sequestration of serine phosphorylation, plays a major role in different models of insulin resistance. IRS proteins are not only phosphorylated on tyrosine residues but also on dozens of serine residues (estimated around 70 sites [29]) which inhibits their activation of downstream target in the majority of cases (Fig. 3).
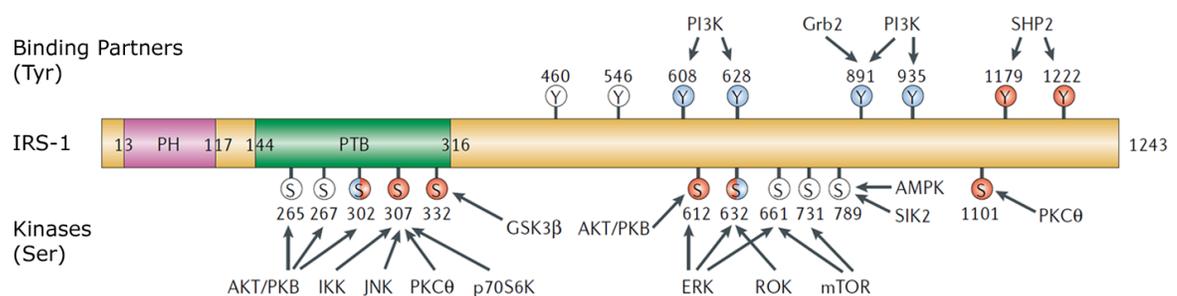
Figure 3. IRS-1 is phosphorylated on multiple tyrosine and serine residues.
Tyrosine sites phosphorylated by IR are shown on top along with the proteins binding to them. Serine sites are shown at the bottom along with the kinases phosphorylating them. Activating phosphorylations are shown in blue, inhibitory ones in red and those with unclear function in white. ROK- rho-associated protein kinase, SIK2 -serine/threonine-protein kinase 2. Reprinted by permission from Macmillan Publishers Ltd: [26].

Introduction

The different serines are phosphorylated by a broad group of kinases, some of which belong to the insulin signaling pathway and may pose feedback inhibition (e.g. Akt, extracellular-signal-regulated kinase (ERK), glycogen synthase kinase 3 (GSK3)) and some of which belong to other pathways (e.g. protein kinase C θ (PKC-θ) or IκB kinase (IKK)) (Fig. 3). IRS-1 is the best studied IRS isoform in this regard. While there is large body of evidence which kinases can phosphorylate IRS-1, the functional relevance of individual sites is often unclear (for comprehensive reviews see [29, 38]). However, the Ser307 phosphorylation is well characterized and has an established role in DAG-PKC mediated insulin resistance in muscle (see 1.3.3.1).

The existence of IRS-1 and 2 has led to the question if they have tissue specific roles. IRS-1$^{-/-}$ mice show growth retardation and glucose intolerance [39]. The facts that PI3K activation through insulin is stronger impacted in muscle than in liver in IRS-1$^{-/-}$ mice and that a compensatory upregulation of IRS-2 happens in their liver but not muscle has led to the view that IRS-2 is the main isoform responsible for insulin signaling in the liver [40]. However, hepatic insulin sensitivity was never assessed in IRS-1$^{-/-}$ mice. While global IRS-2$^{-/-}$ mice develop hepatic and peripheral insulin resistance [41], liver specific IRS-2 knock-out does not lead to hepatic insulin resistance [42]. A study with heterozygous IR and IRS-1 or 2 deficient mice showed that IR$^{+/-}$/IRS-1$^{+/-}$ mice developed insulin resistance in muscle, liver and WAT while IR$^{+/-}$/IRS-2$^{+/-}$ mice developed only hepatic insulin resistance [43]. These results show that caution is warranted when making conclusions about the functional relevance of IRS-1 and 2 in specific tissues. However, it would appear that both isoforms mediate the effects of insulin in liver while IRS-1 may be more important in muscle. In line with this observation, adenovirus mediated liver specific knock-down of both IRS-1 or 2 but not one or the other using shRNA led to glucose intolerance and blunted insulin stimulated Akt activation [44]. However, only knock-down of IRS-1 affected expression of gluconeogenetic enzymes while only knock-down of IRS-2 affected lipogenic enzymes [44]. This would imply that both isoforms have complementary roles within the liver. This is consistent with knock-down experiments in myotubes, that showed that only IRS-1 depletion affected GLUT4 translocation while only IRS-2 depletion led to impaired ERK activation [45].

1.2.2 Branches of the insulin signaling pathway

1.2.2.1 Control of glucose uptake - GLUT4 translocation

GLUT4 is of major importance in the uptake of glucose in muscle and adipose tissue but not in liver which expresses GLUT2. GLUT4 is synthesized in storage vesicles that fuse with the plasma membrane upon insulin stimulation and lead to a fast adaptation of the transport capacity of cells. Three pathways are required for GLUT4 translocation involving IR, PI3K and Akt (Fig. 2b, light blue nodes). IR phosphorylates Cbl which forms a complex with Crk, CAP and the GTP exchange factor (GEF) C3G. C3G activates the monomeric G-protein TC10 (Rho family) by GTP/GDP exchange which causes GLUT4 translocation [27]. In parallel, PI3K activates the atypical PKC-λ and ζ by a mechanism possibly involving PDK1 and PIP_3. Atypical PKCs cause GLUT4 translocation by an unknown mechanism. Finally, Akt phosphorylates Akt substrate of 160kDa (AS160), which relieves inhibition of small monomeric G-proteins to induce GLUT4 translocation. The final steps downstream of these effectors mediating transport and fusion of the vesicles are incompletely understood [46].

1.2.2.2 Control of glucose and glycogen metabolism

The control of glucose and lipid metabolism through insulin (Fig. 2c-e, red nodes) is intrinsically connected to its ability to antagonize the catabolic hormones glucagon and catecholamines (norepinephrine and epinephrine). The receptors of these hormones employ G_s proteins (the β1 and 2 adrenoceptors are relevant for the tissues discussed here) to activate adenylate cyclase (AC) and raise cyclic AMP (cAMP) levels, activating protein kinase A (PKA) [32]. One important component of the effects of insulin is the direct competition to this process by lowering cAMP levels using a phosphodiesterase (PDE). In adipocytes and hepatocytes PDE3B is activated by insulin [47], very likely through phosphorylation by Akt [48].

Glycogen storage is regulated by replenishment and depletion of glycogen through the enzymes glycogen synthase (GS) and glycogen phosphorylase (GP). Insulin activates GS and inhibits GP by influencing their phosphorylation states through GSK3 and protein phosphatase 1 (PP1) (Fig. 2c). GSK3 phosphorylates and inactivates GS. Akt inactivates GSK3 through phosphorylation and activates PP1 to dephosphorylate and activate GS. PP1 is a general serine/threonine protein phosphatase with a highly complicated regulation and intracellular targeting system. Insulin has been described to activate PP1 but the mechanism

is currently not understood [30]. PKA employs phosphorylase kinase (PhosK) to phosphorylate and activate GP leading to glycogen breakdown. Similar to GS regulation, PP1 dephosphorylates GP, shifting it back to inactivity. The net effect of insulin is GS activation and GP inhibition leading to glycogen storage. Conversely, glucagon leads to glycogenolysis.

Glycolysis and gluconeogenesis are mutually exclusive pathways. Insulin switches the flux to glycolysis in liver and enhances glycolysis in muscle. This is achieved by phosphorylation and expression changes of key enzymes (Fig. 2d).

An important modulation of glucose flux in the liver is 6-Phosphofructo-2-kinase (PFKBP). This enzyme produces fructose-2.6-bisphosphate (Frc-2,6-P) which potently inhibits gluconeogenesis at the level of fructose-1,6-bisphosphatase (Frc-1,6-Pase) and stimulates glycolysis at the level of phosphofructokinase 1 (PFK1). Phosphorylation of liver PFKBP (PFKBP1) by PKA inhibits its kinase and activates its phosphatase activity, effectively decreasing Frc-2,6-P [49]. Insulin counteracts PKA through decrease of cAMP levels elevating Frc-2,6-P and reversing the flux from gluconeogenesis to glycolysis. In contrast to the liver, the heart isoenzyme found in muscles and adipocytes, PFKBP2 [49], is activated through direct phosphorylation by Akt as well as PKA [50]. In addition, PKA can phosphorylate pyruvate kinase (PK) in liver, decreasing glycolysis.

Expression changes by insulin follow and reinforce the effects on phosphorylation. Activated Akt translocates to the nucleus and phosphorylates forkhead box (FOX) transcription factors, leading to their nuclear export. The most important factors for glycolysis are FOXO1 and FOXO4 [26] but other FOXO transcription factors and factors involved in lipogenesis like SREBP-1c are also influenced [51]. Glycolysis relevant expression changes include induction of glycolysis enzymes (glucokinase (GK), PFK1 and PK) and repression of gluconeogenesis enzymes (glucose-6 phosphatase (G-6-Pase), Frc-1,6-Pase and phosphoenolpyruvat carboxykinase kinase (PEPCK)).

1.2.2.3 Control of lipid storage and release

Insulin also potently influences lipid storage in WAT (Fig. 2e). The importance of adequate control of TG homeostasis in WAT through insulin is underscored by the important role of ectopic TG accumulation in T2D (see 1.1.1). Under normal circumstances, the plasma concentrations of FFA are much lower than TG, which exist in plasma in the form of lipoproteins. Exchange between plasma and tissue occurs through hydrolysis of TG, transport of the resulting FFAs, and re-

esterification [33]. Insulin decreases lipolysis in WAT through inhibition of PKA mediated activation of hormone sensitive lipase (HSL) [47]. Like for glycolysis, this mechanism depends on a decrease of cAMP through activation of PDE3B by insulin. In addition, insulin induces expression of lipoprotein lipase (LPL) in WAT, increasing plasma TG uptake.

1.2.2.4 Control of protein biosynthesis and proliferation

Insulin also has the ability to influence ribosomes and translation through its activation of the mTOR pathway (Fig. 2f, yellow nodes). Without insulin, the monomeric G-protein Rheb is inactivated by the tuberin/hamartin (Tsc1/Tsc2) GTPase activating complex. Active Akt phosphorylates and inhibits Tsc1/Tsc2 relieving the inhibition on Rheb which in turn activates mTORC1. Subsequently, mTORC1 phosphorylates p70S6 kinase [52], which activates ribosomes by phosphorylation of the S6 structural protein. In parallel, mTOR phosphorylates and inactivates an important translation inhibitor, 4E-BP1 [53], relieving eukaryotic translation initiation factor 4E from inhibition.

Insulin also activates the well-known RAS/RAF pathway (Fig. 2g, green nodes). Upon binding of Grb2 to phosphotyrosines, it activates the GEF son-of-sevenless (SOS). SOS activates the monomeric G-protein RAS, which in turn activates the kinase RAF. RAF phosphorylates MEK, which phosphorylates and activates mitogen activated kinases (MAPK). All three classes of MAPKs are activated by insulin including ERK, c-Jun N-terminal kinase (JNK) and p38 [26].

1.3 Roles of individual organs in T2D

In the following sections, some tissue specific aspects along with classes of anti-diabetic drugs targeting these tissues will be discussed.

1.3.1 Endocrine pancreas

The endocrine part of the pancreas is located in the islets of Langerhans, which are embedded in the exocrine part of the organ. Pancreatic islets mainly consist of insulin producing β-cells and, to a smaller extent, glucagon secreting α-cells (Fig. 4a). Minor cell types include somatostatin producing δ-cells and others. Hormones produced by one cell type usually provide feedback to other cell types generating a network that is beyond the scope of this thesis [32]. The most important cells for T2D are β-cells. ß-cells express the glucose transporter GLUT2 and glucokinase (hexokinase IV). These enzymes regulate the level of glucose-6-

phosphate entering glycolysis. These enzymes are characterized by high K_m values in relation to plasma glucose concentration [31, 32]. Consequently, they function in the linear part of their Michaelis-Menten kinetic, enabling them to function as plasma glucose sensors (Fig. 4b, A). The secretion of insulin is regulated by the ratio of ATP/ADP which is in turn regulated by the oxidative breakdown of glucose in mitochondria (Fig. 4b, B). Increasing ATP levels close the K_{ATP} potassium channel, depolarizing the plasma membrane (Fig. 4b, C). From this point secretion of insulin is similar to neurotransmitter release from presynapses: Depolarization causes Ca^{2+} influx which activates the exocytosis apparatus of preformed insulin containing vesicles (Fig. 4b, D) [54]. The K_{ATP} channel is the target of three classes of anti-diabetic drugs: sulfonylureas, meglitinides and indirectly also for incretins, all of which enhance glucose mediated insulin secretion [55].
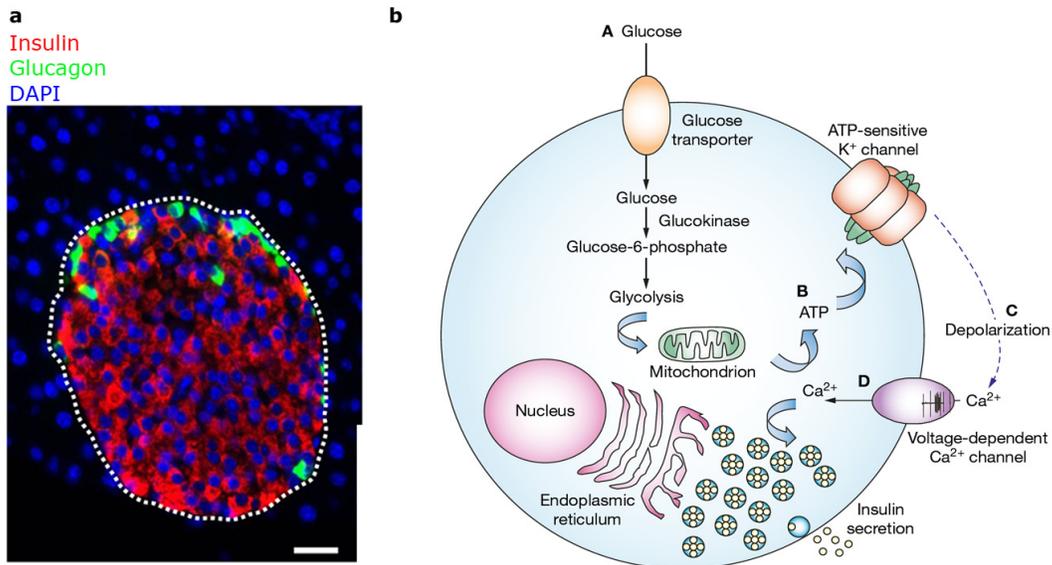
Figure 4. Insulin secretion by pancreatic β-cells is coupled to blood glucose levels.
(**a**) Langerhans islet in mouse pancreas. α-cells are labeled with a glucagon antibody, β-cells with an insulin antibody. Nuclei are stained with DAPI. Scale bar = 25μm. Modified after [56]. (**b**) Glucose stimulated insulin secretion from β-cells. See text for details. Reprinted by permission from Macmillan Publishers Ltd: [54].

The depicted mechanism enables ß-cells to tightly couple plasma insulin levels to changes in blood glucose. When challenged with increasing levels of fasting hyperglycemia, they can more than double plasma insulin concentrations. However, when hyperglycemia exceed 120mg/dl or 140mg/dl for basal and glucose stimulated conditions, respectively, insulin secretion deteriorates [12].

ß-cells are in a state of low grade apoptosis and renewal throughout life [57]. Obesity without T2D is known to increase ß-cell mass, but T2D patients commonly have reduced ß-cell mass in late stages [58]. While physiological

levels of FFA influence glucose stimulated insulin secretion [59], excess of plasma glucose and FFA are thought to cause ß-cell dysfunction and loss in T2D, designated glucotoxicity and lipotoxicity, respectively.

One of the major lines of evidence for glucotoxicity is that decreasing blood glucose by increasing its urinary excretion has been shown to restore impaired insulin secretion in partly pancreatomized rats [60]. Both glucose and FFA seem to induce apoptosis in isolated islets, which is associated with reactive oxygen species production and can be rescued by antioxidant administration [61]. However, a variety of other pathways have also been implicated in both gluco- and lipotoxicity [61].

1.3.2 Liver

The liver is the main factor determining fasting hyperglycemia and also has a major contribution to glucose intolerance in T2D. This is in agreement with its anatomical characteristics making it the gatekeeper of the entry of carbohydrates and proteins into the body. In contrast to all other organs, the liver has an afferent vein, the portal vein, which drains blood from the intestine, spleen and pancreas. Therefore, all dietary carbohydrates from the intestine and newly secreted insulin from the pancreas first enter the liver before the systemic circulation. Note that dietary lipids bypass the portal vein through the lymphatic system [62]. The liver is the second main glucose sensor of the organism, as hepatocytes express GLUT2 and glucokinase, just like pancreatic β-cells [31, 32]. Non-alcoholic fatty liver disease (NAFLD) is a benign condition with ectopic TG accumulation inside hepatocytes (Fig. 5a, b). A subset of NAFLD cases progress to non-alcoholic hepatosteatitis (NASH) which is defined by inflammation and fibrosis of the liver [63]. Obesity is the major determinant of NAFLD - its prevalence is approximately 20% among the general population but almost 75% among obese persons [63]. NAFLD is also very closely associated with T2D and the metabolic syndrome. The incidence of NAFLD among T2D patients is estimated to be 50-75% [63, 64] and approximately 50% among patients with metabolic syndrome [63].

Studies to determine the prevalence of hepatic insulin resistance in NAFLD have suffered from low numbers of studied subjects due to the laborious hyperinsulinemic-euglycemic clamp procedure involved. Nonetheless it was found that NAFLD patients without T2D had similar hepatic insulin resistance as T2D patients [65]. A different study found that NAFLD in T2D patients exacerbates

the degree of hepatic insulin resistance in comparison to patients without NAFLD [66]. Fat deposits in the liver were found to correlate with WAT mass [66]. This may be a confounding factor in its association with T2D. On the other hand, both humans and mice with no WAT due to congenital lipodystrophy still develop NAFLD and hepatic insulin resistance [67, 68].
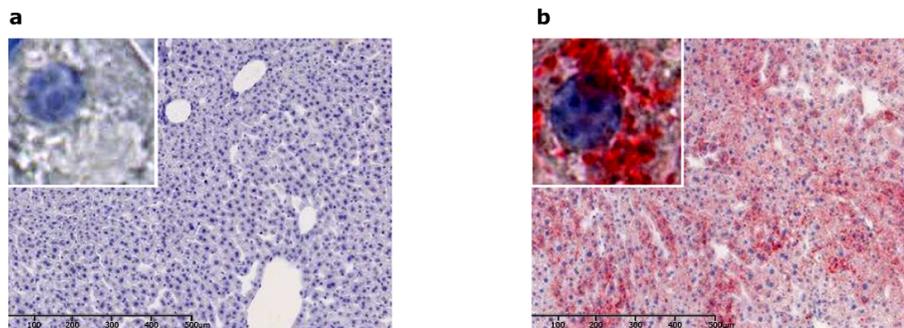
Figure 5. Intrahepatocellular TGs accumulate in NAFLD.
TG specific oil red staining from low fat diet (**a**) and high fat diet (**b**) fed C3H/FeJ mice. Courtesy of Dr. Susanne Neschen (HMGU, IEG) - Pictures taken by Anett Selig.

Ectopic lipid accumulation in the liver is due to dietary fat, redistribution of fat from WAT to the liver and stimulation of lipogenesis. The latter is fostered by enzyme induction through hyperinsulinemia and hyperglycemia, mediated by sterol response element binding protein 1 (SREBP-1) [69] and carbohydrate response element binding protein (ChREBP) [70], respectively. Interestingly, SREBP-1 activation has been shown to play a major role in hepatic insulin resistance in the *lep/lep* T2D mouse model. These mice are hyperinsulinemic, and display severely blunted insulin mediated Akt activation owing to downregulation of IRS-2 [71]. At the same time, insulin effectively activates SREBP-1c, inducing de novo lipogenesis and causing ectopic fat accumulation in their livers [71]. Further investigation of this mechanism showed that transgenic overexpression of SREBP-1c strongly reduced IRS-2 expression [72]. Adenoviral gene transfer of SREBP-1c to primary hepatocytes could cause severe insulin resistance, manifested as blunted Akt activation by downregulation of IRS-2 while at the same time strongly inducing lipogenesis [72]. Furthermore, SREBP-1c was shown to compromise insulin signaling in two ways: it binds to the IRS-2 promotor directly to inhibit its transcription and it competes with the activating transcription factors FOXO1 and FOXO3a for binding to the IRS-2 promotor [72]. Considering the close association of NAFLD with T2D and the fact that most of the data from human studies is association and correlation, it is difficult to tell if NAFLD is cause or effect in T2D. Interestingly, liver specific IR knock-out mice do not develop hepatic steatosis, implying that NAFLD may be cause rather than

effect [18]. However, it is clear that induction of NAFLD with high fat diet (HFD) in mice specifically causes hepatic insulin resistance. The safflower oil model (Fig 5b, c) used as the basis for this thesis is just such a model [73]. Saff-diet feeding in rats led to accumulation of TG and FFA as CoA esters specifically in liver but not in muscle. Concurrent with this accumulation, hepatic insulin resistance developed, while peripheral insulin sensitivity was unaffected [64].

The liver is the main target of metformin, one of the most effective anti-diabetic drugs, which has been used for decades as it does not increase body weight in contrast to many other anti-diabetic drugs [2]. Metformin reduces hepatic glucose production by inhibiting gluconeogenesis through activation of AMP activated kinase (AMPK) although the exact mechanism is unknown [3, 74].

1.3.3 Muscle

In contrast to pancreas and liver, skeletal muscle expresses GLUT4 and hexokinase (hexokinase II). These enzymes have much lower K_m values than the isoenzymes in pancreas and liver and consequently operate almost at V_{max} [31, 32]. Therefore, glucose-6-phosphate concentration is mainly determined by the amount of GLUT4 in the membrane, with plasma glucose concentration playing a minor role. In contrast to GLUT2, GLUT4 is not constitutively localized in the plasma membrane but is translocated though events in the insulin signaling cascade (see 1.2).

Skeletal muscle accounts for the majority of glucose uptake following glucose ingestion. While this is only approximately 50% for an oral glucose load it can be 80-90% of intravenously applied glucose [75]. Muscles can either burn the carbohydrates via glycolysis, pyruvate dehydrogenase and the tricarboxylic acid cycle (TCA) or store them in the form of glycogen. A minor fraction is also converted to lactate and serves as a substrate for gluconeogenesis in the liver (Cori cycle), which is important in the anaerobic phase of exercise [33]. Hyperinsulinemia induces both breakdown and storage of carbohydrates in muscles, but quantitatively, glycogen synthesis is stimulated more strongly than oxidation [75, 76]. This is in accordance with the finding that reduced glycogen synthesis in response to insulin in T2D patients accounts for most of the impaired glucose clearance through muscles [77]. The underlying defect was subsequently shown to be at the level of glucose transport into muscle rather than steps in its metabolism (reviewed in [78]). Specifically, the insulin stimulated translocation of GLUT4 is blunted in T2D patients.

Introduction

Muscles are currently not the main target tissue of any anti-diabetic drugs, although metformin, incretins and thiazolidinedione can also affect their metabolism favorably [55].

1.3.3.1 DAG-PKC mechanism of insulin resistance

One of the best characterized mechanisms of insulin resistance proposed by Shulman and associates is mediated by diacylglycerol (DAG) accumulation in muscle. Elevation of serum FFA through infusion of a phospholipid-stabilized soybean oil emulsion for five hours led to accumulation of lipids in the muscles of healthy volunteers [79] and was associated with increased IRS-1 Ser307 phosphorylation, blunted PI3K activation and glucose utilization [80] in muscle. The same effects could be induced in rats where they were associated with PKC-θ activation and insulin resistance [81]. These findings led to the hypothesis that a lipid intermediate was responsible for PKC-θ activation. In contrast to classical PKCs, which are activated by Ca^{2+} and DAG, novel PKCs like PKC-θ and PKC-ε are not sensitive to Ca^{2+} and their activity is mainly regulated by DAG [82].

FFA are rapidly converted to acyl-CoA intracellularly and esterified to sn-glycerol-3-phosphate generating lysophosphatidic acid (LPA) [83]. LPA is converted to DAG by the addition of a second acyl-group and removal of the phosphate. DAG is then converted to TG by the addition of the third acyl-moiety through DAG-acyltransferase 1 (DGAT1). Evaluation of lipid species in acutely FFA infused rats showed that PKC-θ activation coincided with the accumulation of DAG but not acyl-CoA or TG [84]. Muscle specific DGAT overexpression in mice lowered DAG, increased TG levels [85] and protected mice from HFD induced peripheral insulin resistance. This protective effect was accompanied by improved insulin signaling and GLUT 4 translocation [85], confirming the DAG hypothesis.

Further experiments showed that PKC-θ$^{-/-}$ mice were protected from lipid infusion mediated defects in insulin signaling and glucose transport in muscle [86]. The role of IRS-1 Ser307 phosphorylation was confirmed using muscle specific overexpression of a mutant form of IRS-1 in which serines 302, 307 and 612 were mutated to alanine. These mice were protected from HFD induced insulin resistance and impairment of insulin signaling in muscle at the levels of PI3K and Akt [87]. Translation of these result to humans showed that both content and activity of PKC-θ was also elevated in obese T2D patients relative to obese control subjects [88]. In summary, these results confirm the DAG hypothesis as a major mechanism of insulin resistance in muscle (Fig. 6). This mechanism

starts with an imbalance in lipid metabolism that causes the accumulation of DAG which activates PKC-θ. Next, PKC-θ phosphorylates IRS-1 on Ser307, interfering with its activation by IR and diminishing the stimulation of downstream targets, most notably the translocation of GLUT4.
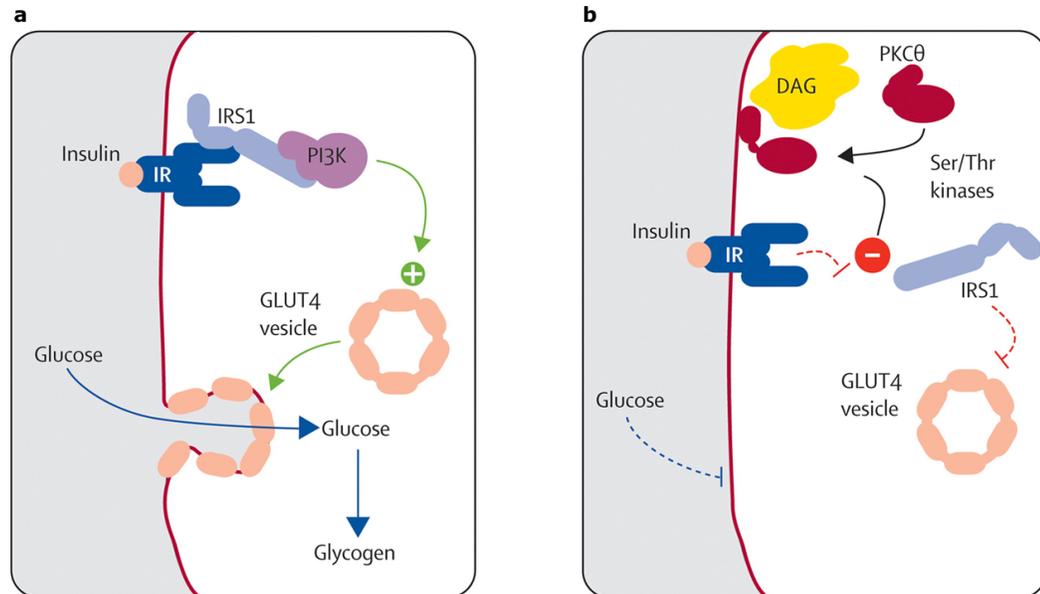
Figure 6. DAG accumulation induced PKC-θ activation causes insulin resistance in muscle.
(**a**) Under normal conditions, insulin activates IR, which leads to GLUT4 translocation through the insulin signaling pathway. Glucose is taken up and utilized. (**b**) Insulin resistance. DAG accumulation activates PKC-θ which phosphorylates IRS-1 on Ser307, impairing its activation by IR. GLUT4 translocation is blunted and glucose uptake is prevented accordingly. Reprinted from The Lancet [89] Copyright (2010), with permission from Elsevier.

There is also evidence that this mechanism may play a role in hepatic insulin resistance. Three day saff-diet feeding led to impairment of insulin signaling at the levels of IRS-1, IRS-2, PI3K, Akt, GSK3 and GS in rats in one study. Investigation of different PKC isoforms (conventional: α, β-1, novel: δ, ε and atypical: ζ) revealed specific activation of PKC-ε [64]. The shift in isoforms from muscle to liver was attributed to the low expression of PKC-θ in the liver. In addition, PKC-ε was implicated in insulin resistance by the finding that mice deficient in acyl-CoA-glycerol-sn-3-phosphate acyltransferase 1 (GPAT 1), which catalyzed the formation of LPA from acyl-CoA, were protected from HFD induced hepatic insulin resistance. This was accompanied by increased acyl-CoA but decreased DAG and TG levels in liver. Conversely, GPAT1 overexpression in liver caused hepatic insulin resistance associated with increased DAG levels and PKC-ε activation [90]. Nevertheless, the role of PKC-ε in hepatic insulin resistance requires further investigation.

1.3.4 Adipose tissue

The bulk of adipose tissue in the human body is subcutaneous WAT. However, WAT deposits are distributed in different parts of the body and a significant reservoir is the visceral WAT around the mesenteric vessel, intestine and omentum majus. These two types of WAT are distinguished based on different metabolic and secretory characteristics [91]. Adipose tissue consists of adipocytes and is not to be confused with the ectopic lipid depositions in muscle and liver, occurring in myocytes and hepatocytes, respectively. The masses of both visceral and subcutaneous fat correlate with insulin resistance, but this correlation is stronger for visceral fat [92]. Visceral fat mass was found to correlate with both, hepatic and peripheral insulin resistance [93] and to be a risk factor for developing glucose intolerance in a longitudinal study [94].

It has been established that obesity leads to a state of chronic low grade inflammation, which is associated with macrophage infiltration into WAT [95]. While some studies have identified higher macrophage infiltration in visceral than in subcutaneous WAT [96, 97] others have found no such difference [98].

Today, the role of WAT in T2D is attributed mainly to release of circulating mediators, both FFA and proteins called adipokines, that influence liver, muscle and pancreas. Insulin resistance of WAT promotes the release of FFA from stored TG [7]. Increasing plasma FFA concentrations foster ectopic lipid accumulation but they also have direct negative effects on insulin sensitivity. The effect of FFA is closely associated with the DAG-PKC mechanism of insulin resistance (see 1.3.3.1). Reduction of plasma FFA levels and redistribution of ectopic fat to WAT are also the main mechanisms underlying the insulin sensitizing effects of thiazolidinediones [89]. This class of anti-diabetic drugs are PPAR-γ agonists that promote pre-adipocyte differentiation and FFA uptake into WAT [55].

1.3.4.1 Adipokine mediated insulin resistance

The best characterized adipokines in T2D are tumor necrosis factor α (TNF-α), interleukin 6 (IL-6) and adiponectin but a plethora of others exist [99].

TNF-α is a proinflammatory cytokine secreted by non-adipocyte cells in WAT [100]. It causes adipocytes to reduce TG storage, release FFA and even induces their dedifferentiation [101]. Interest in TNF-α increased after it was implicated in the T2D model of genetically obese *fa/fa* rats. TNF-α was upregulated in WAT of these rats, increasing its circulating levels [102]. Neutralization of TNF-α improved peripheral but not hepatic insulin resistance in these rats, implicating it

in obesity related insulin resistance in muscle. Subsequent work by the same group showed that TNF-α neutralization also lowered plasma FFA levels and improved insulin signaling at the level or IR and IRS-1 in the muscles but not liver of *fa/fa* rats [103]. Moreover, plasma levels of TNF-α and its expression in WAT were also elevated in healthy obese volunteers, which could be ameliorated by weight loss [104]. Furthermore, infusion of TNF-α into rats could induce peripheral insulin resistance and decrease the effect of insulin on the liver [105]. However, TNF-α failed to induce insulin resistance in isolated rat muscle strips [106]. Two studies investigating TNF-α$^{-/-}$ mice found improved glucose tolerance in GTT, which was clear in one [107] but only marginal in the other study [108]. TNF-α induced IRS phosphorylation on Ser307 though ERK [109] and JNK [110] activation in cell lines, which inhibited insulin signaling at the level of IRS-1 [111]. The same IRS-1 Ser307 phosphorylation occurred in WAT and muscle of *fa/fa* rats [111]. TNF-α mediated increase in intracellular ceramide levels have been associated with MAPK activation [112] and IRS-1 Ser307 phosphorylation [113], but the mechanism is incompletely understood. In addition, there is evidence for multiple other mechanisms by which TNF-α can interfere with insulin signaling (reviewed in [114]), for instance by downregulation of PPAR-γ [115] or induction of suppressor of cytokine signaling 3 (SOCS-3) which in turn interfere with IRS-1 tyrosine phosphorylation by IR [116]. In conclusion, TNF-α from WAT seems to play a role in insulin resistance of muscles in T2D mouse models but the relevance for humans remains to be explored.

Adiponectin is produced by adipocytes [117] and in contrast to all other adipokines it is found downregulated in T2D patients, despite increased fat mass in patients [118]. Adiponectin$^{-/-}$ mice show a metabolic syndrome like phenotype with insulin resistance, glucose intolerance, hyperlipidemia and hypertension [119]. Downregulation of adiponectin receptors was found in muscles and WAT of insulin resistant *lep/lep* mice [119] and exogenous adiponectin improved glucose tolerance in genetically obese insulin resistant *db/db* mice. This was accompanied with increased TG oxidation in muscles of these mice [120]. Further investigation showed that adiponectin also inhibits gluconeogenesis by changing enzyme expression in the liver. The effects on both muscle and liver were mediated by and dependent on AMP activated kinase [121]. The cause of lowered adiponectin levels in T2D is unknown but they may contribute to peripheral and hepatic insulin resistance.

IL-6 was identified as another WAT derived cytokine whose plasma levels were elevated in T2D patients [118]. It is mainly produced by non-adipocyte cells in WAT [122], possibly macrophages. In addition, weight reduction decreased IL-6 plasma levels in obese subjects [99]. In accordance with its putative pathogenic role in T2D, IL-6 could indeed inhibit insulin signaling at the receptor and post receptor level in primary hepatocytes [123]. This was attributed to its induction of SOCS-3, which blocked the phosphorylation of both IR and IRS-1 [124] and targeted IRS-1 and IRS-2 to proteasomal degradation [125]. In agreement with this, IL-6 administration caused hepatic, but not peripheral insulin resistance in mice, associated with reduced IR and IRS-1 phosphorylation in response to insulin [126]. Conversely, IL-6 neutralization with an antibody ameliorated hepatic insulin resistance in *lep/lep* mice [127]. Strikingly, IL-6$^{-/-}$ mice are obese and have slightly worse glucose tolerance than wild type littermates [128]. This is most likely an artefact of the global knock-out as administration of IL-6 to the CNS but not systemic circulation can rescue their phenotype [128]. Administration of IL-6 to healthy volunteers caused a slight increase in plasma glucose but not hyperglycemia [129]. A second study investigated the effect of IL-6 on insulin in healthy subjects using hyperinsulinemic-euglycemic clamp. Surprisingly, IL-6 improved rather than impaired glucose disposal in muscle and had no effect on the liver [130]. These ambiguous results call a possible role of IL-6 in hepatic insulin resistance into question.

1.3.5 Complications of chronic diabetes

Chronic hyperglycemia leads to different diabetic complications, which can be quite severe and are mainly responsible for earlier mortality and loss of life quality for patients. These complications usually occur years after the progression of patients from impaired glucose tolerance to T2D and are tightly correlated to the level of glycemic control achieved through treatment [131]. This point is beyond the scope of this thesis, but most of the complications are caused by glucose mediated damage to blood vessels. The developing macro- and microangiopathy predispose for cardiovascular disease and damage peripheral nerves, the retina and the kidney.

1.4 Proteomics

Proteomic analysis describes the study of a population of proteins from an experimental system in a given state at a given time. In contrast to the much

more static genome of an organism, which is almost identical for all compartments, the proteome of different compartments (e.g. organs in the body) can vary considerably and is subject to constant changes over time [132]. One of the most illustrative examples is that of a caterpillar transforming into a butterfly. In this example, the proteome changes completely along with morphology while the genome remains the same [132]. The major advantage of proteomics is that this approach can assess changes at the effector level in a system-wide fashion. While transcriptomics approaches are more readily available today, expression changes at the RNA level do not necessarily translate into changes at the protein level. In fact, the correlation between changes at the mRNA and protein levels is much weaker than would be expected [133]. Taken together, proteomics assesses molecular changes in biological systems that are much more dynamic than those captured by genomics while being much closer to the functional level than transcriptomics. Furthermore, posttranslational modifications become amenable to study in addition to expression [134].

One of the major disadvantages in contrast to nucleic acid based techniques, like genetics and transcriptomics, is that no amplification of proteins is possible before analysis. Moreover, proteins are much more heterogeneous in their physicochemical properties than, for example, RNA [135]. In addition, the abundance of different protein species in a given proteome can span more than six order of magnitude [136].

In practice, a state of the art proteomic experiment has three main technical aims: Separation, identification and quantification of individual proteins. Currently, there are two major technical approaches to implement proteomics - 2D-gel based and liquid chromatography – tandem mass spectrometry (LC-MS/MS) based approaches. The 2D-gel based approach is older and relies on the two dimensional separation of intact proteins in an acrylamide gel. In the first dimension of the gel, proteins are separated based on their isoelectric point (pI) through isoelectric focusing (IEF). Subsequently, proteins are separated according to their apparent molecular weight (MW) in the second dimension of the gel which is orthogonal to the first [137, 138]. A major improvement was the use of immobilized ampholytes for the first dimension, improving reproducibility [139]. Individual spots on the gel correspond to different proteins or proteins with different chemical modification, posttranslational or otherwise. Therefore, the 2D-gel approach is protein-centric. While protein spots were stained with dyes or silver in the beginning, the use of fluorescent dyes improved sensitivity

and quantification accuracy of the approach [140]. The most advanced approach in this regard uses covalent labeling of proteins with Cy dyes before electrophoresis and is called difference gel electrophoresis (DIGE) [140]. The identification step is the last process in 2D-gel based approaches. Protein spots are excised from the gel, subjected to proteolytic digestion and resulting peptides are analyzed using mass spectrometry (MS). The peptide mix from one protein is ionized using matrix-assisted laser desorption ionization (MADLI) [141]. Traditionally, MALDI sources are coupled to time-of-flight (TOF) mass spectrometers. Proteins are identified either by the pattern of their peptide masses (peptide mass fingerprint) or by inferring the sequence of peptides from their fragment masses following dissociation [142]. As a consequence, each protein spot has to be processed manually, limiting the identification rate drastically. Therefore, 2D-gel approaches are usually limited to identifying a small set of differently expressed proteins (around 5-20) in each experiment. In this regard, the 2D-gel approach generates only limited system-wide information. This drawback, along with reproducibility problems, has led to a decline in the use of 2D-gel based approaches and a shift to LC-MS/MS based approaches [143].

In non-targeted LC-MS/MS based approaches, also called shotgun or discovery proteomics, proteins are proteolytically digested before separation and quantification. The resulting peptides are separated by high performance liquid chromatography (HPLC) in reverse phase (RP) mode on a C18 stationary phase according to their hydrophobicity. The post column flow is directly coupled to an electrospray ionization (ESI) source [144]. In ESI, the eluate is set to a high potential (1-2 kV) relative to the inlet of the mass spectrometer. Under these conditions a Taylor cone is formed that sprays the eluate into small charged droplets. These droplets are subject to desolvatization which concentrates H^+ and thus charges the droplets positively. As charge density increases the droplets dissolve into smaller and smaller particles due to electrostatic repulsion (coulombic explosion). While the final steps in ESI are not completely understood the whole process leads to single molecular ions that are completely desolvatized [145].

Peptide ions are measured in the mass spectrometer in MS1 mode as intact precursor ions determining their MW based on their mass to charge ration (m/z) and the spacing of the C_{13} isotopic peaks. Additional structural information is generated in MS2 mode after fragmentation of these precursors and generation

of fragment mass spectra (also called tandem mass spectra, or MS/MS). The combination of both MS1 and MS2 information enables inference of sequence information and identification of peptides [145]. Moreover, different strategies can be used to quantify peptides from either MS1 or MS2 data (see 1.4.1). In contrast to the protein-centric approach from 2D-gels, LC-MS/MS proteomics is peptide-centric. The reason for this is that LC separation, ESI ionization and the interpretation of fragment spectra is much more effective for peptides than for proteins [146]. Nevertheless, this peptide-centric approach also has disadvantages - proteolytic digestion before quantification can be a significant source of error for quantification and the proteome has to be reconstructed computationally like a puzzle afterwards [147, 148].

The development of LC-MS/MS based proteomics has been strongly advanced by improvements in sensitivity through the use of nano-HPLC and the development of nano-ESI [149] as well as the development of high-end mass spectrometers that fit the requirements of proteomics. These mass spectrometers needed to be able to generate MS1 as well as MS2 spectra. In order to deliver best performance, they required two synchronized mass analyzers, one of which also needed to be able to generate high mass accuracy measurements of precursor ions. This stems from the fact that identification of peptides and hence proteins is strongly improved by mass accuracy of MS1 [150]. In theory, only TOF, Fourier transform ion cyclotron resonance (FT-ICR) and orbitrap mass analyzers were eligible for high mass accuracy [151]. In practice, quadrupole-TOF, linear trap quadrupole (LTQ)-FT-ICR and LTQ-orbitrap hybrid instruments proved suitable for these requirements and enabled the identification and quantification of hundreds of proteins in a few hours [152]. However, it should be emphasized that proteomics has not advanced to the point where every single protein in a proteome can be investigated. While there are proof-of-principle projects that use extensive fractionation to almost completely assess the proteome of unicellular organisms like yeast [153], each proteomics experiment can usually just measure a fraction of proteins present in a given sample [148].

Today, the most commonly used MS for proteomics are LTQ-orbitrap hybrids, and the MS used for discovery proteomics in this thesis is just such an instrument.

1.4.1 Quantification strategies in LC-MS/MS based discovery proteomics

Quantifying proteins from LC-MS/MS data is not trivial. The primary readout is usually MS intensity of peptides, which is determined by ionization efficiency. However, ionization efficiency is different for each peptide and can be unstable over time in nano-ESI [148]. In addition, sample preparation before LC-MS/MS can introduce technical variability and efficiency of proteolysis is particularly hard to control between different samples [148].

Quantification can either be relative or absolute. Relative quantification aims to identify differences between samples only in relation to each other. Absolute quantification aims to determine the precise amount of a protein in a unit of sample. The difference lies mainly in the standard used, since absolute quantification requires a standard with known amount or concentration of a substance. Because hundreds of proteins are compared in discovery proteomics, quantification is almost exclusively relative.
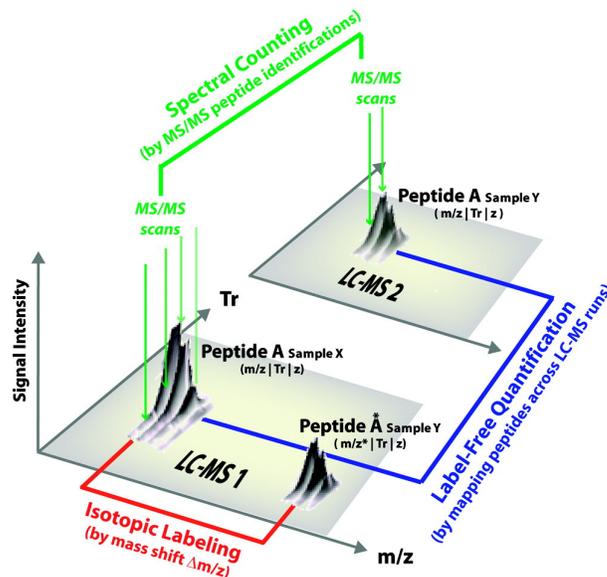
Figure 7. Comparison of isotopic labeling and label-free quantification in proteomics.
Using isotopic labeling, a peptide derived from differently labeled samples will be present in the same run in two forms with a distinct difference in m/z (red). Quantification can be performed from the same mass spectrum. In label free approaches, peptides signals from two separate runs are assigned to each other based on retention time (RT) and m/z by alignment of the runs (blue). Quantification can then be performed based on MS1 intensity like in isotopic labeling. Alternatively, peptides are compared without alignment of runs by their number of MS/MS spectra (green, spectral counting). Reprinted with permission from [154]. Copyright (2008) American Chemical Society.

All quantification strategies in discovery proteomics fall into two main categories – isotopic labeling and label-free quantification (Fig. 7). In isotopic labeling, stable heavy isotopes are incorporated into every protein in the proteomes to be

compared. Differently labeled proteomes are combined and analyzed by LC-MS/MS. The resulting peptides have slightly different masses (usually 2-10 Da) by which peptides derived from one sample or the other can be distinguished based on their mass to charge ratio m/z (Fig. 7, red). Differences in peptide abundance can be related directly to the ratio of the peaks of both peptides in the same mass spectrum [155].

The major advantage of this approach lies in the principle of isotopic dilution. As different isotopes behave chemically identical, differently labeled proteins or peptides will behave identical in all biochemical procedures following mixing of the samples after labeling up until the point where they behave slightly different in the mass analyzer and can be distinguished again [135]. Due to this principle, the ratio measured in LC-MS/MS is not influenced by work-up steps after mixing, minimizing technical variability. The disadvantage lies in the cost of heavy isotopes and the additional steps in introducing them into proteins quantitatively. Approaches to introduce isotopic labels include metabolic labeling of cells in culture with heavy essential amino acids, (stable isotope labeling by amino acids in cell culture (SILAC) [156]) and chemical labeling of proteins on lysine (isotope coded protein label (ICPL) [157]) or cysteine residues (isotope coded affinity tag (ICAT) [158]).

Alternative strategies are chemical labeling of peptides after digestion using so called isobaric labeling, e.g. tandem mass tag (TMT) [159, 160], although additional variations of these labeling schemes exist [161]. In general, the earlier samples can be mixed, the lower the technical variability will be [161]. Hence metabolic labeling is superior to chemical protein labeling, which is superior to peptide labeling. However, metabolic labeling of tissues becomes very cumbersome and costly [162]. Hence chemical protein labeling is the method of choice for isotopic labeling of tissues [163].

Label-free quantification can either be based on comparing MS1 intensities (Fig.7, blue) or the number of fragment spectra (Fig.7, green) of peptides between runs. Comparing the MS1 intensities generates much more accurate results, as the software of the mass spectrometer usually tries to minimize multiple sequencing events of the same precursor (dynamic exclusion). In addition, the number of fragment spectra and peptide abundance correspond only in rough approximation [161]. Key advantages of MS1 based label-free quantification are that no laborious and costly introduction of isotope labels is necessary and that LC-MS/MS runs have to aligned, which allows the pooling of

MS/MS based identification. In this way the number of identified proteins grows with increasing numbers of replicates (unpublished observation). The disadvantage is that MS1 based label-free quantification demands the most sophisticated software solution of all strategies presented here and that the LC-MS system has to work very reproducibly for days or weeks on end, depending on the number of replicates investigated.

1.4.2 Targeted proteomics - SRM

Selected reaction monitoring (SRM) is a mass spectrometric technique that enables data acquisition to be restricted to a small subset of peptides even when thousands of other peptides are present in the ion source [164]. In this way proteins can be detected with very high specificity from complex samples. Targeted proteomics has become a field of great interest in the proteomics community because it represents a paradigm shift from non-targeted discovery studies to a hypothesis driven approach [165]. Usually, only a subset of the proteome is quantified in discovery proteomics. However, researchers have limited control over which proteins will be contained in the final datasets. The significant advantage of the targeted approach is that investigations can be narrowed down to a much smaller panel of proteins already implicated in the system under study by different lines of evidence. Of course, all antibody based approaches, including ELISA and western blots, are targeted approaches. What sets SRM apart is its ability to measure a multiplexed panel of dozens of proteins in a single LC-SRM run [166] and to process a large number of samples sequentially in an automated fashion. These features are combined with high analytical accuracy [167], making it suitable even for clinical applications. This led the journal Nature Methods to select it as method of the year 2012 [168]. LC-SRM analysis is performed using a triple quadrupole MS. Quadrupoles are the worst mass analyzers in terms of mass accuracy when used to record a full spectrum [152]. However, in SRM they are used as a mass filter rather than in spectrum scanning mode. At unit resolution the transmission efficiency of this mass filter drops steeply outside a deviation of 0.35 Da from the targeted m/z. The high specificity of SRM is achieved by using two of these filters in tandem. A specific peptide is targeted by using the first quadrupole Q1 as a filter for the intact precursor ion, fragmenting the peptide in the second quadrupole Q2 though collision with inert gas molecules and filtering selected fragments

sequentially through the third quadrupole Q3 after which they hit the detector (Fig. 8).
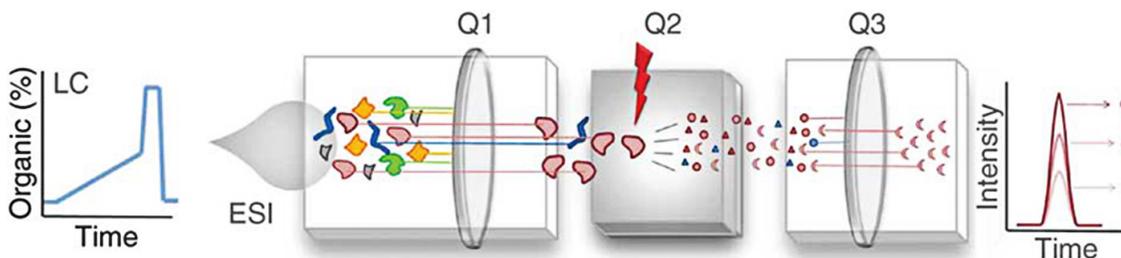
Figure 8. Principle of SRM.
Peptides elute from the nano-HPLC and are ionized by ESI like in LC-MS/MS based analysis. The example here shows detection of one peptide by three transitions. Q1 is operated like a mass filter allowing only the intact peptide ion to pass. Q2 fragments the peptide precursor through collision induced dissociation (CID). Q3 works like Q1 as a filter and lets three fragments pass sequentially based on their m/z. This process is repeated in a loop over the course of the chromatography and a plot of the intensity of the different fragments over time allows the detection of the peptide. Reprinted by permission from Macmillan Publishers Ltd [165].

The combination of a specific Q1 mass, representing the precursor and a specific Q3 mass, representing a fragment, is referred to as a transition. Multiple transitions for different fragments are monitored throughout the whole chromatographic run. When the intensity of the transitions is plotted, the presence of the peptide along the gradient is indicated by simultaneous appearance of all its fragments. This process takes only milliseconds for one peptide. Hence a number of peptides can be assayed sequentially in this fashion in a matter of seconds. The sequential scanning for all fragments from all target peptides constitutes one MS cycle and usually takes 2-10s. The MS is capable of monitoring all target peptides throughout the run by repeating this cycle over and over [169]. The vast majority of not-targeted peptides already collide with the rods of Q1. Therefore, SRM is a so called high duty cycle technique as the MS spends almost all of its time during the run detecting peptides of interest only [169].

In non-targeted discovery proteomics as many peptides per protein as possible are quantified, irrespective of their (unknown) quantitative properties. In contrast, SRM assays rely on a small number of so called proteotypic peptides (PTPs) [170], usually between one to five per protein [169]. PTPs need to be readily observable in the majority of samples and have favorable properties concerning quantification. Specifically, PTP need to have low limit of quantification (LOQ) values and linearity of response over a wide concentration range. PTPs can be considered the analogue of epitopes for antibody based techniques.

Introduction

Quantification strategies for SRM generally employ synthetic heavy isotope labeled peptides (absolute quantification or AQUA peptides). AQUA peptides are spiked into the sample as early as possible, enabling accurate absolute quantification [167].

Through the principles outlined above, gradient time can be shortened significantly, as the MS does not need to fragment ten thousands of peptides, increasing throughput of samples accordingly. The watershed study for the application of SRM in proteomics has been the description of protein dynamics during the growth of *S. cerevisia* [171]. The authors demonstrated accurate absolute quantification of proteins ranging in abundance from 50 to 10^6 copies per cell in a time resolved fashion.

1.5 Aims of the study

Type 2 diabetes mellitus is a heterogeneous disease which develops over many years in patients and often goes unnoticed in its early asymptomatic stages. Consequently, the transition from normal glucose tolerance to insulin resistance has not been studied as well as the condition in clinically apparent T2D. Study of the disease is further complicated by the involvement of multiple organ system. Owing to these complicating factors, insights into the molecular alterations occurring at defined stages of T2D pathogenesis in specific organs have been limited.

On the systemic level, pre-diabetic and early diabetic states are characterized by insulin resistance of liver, WAT and skeletal muscle, abnormal insulin secretion of the endocrine pancreas or a combination thereof. Therefore, studying proteomic changes in these organs is a promising approach to discover new pathways involved in the early events of T2D pathogenesis.

Here, we focused on finding a new pathway functionally relevant for insulin signaling and resistance. To this end, we monitored early protein expression alterations in the liver in a well characterized dietary T2D mouse model. The liver was investigated due to the crucial role of this organ in insulin resistance and glucose homeostasis. Hepatic insulin resistance could be induced by HFD feeding in a controlled manner and changes in protein expression levels monitored through the use of state-of-the-art quantitative proteomics.

In order to achieve the goal of finding a new pathway functionally connected with the development of early hepatic insulin resistance through HFD feeding, we defined the following milestone objectives:

1. Establishment of a robust workflow for non-targeted discovery proteomics of liver tissue. For this purpose we optimized sample preparation and compared and evaluated different quantification strategies for the analysis of liver proteomes with emphasis on the generation of consistent datasets for studies encompassing 30-70 mice.

2. Development of an SRM-based targeted approach so assay proteins implicated in T2D through other sources of evidence (e.g. literature, GWAS). Here we needed to improve the sensitivity of the approach from the currently evolving field of SRM based proteomics for tissue in order to access interesting candidates and set up a tailored quantification method.

3. Application of the whole workflow, encompassing non-targeted and targeted proteomics, to saff-diet fed versus control mice for different time points. High quality analytical performance over dozens of samples had to be ensured and differentially expressed proteins identified by appropriate statistical means. Based on the outcome we planned to formulate hypotheses that could be tested in the last step.

4. Functional validation of one candidate pathway in a cell culture system of insulin signaling. For the last step a whole new experimental setup had to be developed through which the influence of perturbations of the selected EET pathway on insulin signaling in isolated hepatocytes could be studied and evaluated.

2. Material and Methods

2.1 Material

2.1.1 Chemicals

NaOH 1M was purchased from AppliChem (Darmstadt, Germany). Trifluoroacetic acid (TFA) was purchased from Applied Biosystems (Foster City, USA). Ultrapure urea was purchased from Biomol (Hamburg, Germany). Ammonium persulphate (APS), Blotting-Grade Blocker and tetramethylethylenediamine (TEMED) were purchased from Bio-Rad (Hercules, USA). Agarose was purchased from Biozym (Oldenburg, Germany). (±)11(12)-epoxy-5Z,8Z,11Z-eicosatrienoic acid (11(12)-EET), (±)14(15)-epoxy-5Z,8Z,11Z-eicosatrienoic acid (14(15)-EET), (±)14(15)-epoxy-5Z,8Z,11Z-eicosatrienoic-16,16,17,17,18,18,19,19,20,20,20-d11 acid (d11-14(15)-EET), (±)14,15-dihydroxy-5Z,8Z,11Z-eicosatrienoic-16,16,17,17, 18,18,19,19,20,20,20-d11 acid (d11-14(15)-DHET), (±)5(6)-epoxy-5Z,8Z,11Z-eicosatrienoic acid (5(6)-EET) and (±)8(9)-epoxy-5Z,8Z,11Z-eicosatrienoic acid (8(9)-EET) were purchased from Cayman Chemicals (Ann Arbor, USA). Tris was purchased from GE Healthcare (Uppsala, Sweden). Acid-Phenol/Chloroform pH 4.5 and Lipofektamine 2000 were purchased from Life Technologies (Carlsbad, USA). 32% HCl, acetic acid, acetone, bromphenolblue, $CaCl_2*2H_2O$, chloroform, D(+)-glucose$*H_2O$, dithiotreitol (DTT), ethanol, ethylenediaminetetraacetic acid (EDTA), glycerin, HPLC grade H_2O, iodoacetamide (IAA), L-ornithine, L-proline (P), L-serine (S) and methanol were purchased from Merck (Darmstadt, Germany). BSA Fraction V was purchased from PAA (Pasching, Austria). Ni-NTA Agarose beads were purchased from Qiagen (Erlangen, Germany). Complete Protease Inhibitors and NP40 were purchased from Roche (Basel, Switzerland). Agar, guanidiniumthiocyanat (Gua-SCN), H_3BO_3, isopropanol (HPLC-grade), L-alanine (A), L-arginine (R), L-aspartic acid (D), L-cysteine (C), L-glutamic acid (E), L-glutamine (Q), L-glycine (G), L-histidine (H), L-isoleucine (I), L-leucine (L), L-methionine (M), L-phenylalanine (F), L-threonine (T), L-tryptophane (W), L-tyrosine (Y), tryptone and yeast extract were purchased from Roth (Karlsruhe, Germany). Acrylamide/Bis 30% (w/v), DNA Stain Clear and sodium dodecylsulphate (SDS) were purchased from Serva (Heidelberg, Germany). 3,5-Di-tert-4-butylhydroxytoluene (BHT), 3-[(3-Cholamidopropyl)dimethylammonio]-1-propanesulfonate (CHAPS), 4-(2-Hydroxyethyl)piperazine-1-ethanesulfonic acid (HEPES), acetonitrile (ACN, HPLC grade), ampholytes pH 3-10, ampicillin,

beta-mercaptoethanol (beta-ME), dexamethasone, diethylpyrocarbonat (DEPC), dimethyl sulfoxide (DMSO), ethyleneglycol-O, O'-bis(2-aminoethyl)-N, N, N', N'-tetraacetic acid (EGTA), formic acid (FA, MS-grade), H_2SO_4 40%, imidazole, insulin, kanamycin, KH_2PO_4, L-citrulline, L-lysine (K), $MgSO_4$, Na_2CO_3, Na_2HPO_4, NaCl, NaN_3, NH_4HCO_3, Phosphatase Inhibitor Cocktail 2, Phosphatase Inhibitor Cocktail 3, sodium acetate, sodiumdeoxycholate, Triton X-100 and Tween-20 were purchased from Sigma-Aldrich (Steinheim, Germany). $^{13}C_6$ $^{15}N_2$-L-Lysine 98 atom% and $^{13}C_6$ $^{15}N_4$-L-Arginine 98 atom% were purchased from Silantes (Munich, Germany). The synthetic peptide FAILTEK (AQUA Ultimate) was purchased from Thermo Scientific (Waltham, USA). Rapigest was purchased from Waters (Eschborn, Germany).

2.1.2 General lab equipment

Equipment	Manufacturer
Analytical scale ABT 220-5DM	Kern, Balingen, Germany
Camera Easy 400K	Herolab, Wiesloch, Germany
Centrifuge 5415R	Eppendorf, Hamburg, Germany
Centrifuge 5430R	Eppendorf, Hamburg, Germany
Centrifuger 3-18K	Sigma Laborzentrifugen, Osterode, Germany
Electrophoresis & blotting chamber Mini Protean Tetra Cell	Bio-Rad, Munich, Germany
Electrophoresis chamber SubCell GT	Bio-Rad, Freiburg, Germany
Electrophoresis chamber PROTEAN II XL Cell	Bio-Rad, Munich, Germany
Homogenizer Precellys 24	Peqlab, Erlangen, Germany
Incubator/Shaker E.coli	Memmert, Schwabach, Germany
Incubator Heracell 150i	ThermoFisherScientific, Waltham, USA
Laminar flow	BDK, Sonnenbühl-Genkingen, Germany
Liquid Nitrogen Tank Chronos	Messer, Sulzbach, Germany
PCR machine Peqstar	Peqlab, Erlangen, Germany
pH Electrode inlab micro	Mettler-Toledo, Greifensee, Switzerland,
pH Meter PB-11	Sartorius, Göttingen, Germany

Material and Methods

Equipment	Manufacturer
Power supply PowerPac 300	Bio-Rad, Freiburg, Germany
Power supply PowerPac HC	Bio-Rad, Freiburg, Germany
Shaker Titramax 100	HeidolphInstruments, Schwabach, Germany
SpeedVac SPD111V	Savant, FisherScienfic, Schwerte, Germany
Thermomixer comfort	Eppendorf, Hamburg, Germany
TransilluminatorUVT-40 M-HC	Herolab, Wiesloch, Germany
Ultracentrifuge OptiMax	BeckmanCoulter, Krefeld, Germany
Ultrasonic bath Transsonic 310/H	ElmaUltrasonic, Singen, Germany
Vortex Genius 3	IKALabortechnik, Staufen, Germany
Digital Developer FusionFx7	VilberLourmat, Eberhardzell, Germany

2.1.3 Consumables

Consumable	Manufacturer
96 well plates	BD Bioscience, San Jose, USA
BCA Reagents	Pierce, Rockford, USA
Bradford Reagent	Bio-Rad, Munich , Germany
Cell scraper 25 cm	Sarstedt, Nümbrecht, Germany
Cell strainer 100µM Nylon	BD Bioscience, San Jose, USA
ECL Prime	Amersham, Little Chalford, UK
Falcon conical tubes	BD Bioscience, Heidelberg, Germany
Flasks T-25, T-75, T-175	Greiner, Frickenhausen, Germany
Hybond-P PVDF membrane	Amersham, Little Chalford, UK
IPG strips pH 3-10 7cm	GE Healthcare, Uppsala, Sweden
IPG strips pH 4-7 24cm	Agilent, Santa Clara, USA
PepMap100 C18 HPLC column (C18) 150x0.075mm (3µm;100A)	Dionex, Idstein, Germany
Petri dishes	Greiner, Frickenhausen, Germany
Polysulfoethyl A HPLC column (SCX) 150x0.3mm (5µm;300A)	PolyLC Inc, Columbia, USA

Consumable	Manufacturer
PP-tubes bacteria	BD Bioscience, San Jose, USA
Precellys tubes CKM	Peqlab, Erlangen, Germany
Serological pipettes 5ml, 10ml, 25ml	Greiner, Frickenhausen, Germany
Six well plates	Nunc, Wiesbaden, Germany
Slide-A-Lyzers	Pierce, Rockford, USA

2.1.4 Kits and Standards

Kit or Standard	Manufacturer
1kb DNA ladder	New England Biolabs, Ipswich, USA
Big Dye Terminator v3.1 Sequencing Kit	Applied Biosystems, Foster City, USA
Gel Extraction kit	Thermo Scientific, Waltham, USA
Glucose Oxidase Kit	Sigma-Aldrich, Steinheim, Germany
ICPL duplex kit	Serva, Heidelberg, Germany
Lambda DE3 lysogenization kit	Novagen (Merck), Darmstadt, Germany
PageRuler™ Prestained Protein Ladder	Thermo Scientific, Waltham, USA
Plasmid Maxiprep kit	Qiagen, Hilden, Germany
Plasmid Miniprep kit	Thermo Scientific, Waltham, USA
RevertAid cDNA synthesis kit	Thermo Scientific, Waltham, USA

2.1.5 Enzymes

Enzyme	Manufacturer
Amyloglucosidase from *Aspergillus niger*	Sigma-Aldrich, Steinheim, Germany
Benzonase 99% pure	Merck, Darmstadt, Germany
Collagenase type IV from Clostridium histolyticum ≥125 CDU/mg	Sigma-Aldrich, Steinheim, Germany
Gateway BP Clonase II	Invitrogen, Carlsbad, USA
Gateway LR Clonase II	Invitrogen, Carlsbad, USA
Lysozyme	Sigma-Aldrich, Steinheim, Germany
Pfu polymerase	Thermo Scientific, Waltham, USA
Phusion High-fidelity PCR Kit	New England Biolabs, Ipswich, USA

Enzyme	Manufacturer
Restriction Enzymes	New England Biolabs, Ipswich, USA
Taq polymerase	Thermo Scientific, Waltham, USA
Trypsin (Sequencing grade modified trypsin)	Sigma, Steinheim, Germany

2.1.6 Cell culture reagents and media

Medium or Reagent	Manufacturer
DMEM High Glucose	Gibco, Paisley, UK
PBS without Ca^{2+}/Mg^{2+}	Gibco, Paisley, UK
Willams E Medium	Gibco, Paisley, UK
FCS	Gibco, Paisley, UK
Trypsin-EDTA 0.05% (w/v)	Gibco, Paisley, UK
Collagen I, rat tail, 0.3% (w/v)	Gibco, Paisley, UK
LB Medium	self-made (10g/l NaCl, 10 g/l Tryptone, 5g/l Yeast extract)
M9 minimal heavy medium	self-made (4g/l Glucose, 8.5mM NaCl, 22mM KH2PO4, 48mM Na2HPO4, 1mM MgSO4, 0.3mM CaCl2, 0.1g/l [13C615N4]-L-arginine, $[^{13}C_6{}^{15}N_2]$-L-lysine, 0.1g/l 18 other amino acids)

2.1.7 Analytical instruments

Instrument	Manufacturer
Off-gel fractionator G3100A	Agilent Technologies, Santa Clara, USA
Ettan microLC	GE Healthcare, Freiburg, Germany
Micro fraction collector SunCollect	SunChrom GmbH, Friedrichsdorf, Germany
Mass spectrometer Orbitrap XL	Thermo Fisher Scientific, Waltham, USA
HPLC Ultimate 3000	Dionex, Idstein, Germany
HPLC ultimate 3000 RSLC	Dionex, Idstein, Germany
HPLC Tempo nano-HPLC	Eksigent, Redwood City, USA
Mass spectrometer Q-Trap 4000	AB Sciex, Framingham, USA
Inverse microscope DMIRE2	Leica Microsystems, Wetzlar, Germany
Photometer Implen P330	Implen GmbH, Munich, Germany
Plate Reader Synergy HT	Biotek, Bad Friedrichshall, Germany

Instrument	Manufacturer
Photometer Ultraspec Pro 3300	GE Healthcare, Freiburg, Germany

2.1.8 Western blot antibodies

Primary antibody	Clonality, host species	Dilution	Manufacturer
Akt (pan) (C67E7)	monoclonal, rabbit	1:6000	Cell Signaling
Ephx2	polyclonal, rabbit	1:1000	Santa Cruz
IRS-1 (D23G12)	monoclonal, rabbit	1:2000	Cell Signaling
mTOR (7C10)	monoclonal, rabbit	1:1000	Cell Signaling
Phospho-Akt (Ser473)	monoclonal, rabbit	1:1000	Cell Signaling
GAPDH (6C5)	monoclonal, mouse	1:30.000	Millipore
Phospho-Insulin Receptor (Tyr1161/1162)	monoclonal, mouse	1:250	Millipore
Phospho-IRS-1 (Tyr608)	polyclonal, rabbit	1:25.000	Millipore
Phospho-mTOR (Ser2448) (D9C2)	monoclonal, rabbit	1:1000	Cell Signaling
β-Actin	monoclonal, mouse	1:25.000	Sigma
Flag (M2)	monoclonal, mouse	1:10.000	Sigma

Secondary antibody	Manufacturer
anti-rabbit HRP conjugated Fab fragment (goat)	Jackson ImmunoResearch, West Grove, USA
anti-mouse HRP conjugated Fab fragment (goat)	Jackson ImmunoResearch, West Grove, USA

2.1.9 Mammalian cell lines

Cell line	Derived from	Supplier
Hepa 1-6	Liver, hepatoma, C57/L	ATCC, Manassas, USA
BNL Cl.2	Liver, embryonic, normal, BALB/c	ATCC, Manassas, USA

Material and Methods

2.1.10 E.coli strains

Strain	Supplier	Genotype
BL21(DE3)	Stratagene, La Jolla, USA	F– ompT gal dcm lon hsdSB(rB- mB-) λ(DE3 [lacI lacUV5-T7 gene 1 ind1 sam7 nin5])
BL21 Gold	Stratagene, La Jolla, USA	E. coli B F- dcm ompT hsdS(rB- mB-) gal [malB+]K-12 endA hte
AT713	E.coli Genetic Stock Center, Yale, USA	F-, glnV44(AS), λ-, cysJ43, argA21, lysA22, rpsL104, malT1(λR), xyl-7, mtlA2, thi-1
AT713 (DE3)	derived from AT713	F-, glnV44(AS), λ(DE3 [lacI lacUV5-T7 gene 1 ind1 sam7 nin5]) , cysJ43, argA21, lysA22, rpsL104, malT1(λR), xyl-7, mtlA2, thi-1

2.1.11 PCR Primer

All Primers were purchased from Metabion ((Martinsried, Germany). Capitalized parts are part of the attB PCR, lower case sequence parts are gene specific. See 2.2.3.6 for details.

Primer name	Sequence
Ephx2 PCR_fwd	AAAAAGCAGGCTTCtcgtgtctgtgtcagcttg
Ephx2 PCR_rev	AGAAAGCTGGGTTtagatcaggctgtgttccag
CYP2C29 PCR_fwd	AAAAAGCAGGCTTCGCCGCCatggatctggtcgtgttcc
CYP2C29 PCR_rev	AGAAAGCTGGGTTtatgtgtttgctgggtcttg
CYP2C50a PCR_fwd	AAAAAGCAGGCTTCGCCGCCatggatccaatcctggtc
CYP2C50a PCR_rev	AGAAAGCTGGGTTaaagcagtgtgtccagtgtg
CYP2C70 PCR_fwd	AAAAAGCAGGCTTCGCCGCCatggctctcttcatctttctg
CYP2C70 PCR_rev	AGAAAGCTGGGTTcagccatccatgtgaaatac
CYP2J5 PCR_fwd	AAAAAGCAGGCTTCGCCGCCatgattatgtttttgagctccc
CYP2J5 PCR_rev	AGAAAGCTGGGTTtagcacatgtcagctcttcc
attB1 PCR	GGGGACAAGTTTGTACAAAAAAGCAGGCT
attB2 PCR	GGGGACCACTTTGTACAAGAAAGCTGGGT

2.1.12 Plasmids

Vector	Function	Resistance	Manufacturer
pDONR201	GATEWAY donor vector	KAN	Invitrogen
pcDNA3/DEST	GATEWAY expression vector	AMP	Invitrogen
pDEST-N-SF-TAP	GATEWAY SF-TAP vector	AMP	Dr. Johannes Gloeckner [172]

Construct	Insert (Reference)	Resistance	Constructed by
pET21(+)a-6xHisQconCAT	6xHisQconCAT	AMP	Polyquant GmbH, Regensburg, Germany
pDEST-mEphx2a	mEphx2a (NM_007940.4)	AMP	this study
pDEST-CYP2C29	CYP2C29 (NM_007815.3)	AMP	this study
pDEST-CYP2C50a	CYP2C50a (NM_134144.2)	AMP	this study
pDEST-CYP2C70	CYP2C70 (NM_145499.2)	AMP	this study
pDEST-CYP2J5	CYP2J5 (NM_010007.4)	AMP	this study
pCMV-GFP	eGFP	AMP	Addgene Plasmid 11153

2.1.13 Software

Software	Version	Manufacturer
Mascot	2.3.0.2	Matrix Science, Boston, USA
Proteome Discoverer	1.3	Thermo Fisher Scientific, Waltham, USA
Multiquant	1.2.0.6	AB Sciex, Framingham, USA
Progenesis LC-MS	3.1	Non-Linear Dynamics, Newcastle, UK
Photoshop	CS5	Adobe, San Jose, USA
Vector NTI	11.5.2	Life Technologies, Carlsbad, USA

2.2. Methods

2.2.1 Protein and peptide biochemistry

2.2.1.1 Mouse dietary treatment and liver sample acquisition

Mouse housing, dietary treatment and organ sample acquisition were performed by our collaboration partners Dr. Susanne Neschen and Melanie Kahle in the Institute of Experimental Genetics (IEG) at HMGU and are described in detail in [173].

C3HeB/FeJ (C3H) mice were housed under standard vivarium conditions (12:12 light-dark-cycle) and maintained on low-fat diet (LFD, 13% fat-derived calories, 17.0 kJ/g, Diet#1310, Altromin, Germany). At 14 weeks of age, male mice were single-housed (cages included domehouse, nestlet), body mass-, and litter-matched. Mice were fed a high-fat diet (HFD, 58% fat-derived calories, main fat-source safflower oil containing ~78% C18:2 ω-6 FAs, exchange every third day, 24.3 kJ/g, Ssniff, Soest, Germany) for 7, 14, or 21 days. One group of mice (rev) was treated with HFD for 14 days and switched back to LFD for 7 days. Initial body mass-, age-, and litter-matched control groups were continued on LFD for 7, 14, or 21 days. Body mass and body composition (MiniSpec LF60, Bruker Optics, Germany) were measured one day prior to the experiment start and end. At the study end, between 9-11 a.m., random-fed mice were killed with isoflurane. Liver and musculus gastrocnemius were dissected and immediately freeze-clamped in liquid nitrogen. All animals received humane care according to criteria outlined in the NAS "Guide for the Care and Use of Laboratory Animals". All animal experiments were approved by the Upper-Bavarian district government (Regierung von Oberbayern, Gz.55.2-1-54-2532-4-11).

2.2.1.2 Extraction of soluble proteins from mouse liver samples

Frozen liver samples were ground to powder using mortar and pestle under liquid nitrogen and stored at -80°C until use. Powdered liver samples were mixed with tenfold excess of extraction buffer in CKM homogenization tubes (Precellys lysing kit, Bertin Technologies) on ice. For SRM analysis and western blot, RIPA buffer was used (50 mM Tris, 150 mM NaCl, 0.1% (w/v) SDS, 0.5% (w/v) deoxycholate, 1% (v/v) NP40, 1x protease inhibitors, pH 7.4) and for ICPL proteins were extracted in labeling buffer (6 M guanidine-HCl, 100 mM HEPES, 1% (v/v) NP40, pH 8.5). Proteins were extracted by bead-based mechanical homogenization in a Precellys 24 Homogenizer (Bertin Technologies) pre-chilled

to 0°C by 25 s cycles of grinding at 5500 rpm. Homogenates were cleared by centrifugation at 16.000g for 10 min at 4 °C and protein concentration determined by BCA assay (Pierce) according to the manufacturer's instructions. Extracts were stored at -20 °C until use.

2.2.1.3 Enrichment of membrane proteins from mouse liver samples

Frozen liver samples were ground to powder using mortar and pestle under liquid nitrogen and stored at -80 °C until use. Protein extraction followed by membrane protein enrichment was done using a modified version of the protocol of Nagaraj et al [174]. Powdered liver samples were mixed with extraction buffer (2 M NaCl, 1 mM EDTA, 10 mM HEPES, pH 7.4) in CKM homogenization tubes using a 20-fold excess of buffer relative to tissue. Proteins were extracted by bead-based mechanical homogenization in a Precellys 24 Homogenizer (Bertin Technologies) pre-chilled to 0 °C by two 25 s cycles of grinding at 5500 rpm. Homogenates were cleared by centrifugation at 10.000 g for 30 min at 4 °C. Membrane vesicles were harvested at 100.000g at 4 °C for 30 min. Pellets were subjected to two steps of carbonate extraction in 500 µl 0.1 M Na_2CO_3; 1 mM EDTA pH 11.4 for 30 min on ice followed by centrifugation at 16.000g 4 °C for 30 min. Afterwards, pellets were washed with 500 µl urea buffer (4 M Urea, 100 mM NaCl, 10 mM HEPES, 1 mM EDTA, pH 7.4) and subjected to tryptic digestion.

Soluble proteins were prepared for SDS-PAGE analysis by pooling all discarded supernatants (high salt, carbonate and urea buffer), dialyzing thrice against 2 l 15 mM Tris pH 7.4 for 1 h at 4 °C using 30 kDa cutoff membranes and precipitation with acetone. Briefly, four volumes ice cold acetone were added to the dialyzed sample and the mix was incubated overnight at -20 °C. The next day, proteins were pelleted at 16.000g 4 °C for 30 min, washed with ice cold 80% (v/v) acetone, air dried and redissolved in 2x Laemmli buffer.

2.2.1.4 Extraction of proteins from cultured cells

Cells on six-well plates were washed twice with ice-cold PBS. Subsequently, 50 µl pre-chilled RIPA lysis buffer supplemented with protease inhibitors (Roche) as well as serine/threonine and tyrosine phosphatase inhibitors (Sigma) were added and cells were scraped into lysis buffer while cooling the culture plate on ice. Lysates were transferred into 1.5 ml Eppendorf tubes and incubated on ice for 15 min with vortexing every 5 min. Afterwards, lysates were centrifuged at 20.000g

4 °C for 5 min, pellets were discarded and protein concentration determined using the BCA protein assay. Lysates were stored at -20 °C until use.

2.2.1.5 Preparation of secreted proteins from cell culture supernatants

Cells were grown to 80% confluency in T-75 flasks in full medium (containing 10% serum). Cells were washed two times with PBS and 10 ml DMEM were added. Cells were allowed to secrete proteins for 48 h at 37 °C 5% CO_2. The 48 h conditioned medium was centrifuged at 500g for 10 min at RT to remove dead cells. Proteins were precipitated from the conditioned medium by acetone precipitation. Briefly, 40 ml ice cold acetone was added and the mix was incubated overnight at -20 °C. The next day, proteins were pelleted at 16.000g and 4 °C for 30 min, washed with ice cold 80% (v/v) acetone, air dried and redissolved in 100 µl TBS 0.5% (w/v) SDS. Resuspended proteins were separated from low molecular weight substances by ultrafiltration on 10 kDa Amicon centrifugal filters. Filters were spun at 10.000g until the volume was reduced to ~20 µl. Then 100 µl TBS (20 mM Tris-HCl, 150 mM NaCl, pH 7.4) 0.5% (w/v) SDS were added and samples spun again to concentrate proteins. This wash step was repeated two more times. Finally, concentrated, purified proteins were redissolved in 100 µl 2x Laemmli buffer, of which 60 µl were subjected to SDS-PAGE (2.2.1.7). The gel was run until the bromphenolblue had migrated approximately 1 cm into the separating gel. The piece of gel containing the secreted proteins was excised, proteins digested in gel with trypsin (2.2.1.13) and resulting peptides were analyzed by LC-MS/MS on an Orbitrap XL (2.2.2.2).

2.2.1.6 Colorimetric protein assays

Protein concentrations in mouse liver extracts and cell lysates were determined by colorimetric protein assays depending on the composition of lysis buffer. The BCA assay (Pierce) based on the reduction of Cu^{2+} by peptide backbones [175] was used for detergent containing samples because of its robustness against these interfering substances. Assays were conducted on 96 well microtiter plates (Falcon) with 200 µl final volume in each well. Standard curves with eight points measured in duplicates were generated using bovine serum albumin (BSA) standards (Bio-Rad). Final BSA concentrations on the plates ranged from 0.001 to 0.05 µg/µl. Lysis buffer was added to standard wells to give the same concentration of interfering substances as in sample wells for each plate.

Samples were measured in triplicates, mostly with 1µl samples per well. Absorption at 562 nm (BCA) was determined with a Synergy HT plate reader (Biotek). Linear-regression curves were accepted if r^2 was 0.97 or better. Sample measurements were only accepted if coefficients of variation (CV) of triplicates were below 20%. Initial protein concentrations of samples were calculated using Excel 2010.

2.2.1.7 SDS-PAGE

Electrophoretic separation of intact proteins was used as a simple analytical tool (Coomassie staining) but also as a prefractionation technique for proteomics (in-gel digestion 2.2.1.13) and as a part of the western blot technique (2.2.1.9).

Complex mixtures or proteins were separated by denaturing sodium dodecyl sulphate-polyacrylamide gel electrophoresis (SDS-PAGE) according to the discontinuous method originally published by Laemmli [176]. Proteins are incorporated into mixed micelles with SDS yielding constant mass to charge ratio. Protein-SDS micelles are compressed in the stacking gel through isotachophoresis between the leading chloride and trailing glycine ions. Upon entering the separating gel, the pH value changes from 6.8 to 8.8, ending isotachophoresis of proteins which are then separated through zone electrophoresis according to their apparent molecular weight.

Discontinuous polyacrylamide gels of dimensions 8.5 x 6.5 x 0.1 cm (mini) were cast in a Mini Protean 3 system (Bio-Rad) and gels of dimensions 16 x 20 x 0.1 cm (midi) were cast using the Protean II casting stand (Bio-Rad). 8-12% separation gels and 4% stacking gels were used for all experiments. The components (Table 1) were mixed a 15 ml tube. APS and TEMED were added last to initiate polymerization. Separation gels were cast first, overlaid with isopropanol and allowed to polymerize for 1 h at RT. Next, the stacking gels were cast and allowed to solidify for 15 min before wrapping the gel in wet tissues and storing it at 4°C overnight in the dark to ensure complete polymerization. Samples were mixed 1:4 with 5x Laemmli buffer (250 mM Tris-HCl, 50% (v/v) glycerol, 5% (w/v) SDS, 0.04% (w/v) bromphenol blue, 500 mM 2-mercaptoethanol, pH 6.8) and heated to 80 °C for 5 min to achieve denaturation through SDS and reduction through 2-mercaptoethanol. The gel was inserted into a Mini Protean Tetra Cell electrophoresis chamber (Bio-Rad), filled with running buffer (25 mM Tris, 192 mM glycine, 0.1% (w/v) SDS). Samples and standard were loaded onto the stacking gel and gels were run at 80 V for 15 min

and 160 V for approximately 90 min until the bromophenol blue front reached the end of the separating gel. Midi gels were run in a protean II chamber (Bio-Rad) at 25 mA constant current for 3 h.

Component	4%	8%	10%	12%
Type of gel	Stacking	Separating		
dH$_2$0	3.85	4.7	4	3.3
1.5 M Tris-HCl pH 8.8	-	2.5	2.5	2.5
1.5 M Tris-HCl pH 6.8	0.416	-	-	-
30% (w/v) Acrylamide:Bis	0.666	2.6	3.3	4
SDS 10% (w/v)	0.05	0.1	0.1	0.1
TEMED	0.01	0.01	0.01	0.01
APS 10 % (w/v)	0.05	0.05	0.05	0.05
Σ	5	10	10	10

Table 1. Composition of discontinuous SDS-PAGE gels.
All volumes given in ml.

2.2.1.8 Coomassie staining

Following electrophoresis, gels were stained with Coomassie Brilliant Blue. Depending on the required sensitivity the conventional or the more sensitive but more time consuming colloidal coomassie staining [177] was chosen. In this modification of the staining procedure microprecipitates of the dye Coomassie Brilliant Blue G-250 with ammonium sulphate specifically stain proteins in the polyacrylamide gel with increased sensitivity and specificity as compared to conventional coomassie staining.

Gels were fixed for 20 min in 50% methanol, 12% acetic acid and incubated with either 0.04% (w/v) Coomassie R-250 in 50% methanol, 12%acetic acid for 30 min or colloidal coomassie solution (Roti-Blue diluted 1:5 in 20% methanol) overnight. Destaining was necessary for conventional coomassie only and was done in 50% methanol, 12% acetic acid for 30 min or until background was reduced sufficiently.

2.2.1.9 Western blot

Specific detection of individual proteins and their phosphorylated forms from complex cell lysates was done by western blot [178]. 10-20 µg of total protein were separated by SDS-PAGE and blotted onto 0.45 µM pore size polyvinylidene fluoride (PVDF, Hybond-P, Amersham) membranes using the wet blot technique. Membranes were activated in methanol (p.a.) for 30 s and hydrated in transfer buffer (20 mM Tris, 150 mM glycine, 10% (v/v) methanol, pH 8.7). Gels were

equilibrated in transfer buffer for 5 min before proteins were transferred by wet blotting in a Mini Protean Tetra Cell equipped with a Trans blot central core unit (Bio-Rad) filled with pre-chilled transfer buffer (4 °C). Electrophoretic transfer was done in a cold room (4 °C) with a constant voltage of 110 V for 90 min. For all subsequent steps membranes were transferred to 50 ml Falcon tubes and incubated with solutions under constant rolling. Non-specific binding sites were blocked in TBS-T (20 mM Tris-HCl, 150 mM NaCl, 0.1% (v/v) Tween-20, pH 7.4) supplemented with 5% (w/v) skim milk for 1 h at RT.

Specific proteins were detected with primary antibodies recognizing the proteins or phospho-proteins and horseradish peroxidase (HRP) conjugated secondary antibodies binding to the primary ones. Bound secondary antibodies were detected by luminol oxidation through H_2O_2 catalyzed by HRP and the resulting luminescence.

Membranes were washed in TBS-T for 10 min, incubated with the primary antibody diluted in TBS-T 5% (w/v) BSA (except phospho-IRS-1 Y608 which was used in TBS-T 5% (w/v) skim milk) for 2 h at RT or overnight at 4 °C. Membranes were washed thrice in TBS-T for 10 min incubated with the secondary antibody diluted 1:7500 in TBS-T 5% (w/v) BSA for 1 h at RT. After washing the membranes four times for 10 min in TBS-T, they were immersed in enhanced chemoluminescent (ECL) solution for 3 min and transferred to a hypercassette (Amersham). Chemoluminsecence was detected with a digital developer (Fusion FX7, Vilber Lourmat) with the high sensitivity setting of the camera and a resolution of 2048 x 2048 pixel and exported to Photoshop CS5 (Adobe) for further processing.

2.2.1.10 Isotope coded protein label (ICPL) labeling of proteins

ICPL is a method of stable isotope labeling of proteins though the quantitative conjugation of lysine residues with nicotinic acid. It takes advantage of the principle of stable isotope dilution to enable high quantitative accuracy [157] and is well suited for the quantitative proteomic analysis of tissues [163]. In this study it was used to quantify proteins from mouse liver.

Proteins from mouse liver were extracted as described under 2.2.1.2 in labeling buffer and quantified using the BCA assay. Subsequently, 100 µg protein were conjugated at 5 µg/µl protein concentration with either [U-$^{12}C_6$] or [U-$^{13}C_6$] N-nicotinoyloxy-succinimide (Nic-NHS) according to [157]. Briefly, cysteines were reduced with 5 mM tris(2-carboxyethyl)phosphine (TCEP) for 15 min at 60 °C

and alkylated using 10 mM iodoacetamide (IAA) at RT for 30 min in the dark. Excess IAA was inactivated using N-acetyl-cysteine at a final concentration of 12.5 mM for 15 min at RT. The pH value was checked with a microelectrode and adjusted to 8.3 ± 0.1 if necessary. Subsequently, lysine residues were conjugated with Nic-NHS at a final concentration of 22.5 mM for 2 h at room temperature under exclusion of oxygen though argon overlay. The reaction was stopped by the addition of hydroxylamine to a final concentration of 150 mM for 30 min at room temperature. Differently labeled samples were combined and nicotinic acid protein esters were hydrolyzed by raising the pH to 11.9 ± 0.1 using 1 N NaOH for 20 min. Finally, samples were neutralized to pH 7-8 using 1 N HCl and excess chemicals were removed using dialysis (2.2.1.11).

2.2.1.11 Purification of ICPL labeled proteins by dialysis

Dialysis allows the complete change of buffer conditions of macromolecules. Protein samples were purified of undesired low molecular weight species after ICPL labeling as the diverse chemicals used in labeling are not compatible with downstream applications. Particularly, 6 M guanidine is detrimental for SDS-PAGE as it causes precipitation of proteins when mixed with low amounts of SDS. The protein sample is brought into contact with the dialysis buffer through a membrane retaining the proteins permeable for low molecular weight substances. Dialysis is continued until the concentrations of low molecular weight components of sample and dialysis buffer have equilibrated. As the volume of dialysis buffer far exceeds that of sample buffer, the composition of sample buffer after dialysis is effectively that of the dialysis buffer.

50 µl of ICPL labeled proteins were dialyzed against 2 l of dialysis buffer (2 M urea, 50 mM Tris, pH 7.4) overnight at 4 °C using 2 kDa cutoff membranes under constant stirring of the dialysis buffer (Slide-A-Lyzers, Pierce). Under these conditions, low molecular weight components of the sample are depleted by a factor of 40.000. Samples were retrieved from dialysis devices, mixed with 5x Laemmli buffer and separated by SDS-PAGE (2.2.1.7) as pre-fractionation technique for proteomics.

2.2.1.12 Purification of recombinant QconCAT by IMAC and isoelectric focusing

Recombinant 6xHis-QconCAT was expressed in *E.coli* as described in 2.2.3.2. Subsequently, the recombinant protein was purified under denaturing conditions by the combination of two orthogonal purification technique in order to produce a

highly pure internal standard for MS [179]. Immobilized metal affinity chromatography (IMAC) was the first step. Here the high affinity of the His-tag for transition metal ions, specifically Ni^{2+}, is used to remove the bulk of contaminants [180], which bind much weaker to the Ni-NTA resin. The recombinant protein is eluted by disrupting the His-tag-Ni^{2+} interaction with imidazole and lowering the pH from 8 to 4. In the second step, IEF was used to polish the QconCAT, as it offers highest resolution and loading capacity [181]. Buffer components incompatible with the second step of the purification, NaCl and ionic detergents, were removed by methanol chloroform precipitation. The protein was then focused over a long shallow pH gradient achieving pH increments of 0.1 between fractions and retrieved from the two fractions corresponding to its calculated pI.

For the first step, 20 ml crude *E.coli* lysate (8 M urea, 300 mM NaCl, 14 mM KH_2PO_4, 86 mM Na_2HPO_4, 50 mM imidazole, 1% (v/v) Triton X-100, 0.5% (w/v) CHAPS, 0.2% (w/v) SDS, Complete Protease Inhibitors w/o EDTA, pH 8.5) were incubated with 2.5 ml Ni-NTA agarose (Qiagen) for 3 h at 4 °C. Subsequently, the resin was washed four times with 4 ml of the same buffer used for lysis and the tagged protein was eluted eight times with 0.5 ml of the same buffer used for lysis without detergents supplemented with 500 mM imidazole and pH lowered to 4. Eluted 6xHis-QconCAT was precipitated using methanol/chloroform [182], resuspended in off-gel protein sample buffer (7 M urea, 2 M thiourea, 60 mM DTT, 1% (w/v) CHAPS, 0.4% (w/v) ampholytes pH 4-7) and separated on a 24 cm linear IPG strip pH 4-7 (Agilent) using an Agilent 3100 OFFGEL Fractionator (Agilent, G3100A) into 24 fractions according to the manufacturer's instructions. Isoelectric focusing was conducted with the settings: 5000 V, 50 µA, 250 mW 15 °C until 50 kVh were reached. Purified QconCAT was retrieved from two fractions corresponding to pI 5.1-5.2 and precipitated using methanol/chloroform. Purity was assessed by SDS-PAGE followed by colloidal coomassie staining (2.2.1.8).

2.2.1.13 In-gel tryptic digestion of proteins

Protein samples were fractionated by SDS-PAGE (2.2.1.7) and subjected to in gel tryptic digestion as described in [172]. Briefly, 60 µg soluble liver proteins or 100 µg ICPL labeled liver proteins were separated on a 10% discontinuous SDS-PAGE gel, stained with coomassie and the lanes cut into five fractions. Gel slices were destained by repeated washes with 60% acetonitrile (ACN). Dehydrated gel

pieces were swollen in 5 mM DTT in 50 mM ammoniumbicarbonate (ABC) and heated to 60 °C for 15 min to reduce cysteines. Cysteines were alkylated with 25 mM iodoacetamide (IAA) in 50 mM ABC for 15 min at RT in the dark. Residual alkylation reagents were removed by dehydrating the gel pieces fully in ACN, reswelling in 50 mM ABC followed by a second dehydration in ACN. Dehydrated gel plugs were air dried completely and swollen in 100 µl 10 ng/µl trypsin in 50 mM ABC. Proteins were digested for 16 h at 37 °C and eluted two to three times using 100% ACN 0.5% TFA. Pooled eluates were dried by vacuum centrifugation, reconstituted in 2% ACN 0.5% TFA and stored at -20 °C until use.

2.2.1.14 In-solution tryptic digestion of proteins

In solution digestion protocols for three different types of sample were used. In each case conditions were adjusted according to the characteristics of the sample.

Soluble protein extracts from mouse liver: Highest efficiency of extraction was achieved with a mix of detergents. Samples needed to be diluted to prevent inactivation of trypsin. Acid labile detergent Rapigest (Waters) was added to a final concentration of 2% (w/v) to protein samples (from 2.2.1.2). Samples were denatured and reduced using DTT at a final concentration of 3.5 mM at 60 °C for 10 min. Cysteines were alkylated using IAA at a final concentration of 11.25 mM for 30 min at RT in the dark. Subsequently, samples were diluted tenfold with 50 mM Tris pH 8.5 and digested with trypsin at 1:20 enzyme/protein for 18 h at 37 °C. Afterwards, Rapigest was hydrolyzed by lowering the pH below 2 for 30 min on ice and samples were stored at -20 °C until use.

Membrane proteins from mouse liver: Protein concentrations could not be determined and protein pellets were difficult to solubilize. Therefore excess reagents and sonication were used. Protein pellets (from 2.2.1.3) were resuspended in 50 mM Tris pH 8.5 0.5% (w/v) Rapigest (Waters) and resolubilized by three 10 s bursts of sonication with 30 s pauses on ice. Proteins were denatured and reduced using DTT at a final concentration of 7 mM at 60 °C for 10 min. Cysteines were alkylated using IAA at a final concentration of 22 mM for 30 min at RT in the dark. Proteins were digested with 5 µg trypsin for 18 h at 37 °C. Afterwards Rapigest was hydrolyzed as described above. Residual insoluble matter was removed by centrifugation and samples were stored at -20 °C until use.

Purified QconCAT: The necessary complete digestion of the hydrophobic and unstructured QconCAT was achieved by supplementing the reaction mix with ACN and digesting with very high amounts of trypsin. Precipitated QconCAT (from 2.2.1.12) was resuspended in 50 mM Tris pH 8.5, 10% (v/v) ACN 0.2% (w/v) Rapigest to a final concentration of 1 pmol/µl protein. Trypsin was added at 1:2 enzyme/protein and the QconCAT was digested for 8 h at 37 °C. Rapigest was hydrolyzed as described above. Aliquots of Q-Peptides were stored at -80 °C until use.

2.2.1.15 Peptide fractionation by offline SCX HPLC

Prefractionation of peptides for proteomics was performed with strong cation exchange (SCX) chromatography in off-line HPLC format. Tryptic peptides were desalted by a C18 pre-column and transferred to the preparative SCX column by a short organic bump. Tryptic peptides are separated at pH 2.7 because the carboxyl groups of acidic amino acids are protonated while basic amino acids and N-termini carry positive charges. Hence non PTM carrying tryptic peptides have at least one positive charge in acidic solution and can be bound to negatively charged SCX resins. Fractionation is based on the elution of peptides with increasing amounts of competing cations in order of their charge state and hydrophobicity [183].

Off-line SCX fractionation of peptides was conducted on an Ettan micro-HPLC (GE Healthcare) equipped with a C18 trap-column (1 × 5 mm, PepMap100 C18, 5 µm, 100 Å; LC Packings) and an SCX preparative column (0.3 x 150 mm, PolysulfoethylA SCX [183], 5 µm, 300 Å, PolyLC) in backflush configuration. 20 µg peptides were loaded onto the trap column in 0.1% (v/v) trifluoroacetic acid (TFA) and desalted at 30 µl/min for 10 min. Transfer of peptides from C18 to SCX was achieved by a short organic bump using 80% (v/v) acetonitrile, 0.1% formic acid in water at 3 µl/min for 3 min. Subsequently, peptides were separated using 5% (v/v) acetonitrile, 0.1% (v/v) formic acid in water (A) and 5% (v/v) acetonitrile, 0.1% (v/v) formic acid 500mM NaCl in water (B) at a flow rate of 5 µl/min, according to the following gradient schedule: 0-5 min: 2% B, 5-25 min: 2-30% B, 25-30 min: 30-65% B, 30-31 min: 65-95% B, hold 95% B for 6 min and re-equilibrate at 2% B for 15 min. Peptide elution was monitored at 214 nm and 5 min fractions were collected.

2.2.1.16 Isoelectric focusing of peptides

Peptides were also prefractionated for proteomics using off-gel electrophoresis (OGE) [184], which refers to IEF in a specialized format. Peptides are separated according to their isoelectric point along a preformed immobilized pH gradient (IPG) formed by ampholytes covalently attached to a polyacrylamide gel matrix under high electric field strength. The unique feature of OGE is a second liquid phase overlaying the IPG that is separated into discrete compartments. Peptides move between the liquid phase and the gel through diffusion and within the gel through electrophoresis. At equilibrium, peptides mainly occupy the liquid phase compartment overlaying the stretch of gel corresponding to their pI and can be retrieved easily by collecting the liquid phase fractions in different compartments [185].

OGE was performed on an Agilent 3100 OFFGEL Fractionator with an optimized protocol using consumables from Agilent: IPG strips (pH 3-10, linear, 7 cm, GE Healthcare) were swollen in 30 ml H_2O overnight at RT. The next day, strips were dehydrated in 10 ml acetonitrile (ACN) for 20 min at RT. Dehydrated strips were inserted into off-gel trays, fixed with frames, which had been clipped to 7 wells, and rehydrated using 100 µl 0.2% ampholytes pH 3-10 in H_2O per well for 20 min at RT. 50 µg peptides were diluted in 525 µl 0.2% (w/v) ampholytes pH 3-10 in H_2O and applied to the strip at 75 µl/well. Isoelectric focusing was conducted with the settings: 2000 V, 50 µA, 200 mW, 12 °C until 15 kVh were reached. Fractions were collected and wells were rinsed with 100 µl 80% methanol 0.5% TFA for 5 min to improve peptide retrieval. Corresponding fractions were pooled. Highly acidic and basic peptides were extracted from electrode papers using 100 µl 50% (v/v) ACN 0.1% (v/v) TFA and combined with the most acidic and most basic fractions, respectively. Organic solvents were removed by 45 min vacuum centrifugation at 35 °C and fractions were concentrated using PepClean (Pierce) according to the manufacturer's instructions to a final volume of 20 µl. Fractions five and six, counted from the anode, were pooled. Average pH values were measured on a strip run without peptides in parallel using a micro pH electrode (Mettler Toledo).

2.2.2 LC-MS based proteomics

2.2.2.1 Peptide solid phase extraction on C18 spin columns

Peptides were purified by C18 solid phase extraction (SPE) after digestion, if necessary. This step was omitted if possible as it contributes to the overall

technical variability of workflows. A spin column format for SPE, PepClean (Thermo), was used. All steps were done by adding the indicated solutions to the spin columns and centrifugation for 3 min at 1500g at RT. The C18 material was activated twice with 200 µl 50% methanol and equilibrated twice with 200 µl loading buffer (5% (v/v) ACN 0.5% (v/v) TFA). Peptides were dissolved in 200 µl loading buffer and bound to the C18 material. Spin columns were washed once with 200 µl loading buffer and peptides were eluted twice with 35 µl 70% (v/v) ACN. Organic solvent was evaporated from eluates by vacuum centrifugation and the remaining 10-20 µl acidified with 2% (v/v) ACN 0.5% (v/v) TFA and stored at -20 °C until use.

2.2.2.2 LC-MS/MS on Orbitrap XL systems

Quantitative non-targeted proteomics data were generated with LC-MS systems composed of reverse phase (C18) nano LC coupled on-line to Orbitrap XL mass spectrometers. Peptides are separated in reverse phase chromatography (C18) according to their hydrophobicity. This process is supported through the use of the ion pairing reagents TFA and FA. TFA enables efficient binding of more hydrophilic peptides to the C18 material but is exchanged during chromatography for FA as it suppresses ionization in the ESI source [186]. Peptides that have eluted from the column are subjected to electrospray ionization (ESI) [144]. The format of choice for the efficient ionization and sensitive detection of peptides, nano ESI [149], is used to desolvatize and ionize the peptides.
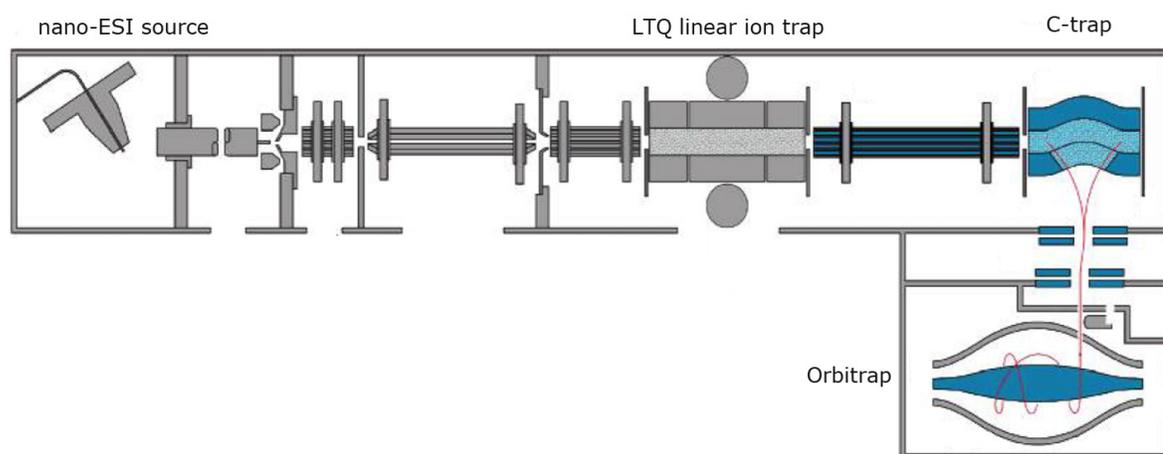
Figure 9. Schematics of the Orbitrap XL mass spectrometer.
Ions from the nano ESI source are transmitted by the front end ion optics to the LTQ linear ion trap. Here they are either transmitted to the Orbitrap analyzer via the intermediate C-trap or subjected to CID fragmentation. Reprinted (adapted) with permission from ([187]). Copyright (2006) American Chemical Society.

Material and Methods

MS and MS/MS spectral data are generated by the hybrid linear ion trap-orbitrap mass spectrometer Orbitrap XL. The instrument is composed of a nano ESI source, the linear LTQ ion trap, the C-trap, which is crucial for transmitting ions from the LTQ to the orbitrap, and the electrostatic orbitrap [188] itself, which is used for the generation of high resolution MS spectra (Fig. 9).

Data was acquired in the parallel TOP 10 method design. During each cycle, ions are first transmitted to the orbitrap for a lower resolution fast preview scan in order to identify multiply charged ions for fragmentation. Next a second packet of ions is introduced into the orbitrap to acquire a more time consuming high resolution MS full scan. During this time the putative peptide ions identified in the preview scan are sequentially isolated and subjected to collision induced fragmentation (CID) in the LTQ, in order to generate moderate resolution MS/MS spectra. This proceeds to a maximum of ten MS/MS per cycle if a sufficient number of precursor ions have been identified in the preview scan. In this fashion each cycle generates a maximum of one high resolution MS and ten MS/MS scans in parallel. For all spectra, automatic gain control ensures best possible trap filling and thereby spectra quality. In order to target as many different peptide precursors as possible, dynamic exclusion is used: Precursor selection is based on highest MS intensity. Peptides fragmented in one cycle are excluded from selection from the precursor list for 30 s to have the chance to select lower intensity precursors of different peptides and thus reduce redundancy of MS/MS data. In order to obtain the best possible mass accuracy, continuous internal calibration with polysiloxane as lock mass was used [189].

Two LC-MS systems were used: System 1 consisted of a standard HPLC adapted to constant nanoflow operation by an active flowsplitter (Ultimate 3000, Dionex) coupled to an Orbitrap XL. System 2 consisted of a splitless ultra high pressure LC (RSLC, Dionex) coupled to a second Orbitrap XL. MS settings were identical for both systems but columns and chromatography settings differed slightly.

Peptides were loaded onto a nano trap column (0.3 × 5 mm, PepMap100 C18, 5 µm, 100 Å; LC Packings) in 0.1 % (v/v) TFA at a flow rate of 30 µl/min for 5 min and separated by reversed phase chromatography on a C18 column heated to 40 °C.

Separations were conducted on system 1 (standard HPLC) using a PepMap column, 0.075 x 150 mm, 3 µm, 100 A° pore size (Dionex, Idstein, Germany) with a nonlinear 170 min gradient using 2% (v/v) acetonitrile in 0.1% formic acid (v/v) in water (A) and 0.1% (v/v) formic acid in 98% (v/v) acetonitrile (B)

at a flow rate of 300 nl/min with the gradient settings: 5–140 min: 5–31% B, 140–145 min: 31–99% B, 145–150 min: 99% B and equilibrate for 10 min at starting conditions. Separations were conducted on system 2 (RSLC) using a PepMap column, 0.075 x 250 mm, 2 µm, 100 A° pore size (Dionex, Idstein, Germany) with a nonlinear 170 min gradient using 2% (v/v) acetonitrile in 0.1% (v/v) formic acid in water (A) and 0.1% (v/v) formic acid in 75% (v/v) acetonitrile (B) at a flow rate of 300 nl/min. The gradient settings were subsequently: 5–140 min: 5–50% B, 140–145 min: 50–95% B, 145–150 min: Stay at 95% B and equilibrate for 10 min at starting conditions.

Both nano-HPLCs were connected to LTQ Orbitrap XL mass spectrometers (Thermo Fisher, Bremen, Germany) equipped with nano-ESI sources. ESI was maintained with a spray voltage between 1.25–1.4 kV without sheath or auxiliary gas flow and transfer capillaries heated to 200 °C. The mass spectrometers were operated in data-dependent mode to automatically switch between Orbitrap-MS and LTQ-MS/MS acquisition. Survey full scan MS spectra (from m/z 300 to 1500) were acquired in the Orbitrap with resolution R= 60,000 at m/z 400. The method used allowed sequential isolation of up to ten most intense ions depending on signal intensity. Precursors were fragmented in the linear ion trap using collision-induced dissociation at an AGC target value of 10.000 with a normalized collision energy of 35% and an activation time of 30 ms. Minimum signal intensity required was 200, isolation width 2 amu and default charge state 2. Precursor masses were selected in a data-dependent manner. High resolution MS scans in the orbitrap and MS/MS scans in the linear ion trap were performed in parallel. Target peptides already selected for MS/MS were dynamically excluded for 30 s.

2.2.2.3 Label-free quantification using Progenesis LC-MS

Label-free quantification was performed in Progenesis LC-MS based on peptide MS intensity. Retention times versus m/z graphs for each run are aligned to match peptide signals between runs. Peptides are quantified by integrating the extracted ion chromatograms (XIC). By extension, protein quantification is straightforward by summing peptide areas belonging to one protein. For all experiments the normalization implemented in Progenesis LC-MS was used. Here a correction factor is calculated for each run based on the total MS intensity of features. Specifically, the robust mean of all feature intensities is calculated and used as correction factor to compensate for unequal loading.

Thermo raw files were imported into Progenesis LC-MS (Non-Linear Dynamics, version 3.0) and aligned semi-automatically to compensate retention time shifts between runs. MS/MS spectra were exported in mgf format and searched against the Ensembl Mouse database using Mascot (Matrix Science, version 2.3.02) with the following parameters: Precursor mass tolerance: 7 ppm, fragment tolerance: 0.7 Da, enzyme: trypsin, allowed missed cleavages: 1, instrument: ESI-TRAP, fixed modifications: carbamidomethylation (C), dynamic modifications: oxidation (M) deamidation (N,Q), acetylation (K). Peptide FDR was set to 2% by adjusting cutoff values for Mascot score and p-value using the decoy database approach. Peptide identifications were re-imported into Progenesis LC-MS. Peptides were excluded from quantification if they were not unique. Proteins were excluded if they were identified by less than two unique peptides. Results were exported into Excel 2007 (Microsoft) for further analysis. Average fold changes were calculated for each protein as the sum of protein intensities in group 1 divided by the sum of protein intensities in group 2. In addition, p-values for significant differences were calculated by t-tests in combination with multiple testing correction using the Benjamini Hochberg method [190]. Here q-values were calculated to allow flexibility during further analyses.

2.2.2.4 Isotopic labeling quantification using Proteome Discoverer

Identification and quantification of peptides and proteins was done using Proteome Discoverer 1.3 (Thermo Fisher Scientific). Acquired MS/MS spectra were searched against the Ensembl Mouse database using Mascot (Matrix Science, version 2.3.02) with the following parameters: Precursor mass tolerance: 7 ppm, fragment tolerance: 0.7 Da, enzyme: trypsin, allowed missed cleavages: 1, instrument: ESI-TRAP, fixed modifications: carbamidomethylation (C), dynamic modifications: oxidation (M) deamidation (N,Q). Heavy and light ICPL labels of lysines were set as variable modifications. Resulting peptides hits were filtered with a Mascot score cutoff of 13, further processed with Percolator [191] and filtered to a peptide false discovery rate of 2% using the estimation method implemented in Percolator. Proteins with at least two peptides were considered identified. Peptides were quantified by their heavy/light ratio determined from their XICs at the MS level. Protein heavy/light ratios were calculated as the median of peptide ratios and normalized by shifting the median of the protein ratio distribution to one by multiplication with a normalization factor. Results were exported to Excel 2007 (Microsoft) for further analysis.

2.2.2.5 LC-SRM on a Q-Trap 4000/Eksigent nano-HPLC system

Development of SRM assays and quantitative LC-SRM analysis were performed on an LC-MS system composed of a splitless nano-HPLC (Tempo MDLC, Eksigent) and a Q-Trap 4000 mass spectrometer (ABSciex). Peptides were separated by reverse phase chromatography analogous to LC-MS analysis on the orbitrap systems (see 2.2.2.2.) The nano-HPLC was coupled online to the mass spectrometer by a nano spray III ion source. Mass spectrometers of the Q-Trap series are a combination of triple quadrupole and linear ion trap (LIT) (Fig. 10). The main advantage of the instrument is that it can switch from normal quadrupole operation to using quadrupole 3 (Q3) as an ion trap [192]. In this manner, fragment ions of lower abundance precursors can be collected, if necessary, and MS/MS spectra can be generated with better resolution than with normal quadrupole scans. This facilitates the setup of SRM assays as the instrument can switch to improved MS/MS data acquisition once a transition exceeds a defined threshold. Successful MS/MS coinciding with transitions can validate the identity of signals during SRM assay development.

Two types of methods were used with the Q-Trap system. The method used in assay development (LC-SRM-MS/MS) monitored candidate transitions without scheduling in SRM mode and triggered MS/MS data acquisition when transitions exceeded a certain threshold. The method used for quantification with the final assays (LC-SRM) used scheduled SRM [193] only. HPLC separations for both types of methods were identical.
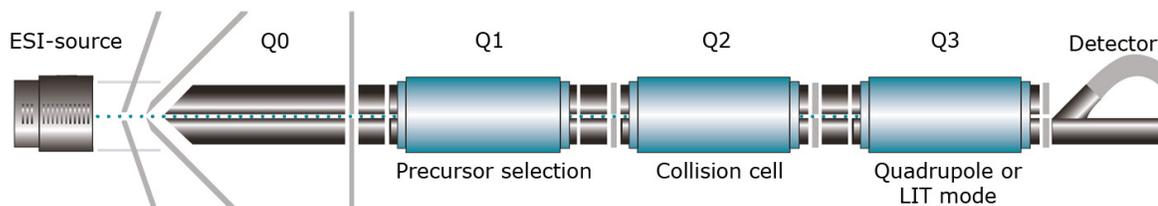
Figure 10. Schematics of the Q-Trap 4000 mass spectrometer.
Ions Produced in the ESI source are transmitted to the triple quadrupole path through Q0. Subsequently they pass Q1 Q2 and finally Q3 before hitting the detector. Q3 can be operated in quadrupole or linear ion trap (LIT) mode. Reprinted (adapted) from [194] Copyright (2004), with permission from Elsevier.

Peptides were loaded onto a nano trap column (0.3 × 5 mm, PepMap100 C18, 5 µm, 100 Å; LC Packings) in 0.1 % TFA at a flow rate of 20 µl/min for 5 min and separated on a C18 analytical column (0.075 × 150mm, PepMap100 C18, 3 µm, 100 Å, LC Packings) by a 90min gradient using 2% acetonitrile in 0.1% formic acid in water (A) and 0.1% formic acid in 98% acetonitrile (B) at a flow rate of 250 nl/min. The 90min gradient settings were: 5–65 min: 5–40% B, 65–70 min:

40–90% B, 70–72 min: 90% B, 72-79 min: 90-5% B, re-equilibration for 10 min. Electrospray ionization was maintained with curtain gas set to 14 psi, a spray voltage of 2.6 kV, ion source gas set to 30 psi and an interface heater temperature of 170 °C. During establishment and validation phase the LC-SRM-MS/MS method was used. Peptides were detected in SRM mode with Q1 and Q3 set to unit resolution and dwell times ranging from 20 ms to 50 ms. SRM dependent MS/MS spectra acquired in enhanced product ion scan (EPI) mode were triggered if transitions exceeded a threshold of 200 counts. EPI scans were acquired by summing two scans at speed 4000 Da/s, Q1 set to unit, Q0 trapping enabled and fixed fill times ranging from 300 ms to 800 ms. Collision energy for EPI scans was determined from a charge state specific linear curve dependent on m/z.

Quantification for saff-diet samples was performed using the LC-SRM method. Validated SRM assays were combined into one multiplex method in which peptide measurements were conducted at unit resolution in Q1 and Q3 using scheduled SRM with a retention time window of 2 min and target scan time set to 5 s.

2.2.2.6 SRM assay development

Proteotypic peptides (PTPs) [170] were selected based on the criteria outlined in [169]: length 5-30 aa, no cysteine or methionine containing peptides, no missed cleavage sites, unique to the target protein as assessed by BLAST search (http://blast.ncbi.nlm.nih.gov) against the "all non-redundant GenBank CDS translations+PDB+SwissProt+PIR+PRF" database with organism filter set to mus musculus. During the establishment phase, gel-fractionated mouse liver samples (see 2.2.1.13) were subjected to non-targeted proteomics analysis as described for the orbitrap LC-MS systems (see 2.2.2.2) and peptides of target proteins detected in this analysis were preferentially selected from the list of proteotypic peptides.

Assays were established by screening for PTPs of each protein in the fraction corresponding to its molecular weight (MW) using the 90min SRM-MS/MS method described before. Up to 14 peptides per protein and up to 16 transitions per peptide were screened with the objective of obtaining three peptides with three transitions for each protein. PTPs were screened for SRM observability by searching for occurrence of multiple transitions at the same retention time, supported by the generation of SRM triggered MS/MS data during the screening runs. MS/MS spectra were exported with the built-in Mascot script of Analyst and

searched against the Ensembl mouse database using Mascot (Matrix Science, version 2.3.02) using the following settings: precursor mass tolerance: 0.8 Da, fragment tolerance: 0.8, allowed missed cleavages: 1, fixed modifications: carbamidomethylation (C), variable modifications: oxidation (M), deamidation (N,Q), instrument: ESI-TRAP.

Annex tables A1 and A2 contain full lists of tested peptides and transitions, respectively. Peptides in the final assay were validated by manual inspection of MS/MS as well as coelution with their corresponding heavy Q-peptide.

Collision energy (CE) optimization of selected transitions for the final assay was done by testing nine CE values in two volt increments centered on the initial value determined by charge state and m/z during LC-MS runs using gel-fractioned samples used for establishment. The optimum value was determined by manual inspection of LC-SRM runs in the Analyst 1.5 software.

2.2.2.7 SRM quantification using Multiquant

Raw data acquired using Analyst 1.5 was imported into Multiquant 2.0 (AB Sciex) for quantitative analysis. Peak areas were determined by integration of SRM traces with the MQ4 algorithm using the following settings: Gaussian smooth width: 3 points, min peak width: 3 points, noise percentage: 85%, baseline subtraction window: 2 min, peak splitting: 2 points. Signal-to-noise ratios were determined using the SignalFinder algorithm with the settings: confidence threshold: 50%, no global baseline, allow non-linear baseline. Multiquant results were exported to Excel 2007 for further analysis. Visual comparison of SRM traces was done with Skyline 1.2 using Savitzky–Golay smoothing of all traces.

2.2.3 Molecular biology

2.2.3.1 General culture of *E.coli* and heat shock transformation

Different strains of *E.coli* were made chemically competent by the $CaCl_2$ method [195]. Cloning was done in the BL21 Gold strain cultured in LB medium and protein expression was done in the strain AT713(DE3) cultured in M9 minimal heavy medium (4 g/l Glucose, 8.5 mM NaCl, 22 mM KH_2PO_4, 48 mM Na_2HPO_4, 1 mM $MgSO_4$, 0.3 mM $CaCl_2$, 0.1 g/l $[^{13}C_6{}^{15}N_4]$-L-arginine, $[^{13}C_6{}^{15}N_2]$-L-lysine, 0.1 g/l 18 other amino acids).

Bacteriological agar plates were prepared by dissolving agar in medium under heating to a final concentration of 1% (w/v). After cooling the mixture down, antibiotics were added before pouring the plates. Ampicillin was used at a final

concentration of 100 µg/l and Kanamycin at 50 µg/µl. Antibiotic concentrations for agar plates and growth media were identical.

For heat shock transformation 50 ng intact plasmid or 5 µl recombination mixture (BP or LR gateway reaction, theoretically 75 ng DNA) were added to competent cells in 1.5 ml Eppendorf tubes and incubated for 30 min on ice. Bacteria were subjected to heat shock at 42 °C for 45 s on a heating block and incubated for 2 min on ice. Afterwards, the transformed bacteria were mixed with 200 µl medium (pre-warmed to 37 °C) and allowed to grow for 1 h without antibiotic. The outgrown suspension was spread on pre-warmed LB or M9 heavy agar plates with the appropriate antibiotic and incubated overnight at 37 °C. Colonies were picked the next day with sterile inoculation loops and transferred to vented bacteriological tubes containing 2.5 ml LB medium with antibiotic. These cultures were grown overnight at 37 °C under vigorous shaking. 2 ml of the culture were used for DNA preparation on miniprep scale and 500 µl were used for the generation of cryostocks, by adding 100 µl 80% (v/v) glycerol and freezing at -80°C.

Clones were screened for the desired constructs using restriction endonuclease digestion and/or sequencing. Larger cultures for recombinant expression (100 ml, 2.2.3.2) or plasmid preparation on maxiprep scale (200 ml 2.2.3.3) were inoculated from cryostocks and grown overnight at 37 °C.

2.2.3.2 Recombinant expression of QconCAT

Stable isotope labeled Q-peptides were generated using the QconCAT approach according to [180]. 6xHis-QconCAT was synthesized and subcloned into pET21a-(+) by PolyQuant GmbH (Regensburg). In order to achieve complete labeling of the QconCAT, possible sources of light lysine and arginine have to be eliminated. These include endogenous synthesis as well as the growth medium. To address endogenous synthesis, the lysine and arginine auxothrophic *E.coli* strain AT713 was used. The AT713 strain was converted to AT713(DE3) by using the λ DE3 lysogenization kit (Novagen). The DE3 phage introduces the IPG inducible T7 polymerase which allows tight control of expression from pET21 plasmid containing the QconCAT under control of the T7 promotor. In order to eliminate exogenous lysine and arginine, the LB medium was exchanged for M9 minimal heavy medium after transformation.

QconCAT expression in 100 ml culture was induced after bacteria had reached an OD600 of approximately 0.6 by addition of IPG to a final concentration of 2 mM

for 4 h at 37 °C under vigorous shaking. Induced bacteria were harvested by centrifugation at 4000g for 10 min and subjected to two freeze thaw cycles. Bacteria were lysed by lysozyme treatment (1 μg/μl lysozyme in 15 mM NaCl, 50 mM Tris, 1 mM EDTA, 0.1% (v/v) Triton X-100, pH 7.4) for 30 min on ice followed by addition of denaturing Ni-NTA lysis buffer (8 M urea, 300 mM NaCl, 14 mM KH_2PO_4, 86 mM Na_2HPO_4, 50 mM imidazole, 1% (v/v) Triton X-100, 0.5% (w/v) CHAPS, 0.2% (w/v) SDS, Complete Protease Inhibitors w/o EDTA, pH 8.5) on ice.

2.2.3.3 Plasmid DNA preparation

For all plasmid preparations bacteria were grown for 16-20 h at 37 °C under vigorous shaking. Plasmids were prepared on two scales using kits, Miniprep (2 ml) and Maxiprep (200 ml). In both cases bacteria were pelleted by centrifugation at 6000g for 5 min at RT. Pellets were then processed according to the manufacturer's instructions for each kit. In each case bacteria were subjected to alkaline lysis to remove genomic DNA and debris in the insoluble fraction. For Minipreps (Thermo Scientific) DNA was bound to a silica stationary phase washed with ethanol containing buffer and eluted with TE buffer (10 mM Tris, 1 mM EDTA, pH 8) under low ionic strength. For Maxiprep (Qiagen), plasmids were separated from RNA and protein by anion exchange chromatography and eluted under high salt conditions. DNA was then precipitated using isopropanol and redissolved in TE buffer. DNA concentration and purity of plasmid preparations was measured by spectrophotometry and identity of prepared plasmids was confirmed by restriction fragment analysis. Only preparation giving the expected fragment pattern and with OD260/280>1.8 and OD 260/230>2 were used for transfections. Plasmid preparations were adjusted to 1 μg/μl in TE buffer and stored at -20 °C until use.

2.2.3.4 DNA restriction digestion and agarose gel electrophoresis

Enzymes and buffers from New England Biolabs (NEB) diluted in ddH_2O were used for all digestions. Analytical digestions were set up in a total volume of 10 μl 1x NEBuffer with 0.5 μg plasmid DNA. Enzymes were used at a ratio of 10 $U_{Enzyme}/\mu g_{DNA}$ in all reactions and if required, BSA was added to a final concentration of 100 μg/ml. Reactions were carried out at 37 °C for 45 min in a thermoblock.

In order to cast 1% (w/v) agarose gels, an appropriate amount of agarose powder was added to Tris-borate-EDTA (TBE, 89 mM Tris, 89 mM boric acid, 2

mM EDTA) buffer and heated in a microwave oven until the solution was clear and homogenous. The flask was cooled down and SERVA DNA Stain Clear G was added to a final concentration of 0.005% (v/v). The gel was cast and allowed to solidify for 1 h at RT and placed in an electrophoresis chamber (Sub-Cell GT Cell, Bio-Rad). Samples were mixed with 6x loading buffer (10 mM Tris-HCl, 0.15% (w/v) Orange G, 60% (v) glycerol, 60 mM EDTA) and loaded onto the gel. Gels were run at a constant voltage of 100 V for 30-50 min. Serva stain intercalates into nucleic acids and its fluorescence emission at 530 nm increases. In this way, separated fragments could be visualized as bands using an UV light box and documented with a CCD camera. 1 kbp linear dsDNA standards were used for size determination of bands.

2.2.3.5 RNA isolation and cDNA synthesis from mouse liver

In order to generate coding DNA sequences for cloning, mRNA from mouse liver was extracted, purified, subjected to reverse transcription (RT) to cDNA. Total RNA from mouse liver was extracted by acidic guanidinium thiocyanate–phenol–chloroform extraction [196], which separates genomic DNA from RNA into an organic and aqueous phase respectively. Proteins are denatured, precipitate and removed efficiently during the procedure. In this manner, pure RNA can be prepared as template for the viral reverse transcriptase enzyme.

All solutions were prepared in DEPC treated ddH$_2$O. Ground liver tissue from C3HeB/FeJ mice (50 mg) was homogenized by mechanical grinding as described for protein extraction from liver in 500 μl denaturing solution (4 M guanidinium thiocyanate, 25 mM sodium citrate, 0.5% (w/v) N-laurosylsarcosine 100 mM 2-mercaptoethanol, pH 7). Homogenates were transferred to 2ml Eppendorf tubes, 50μl 2M sodium acetate (pH 4) and 600 μl phenol:chloroform:isoamylalcohol (125:24:1, pH 4.5) were added followed by vigorously vortexing for 10 s. Samples were then cooled on ice for 15 min and complete phase separation achieved by centrifugation at 20.000g for 10 min at 4 °C. The aqueous upper phase, containing RNA, was transferred to a fresh tube and precipitated by adding 500 μl isopropanol and incubating for 1 h at -20 °C. The RNA pellet was washed twice with 1 ml 75% (v/v) ethanol at RT for 10 min and air dried completely afterwards. RNA pellets were redissolved in 120 μl DEPC treated H$_2$O. Purity and concentration were determined spectrophotometrically using a nanophotometer (Implen). Only preparation with OD260/280>2 and OD260/230>1.8 were used as these were sufficiently free of protein or phenol

(280nm) and guanidinium (230 nm). Integrity of RNA preparation was checked by denaturing agarose gel electrophoresis. Only preparations showing distinct 28S and 18S ribosomal RNA bands were used for cDNA synthesis.

cDNA was synthesized from 5 µg total RNA in a volume of 12 µl using oligo dT primer with the RevertAid First Strand cDNA Synthesis Kit (Thermo Scientific) according to the manufacturer's instructions. Both RNA and cDNA were stored at -80 °C until use.

2.2.3.6 RT-PCR and Gateway cloning of EET enzymes

EET enzymes were cloned into expression vector by a four step procedure using the Gateway cloning system based on recombination of specific DNA sites from bacteriophage λ [197] rather than the classical restriction enzyme DNA ligase based approach. In the first step inserts containing coding sequences were amplified with gene specific primers (gsp) from cDNA by polymerase chain reaction (PCR) [198]. The primer for this first reaction contained partial attB sites which provided the binding sites for the PCR primers in the second step which introduced the full attB sites on the ends of the insert. In the third step, the attB flanked inserts were recombined with the attP sites of the entry vector pDONR201, yielding entry constructs. In the final step insert were transferred from entry constructs to the target expression vectors using recombination of attL and attR sites.

Both PCRs were carried out with a mix of *Taq* and *Pfu* polymerase at a ratio of 10:1 to increase fidelity though the proofreading activity of *Pfu* with a total of 25 cycles for both PCRs to minimize introduction of mutations. Composition of PCR mixtures and the PCR programs are provided in Table 2 and 3, respectively. Gene specific primers for the first PCR are listed in Table 2.1.11.

The first reaction was run for ten cycles using 2µl cDNA mixture with different annealing temperatures: 59 °C for mEphx2a and CYP2C29, 63 °C for CYP2C50a, 57 °C for CYP2C70 and 61 °C for CYP2J5. 10 µl of the first PCR were used as template for the second PCR with attB adapter primers. The second PCR was run for ten cycles with an annealing temperature of 45 °C and then for another five cycles with an annealing temperature of 55 °C.

Final PCR products were separated by agarose gel electrophoresis, bands of the correct size excised with a scalpel and DNA inserts were purified with a gel extraction kit (Thermo Scientific) according to the manufacturer's instructions. Purified insert DNA was quantified using a nanophotometer (Implen).

Material and Methods

For BP recombination 150 ng attB flanked inserts were mixed with 150 ng pDONR201 in a final volume of 8 µl. 2 µl BP clonase II mix (Life Technologies) were added and the mixture was incubated at 25 °C for 1 h. Afterwards enzymes were degraded by adding 1 µl Proteinase K and incubating at 37 °C for 10 min. Five microliter of the recombination reaction were transformed into chemically competent *E.coli* (BL21 Gold) as described in 2.2.3.1.

Component	Stock	Final conc	1 rxn 50 µl
DNA Template	varies	varies	x µl
Taq buffer 10x	10x	1x	5 µl
MgCl$_2$	25 mM	1.5 mM	3 µl
Primer fwd	20 µM	0.5 µM	1.25 µl
Primer rev	20 µM	0.5 µM	1.25 µl
dNTPs	10 mM each	250 µM each	1.25 µl
Taq	5 U/µl	25 mU/µl	0.25 µl
Pfu	2.5 U/µl	2.5 mU/µl	0.05 µl
ddH$_2$O			Ad 50 µl

Table 2. Composition of PCR reactions used for cloning.

Temp	Time	Step	
96 °C	2 min	Initial Denaturation	
96 °C	20 s	Denaturation	
See text	40 s	Annealing	gsp PCR 10 cycles
72 °C	2 min (1.5-2 kbp amplicons)	Extension	attB PCR 20 cycles
72 °C	5 min	Final Extension	

Table 3. PCR programs for Gsp and attB PCR.

Generated entry constructs were first screened by restriction fragment analysis before sequencing the coding sequences of two clones obtained from cDNA from different animals completely by multiple sequencing primers (Annex table A9). By comparing two clones from different animals, mutations introduced by cloning and variations of the canonical sequences (see 2.1.12) in the C3HeB/FeJ mouse strain could be distinguished. In this way, correct entry constructs were obtained for all genes.

In the final step, coding sequences were transferred from pDONR201 vectors to the expression vectors pcDNA3/DEST and pDEST-N-SF-TAP according to the manufacturer's protocol. Final constructs were verified by restriction fragment analysis only and constructs were produced by Maxiprep (2.2.3.3) for transfection.

66

2.2.3.7 Sanger Sequencing of plasmid DNA

Plasmid DNA was sequenced using the four fluorescence ddNTP variant of the Sanger method [199]. Here DNA molecules are synthesized from a single primer bound to the plasmid. The reaction contains ddNTPs that are labeled with a different fluorophore for each nucleotide and terminate DNA strand synthesis once they are incorporated. This generates a population of ssDNA molecules differing in length by one nucleotide increments which carry a color coded label indicating the last nucleotide incorporated. These are separated according to length using capillary electrophoresis. The sequence can be read back from the electropherogram of the four fluorescence channels.

Reactions were set up with 150 ng plasmid and 5 pmol primer in a reaction volume of 10 µl using components of the BigDye3.1 kit. Sequencing product synthesis was carried out in a PCR machine Peqstar thermocycler (Peqlab) using the program provided in Table 4. ssDNA products were precipitated by adding 45 µl 80% (v/v) ethanol and incubating for 15 min in the dark and collected at 6000g for 10 min at RT. After washing the pellets once with 70% (v/v) ethanol they were air-dried and resuspended in 75 µl HPLC grade water. Products were analyzed by the Institute of Experimental Genetics, HMGU. The electropherograms were analyzed using the Vector NTI software.

Step	Duration	Temperature	
Initial Denaturing	2 min	95 °C	
Denaturing	15 s	95 °C	
Annealing	15 s	50 °C	20 Cycles
Extension	4 min	60 °C	
Final Extension	6 min	60 °C	

Table 4. Thermocycler program used for Sanger Sequencing.

2.2.3.8 Routine cell culture of mouse liver cell lines Hepa 1-6 and BNL Cl.2

For routine culture, Hepa 1-6 and BNL Cl.2 were grown in full medium (Dulbecco's modified eagle medium (DMEM), 10% (v/v) Fetal calf serum (FCS), 25 U/ml Penicillin and Streptomycin) in T-75 flasks or T-175 flasks at 37 °C and 5% CO_2 in a cell culture incubator. Cells were routinely passaged at a ratio of 1:6 (Hepa 1-6) and 1:10 (BNL CL.2) every three day corresponding to a density of ~80% at the time of splitting. Passaging included trypsinization and splitting. Cells were trypsinized by removing the medium, washing the cells once with phosphate buffered saline (PBS) and adding 1 ml trypsin/EDTA for a T-75 or 2 ml

for a T-175. Detached cells were suspended in full medium, inactivating trypsin in the process, and either split or counted and seeded (2.2.3.10).

Hepa 1-6 and BNL Cl.2 were obtained from the American Type Culture Collection (ATCC). Initial cultures were expanded and frozen in four cryovials for each cell line in DMEM 20% (v/v) FCS and 7.5% (v/v) DMSO in a liquid nitrogen tank. Active cultures were discarded if they had grown to confluency. Fresh cultures were started from cryostocks, replenishing the used cryostock with excess cells during the first passage of the fresh culture.

2.2.3.9 Isolation and culture of primary mouse hepatocytes

Primary mouse hepatocytes were isolated by a combination of collagenase and EGTA perfusion [200]. Extracellular matrix is degraded by the collagenase treatment while cell adhesion molecules like cadherins are deprived of their essential divalent cation cofactors through the strong chelator EGTA. Prior to perfusion, 25 weeks old male C3HeB/FeJ mice were terminally anesthetized by isoflurane insufflation through a nose cone.

All buffers were prepared freshly on the day of isolation from sterile frozen stock solutions. The mentioned amino acid mix in the buffer compositions consisted of the twenty proteinogenic amino acids as well as L-citrulline and L-ornithine.

Perfusion was performed in the German Mouse Clinic under non-sterile conditions. The peritoneal cavity was carefully opened, exposing liver portal vein and lower vena cava. The portal vein was carefully perforated using a 25G catheter. Perfusion was then started with EGTA solution (31.5 mM glucose, 105 mM NaCl, 2.4 mM KCl, 0.95 mM KH_2PO_4, 25.5 mM HEPES, 25.5 mM amino acid mix, 0.5 mM EGTA, pH 8.5) at 8 ml/min using a syringe pump. The vena cava inferior was cut when the liver started to swell due to perfusion to release pressure. While EGTA solution perfusion was continued for another 5min, collagenase type IV (125 CD/mg) was added freshly to collagenase buffer (31.5 mM glucose, 105 mM NaCl, 2.4 mM KCl, 0.95 mM KH_2PO_4, 25.5 mM HEPES, 12.5 mM amino acid mix, 5.3 mM $CaCl_2$, 46 CD/ml Collagenase IV, pH 8.5). Perfusion was then switched from EGTA to collagenase solution and continued for another 8 min. The liver was moisturized with suspension buffer (31.5 mM glucose, 105 mM NaCl, 2.4 mM KCl, 0.95 mM KH_2PO_4, 25.5 mM HEPES, 15.5 mM amino acid mix, 1 mM $CaCl_2$, 0.4 mM $MgSO_4$, 0.2% BSA, pH 7.6) in between. Subsequently, the liver was excised and transferred to a 50 ml Falcon tube in 20 ml suspension

buffer and transferred to a laminar flow hood. All following steps were performed under sterile conditions.

The liver capsule was opened and cells filtered through a 100µm cell strainer by pouring of suspension buffer to a final filtrate volume of 40 ml. Cells were pelleted at 50g for 2 min at RT. The supernatant was discarded and the cell pellet washed with 30 ml suspension buffer. After pelleting the cells again at 50g for 5 min at RT, they were resuspended in 20 ml adhesion medium (Williams E Medium, 10% FCS, 25 U/ml Penicillin and Streptomycin, 100 nM dexamethasone). Cell viability was assessed by trypan blue exclusion. Only preparations with vitality>80% were used. Primary hepatocytes were then counted and seeded onto collagen coated six well plates.

2.2.3.10 Collagen coating and seeding of eukaryotic cells

Primary hepatocytes and hepatocyte cell lines were seeded on collagen I coated six-well plates for insulin stimulation and transfection experiments. Each well was coated with 1 ml 0.005% (w/v) type I collagen from rat tail in 20 mM acetic acid pH 4 for 2-4 h at RT. Wells were then washed twice with 2 ml PBS, all liquid was removed and plates were air-dried completely under a laminar flow hood. Dried plates were stored at 4 °C until use.

For seeding, cell numbers in suspensions were counted using a Neubauer chamber with 0.1 mm depth under an inverted microscope. The number of cells in four counting fields was averaged and multiplied by 10.000 to yield cells/ml. If concentrations exceeded 10^6 cells/ml, suspensions were diluted four-fold and counted again. Finally, cells were diluted in full medium (DMEM based for cell lines or Williams E medium based for primary hepatocytes) and the required number of cells for the respective application was seeded in 2 ml cell suspension per well. Cells were allowed to adhere overnight at 37 °C, 5% CO_2.

2.2.3.11 Transfection of Hepa 1-6

Hepa 1-6 cells were transfected with Lipofektamine 2000 based on liposomes formed by DNA and positively charged lipids. In pilot experiments, the DNA/lipid ratio and the total amount of liposomes per well were optimized using the eGFP reporter construct pCMV-GFP. Hepa cells were seeded to give a cell density of 80-90% on the day of transfection as they stopped growing afterwards.

Hepa 1-6 were seeded at a density of 160.000 cells per well 24 h before transfection. On the day of transfection 3 µg DNA were diluted in 300 µl DMEM. 10.5 µl Lipofektamine 2000 were diluted in another 300 µl DMEM and mixed with

the plasmid containing medium. The mix was vortexed for 10 s and incubated at RT for 10 min. Subsequently, the full medium was removed from the cells and the liposome mix added. Cells were incubated at 37 °C, 5% CO_2 for four hours, then the liposome mix was removed, cells were washed with 2 ml PBS and 2 ml full medium were added. Cells were incubated at 37 °C, 5% CO_2 for 1h before the medium was changed again.

Cells were used for experiments 24 h or 48 h after the start of transfection. Transfection efficiency was assessed with the reporter construct pCMV-GFP expressing eGFP driven by the strong cytomegalovirus (CMV) immediate early promotor using an inverted epifluorescence microscope (DMIRE2, Leica) for life cell imaging. eGFP fluorescence was excited with a mercury arc lamp combined with a FITC filter cube (Excitation: BP490/15, Emission: BP525/20). Phase contrast and fluorescence images were documented with a 10x objective and a CCD camera connected to the microscope.

2.2.3.12 Insulin stimulation with or without EETs

Cells were subjected to insulin stimulation in a six well plate format. Lyophilized recombinant human insulin produced in *S. cerevisiae* was used for all experiments. Assuming a specific activity of 24 IU/mg for human insulin, 100 U/ml stock solution aliquots in sterile PBS were generated and stored at -20 °C. Aliquots were only thawed once on the day of the experiment and discarded afterwards, to ensure constant biological activity of preparation.

For insulin stimulation experiments, cells were seeded in full medium as described in 2.2.3.10 to yield a density of approximately 70-80% after serum starvation. 150.000 Hepa 1-6, 140.000 BNL Cl.2 cells or 200.000 primary hepatocytes were seeded per well 48 h before the start of stimulation. Cells were allowed to adhere and proliferate overnight.

Cells were starved overnight before stimulation to lower the activity of signaling cascades activated by components of serum and synchronize cells in a non-proliferative state. The next day, serum starvation was initiated by removing the full medium, washing the cells twice with 2 ml PBS and adding 2 ml starvation medium. DMEM without FCS was used for cell lines and Williams E medium without FCS was used for primary hepatocytes (in both cases supplemented with 25 U/ml Penicillin and Streptomycin).

The next morning, solutions for insulin stimulation were prepared. An appropriate volume of fresh starvation medium was warmed to 37 °C. First, phosphatase

inhibitors were added at 1:200 dilution (Inhibitor Mix 2 & 3, Sigma). Then the solution was split into Falcon tubes for control and different insulin concentrations. Next insulin was added to the desired final concentrations (1 µM, 100 nM or 1.5 nM). For EET costimulations, the solutions with different insulin concentrations or no insulin were split again into fresh falcon tubes and either DMSO or the EET stock solution in DMSO was added to give final EET concentrations of 4 µM for all four isomers. In this manner, differences in insulin or phosphatase concentration were highly unlikely to influence effects elicited by EETs.

The medium was removed from the cells, solutions for stimulation were added and plates were incubated at 37 °C, 5% CO_2 for 20, 40 or 60 min. At the time of harvesting, plates were placed on ice, the medium was removed and cells were lysed as described in 2.2.1.4.

2.2.4 Lipid and carbohydrate biochemistry

2.2.4.1 Preparation of EET mixtures

Synthetic racemic EETs were purchased from Cayman Chemical. The 5(6), 8(9), 11(12) and 14(15) isomers were obtained as 0.1 µg/µl solutions in ethanol. For cell culture experiments, ethanol had to be exchanged for the better biocompatible solvent DMSO. EET ethanol stock solutions (312 µM each) were mixed to produce 2 ml 78 µM stock solution of all four EETs. Ethanol was evaporated by vacuum centrifugation for 2 h at 25 °C until only a small rest of solvent was present. This was evaporated by a stream of dry liquid nitrogen to complete dryness and 2 ml DMSO were immediately added to redissolve EETs. The success of this procedure was evaluated by relative quantification of EET isomers (2.2.4.3) in an aliquot of the ethanol stock solution versus DMSO stock solution. All EET containing solutions were stored at -80 °C until use.

2.2.4.2 Isolation of lipids from supernatants and cell lysates

Lipid extracts of cells were generated by scraping cells on six well plates in 100µl reducing lysis buffer (50 mM Tris, 10% (v/v) methanol, 1 mM TECP, 0.01% (w/v) BHT 0.1% SDS, pH 8). Lysates were incubated on ice for 10 min. For accurate quantification, deuterated isotope labeled internal standards were added before lipid extraction. 2 pmol of d11-14(15)-EET and d11-14(15)-DHET were added. 2 µl of lysate were used for protein quantification to normalize lipid species to total protein content of samples.

Lipids were separated from proteins and hydrophilic compounds by methanol/chloroform extraction [182]. Briefly, 400 µl methanol and 100 µl chloroform were added to the lysate and mixed. Phase separation was initiated by the addition of 300µl ddH$_2$O and led to the formation of an upper aqueous and a lower organic phase, with denatured proteins precipitated in between. Samples were centrifuged at 10.000g and RT for 1 min. The upper aqueous phase was discarded and another 300 µl methanol added which led to the protein pellet sinking to the bottom of the tube. After centrifuging at 10.000g and RT for 1 min the organic phase could be collected into a fresh tube and was dried completely by vacuum centrifugation. Dried samples were reconstituted in 50 µl 65% ACN and subjected to LC-MS analysis (2.2.4.3).

2.2.4.3 Quantification of EETs using LC-SRM

EETs and arachidonic acid were quantified by a custom LC-SRM method developed by Tobias Gaisbauer (genome analysis center (GAC), HMGU). Lipids were separated by reverse phase chromatography on a Shimdazu Prominence HPLC equipped with a C18 analytical column (2.1 × 250 mm, Hypersil C18, 5 µm, 130 Å; Thermo Scientific) using a binary multistep gradient with eluents A (H$_2$O, 0.1% (v/v) FA) and B (ACN, 0.1% (v/v) FA). The HPLC was coupled online to a Q-Trap 4000 mass spectrometer through a Turbo V ion source operated in negative ion mode. Lipids were detected by the MS in SRM mode. Specifics of the HPLC and MS methods are omitted in this thesis to allow for possible publication of the method later.

For quantification of lipids, result files were analyzed using Multiquant 2.0 as described for peptides under 2.2.2.7, but with the following modification: Absolute quantification was performed by comparison of all EET and DHET isomers signals to d11-14(15)-EET and d11-14(15)-DHET, respectively.

2.2.4.4 Glucose oxidase assay

Free glucose monosaccarides were measured using the enzymatic glucose oxidase assay [201] in 96 well format. This assay is highly specific for D(+)-glucose through the use of the enzyme glucose oxidase, which oxidizes D(+)glucose in the presence of oxygen to D-gluconic acid. Hydrogen peroxide formed during this reaction in turn oxidizes the dye o-dianisidine with horseradish peroxidase as catalyst. Oxidized o-dianisidine color development is maximized by lowering the pH drastically through addition of concentrated sulphuric acid which also stops the enzymatic reaction.

Standard curves of a D(+)-glucose with final glucose concentrations of 0, 0.1, 0.5, 1, 2 and 6 ng/µl in duplicate wells were used for quantification throughout.

A glucose oxidase/peroxidase/o-dianisidine mix from Sigma was used. The stock solution of the assay mix was stored in aliquots at -20 °C and diluted 1:4 with ddH$_2$O on the day of use. Samples were measured in triplicate wells. 5-30 µl sample were mixed with 115 µl diluted assaymix for 30 min at 37 °C. The assay was completed by the addition of 80 µl 12 N H$_2$SO$_4$. Absorption of the plate was measure at 540 nm with a Synergy HT plate reader (Biotek). Linear-regression curves were accepted if r^2 was 0.98 or better. Sample measurements were accepted if the coefficient of variation (CV) of triplicates was below 20%. Initial D(+)-glucose concentrations of samples were calculated using Excel 2010.

2.2.4.5 Quantification of intracellular glycogen

Insulin stimulated glycogen synthesis was measured as the accumulation of intracellular glycogen in cells through the amyloglucosidase assay [202]. For this assay, cellular lysates are split in two samples. One is treated with the enzyme amyloglucosidase, which hydrolyzes glycogen to glucose monomers. The glucose monomer concentration is then measured in both samples using the glucose oxidase assay, yielding free intracellular glucose and total intracellular glucose (free+glycogen). Glycogen amounts can be derived by subtraction.

For the synthesis assay, 180.000 Hepa 1-6 cells/well were seeded onto collagen I coated six-well plates. The next day, cells were serum starved overnight as described for insulin stimulations (2.2.3.12). The next day, 2 ml starvation medium with or without insulin in different concentrations were added to wells. Cells were allowed to synthesize glycogen for 5 h at 37 °C, 5% CO$_2$. After synthesis, cells were washed three times with pre-warmed PBS (37 °C) and lysed by scraping into 50 µl 1 M KOH. Lysates were heated to 70 °C for 20 min to complete lysis and reduce free glucose levels. Protein concentration in lysates was measured by BCA protein assay and samples were split in two 25µl parts for the glycogen assay.

Both samples were neutralized by adding 3 µl acetic acid. Then assay buffer (240 mM sodium acetate, pH 5), with or without amyloglucosidase at 5 mg/ml (350 U/ml) was added. Both samples were incubated at 40 °C for 90 min. Afterwards, D(+)-glucose was determined in 3 x 30 µl for each sample using the glucose oxidase assay (2.2.4.4). Intracellular glycogen content was calculated as (total glucose – free glucose)/protein concentration.

3. Results

3.1 Development of workflows for proteomic profiling of mouse liver

In comparison to earlier and more established comprehensive technologies like genomics and transcriptomics the younger field of proteomics has not yet reached the stage where standardized workflows for processing and quantification for different types of sample are readily available. Rather, basic strategies for proteomic analysis have to be optimized for specific sample types and experimental designs to produce data sets that are suited to answer the main questions of a project.

3.1.1 Comparison of sample preparation for discovery proteomics

Here we set up a workflow for protein expression profiling of liver tissue in T2D mouse models. Important considerations were therefore the depth of proteome coverage of the highly complex liver proteome and the quantitative performance of the approach in terms of accuracy and precision. As the study would encompass a time course of treatment versus control groups with 7-10 mice for each time point and group, another important aspect was the consistency of the datasets, in the sense that overlap between proteins identified and quantified in individual biological samples should be as large as possible. Finally the effort in terms of MS-machine time had to be considered given that in total 70 liver samples had to be processed and measured.

The final step of all optimization experiments was tryptic digestion and bottom-up LC-MS/MS analysis on Orbitrap systems, as this is the state of the art technique of quantitative proteomics [134]. Three hour HPLC gradients and TOP10 MS methods were used if not otherwise indicated. As identification criteria throughout the thesis we have used the search engine and software independent parameter peptide false discovery rate (PepFDR) which was always set to 2% for peptides. Proteins were considered identified if at least two peptides at 2% PepFDR were found.

We started with a simple mechanical extraction procedure and in-solution digestions of liver proteins. This analysis yielded a very low number of 450 proteins (Fig. 11a) identified. In light of the total depth of the liver proteome

(>6700 proteins [203, 204]) this is well below 10% of all proteins. However, this finding is not unexpected as high abundance and/or large proteins produce many abundant peptides upon digestion which can mask the main parts of a proteome. In order to alleviate this problem we implemented two optimized biochemical workflows previously used successfully for tissue proteomics – 1D SDS-PAGE fractionation combined with isotopic labeling through the ICPL method [205] and membrane protein enrichment in combination with label-free quantification [206]. For the SDS-PAGE/ICPL approach, lysine residues of all proteins are conjugated with nicotinic acid carrying different heavy isotope labels immediately after extraction. This conversion is quantitative [157] and allows quantification based on the heavy/light peptide rations within runs after mixing. According to the principle of isotopic dilution, biochemical fractionation in the form of 1D-SDS-PAGE can be used to increase proteome coverage without affecting quantification results afterwards. We tested gel fractionation with or without ICPL labeling and found that irrespective of labeling we could increase the number of identified proteins more than two-fold (Fig. 11a).

The second workflow made use of the enrichment of membrane proteins. This class of proteins is of low abundance and unfavorable solubility in aqueous buffers and therefore underrepresented in proteomics datasets [207]. The underlying idea for its application to liver tissue was depletion of highly abundant soluble proteins like carbamoyl phosphate synthetase 1, fatty acid synthase or liver synthesized plasma proteins from protein extracts, while at the same time enriching transmembrane and membrane associated proteins. We adapted an enrichment protocol [174, 206], in which the tissue was homogenized by mechanical grinding in high salt buffer. After removal of debris by low speed centrifugation, membrane enriched fractions were separated from soluble proteins by ultracentrifugation. Comparison of the protein compositions of the soluble and membrane enriched fractions by SDS-PAGE and coomassie staining (Fig. 11c) showed distinctly different patterns. Some proteins were enriched by the procedure while others were depleted. The mechanism of this enrichment technique is most likely due to the spontaneous formation of pelletable membrane vesicles from mechanically homogenized liver tissue in the absence of detergents [208].

We found that the membrane enrichment could increase the number of identified proteins only slightly (Fig. 11a). However, when we compared representation of integral membrane proteins in all samples through prediction of transmembrane

Results
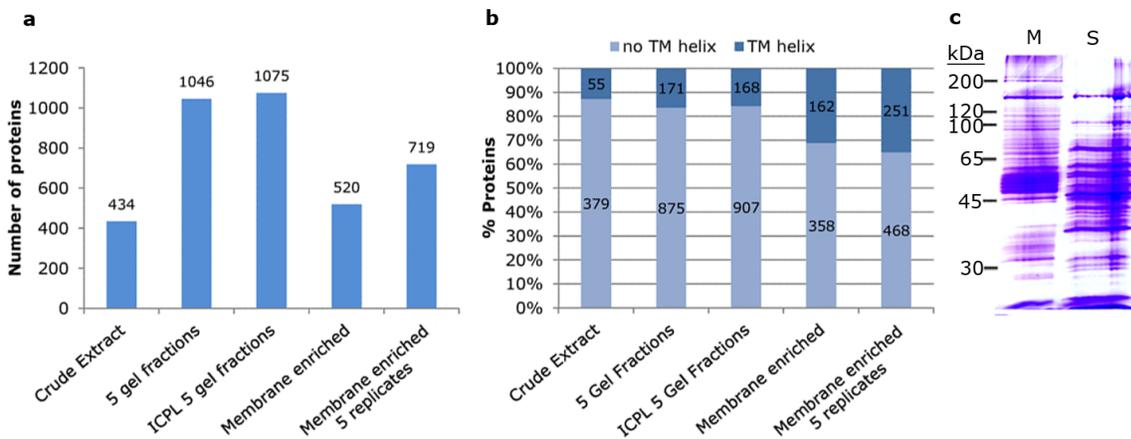
Figure 11. Gel fractionation and membrane protein enrichment increase proteome coverage for mouse liver tissue.
(**a, b**) 20µg liver protein from crude extracts were directly digested in solution (soluble direct). 100µg protein with or without ICPL label were separated on 12% SDS-PAGE gels, cut into 5 fractions and digested in gel. For membrane enriched samples proteins corresponding to 50mg liver tissue were digested after enrichment in solution. (**a**) Proteins were identified using the Mascot/Percolator workflow implemented in Proteome Discoverer 1.3. Identification criteria were PepFDR 2%, and 2 peptides/protein. (**b**) Number of TM helices for proteins from (a) was estimated using the tool Phobius. (**c**) Soluble (S) and membrane enriched (M) fraction proteins from 50mg liver tissue were separated by SDS-PAGE on a 10% gel and stained with coomassie. Soluble fractions of all extraction steps were pooled and purified by dialysis and precipitated using acetone.

helices using Phobius [209] we found that the proportion of integral membrane proteins could be increased from 12-16% (soluble, gel fractionated or ICPL-gel fractionated samples) to more than 30% in membrane enriched samples (Fig. 11b). In this regard, it is interesting to note that approximately 30% of all ORFs of mammalian genomes are predicted to encode transmembrane proteins [210]. Therefore we consider soluble liver extracts and ICPL samples biased against membrane proteins while membrane enriched fractions are slightly biased in favor of membrane proteins. However, they do not represent highly purified membrane protein samples.

Finally, we evaluated the effect of processing of membrane enriched samples with the label-free software (Progenesis LC-MS). During processing, MS/MS of single runs are merged (see below) and consequently we found a sizable increase in protein identification with five merged membrane protein enriched LC-MS/MS runs (Fig.11a) to 719 proteins while conserving the proportion of transmembrane proteins (Fig.11b).

Based on the high number of MS/MS and shift of the TOP n cycle distribution to the maximum of 10 MS/MS per cycle we found that gel fractionated as well as membrane enriched samples were consistently undersampled (data not shown). This strongly implies that all samples were still too complex for the LC-MS/MS system to identify all proteins contained in each sample. Therefore, further fractionation or higher numbers of biological replicates would lead to higher

proteome coverage. However, we decided not to pursue an extensive fractionation strategy in favor of being able to analyze more biological replicates later on.

3.1.2 Label-free and ICPL quantification strategies have good accuracy and reproducibility

Next, we compared both approaches in terms of their performance for quantification. In this regard, the two characteristic analytical parameters accuracy and precision were evaluated. Accuracy refers to how much the measured differ from theoretical values. To test and compare this we used the protein ratio between technical replicates of liver samples. This has the advantage that the ratio of all quantified proteins should ideally be 1. Label-free quantification should inherently be less accurate than the ICPL isotopic labeling based quantification [155]. However, label-free quantification is expected to be more accurate when increasing numbers of replicates are measured because random fluctuations in the determination of peptide peak areas are averaged out.

Therefore we compared the distribution of protein ratios by ICPL quantification (Fig.12 lower right panel, green) to those obtained by measuring increasing numbers of technical replicates for label-free quantification (Fig. 12, blue). To conserve symmetry in ratio distributions ratios were log2 transformed. We found that the standard deviation (SD) of the log2 protein distribution for label-free improves from 0.68 steadily to 0.34 as more replicates are included in the quantification. At 5 versus 5 replicates label-free performs almost as well as ICPL which is still more accurate with an SD of 0.28 (Fig. 12).

Nevertheless, it should be pointed out that averaging of replicates for label-free does not reflect the situation for the actual mouse study where every replicate will be measured once. Rather, it goes to show that the average fold change (FC) for every protein in the mouse groups can be determined with good accuracy using both approaches if comparisons are made between at least 5 versus 5 mice.

Next, we determined precision by calculating the coefficient of variation (CV) for each protein using four technical replicates for both techniques. For this experiment each replicates was subjected to the whole process of sample preparation. Therefore the variability assessed is that of the whole proteomic

Results
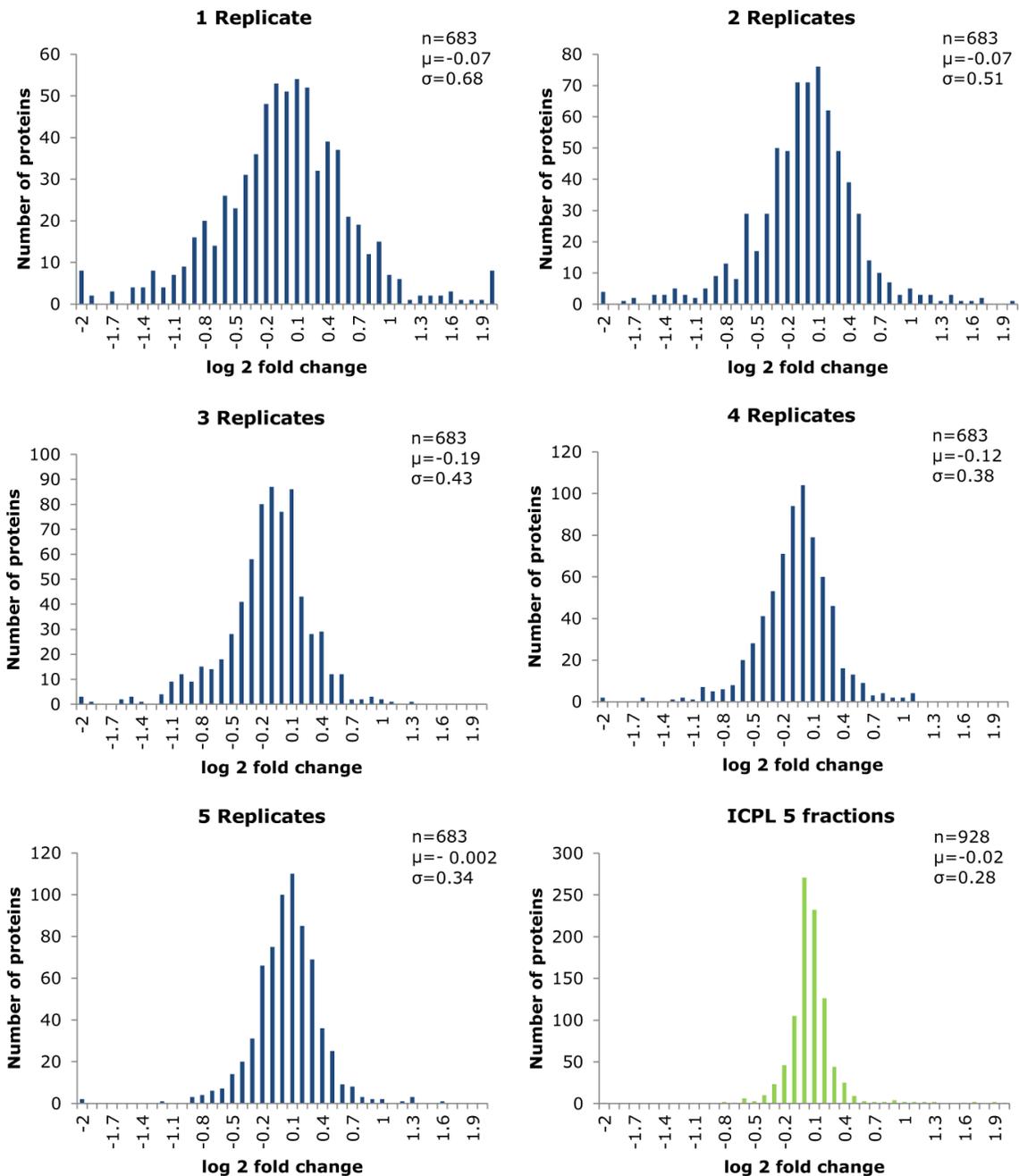
Figure 12. Label-free quantification and ICPL can have comparable accuracy.
Ten technical replicate membrane enriched samples (50mg liver each) were prepared and digested in solution. Samples were run as a single batch on the LC-MS system. Protein MS1 intensity was determined with Progenesis LC-MS. Ratios for each protein were calculated by dividing the average intensity of two randomly assigned groups of samples of the size indicated above each histogram. For ICPL, a mix containing 50μg light and heavy labeled proteins each were fractionated by SDS-PAGE, cut into five fractions and digested. Protein ratios were determined using Proteome Discoverer. All ratios were log 2 transformed and histograms with the indicated mean and SD were calculated.

workflow from sample preparation to calculations by the quantification software. We found average CVs of 12% for ICPL and 20% for label-free quantification. Hence both approaches performed well in terms of precision for discovery proteomics techniques with ICPL being more precise. In addition we noted no

correlation between protein MS1 intensity and CV for either technique (Fig. 13). Hence, no MS1 intensity threshold was used for further experiments. Additionally, we note that although the four replicates for ICPL individually had more than 900 proteins quantified, the overlap of proteins quantified in all four replicates was only 641. Most probably, this stems from the somewhat random nature of LC-MS/MS when undersampling occurs due to too high complexity of individual runs as is the case for mouse liver.
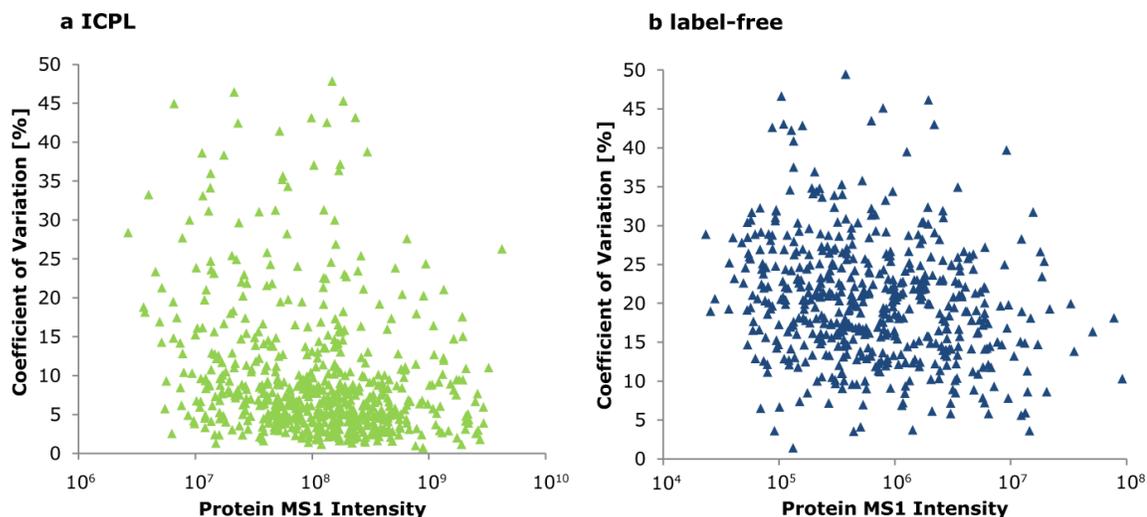
Figure 13. ICPL offers better precision than label-free quantification.
Heavy to light ratios for four technical replicates of gel fractionated ICPL samples (**a**) and protein MS1 intensities for four technical replicates of membrane enriched samples (**b**) were determined. CV values were calculated based on heavy to light ratios for ICPL and protein MS1 intensities for label-free and plotted versus average MS1 protein intensity. Only proteins quantified in all replicates were used for ICPL. Therefore, the number of proteins was 641 for ICPL and 523 for label-free.

3.1.3 Consistency of datasets increases for label-free but decreases for ICPL with increasing numbers of replicates

To conclude our evaluation of discovery proteomics strategies we will illustrate the phenomenon of differing dataset consistency between isotopic labeling and label-free further using the example of datasets from larger scale experiments with dozens of mice, whose background and outcome are not subject of this thesis. The first study focused on the effect of drug treatment in the T2D db/db mouse model (Study 1, Mouse200, Markus Scheerer, IEG). We used membrane enrichment and label-free quantification directly for 50 mice divided into 5 treatment groups (Fig. 14a). The second study concerned the effect of high fat diet in two BL6 substrains, the N and J substrains (Study 2, MiB, Melanie Kahle, IEG). Here a total of 30 mice were included and we used ICPL and gel fractionation. For the second study, a particular concern was the problem of overlap between datasets. In order to maximize this overlap we modified the

Results

labeling design. Four different labels were used (quadruplex ICPL) and the light label (ICPL 0) was used for a global internal standard (GIST) composed of an equal mixture of all 30 samples. Individual mice were labeled with ICPL label with three different isotopic shifts (ICPL 4, 6 and 10). In this manner, ten samples with GIST and three differently labeled mice were generated and subjected to fractionation on a single gel (midi gel) (Fig 14b). The advantage of this modification was that proteins in all gel lanes and biological samples have the same reference proteome (GIST) and that each successful MS/MS identification of a peptide from one gel lane confers identification to three biological samples (Fig 14c). This concept is similar to the pooling of MS/MS based identification in label-free quantification. These two studies were a good opportunity to compare ICPL and label-free as both entailed the same effort in terms of machine time with 50 LC-MS/MS runs each.

Considering all quantified proteins contained in the resulting datasets, ICPL clearly yielded better results with 1496 proteins quantified while the label-free approach led to quantification of 1077 proteins (Fig 14d). In addition, we found a constantly high number of quantifications for each gel lane (840+-50, Fig. 14d). Moreover, the quadruplex design worked as expected, since over 95% of proteins were quantified in all four channels (data not shown). However, on closer examination of datasets, we found a fundamental flaw for the ICPL strategy.

Even with the GIST/quadruplex modification, we found that only a minor fraction of proteins (435, 29%) was quantified in all 30 mice (Fig. 14f).

Most quantified proteins had missing values in the sense that they were not identified in some mice. These missing values were randomly distributed over the dataset, reflecting the somewhat random nature of automatic precursor selection in undersampled LC-MS/MS runs. Moreover, the number of missing values for each protein was variable and led to the heterogeneous distibution of number of mice each protein was quantified in shown in Fig 14f. A significant portion of proteins was even quantified only in one gel lane (321, 21%). Thanks to the quadruplex design this led to quantification in three mice, but these proteins were still worthless for statistical analysis.

In stark contrast, the label-free study led to the generation of a very consistent dataset with more than 920 proteins (85%) quantified in all 50 mice. Another 5% of all proteins were quantified with one missing value and the residual 9% of

proteins were quantified with up to 9 missing values. In other words they were still quantified in more than 40 mice.
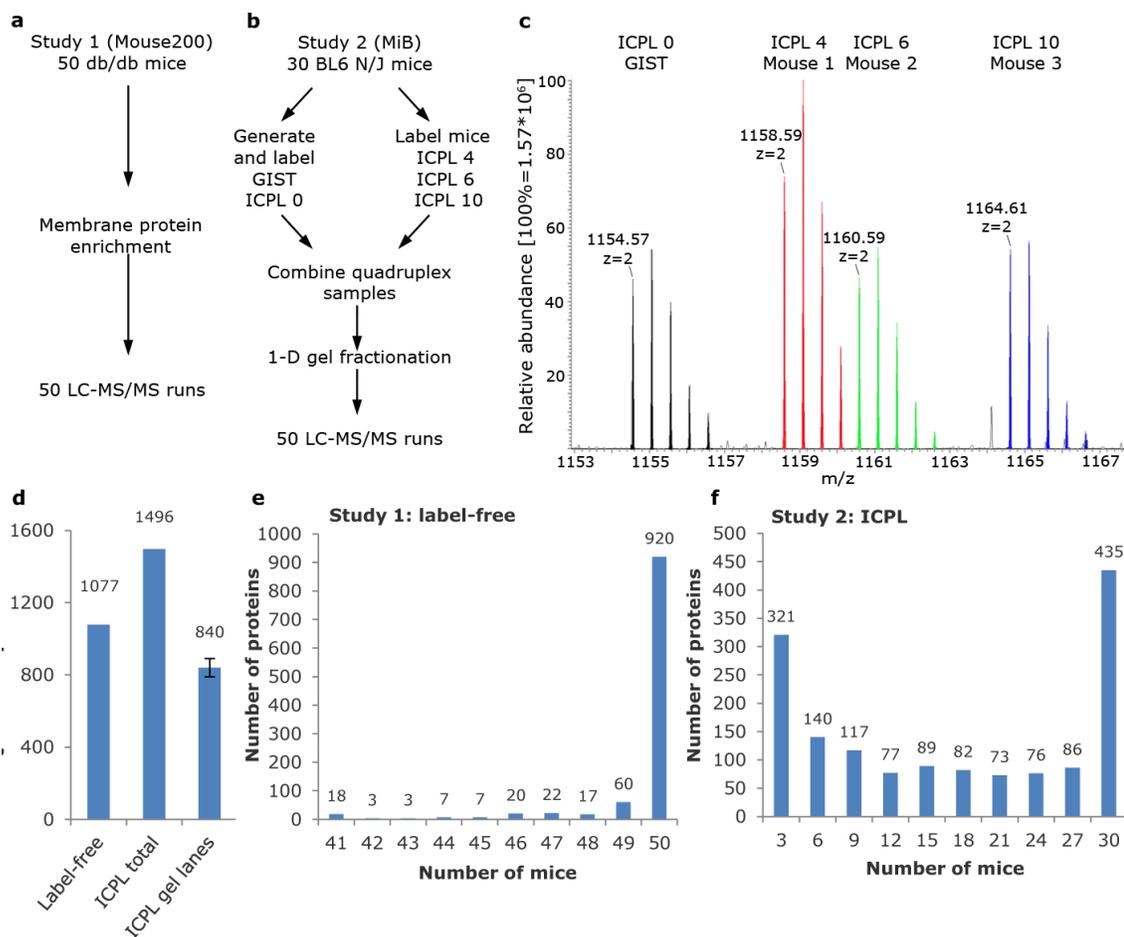
Figure 14. Label-free quantification generates more consistent datasets than ICPL.
(**a, b**) Proteomics workflows for the label-free Mouse200 (**a**) and quadruplex ICPL MiB (**b**) studies. (**c**) MS1 spectrum example of quadruplex ICPL peptide quantification. The GIST was labeled with ICPL 0 and the peptides from three mice were labeled with either ICPL 4, 6 or 10 and can thus be quantified relative to the GIST. (**d**) Cumulative number of protein quantification for both studies. The last column shows the mean and SD of quantifications for the ten ICPL gel lanes. (**e**) Histogram of the number of mice, individual proteins were quantified in for the Mouse200 study. An MS1 intensity threshold of $2*10^4$ was used. Note that the maximum number of mice is 50. (**f**) Corresponding histogram for the ICPL study. Here the maximum number of mice is 30 and increments of 3 mice were chosen due to quadruplex design.

These results may be confounded by the fact that the label-free software assigns some background MS1 intensity to peptides that are actually not detected in a sample. In order to avoid this we used an intensity cutoff of $2*10^4$ for protein MS1 intensity as these were the lowest values detected in the experiment shown in Fig. 13 when evaluating whether a particular protein was actually detected in a particular mouse.

In summary, the label-free study led to the quantification of more proteins in more mice at the same effort in terms of LC-MS/MS analyses. These experiments show that label-free datasets are improved with increasing numbers of biological

replicates while this behavior is the opposite for isotopic labeling datasets. In the example at hand, the label-free approach allowed quantification of 920 proteins in 50 mice. Even if we allow 50% missing values for ICPL (detected in at least 15 mice), which is a very untenable situation for the statistical analysis, we would still only be able to quantify 841 proteins in 30 mice.

However, it is important to point out that this finding is not a specific shortcoming of ICPL. Rather, it is a consequence of the whole concept of isotopic labeling shotgun proteomics (see Discussion).

Note that while all other presented datasets in this thesis were generated with LC-MS system 1 (split standard HPLC) these two datasets were run on LC-MS system 2 (nano UPLC) which allowed label-free batches up to 50 samples due to improved HPLC stability. Therefore, the 68 samples from the saff-diet study had to be split into five batches of 12-16 samples. Nonetheless, the outcome of the comparison of these two studies illustrates an important point concerning consistency of datasets which was recognized before and is also pertinent to the smaller batch size for the saff-diet study presented in chapter 3.3.

Based on the results from the development phase we decided to employ only the membrane enrichment label-free strategy for the C3H saff-diet study. It features good accuracy and precision for a discovery approach, produces highly consistent datasets and facilitates access to the highly interesting group of membrane proteins. As the main phenotype in the C3H safflower oil study is that of insulin resistance and thus a signaling defect we considered this a particular advantage for the project.

3.1.4 Development of a multiplex SRM assay for a panel of T2D candidate proteins

Using discovery proteomics we are able to perform non-targeted quantitative analysis for approximately 1000 proteins in mouse liver in dozens of biological replicates necessary for statistical evaluation in the T2D mouse model under study. Higher proteome coverage would require more high-end instrumentation, which was not available, or extensive prefractionation which comes at the cost of reduced throughput and increased technical variability.

In order to increase the chance of finding protein expression changes that could be correlated with hepatic insulin resistance and lead to the discovery of pathways involved in insulin signaling, we complemented the discovery part of our project with a hypothesis driven SRM based targeted proteomics part. We

selected proteins already implicated in T2D by other sources of evidence, mainly human GWAS studies and literature research. However, we did not select obvious choices like SREBP-1c with already established roles in acquired hepatic insulin resistance [72] as the purpose of the study was to find new pathways associated with hepatic insulin resistance.

Accession	Gene	Protein Name	PTPs	Abundance	Reference
Q8K010	Oplah	5-oxoprolinase	3	1.1	[211]
P56528	Cd38	CD38 ADP Phosporibosyltransferase	3	2.1	[212]
Q921G7	Etfdh	Electron transfer flavoprotein DH	4	12	[213]
Q9JLJ4	Elovl2	Elongation of very long fatty acids 2	1	3.7	[213]
Q920L1	Fads1	Fatty acid desaturase 1	3	3	[214]
P52792	Gck	Glucokinase	4	3.4	[215]
Q91X44	Gckr	Glucokinase regulatory protein	4	2.7	[214, 216]
Q571F8	Gls2	Glutaminase liver	4	3.7	[217]
P41216	Acsl1	Long chain fatty acid CoA ligase 1	4	30	[213]
P51174	Acadl	Long-chain specific acyl-CoA DH	4	31.4	[218]
P45952	Acadm	Medium-chain specific acyl-CoA DH	5	16.7	[214]
P21981	Tgm2	Transglutaminase-2	5	9.7	[219]
Q07417	Acads	Short-chain specific acyl-CoA DH	4	36.7	[213]
P14246	Slc2a2	Solute carrier glucose GLUT2	4	19.6	[213]
Q64442	Sord	Sorbitol dehydrogenase	4	103	[220]
P25688	Uox	Uricase	4	230.7	[221]
			Σ 60		

Table 5. Targeted proteomics SRM multiplex assay.
Proteins targeted in the final version of the SRM assay are listed along with the number of PTPs measured during each run. In addition, the abundance of each protein in fmol/µg total protein determined for one exemplary C3H mouse liver using the standard Q-peptides (see below) is indicated.

The development of SRM assays involves the selection of unique signature peptides called PTPs from target proteins. Suitability of peptides to serve as PTPs can be predicted based on their primary sequence. We used criteria established in the literature [169] to screen for PTPs from an initial list of 25 proteins of interest.

We used gel fractionated pools of mouse liver samples containing the endogenous proteins as source material for the development of our assay. Candidate peptides were selected from these shotgun proteomics datasets preferentially. If no MS/MS were contained in these datasets we queried the online peptide MS/MS database PeptideAtlas [222] for candidates. Screening of

Results

PTPs and MS/MS based verification is described in detail in Material and Methods (2.2.2.6). We were successful in establishing SRM assays for 16 out of 25 candidate proteins. The main reason assay development failed for these nine proteins is most likely the sensitivity of our LC-MS setup. This explanation is based on the observation that not a single peptide for these proteins could be measured in SRM mode, although the target proteins should be expressed in liver. Proteins contained in the final assay, the number of PTPs targeted for quantification and the literature source implicating the protein in the context of T2D are given in Table 5. All peptides and transitions tested and which are used in the final assay are enclosed in annex tables A1 and A2.
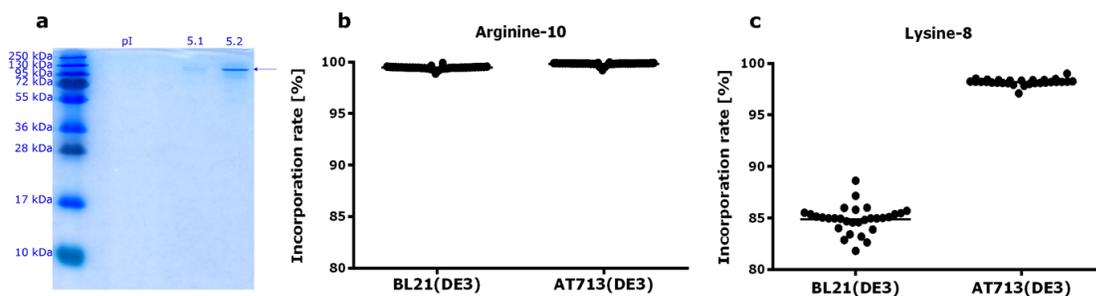
Figure 15. High purity and labeling efficiency for the QconCAT.
(**a**) Heavy labeled QconCAT was expressed in AT713(DE3) and purified by a combination of IMAC and OGE. 0.12% of final OGE fractions containing to the QconCAT (pI 5.1-5.2) were separated by SDS-PAGE and stained with colloidal coomassie. Arrow indicates the full length QconCAT (116 kDa). (**b, c**) QconCATs expressed in AT713(DE3) and BL21(DE3) were digested and analyzed with the final SRM method. Incorporation rates for each peptide were calculated (L/H ratio+1)$^{-1}$ and plotted separately for lysine-8 and arginine-10 in both *E.coli* strains. Reprinted (adapted) with permission from [179]. Copyright (2012) American Chemical Society.

After an extensive process of trial and error, our final SRM assay included 60 out of 232 tested peptides and 359 out of 1494 tested transitions. Quantification and verification of specificity for SRM assays was conducted using isotopically labeled standard peptides. Instead of the expensive AQUA approach we employed the more cost-effective QconCAT [180] approach to synthesize heavy isotope labeled standard peptides. Here an artificial protein containing all the desired PTPs concatenated to each other (QconCAT) is generated through gene synthesis and expressed recombinantly in medium containing the heavy amino acids arginine and lysine. Tryptic digestion of the QconCAT yields an equimolar mixture of the heavy labeled target peptides, designated Q-peptides. It has been shown that Q-peptides are equally well suited as AQUA peptides as internal standards [223].

Our His-tagged QconCAT protein could be prepared in high purity, as evaluated by SDS-PAGE and colloidal coomassie staining (Fig. 15a), through a combination of IMAC chromatography and preparative IEF in off-gel format. However, we initially had problems obtaining the QconCAT in a fully labelled state when

expressing it in the standard strain BL21(DE3). While arginine-10 incorporation was nearly complete (Fig. 15b), lysine-8 incorporation was not sufficient (Fig. 15c). We hypothesized that this was due to endogenous synthesis of light lysine from other amino acids and switched to the lysine/arginine auxotrophic *E.coli* strain AT713 [224]. In this strain we could indeed obtain fully lysine-8 labeled peptides (Fig. 15c). The QconCAT was digested, stored in aliquots and the concentration of the equimolar Q-peptides determined by quantifying one of them with a light labeled AQUA peptide. The specificity of our final assay could be verified by spiking the Q-peptides into a tryptic liver protein digest and measuring both light and heavy peptides together using LC-SRM. By comparing the retention time and order of intensity of individual transitions between light endogenous PTPs and heavy Q-peptides peptides we could confidently verify the specificity of our assay for all peptides.

In the final steps we tuned MS and HPLC parameters in order to enhance signal intensities and thus sensitivity. Specifically we determined optimum values for collision energy, the most important MS parameter in this regard [225], for every transition as described in detail in Material and Methods. Finally, we optimized chromatography gradients and column loading and evaluated sample clean-up through C18 SPE (data not shown).

The SRM based targeted proteomics approach is relatively new compared to non-targeted discovery proteomics [165, 168]. In addition, setting up SRM assays involves an elaborate process of computational analysis as well as LC-MS system performance. Therefore we compared the performance of our final assay to published results with highly similar instrumentation in order to benchmark SRM assay development and instrument performance.

To this end, we determined LOQ and linearity of response for each transition by spiking a serial dilution of the Q-peptide mix in a complex background sample (1µg mouse liver peptides). Only transitions with a linearity of response of $r^2 > 0.95$ over a dynamic range of factor 200 were considered for LOQ calculations. We used only the most intense transition of each peptide to estimate its LOQ [226-228]. The results of the Q-peptide LOQ determination are enclosed in annex table A3. We found LOQ values of <10fmol peptide on column for 52 out of 60 peptides. LOQ values for 36 peptides were even below 500amol on column [179]. These values compare very favorably to a multisite assessment of seven Q-Trap 4000 systems [226]. Therefore we conclude that SRM assay

development and instrument performance reflects the current state of this important field in targeted proteomics.

However, when we applied our final assay to unfractionated liver samples and tried to detect the endogenous peptides we found that only 35 out of 60 PTPs could be detected with three transitions with signal to noise (S/N) >10, a prerequisite we deemed necessary for successful quantification. As the low S/N peptides were not distributed randomly over the panel of target proteins but were concentrated for certain proteins this would entail only being able to quantify eight out of sixteen proteins with at least three peptides. We suspected this outcome to be the result of insufficient sensitivity of our LC-MS setup.

3.1.5 Two-dimensional peptide separation improves sensitivity of SRM-based targeted proteomics

Fractionation and enrichment of specific peptides has been shown to be an effective way to increase sensitivity of SRM assays in plasma. The combination of affinity chromatography (SISCAPA) [229], SCX [227, 228] or IEF [230] with SRM have proven successful in this regard. Therefore, we set up and optimized two techniques for peptide separation – SCX and off-gel electrophoresis (OGE) with the aim of increasing the sensitivity of the assay. Fractionation strategies at the protein level, as shown for SDS-PAGE fractionation in the previous chapter, were not well suited as the internal standard in this instance is a mix of heavy labeled peptides.
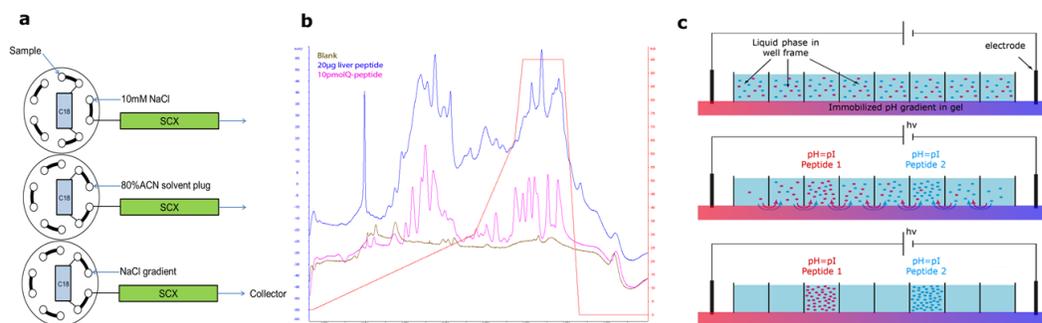
Figure 16. Principles of SCX and OGE peptide fractionation.
(**a**) Off-line HPLC setup. Peptides were retained on the C18 precolumn and desalted before transfer from C18 pre- to SCX analytical column using an ACN solvent plug followed by separation of peptides based on positive charge using a NaCl gradient. (**b**) SCX chromatograms. 20µg liver peptides or 10 pmol Q-peptides were separated with the NaCl gradient and peptide elution monitored at 214nm. (**c**) Principle of OGE (adapted from [231]). Peptides dwell mainly in the liquid phase over an IPG strip. Under high voltage they travel along the IPG to the position corresponding to their pI and are thus separated.

According to the principle of isotopic dilution [135], optimal use of this type of standard requires it to be introduced into the sample as early in the workflow as possible and particularly before fractionation which adds technical variability to the workflow. Both types of fractionation were successful in raising signal to noise of all peptides to the point where they were quantifiable.

In order to clarify which proteins were not detectable without fractionation we sorted proteins in order of increasing abundance and generated a heatmap showing the number of quantifiable peptides for direct injection or fractionation data (Fig. 17a). We could discern a clear pattern in which lower abundance peptides had only one or no quantifiable peptides without fractionation (Fig. 17a, upper left corner). Peptides from low abundance proteins became amenable to quantification through fractionation. Representative examples are shown in Fig.17b. For higher abundance proteins like sorbitol DH direct injection was already sufficient and no fractionation was needed (Fig. 17b). In contrast, enhancement of the signal to noise ratio was necessary for lower abundance proteins like glucokinase. We observed a clear correlation between protein abundance and the benefit of fractionation for SRM assays. We interpret this finding to be the result of increased overall sensitivity when peptide fractionation and SRM were combined. A straightforward explanation for this outcome is that the much higher loading capacity of a two-dimensional peptide separation system led to high concentrations of target peptides in the electrospray ion source and thus facilitated detection of analytes.

3.1.6 OGE peptide fractionation is superior to SCX for targeted proteomics of mouse liver tissue

Both peptide fractionation techniques were extensively optimized prior to their use for SRM. They were miniaturized to reduce losses and facilitate coupling to the nano-HPLC part of the LC-MS system. For SCX, we implemented a custom off-line HPLC setup with microflow dimensions and automatic desalting (Fig. 16a). Q-peptides were used to tailor the NaCl gradient to the demands of our specific application (Fig. 16b). For OGE, we used a customized peptide separation protocol that enabled the direct injection of the liquid phase fractions into the LC-MS system without additional workup, which is a general drawback of the technique due to the incompatibility of ampholytes with C18 HPLC columns.

a
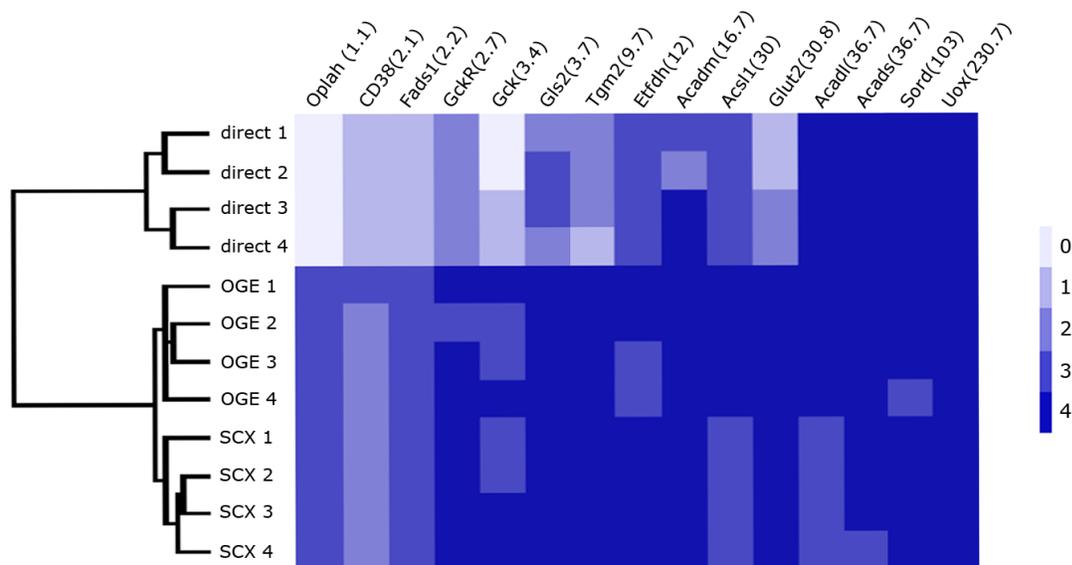
b
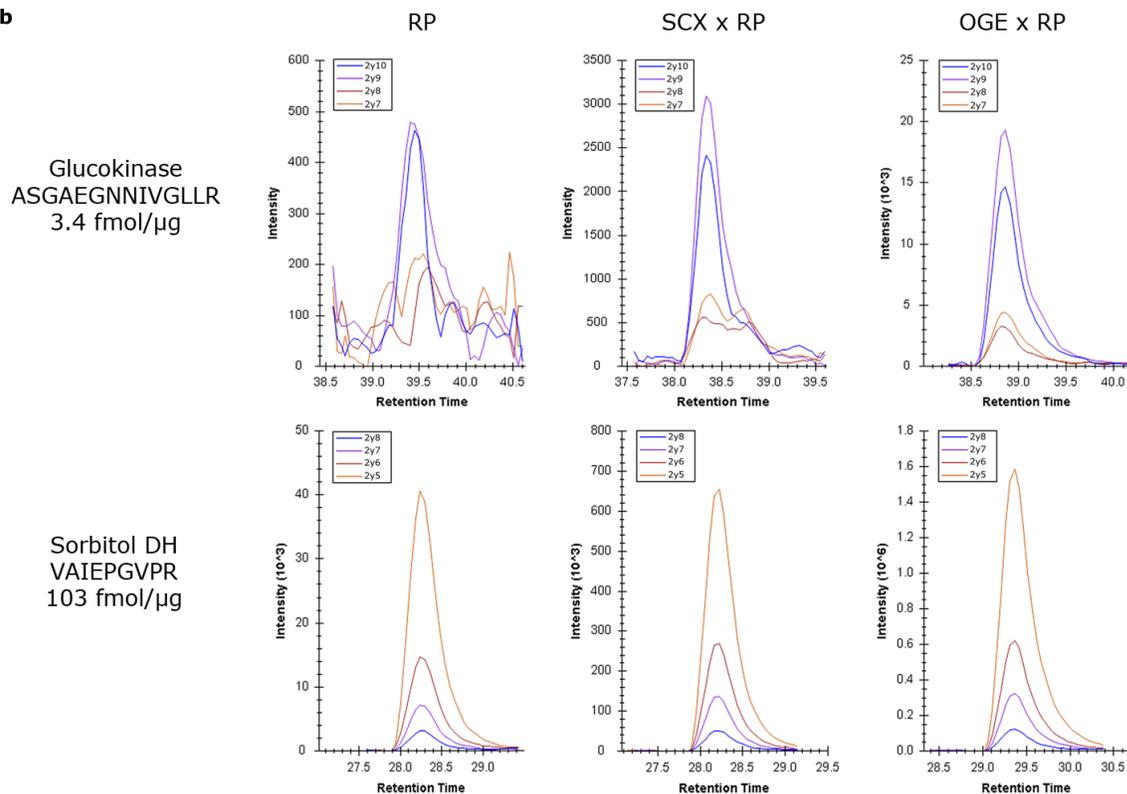
Figure 17. Two-dimensional peptide separation improves detection of low abundance proteins.
(**a**) Four replicates of either directly injected, SCX fractionated or OGE fractionated liver tryptic peptides were analyzed by hierarchical clustering based on the number of quantifiable peptides indicated as color scale on the right. Proteins were sorted in order of abundance from left to right. (**b**) Example of SRM traces of a low abundant (Glucokinase) and a high abundant (Sorbitol DH) peptide. Reprinted (adapted) with permission from [179]. Copyright (2012) American Chemical Society.
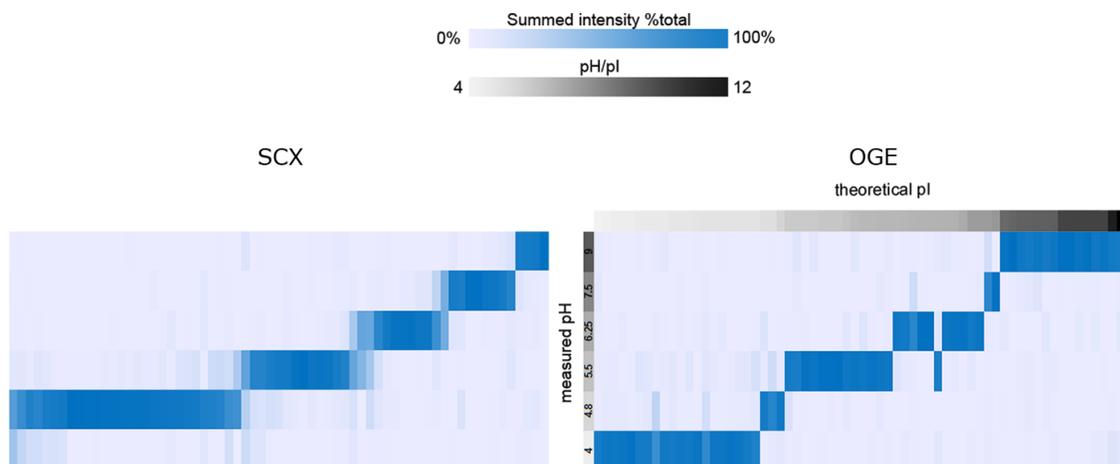
Figure 18. OGE separates peptides with higher resolution than SCX.
50µg tryptic liver digest spiked with 2.5pmol Q-peptides were separated using OGE. 20 µg digest and 1pmol Q-peptides were separated using SCX. In both cases six fractions were generated. Columns and rows correspond to peptides and fractions, respectively. Total intensity of heavy and light isotopologues were summed for each peptide and each fraction. Blue shading indicates %of total intensity for each peptide. For OGE, theoretical pI and measured fraction pH are indicated in grey. Reprinted (adapted) with permission from [179]. Copyright (2012) American Chemical Society.

Both SCX and OGE were found to separate peptides at high resolution (Fig. 18). To compare techniques at optimal performance, titration of loading amounts for each technique were conducted to determine the maximal loading capacity at which resolution was still high. The determined limits of 20µg peptides for SCX and 50µg for OGE were used for all following experiments.
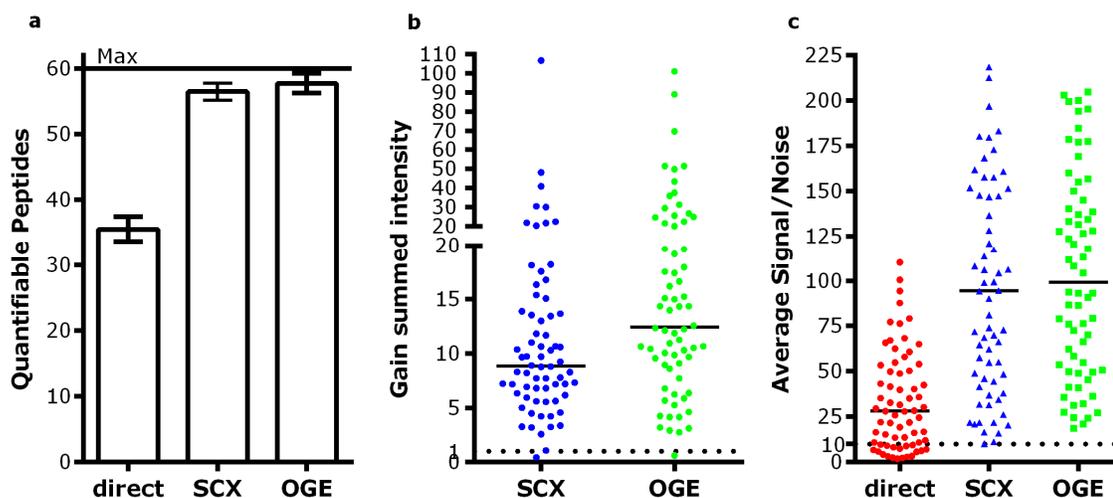
Figure 19. SCX and OGE peptide fractionation improves signal intensity and S/N of SRM assays.
Peptide amounts of 1µg, 20µg and 50 µg were used for direct injection, SCX and OGE respectively. Four technical replicates were performed for each approach. (**a**) Number of peptides suitable for quantification (at least three transitions S/N>10). Bars show mean±SD. (**b**) Improved signal intensity through fractionation. Circles indicate the average signal gain for each peptide relative to direct injection data. Lines show median gain for all peptides. (**c**) Average signal to noise values for each peptide with direct injection or fractionation. Lines indicate median S/N of all peptides. Reprinted (adapted) with permission from [179]. Copyright (2012) American Chemical Society.

Results

We found that both SCX and OGE caused a strong increase in signal intensities of light endogenous peptides (Fig. 19b). This signal gain was more pronounced for OGE than for SCX with median gains in intensity of 8.8 for SCX and 12.4 for OGE. This gain in intensity translated to a strong shift in the distribution of S/N values for both SCX and OGE as compared to direct injection data (Fig. 19c). As a consequence, the number of peptides suitable for quantification almost reached the maximum value of 68 peptides and thus provided an efficient solution of the initial problem (Fig. 19a).

In addition, we noted an excellent correlation between the pH of OGE fractions and the theoretical pI [232] of our target peptides (Fig. 18). This is in accordance with previously published results [185] and can be utilized for the setup of future SRM assays. As OGE provided a stronger boost in signal intensity and signal to noise ratios and had better resolution as well as loading capacity, we decided to use a two-dimensional peptide separation workflow based on the OGE x LC-SRM combination for analysis of the liver samples from the saff-diet study.
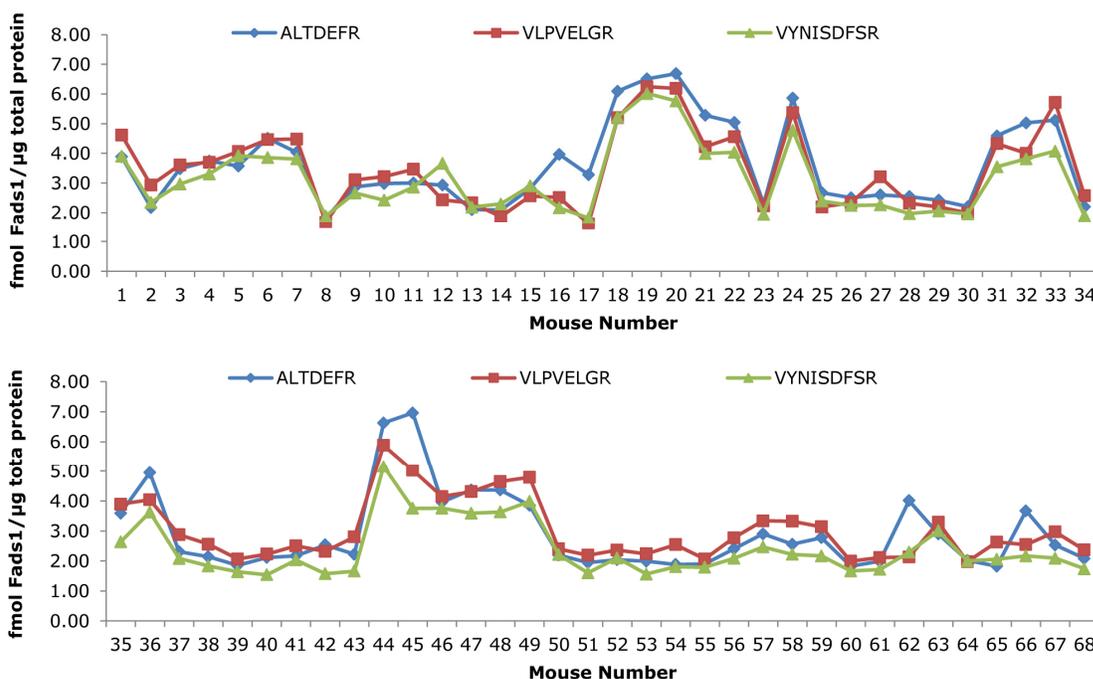
Figure 20. The final OGE x LC-SRM enables precise absolute quantification of target proteins.
68 mice from the saff-diet study were subjected to the final SRM assay. 50µg protein were digested, mixed with 1pmol Q-peptides and separated into five fractions using OGE. Absolute quantification of the three PTPs of fatty acid desaturase 1 are shown (normalized to one µg total protein).

As the final assay is rather complex, we evaluated whether PTPs from the same protein but different fractions would result in the same absolute quantification results. As an example, quantification of fatty acid desaturase 1 in 68 mouse liver samples through the OGE x LC-SRM workflow is shown. Despite its rather low abundance (<10fmol/µg protein) we obtained strikingly similar absolute values for all three PTPs over the whole 68 mouse liver samples (Fig. 20).

3.2 Monitoring protein expression changes over the course of the saff-diet study

The main T2D mouse model under investigation was a high fat dietary model with plant derived TGs from safflower. This saff-diet mouse model was described initially in [73] and was implemented in the C3H/FeJ strain for the present study, although it was also applied to other strains (most notably BL6 N and J). The following paragraph is a brief summary of the findings of Dr. Susanne Neschen and Melanie Kahle (IEG, HMGU) concerning the physiology of this T2D model published in [233] and [173]. Their work forms the basis for the proteomic study presented here and results from the proteomic study are contained in the second publication [173].

Mice were either fed a high fat (saff) or standard low fat (chow) diet for a relatively short period of time (up to three weeks). Diets were not isocaloric - the saff-diet contained 24.3 kJ/g while the chow-diet contained 17 kJ/g. Saff-diet feeding led to mild accumulation of TGs in the liver (hepatosteatosis) after one week. Initial body mass-, age-, and litter-matched treatment and control groups of mice were fed either the saff- or chow-diet for 2, 7, 14 or 21 days (Fig. 21a). Additionally, a reversibility experiment was conducted in which one group of mice was fed the saff-diet for 14 days and then switched back to standard diet for 7 days (rev). In this group of mice hepatosteatosis was reversible. While animals remained normoglycemic throughout, they developed slight hyperinsulinemia. The effect of insulin on glucose homeostasis and particularly the uptake of glucose by the periphery in relation to endogenous glucose production was monitored using the euglycemic-hyperinsulinemic clamp technique [21], the gold standard in this regard. Statistically significant insulin resistance was found after two weeks and to an even larger extent after three weeks of saff-diet feeding. This insulin resistance could be attributed to a blunted inhibition of endogenous glucose production though insulin, rather than a change in insulin stimulated glucose uptake of tissues. As endogenous glucose production is dominated by the

liver, this strongly implied the liver as the main organ responsible for the insulin resistance, which is in line with the pathogenesis of T2D in patients [6].

3.2.1 Proteomic identification of alterations in metabolic pathways induced by high fat diet feeding

We conducted non-targeted discovery proteomic analysis of this model using the membrane enrichment label-free quantification approach as well as targeted proteomics using the candidate panel and OGE x RP-SRM approach described in 3.1.

For each time point, we compared saff- versus control-diet fed groups of mice. Some LC-MS/MS runs had to be excluded for technical reasons. The number of animals in each group included in the final analysis is indicated in Fig 21a. Proteins were classified as regulated by the saff-diet through classical statistical testing for each protein followed by multiple testing corrections for the individual datasets separately without a fold change cutoff. Specifically we calculated p-values using two-tailed t-tests (two sample unequal variance) and q-values using the Benjamini Hochberg (BH) method [24]. This had the advantage that proteins were not excluded based on the effect size of their change as a low fold change does not necessarily entail a low biological effect. Furthermore, the stringency of the analysis could be adjusted afterwards by using different cutoff values for the q-values. The q-value cutoff directly gives the false discovery rate (FDR, i.e. falsely declared regulated) of the list of proteins declared significantly regulated. This approach had statistical validity but was not as overly strict as approaches controlling the family-wise error like Bonferroni or Holms correction and was still flexible in its stringency [234].

We used 5% FDR as high stringency criterion and identified 169 and 95 regulated proteins at d14 and d21 respectively but none at d2 or d7 (Fig 21. b). This was in accordance with the development of hepatic insulin resistance at these time points. For these highly confident hits we noted an overlap of 48 proteins for both time points but also a high number of proteins regulated at one time point only (121 for d14 and 47 for d21). In order to identify proteomic changes before the onset of hepatic insulin resistance, we lowered the q-value cutoffs for the d2 and d7 datasets and found 95 regulated proteins at 10%FDR for the d7 dataset. We noted that, while there was some overlap of these early (d7) with the late (d14 & d21) changes (Fig. 21c), the majority of regulated proteins at d7 (58 proteins) was not found regulated at the other time points. Complete datasets

for all time points with all identified proteins as well as measures used to identify regulated proteins are given in annex tables A4-A8.
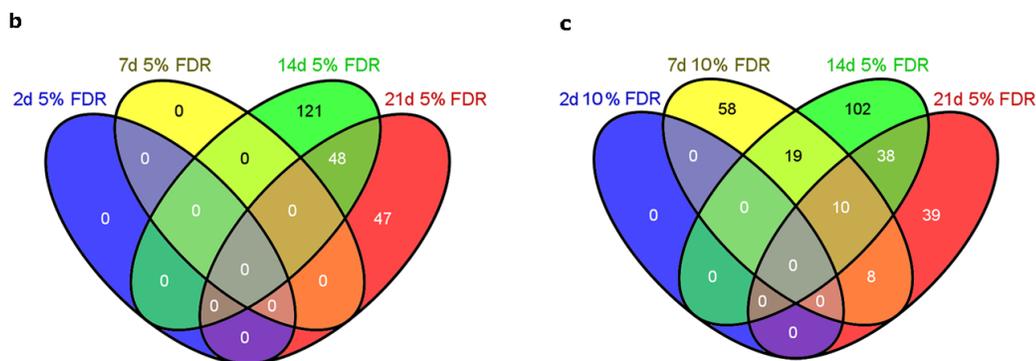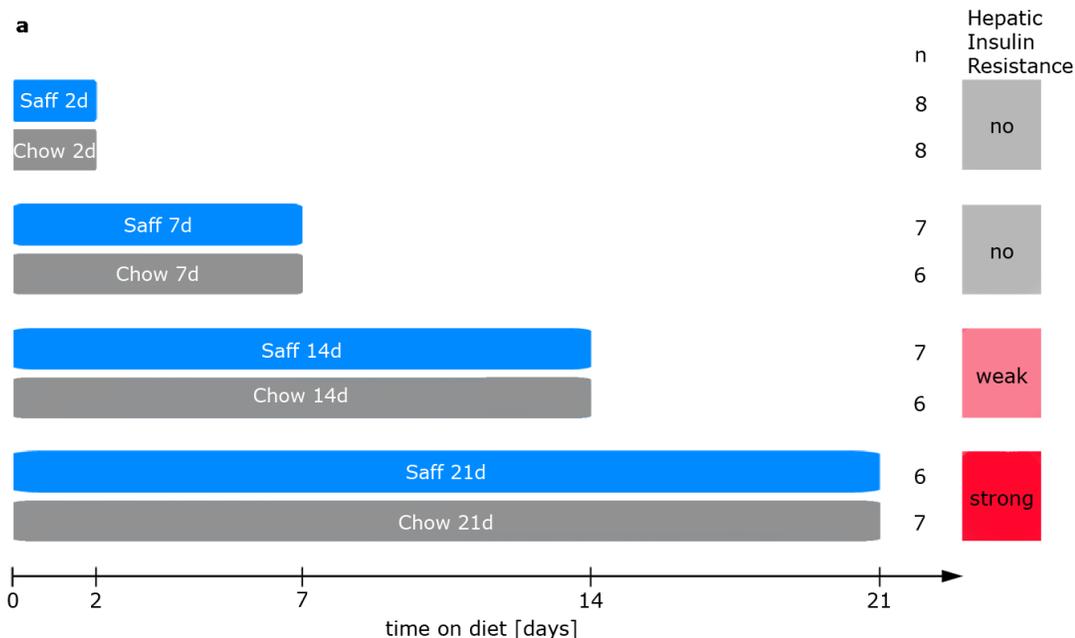
Figure 21. Saff-diet feeding induced hepatic insulin resistance is associated with differential protein expression.
(**a**) Study design. The individual mouse groups with feeding regimens are indicated as bars. The number of mice for each group included in the final proteomics datasets is given behind each bar. Hepatic insulin was evaluated with the hyperinsulinemic-euglycemic clamp technique [173]. Regulated proteins were identified by t-test of HFD-fed versus control diet groups followed by BH correction. Cutoff values for regulation were: (**b**) q<0.05 for all time points and (**c**) q<0.05 for d14 and d21, q<0.1 for d2 and d7.

The numbers of proteins regulated at one time point only were much higher than we would expect for proteins falsely declared regulated. For example, we would expect only 9-10 false positive hits for the d7 dataset instead of 58 (95 proteins at 10% FDR). We used the reversibility experiment as an additional negative control. We identified three regulated proteins at 5% FDR and seven regulated proteins at 20% FDR for this dataset, none of which were found regulated in the other datasets.

Results

While it is possible that these proteins represent lingering effects of two weeks HFD feeding we note that our analysis strategy does not seem to produce many false hits that are apparently regulated. Based on this observation, we hypothesized that time-resolved proteomic changes in the liver represent a multistage process and tried to find pathways underlying the different groups of regulated proteins at the different time points.

To this end, we conducted pathway enrichment analyses of the regulated proteins. We choose to employ a customized background set for enrichment analysis as using the whole mouse proteome would give a mixed result of liver enriched pathways and diet regulated pathways. Therefore, we constructed a custom background set from the largest mouse liver proteome dataset published ([203], >6700 protein), complemented with proteins additional identified in our collected datasets. Therefore, the final background set contained more than 7300 proteins. As we were interested in metabolism and signaling we tested enrichment of pathways contained in KEGG [235] and Reactome. Identified enriched pathways for each time point are listed in Table 6. Fold enrichment versus the liver background set and regulated proteins are given for each pathway.

We could not identify a single signaling pathway, but we found a set of metabolic pathways enriched at both d14 and d21. The increase of enrichment factors from d14 to d21 implies that more components of the individual pathways were found regulated as hepatic insulin resistance progressed. One strongly affected pathway was oxidative phosphorylation. At d21 we found components of all five respiratory chain complexes regulated. All proteins of the respiratory chain were downregulated in all datasets. This finding is very likely connected to alterations in mitochondria which have been found on the ultrastructural level in the saff-diet model [173].

We noted that a large part of the proteins upregulated at d7 were different ribosomal structural proteins, but these changes declined as HFD feeding progressed and the term "Ribosome" was no longer found enriched in the d21 dataset. Therefore, this change was transient and vanished before fully developed hepatic insulin resistance was observed.

KEGG pathway	fold enrichment			Proteins
	d7	d14	d21	
Oxidative phosphorylation	n.s.	4.4	6.4	Atp5f1 Atp5j Atp5k Atp5l2 Atp5o Cox5a Cox6a1 Nd5 Ndufa10 Ndufa3 Ndufa5 Ndufa9 Ndufb3 Ndufb4 Ndufb5 Ndufb7 Ndufb8 Ndufs1 Ndufs2 Ndufs3 Ndufs5 SdhB SdhC Uqcr10 Uqcrb Uqcrc1 Uqcrc2 Uqcrfs1
Ribosome	4.6	2.8	n.s.	Rpl14 Rpl17 Rpl23 Rpl27 Rpl6 Rpl7 Rpl9 RplP0 Rps11 Rps13 Rps14 Rps17 Rps2 Rps26 Rps27l Rps3a Rps4x Rps7 Rps9
Drug metabolism	n.s.	3.6	5.5	Cyp2A12 Cyp2A5 Cyp2C29 Cyp2C50 Cyp2C67 Cyp2C70 Cyp2F2 Dhdh Ephx1 Fmo1 Fmo5 Gstk1 Gstp1 MaoA MaoB Ugt2b1 Ugt2b36
Retinol metabolism	n.s.	3.1	4.8	Cyp2A12 Cyp2A5 Cyp2C29 Cyp2C50 Cyp2C67 Cyp2C70 Cyp4A12 Ugt1a Ugt2b1Ugt2b36
Arachidonic acid metabolism	n.s.	3.5	5.4	Cyp2C29 Cyp2C50 Cyp2C67 Cyp2C70 Cyp2J5 CYP4A12 Ephx2
Linoleic acid metabolism	n.s.	4.0	6.3	Cyp2C29 Cyp2C50 Cyp2C67 Cyp2C70 Cyp2J5
Primary bile acid biosynthesis	n.s.	4.9	7.7	Cyp8B1 Cyp7B1 Cyp7A1 Cyp27A1 Scp2 Hsd17b4
Ascorbate metabolism	n.s.	5.3	8.3	Aldh2 Aldh3a2 Gulo Ugt1a Ugt2b1 Ugt2b36
Steroid hormone biosynthesis	n.s.	n.s.	6.2	Comt1 Cyp7A1 Cyp7B1 Hsd17b2 Hsd17b7 Hsd3b5 Ugt1a Ugt2b1 Ugt2b36
Tryptophan metabolism	n.s.	n.s.	4.2	Aldh2 Aldh3a2 Ehhadh Kmo MaoA MaoB
PPAR signaling pathway	n.s.	3.0	3.5	Hmgcs2 Acsl1 Cyp27A1 Scp2 Cyp4A12 Cyp7A1 Cyp8B1 Ehhadh
Fatty acid metabolism	n.s.	3.3	n.s.	Acaa1b Aldh2 Acaa2 Acsl1 Aldh3a2 Cpt1a Cyp4A12 Dci Ehhadh Hadha Peci

Table 6. KEGG pathways underlying differential protein expression in the saff-diet study.
Enriched pathways from KEGG and Reactome were identified using the tool DAVID [236]. DAVID p-values were corrected for multiple testing using BH with an FDR of 10%. n.s not significant. Up- and downregulated proteins are shown in green and red, respectively. Regulated proteins from the d21 dataset are listed, except for "Ribosome" and "Fatty acid metabolism" where d14 regulated proteins are listed.

Results

We found increasing enrichment of biotransformation enzymes ("Drug metabolism" in Tab. 6). On closer examination of the regulated proteins contained herein, we found that they actually represent a union of various metabolic processes lower on the list. These included synthesis and degradation of linoleic acid and arachidonic acid, retinol, steroid hormones as well as primary bile acids, ascorbate and tryptophan. Finally, we found regulation of peroxisome-proliferator activated receptor (PPAR) target proteins. This was expected as the main fatty acid contained in the saff-diet was linoleic acid (C18:2 ω-6), a natural activator of PPAR-α.

Transcriptome analyses of the C3H saff model [233] allowed the prediction that PPAR-α was activated by saff-diet feeding from d7 to d21. Among these target genes were also enzymes of peroxisomal β-oxidation, a minor lipid catabolic pathway. This pathway as well as mitochondrial β-oxidation appear as the term "Fatty acid metabolism" in our analysis, but were only found enriched at d14. Upregulated proteins of peroxisomal β-oxidation included 3-hydroxyacyl-CoA dehydrogenase (Ehhadh) and 3-ketoacyl-CoA thiolase (Acaa1b) while those of β-oxidation were 3-ketoacyl-CoA thiolase (Acaa2), long chain fatty acid-CoA ligase 1 (Acsl1), and trifunctional enzyme subunit alpha (Hadha). Two additional upregulated enzymes, Scp2 and Hsd17B4, assigned by KEGG to bile acid synthesis, actually have more prominent roles in peroxisomal β-oxidation [237]. In addition, the fatty acid isomerases enoyl-CoA delta isomerase 2 (Peci) and enoyl-CoA delta isomerase 1 (Dci), crucial for the oxidative breakdown of unsaturated fatty acids such as linoleic acid (C18:2 ω-6), were upregulated. Note that most of the enzymes in Table 6 (except for ribosomal and β-oxidation enzymes) are actually transmembrane or membrane associated proteins.

3.2.2 Saff-diet feeding induces an early transient increase in the PUFA synthesis pathway

We choose the interconnected pathways of linoleic acid and arachidonic acid metabolism for closer examination. Upon literature based research we found additional regulated proteins not covered by the pathway enrichment analysis. This led to the identification of two specific processes that were affected: The polyunsaturated fatty acid (PUFA) synthesis pathway and the epoxyeicosatrienoic acid (EET) pathway. Interestingly, we could discern two phases in the deregulation of these pathways.

The first phase was composed of the upregulation of proteins catalyzing the synthesis of arachidonic acid from linoleic acid shown in Figure 22. Linoleic acid (C18:2 ω-6) is not only subject to catabolic processes and finally β-oxidation, but it is also an essential precursor for the anabolic process of PUFA synthesis. PUFAs are fatty acids with two or more double bonds. Relevant natural PUFAs have between 16 and 24 carbons atoms and are therefore long and very long fatty acids [238] (e.g. C18:2 ω-6 or C24:4 ω-6). This is achieved though carbon chain elongation catalyzed by the elongation of very long chain fatty acid proteins (Elovl) and introduction of additional double bonds through fatty acid desaturases (Fads) [238]. Four enzymes are mainly responsible for PUFA synthesis from dietary linoleic acid in liver [238]. Our non-targeted data contained two of these enzymes – Elovl5 and Fads2. Interestingly, the other two enzymes were targeted in our SRM panel (Tab. 5) as they were already implicated in T2D through genetic data from human studies [214]. We found that all enzymes were upregulated at d7 (Fig. 22a).
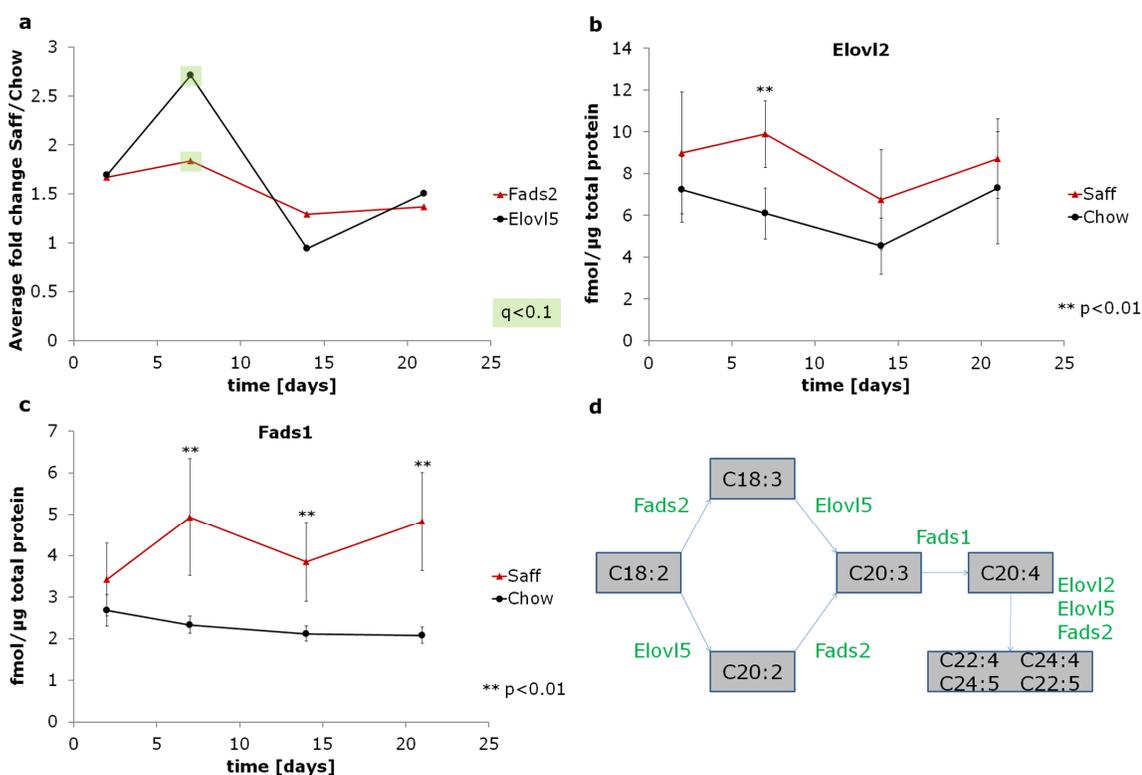
Figure 22. Saff-diet feeding induces a transient upregulation of the PUFA synthesis pathway.
(**a**) Time course of average fold changes of enzymes of the PUFA synthesis pathway. Statistical significance after BH correction at FDR 5% and 10% is shown through blue and green shading respectively. (**b**, **c**) Absolute quantification of Elovl2 (**b**) and Fads1 (**c**) in saff- and chow-diet fed mice over time through targeted proteomics. Mean±SD are shown for each time point and group. (**d**) ω-6-PUFA synthesis pathway according to [238]. Fatty acids are shown in grey, enzymes upregulated at d7 are shown in green.

Note that all PUFAs shown in Fig.22d are of the ω-6 series; although the four investigated enzymes also synthesize PUFA of the ω-3 series (see Discussion). However, this upregulation was only transient for Fads2, Elovl2 and Elovl5 and did not persist at and after d14 (Fig. 22a, b). In contrast, a very clear and protracted upregulation of Fads1 was observed from d7 to d21 (Fig. 22c). Taken together, these enzymes catalyze the conversion of linoleic acid to arachidonic acid and to even longer, highly desaturated PUFAs. These results also pose the question which intermediates and end products increase or decline through the change in enzyme levels. Unfortunately we were unable to assess PUFA levels in the liver samples at this point. This is due to the fact that assessing these lipids requires specialized analytical assays like gas chromatography (GC) [239-241] which were not available. Therefore it is an open question whether the levels of the intermediate arachidonic acid were influenced in a positive or negative manner through a change in the flux of the whole pathway. In this regard it is noteworthy that all four enzymes are transmembrane proteins of the ER [242, 243] and that their upregulation predominantly at d7 was also seen as a concerted reaction on the transcript level (analysis of transcriptomics dataset from [233]).

3.2.3 Saff-diet induced repression of the EET synthesis pathway coincides with hepatic insulin resistance

The second phase involved a group of particular cytochrome P450 (Cyp) enzymes as well as the hydrolase Ephx2, which are responsible for the synthesis and degradation of endogenous eicosanoids, derived from arachidonic acid – EETs. The Cyp enzymes in question were four members of the Cyp2C family (Cyp2C29, Cyp2C50, Cyp2C67, and Cyp2C70) as well as Cyp2J5. We found a progressive downregulation already beginning at d7 and statistically significant at d14 for Cyp2C50, 67 and 70. At d21, all enzymes were significantly downregulated (Fig. 23a). These five Cyps catalyze the synthesis of EETs through epoxygenation of arachidonic acid [244] (Fig. 23c). Conversely, we found a more than threefold upregulation of the EET degrading enzyme Ephx2, statistically significant at d14 and d21 (Fig. 23b). This trend could already be observed at d7 but was not statistically significant as the high fold change was the result of outliers in the saff group with very high Ephx2 MS1 intensities. Ephx2 hydrolyzes the epoxy group introduced by the Cyps. The resulting diol derivatives are called
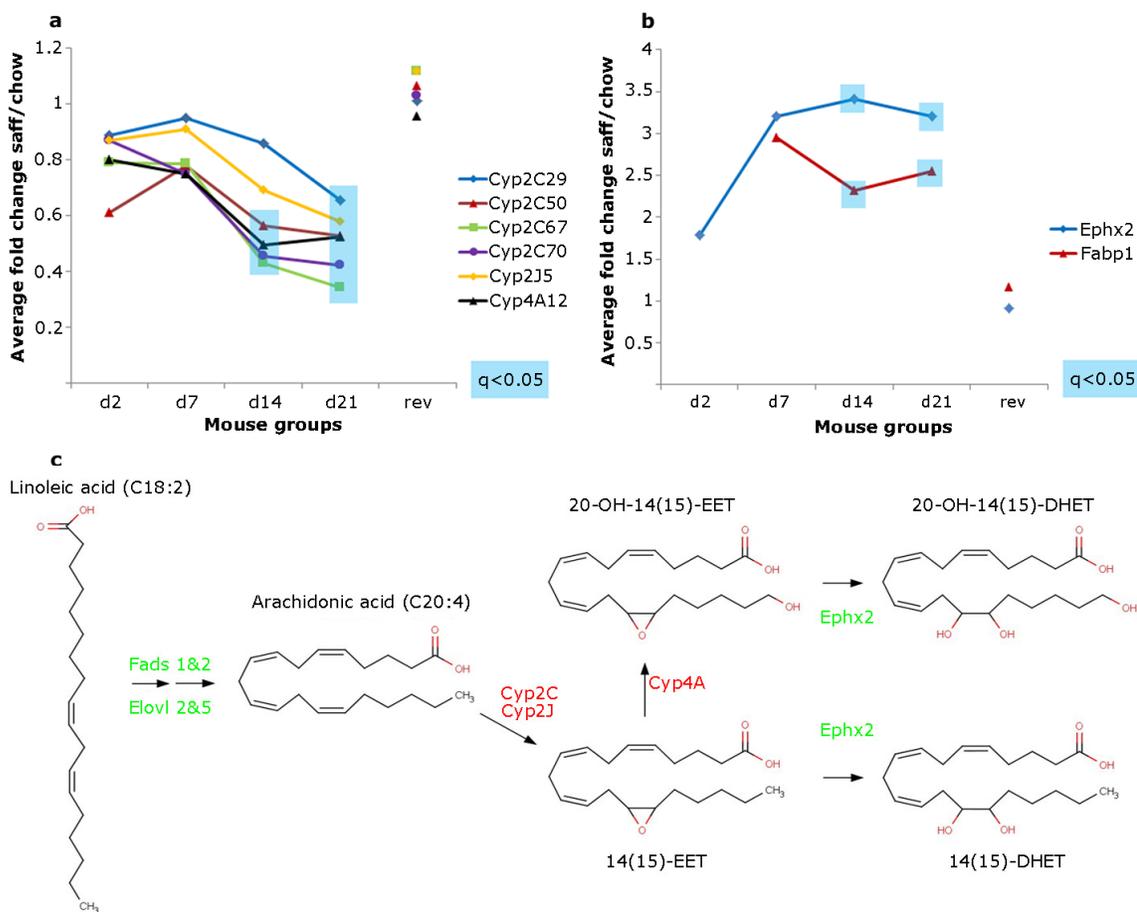
Figure 23. EET pathway enzymes are deregulated through saff-diet feeding.
(**a**) Time course of average fold changes of EET synthesizing Cyp enzymes. (**b**) Upregulation of negative effectors of the EET pathway. Statistical significance after BH correction at FDR 5% is shown through blue shading for **a** and **b**. (**c**) EET synthesis and degradation pathway redrawn after KEGG [235]. Upregulated enzymes are shown in green, downregulated ones in red.

dihydroxytrienoic acids (DHET) and are largely biologically inactive [244] (Fig. 23c).

In addition we found a very similar pattern of downregulation for Cyp4A12 (Fig. 23a). This enzyme is involved in the ω-hydroxylation of EETs [245] which is an intermediate step in the synthesis of 20-OH-DHETs (Fig. 23c). In contrast to unmodified DHETs, 20-OH-DHETs are biologically active but in a different way than EETs. While EETs have been shown to influence intracellular signaling in endothelial cells (see chapter 3.3), 20-OH-DHETs have been shown to be potent PPAR-α agonists [246]. Taken together, we hypothesized that these changes would lead to lowered levels of EETs and 20-OH-DHETs in hepatocytes as the synthesizing enzymes were down- while the degrading enzymes were upregulated. A final observation in this regard is the simultaneous strong upregulation of Fabp1 (Fig. 23b), which has been described to sequester EETs and thus inhibit their action [247]. However, this may be a non-specific

adaptation of hepatocytes to cope with an increased influx of fatty acids through the high fat diet.

3.2.4 Repression of the EET pathway is not caused by changes in subcellular organelle composition or unspecific Cyp repression

At this point much of our speculation concerning deregulation of the EET pathway depended on the concerted downregulation of certain Cyp enzymes. In light of the findings concerning altered structure of mitochondria, we asked the question whether downregulation Cyps could be caused by a change in the ER of the hepatocytes, since most Cyps in general and EET synthesizing Cyps in particular, are localized in or at the ER membrane. By the same token, Ephx2 upregulation may be a result of changes in peroxisomes, as Ephx2 is localized both in cytoplasm and peroxisomes [248].

However, we could find no differences in the abundance of either the ER marker calnexin or the peroxisome marker catalase at any time point (Fig. 24, first two rows). Moreover, the upregulation of Ephx2 and downregulation of Cyp2C67 and Cyp2C70 was also observed at the transcript level, although this was not the case for the four other Cyps (analysis of transcriptomics dataset from [233]). We conclude that the structural changes on the level of subcellular organelles are unlikely to account for the differences in expression of EET pathway enzymes.

Next, we checked if there was evidence that regulation of the Cyps could be the result of a general repression of Cyps that was not specific for the EET synthesizing enzymes. In total, we quantified 31 Cyp enzymes in this study. Of these, 18 were not affected by high fat diet feeding. As an example, we compared the expression change of Cyp2C70 to that of Cyp3A11, a homologue of the human Cyp3A4, whose expression can be induced by a large number of diverse xenobiotics [249]. The expression of Cyp3A11 was very stable across time points and treatment groups, while there was a clear downregulation for Cyp2C70 at d14 and d21 (Fig. 24, two lower rows).

Of the 14 Cyps affected by saff-diet feeding, 12 were associated with the enriched pathways. Six were part of the EET pathway (Fig. 23). Four were part of the synthesis of primary bile acid but may also take part in minor branches of steroid hormone degradation (Cyp7A1, Cyp7B1, Cyp8B1 and Cyp27A1) (Tab. 6). Another two were implicated in the metabolism of retinol (Cyp2A5 and Cyp2A12) and the final two (Cyp4V3 and Cyp2F2) had no straightforward association with

enriched pathways in our analysis. We conclude that Cyp repression is by no means exclusive to EET pathway enzymes but that it is also not overly unspecific. It rather appears that these affected Cyps are components of three to four saff diet sensitive biochemical pathways, of which the EET pathway is the most prominently represented one.
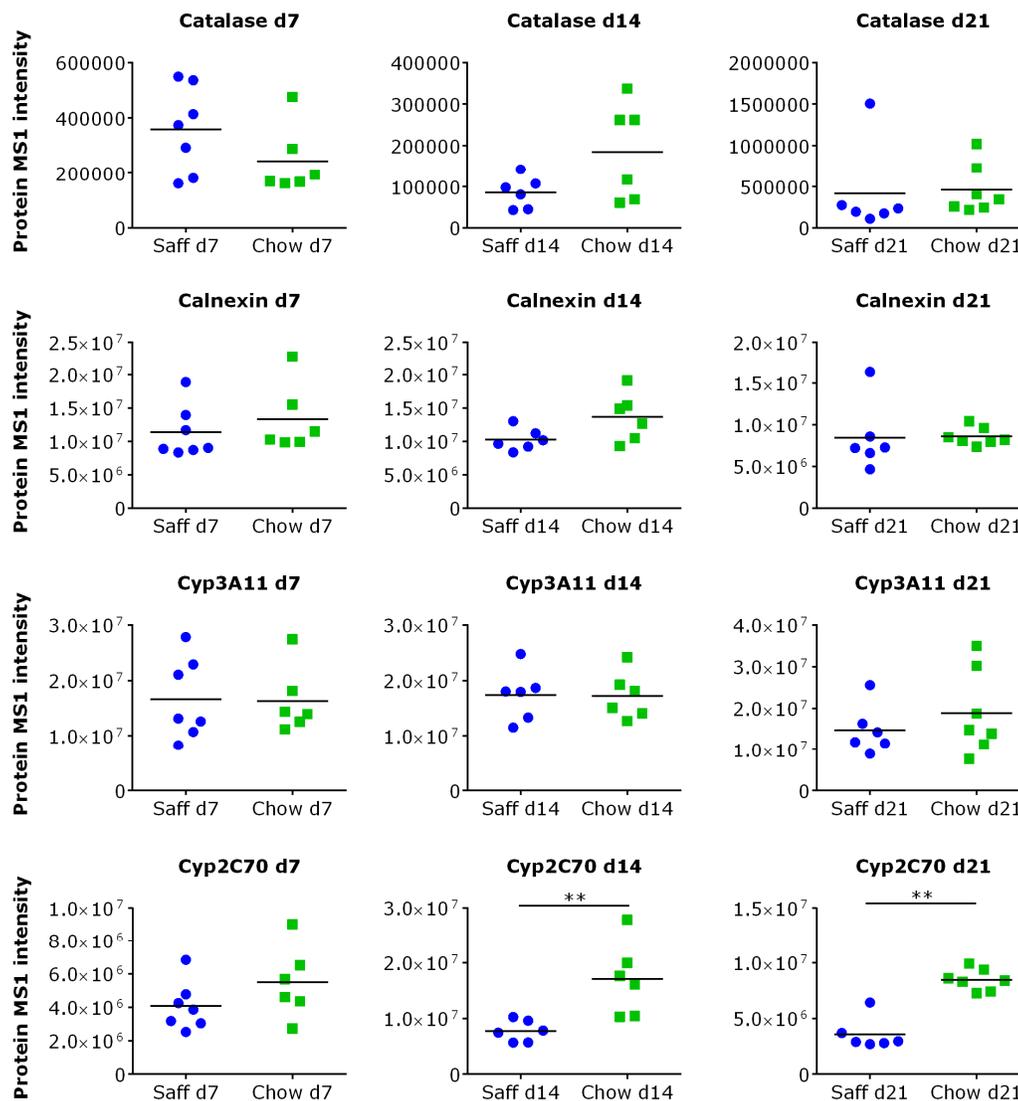
Figure 24. Repression of EET synthesizing Cyps is not a consequence of changes in ER abundance of general Cyp repression.
Each marker corresponds to the MS1 intensity of the indicated protein in one mouse of the indicated groups. Saff animals are shown as blue circles, chow animals as green squares. Group mean values are indicated by bars. Individual graphs show group comparisons of different time points (left to right, d2-d21) for marker proteins and Cyps (top to bottom: Catalase, Calnexin, Cyp3A11, and Cyp2C70). ** $p < 0.01$.

3.2.5 Discovery of a novel lysine acetylation site on Ephx2, which is influenced by saff-diet feeding

A particular advantage of proteomics is that it not only delivers quantitative information at the effector level but also has the potential to identify and quantify posttranslational modifications (PTMs). However, datasets need to be queried in a targeted fashion for PTMs to avoid the combinatorial explosion phenomenon described in the literature [134, 250]. Protein lysine acetylation has recently been discovered as a functionally relevant PTM affecting non-nuclear proteins [251] and as being influenced by high fat diet feeding [252]. We examined our datasets for the presence of acetylated peptides and found 50-100 acetylated peptides per dataset at PepFDR 2%. One of these acetylated peptides was actually derived from Ephx2. In this instance the MS/MS spectrum for the identification had very high quality and could be used to localize the acetylation site precisely through the presence of almost all y fragment ions (Fig. 25a). A drawback of identifying lysine acetylation in this manner is the risk of confusing it with lysine trimethylation as both modifications introduce the same nominal mass shift of 42 Da.

However, both modifications differ by 0.036 Da due to the mass defect of atomic nuclei which corresponds to a mass difference of more than 20ppm. As our
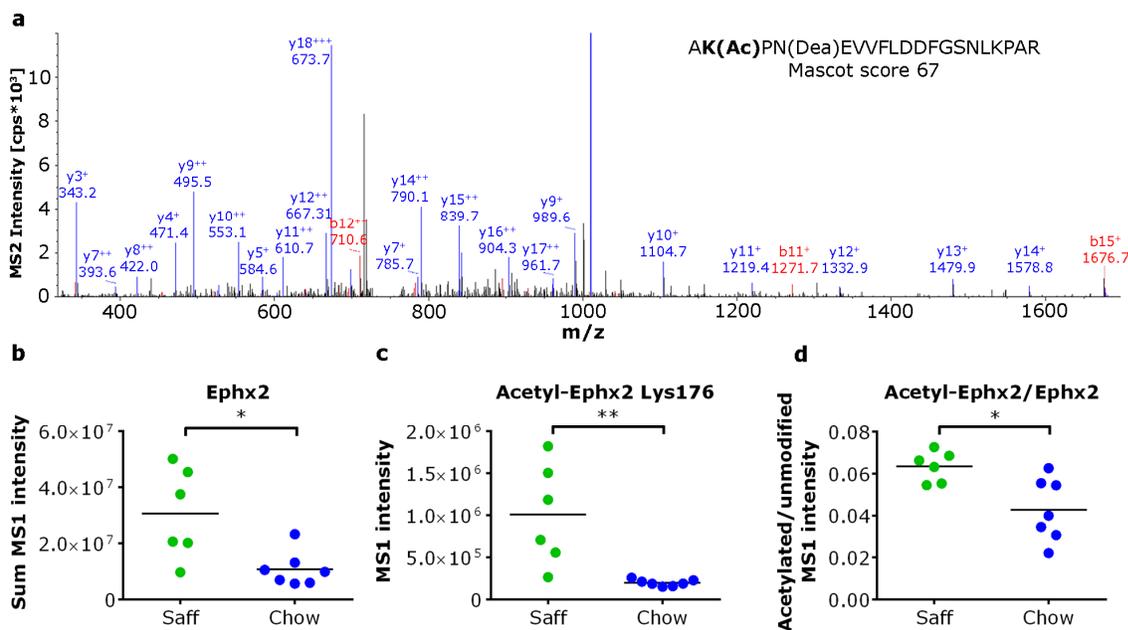
Figure 25. A novel acetylation site on Ephx2 is affected by saff-diet feeding.
(**a**) Annotated MS/MS fragment spectrum of the acetylated tryptic peptide from Ephx2. Mascot score was 67 and peptide confidence>99.9% calculated by Percolator [191]. Unmodified and acetylated Ephx2 peptides were compared for the d21 dataset. Each circle corresponds to one mouse. (**b**) Summed MS1 intensity of all unmodified Ephx2 peptides. (**c**) Lys 176 acetylated peptide MS1 intensities. (**d**) Acetylated MS1 intensity normalized to the summed MS1 intensity of all unmodified peptides (separately for each animal). * p<0.05 **p<0.01.

database search was conducted with a maximum mass deviation of 7ppm for precursors, we can exclude that the peptide was trimethylated.

We were interested whether this novel acetylation site was also affected by saff-diet feeding. We found that both the unmodified protein intensity (represented as the sum of unmodified peptide intensities) and the acetylated peptide intensity were strongly upregulated by saff-diet feeding in the d21 datasets (Fig.25 b, c). In order to determine if the degree of acetylation was affected we normalized the intensity of the acetylated peptide to the unmodified peptides (Fig. 25d). Note that the resulting ratio does not represent the percentage of acetylated Ephx2 but is a surrogate measure of relative acetylation Ephx2. We found that the degree of acetylation of Ephx2 was significantly increased by saff-diet feeding (Fig. 25d).

3.2.6 Saff-diet feeding induces mitochondrial β-oxidation of long chain unsaturated FAs

In line with the results of our discovery analysis we found that the outcome of our targeted proteomics investigation was linked directly to the described perturbations in long chain fatty acid metabolism. The most clearly regulated proteins in the T2D SRM panel (Table. 5) were not only the PUFA synthesis enzymes (Fig. 22) but also four enzymes responsible for directing free fatty acids towards mitochondrial β-oxidation (Fig. 26). These enzymes were: the plasma membrane associated cytoplasmic long chain fatty acid CoA ligase 1 (Acsl1), which forms the activated acyl-CoA thioesters of long chain fatty acids [253] and the three acyl-CoA dehydrogenase (Acad) enzymes acting on acyl-CoA species of different carbon chain lengths.

These enzymes catalyze the first (α, β-dehydrogenation) step of β-oxidation within mitochondria and have preferences for short (C4-C6, Acads), medium length (C6-C12, Acadm) and long chain (C8-C16, Acadl) acyl-CoAs [254]. We found induction of all these enzymes though saff-diet feeding (Fig. 26). This induction was most pronounced for Acsl1 (Fig. 26a) and Acadl (Fig. 26b), which reached statistical significance at and after d7, while the other two enzymes (Acadm and Acads, Fig. 26c and d) showed significant changes at d21 only. In addition, the final fold-change at d21 correlated with the chain length of fatty acids being oxidized by these enzymes with Acadl being 1.5 fold, Acadm 1.4 fold and Acads 1.2 fold upregulated. In this regard, it is interesting that fold changes in this range are usually not detected by discovery proteomics and that the

application of the high accuracy SRM approach could uncover the predominant induction of one of the three isoenzymes which would be challenging with other methods.
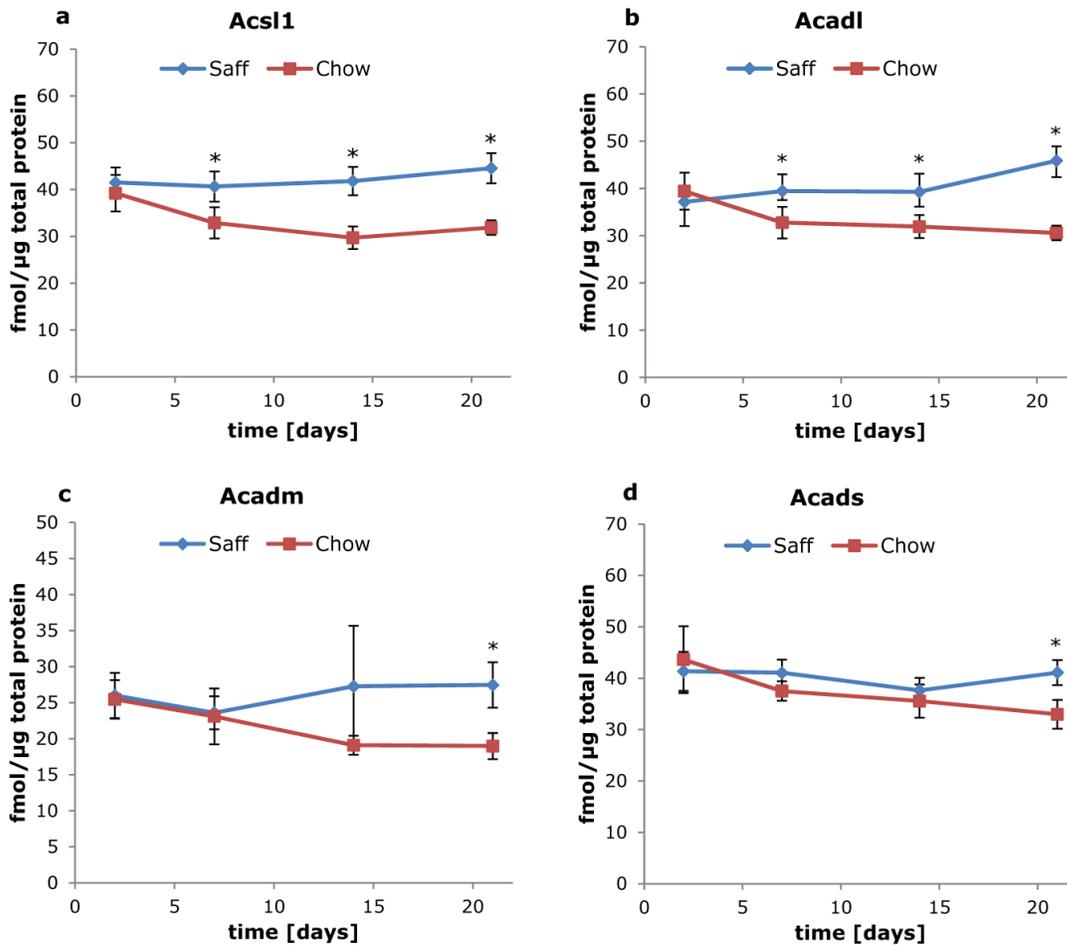
Figure 26. Saff-diet feeding induces expression of long fatty acid β-oxidation enzymes. Absolute amounts of Acsl1 (**a**), Acadl (**b)**, Acadm (**c**) and Acads (**d**) per µg total protein extract from mouse liver was determined using the OGE x RP SRM assay described in chapter 3.2. Blue (Saff) and red (Chow) markers show mean±SD for the respective mouse groups. n=7 for all time points and groups. * $p<0.01$.

While a very long chain acyl-CoA dehydrogenase (Acadv) for fatty acids longer than C16 exists, unsaturated fatty acids have been found to be a poor substrate for Acadv. In fact, Acadl has been shown to have much higher activity towards arachidonic acid than Acadv [255]. Therefore the most likely β-oxidation enzyme responsible for mitochondrial breakdown of the long, unsaturated acyl-CoAs of linoleic and arachidonic acid is Acadl. In this regard, it is tempting to speculate that the concerted action of Ascl1 and Acadl may mediate breakdown of both linoleic and arachidonic acid and would thus be an additional negative effect on the EET pathway as it would reduce the availability of EET precursors. Moreover,

β-oxidation of EETs is an important alternative inactivation mechanism in addition the Ephx2 mediated hydrolysis [244].

3.3 Functional validation of the impact of the EET pathway on hepatic insulin signaling

Based on our results concerning the perturbation of the PUFA and EET synthesis pathway we hypothesized that saff-diet feeding reduces, among other processes, the levels of EET putatively present in hepatocytes. Therefore we formulated the working hypothesis that EETs are positive regulators of insulin signaling and proceeded to test this hypothesis in cell culture. Up to this point it was unknown whether hepatocytes contain EETs or if signaling in hepatocytes was influenced by EETs. However, EETs activate some of the same signaling pathways in endothelial cell as insulin does in the liver (see Discussion). In addition, they are implicated in glucose homeostasis by the recent finding that Ephx2 knock-out or inhibition can reduce blood glucose and enhance insulin secretion in streptozotocin (STZ) treated mice, a model for diabetes [256].

3.3.1 Hepatocyte cell lines and primary hepatocytes as a model for insulin signaling

In order to test our hypothesis we established a system that allowed controlled insulin stimulation of hepatocytes at first with insulin alone. To this end we verified the suitability of cell lines and primary cells as a model for hepatic insulin signaling. Furthermore we characterized their response to insulin in terms of phosphorylation of key nodes of the insulin signaling cascade in dependence on the parameters stimulation time and insulin dose. Once the stimulation protocol had been established successfully we tested the hypothesis by costimulation with synthetic EETs and overexpression of EET pathway enzymes.

As the EET receptor is still unknown [76], we used the mouse hepatoma cell line Hepa 1-6 (Fig. 27, left panel) [257] and the normal liver cell line BNL Cl.2 [258] (Fig. 27, middle panel) in addition to primary hepatocytes to reduce the risk that that cells were not responsive to EETs. While the identity of the primary mouse hepatocytes was readily confirmed by their morphology, specifically their polygonal shape and two nuclei per cell [259] (Fig. 27, right panel), both cell lines did not display characteristic hepatocyte morphology. Therefore, we assayed one of the hallmark activities of hepatocyte – secretion of plasma proteins.
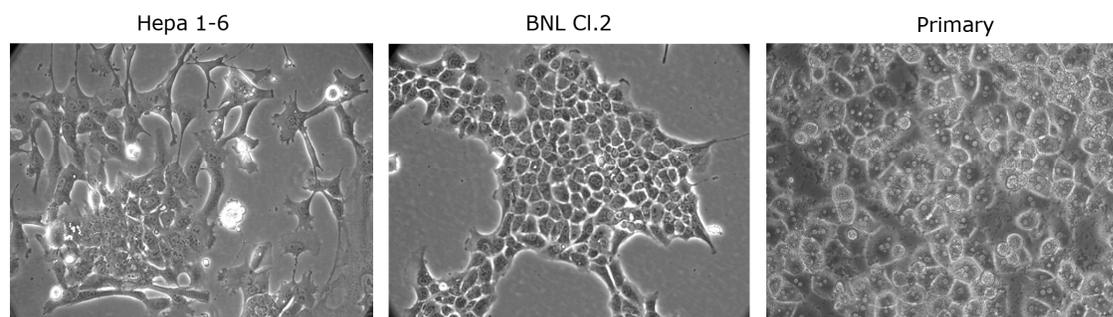
Figure 27. Primary hepatocyte and hepatocyte cell lines morphology.
Hepatocyte cell lines were photographed during routine culture in flasks. Primary hepatocytes were isolated by EGTA/collagenase perfusion and seeded on Collagen I coated six-well plates. Morphology six hours post isolation is shown. All pictures at 200x magnification.

Secreted proteins from 48h conditioned medium were isolated, digested and analyzed by LC-MS/MS. As negative control we used a HEK293T supernatant. As HEK293T cells are kidney derived they should not secrete plasma proteins. We found most of the high abundant plasma proteins [136] in the hepatocyte cell lines supernatants, which were absent from the HEK293T supernatant (Table 7). Not all major blood proteins are synthesized by hepatocytes. Hemoglobin is produced in the bone marrow and immunoglobulins in the lymphatic system. Neither hemoglobin nor immunoglobulins were identified in Hepa 1-6 or BNL Cl.2 supernatants, showing the specificity of plasma proteins secretion by our hepatocyte cell lines (Table 7). As datasets were searched against the Uniref100 database with taxonomy set to mammalia it was possible to distinguish mouse (secreted by Hepa 1-6 and BNL Cl.2), bovine (contaminants from FCS) and human (secreted by HEK293T) proteins.

	Hemoglobin	Immunoglobulin	Albumin	Complement C1s	Complement C3	Complement C2	Serpinb6	Serpinb7	Serotransferrin	Apolipoprotein E	Ceruloplasmin	b2 microglobulin
Hepa 1-6	-	-	17	14	11	7	4	3	24	15	6	3
BNL Cl.2	-	-	9	13	36	12	10	-	6	5	24	-
HEK293T	-	-	-	-	-	-	-	-	-	-	-	-

Table 7. The hepatocyte cell lines Hepa 1-6 and BNL Cl.2 secrete plasma proteins.
Numbers of unique peptides per protein at 2% PepFDR are shown. Proteins from 48h conditioned serum free medium were precipitated using acetone, purified using ultrafiltration before tryptic digestion and LC-MS/MS analysis. Datasets were searched against the Uniref100 database with taxonomy set to mammalia. Proteins from a HEK293T supernatant are shown as control.

This relatively simple test demonstrates that the cell lines were initially derived from mouse cells as it provides amino acid sequence information for secreted proteins. It also shows that the cell lines were initially derived from hepatocytes and not non-parenchymal cells of the liver as these would not secrete plasma proteins. Finally the test shows that the cell lines still retain some of the molecular functions of hepatocytes.

Next, we set up the insulin stimulation protocol. As readout for the insulin signaling cascade we chose phosphorylation of the insulin receptor (IR), insulin receptor substrate 1 (IRS-1) and the kinase Akt. These proteins are key nodes in the branch of the insulin signaling pathway responsible for glucose metabolism in hepatocytes, spanning the receptor binding insulin to the central kinase modulating effector molecules [27]. For the insulin receptor, we used an antibody against the main regulatory three tyrosine motif (Y1175, Y1179, Y1180, inconsistent in the literature, we use the Uniprot entry P15208 as reference) in the cytoplasmatic C-terminus of the receptor, which control kinase activity of the IR [24]. IRS-1 couples IR kinase activity to the main intracellular kinase cascades. Both IRS isoforms expressed in liver, IRS-1 and IRS-2 [26], are extensively phosphorylated at dozens of tyrosines as well as serines and threonines [29]. However, in most cases the importance of individual sites is not well characterized. We chose an activating tyrosine (Y608) which is known to be important for the crucial IRS-1/PI3K interaction [260]. IRS-1 expression levels are very stable [29], while those of IRS-2 undergo strong fluctuations in response to fasting [72] as well as insulin signaling [71]. Therefore, we only targeted the isoform IRS-1 as analysis of IRS-2 phosphorylation would complicate matters considerably. Finally, we assess the activity of Akt by its phosphorylation status at serine 473. This is one of only two phosphosites tightly regulating Akt catalytic activity [261].

Both cell lines were stimulated for three different periods of time (4min, 20min and 40min) with three different insulin concentrations (1.5nM, 100nM and 1000nM). The lowest dose (1.5nM) reflects high physiological insulin concentrations. After a meal (postprandial) insulin levels in the peripheral circulation peak around 0.5nM [6] for humans. The concentrations are very similar in mice as determined by ELISA (personal communication with Dr. S. Neschen, IEG, HMGU). However, the pancreas secretes insulin into the pancreatic veins which drain into the portal vein leading to the liver. Therefore, insulin concentrations in portal vein blood can be two to three times higher than

Results

peripheral circulation levels [262]. Hence 1.5nM insulin mimics acute stimulation of the liver after a meal. In comparison, 100nM insulin was used as it is the most common insulin concentration used in cell culture stimulations. However it is supraphysiological and would lead to severe hypoglycemia in vivo. Additionally we used the very high 1000nM dose to see if signaling pathway activity could be saturated.
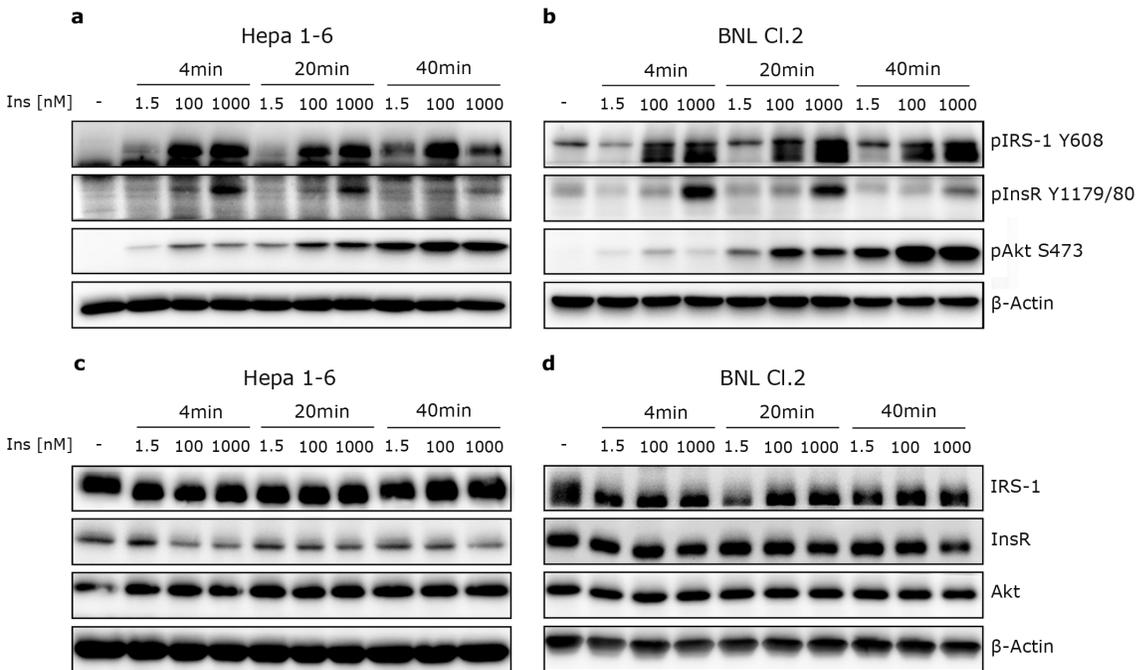
Figure 28. Physiological doses of insulin activate of IR, IRS-1 and Akt in hepatocyte cell lines.
Cells were seeded, starved and stimulated with insulin as described in 2.2.3.12. 10 µg lysate for each condition were separated by SDS-PAGE on 10% gels and blotted onto PVDF membranes. Phosphorylated and total proteins were detected on separate membranes. Bands were recorded with a digital developer at exposure times of 20s to 3min. Apparent MW were: pIRS-1/IRS-1: ~200kDa, pIR/IR: ~100 kDa, pAkt/Akt: ~55 kDa, β-Actin ~40 kDa. Representative example of three experiments.

We found that phosphorylation of all three proteins could be induced in the expected dose and time dependent manner in both Hepa 1-6 (Fig. 28a) and BNL Cl.2 (Fig. 28b). Moreover, the kinetic and extent of phosphorylation, assessed by band intensity, was very similar between both cell lines (Compare Fig. 28 a and b). IR and IRS-1 phosphorylation already occurred after 4min of stimulation and remained almost unchanged until 40min. The phosphorylation of IR at the highest insulin dose (1000nM) was an exception in this regard, as IR phosphorylation decreased from 20min to 40min. In contrast, Akt activation could first be observed after 20min and increased further until 40min. In addition, we note that IR and IRS-1 phosphorylation could be increased in a dose dependent manner from 1.5 to 1000nM insulin. In contrast, Akt activation did

increase from 1.5nM to 100nM but not from 100nM to 1000nM in both cell lines (Fig. 28 a, b). When comparing the total protein levels we found no differences in expression for IRS-1 or Akt under any experimental condition in Hepa 1-6 (Fig. 28c) or BNL Cl.2 (Fig. 28d). However, we noted slight differences in IR expression at very high (1000nM) insulin doses in Hepa 1-6 (Fig. 28c). While the insulin receptor is known to be internalized upon ligand binding, it usually is recycled to the plasma membrane rather than degraded [263].

We conclude that the insulin signaling pathway can be activated with high physiological insulin concentrations (1.5nM) and that activation of the pathway is saturated at the level of Akt at 100nM insulin. As expected, activation on this timescale involves changes in phosphorylation rather than expression. For further experiments we chose 40min as optimal time to see activation of all parts of the pathways targeted in our assay.

3.3.2 EETs boost insulin signaling by enhancing Akt activation without affecting IR or IRS-1 activation

In the next step we tested our working hypothesis with the established stimulation protocol by costimulating BNL Cl.2 cells with synthetic EETs. We used an equimolar 4µM EET mix, as concentrations necessary to induce effects on endothelial cells are in the low micromolar range [264, 265]. Liver EET levels have been investigated in only one study up to now. Here, the concentration of all isomers ranged from approximately 0.3 to 0.6 pmol per gram wet weight [266]. Assuming a water content of ~65% for mouse liver [267] this would translate to tissue concentrations ranging from 0.4-1µM, without taking extra- and intracellular compartments into account. Therefore, the concentrations used in the following experiments are very likely not far from the physiological range in mice.

In order to better control these experiments we could employ an LC-SRM based assay developed in the GAC at HMGU by Tobias Gaisbauer and Prof. Jerzy Adamski. This assay allowed absolute quantification of EETs, DHETs and arachidonic acid from cell culture supernatants and cell lysates. Initial pre-tests showed that all four EET isomers (5(6)-EET, 8(9)-EET, 11(12)-EET and 14(15)-EET) could be introduced into the stimulation medium in the necessary amounts, but that their concentrations in the culture medium were steadily declining. After 40min at 37°C, levels of all EET isomers were reduced to approximately 60%

Results

(data not shown). Nonetheless, we assumed these were sufficient levels for the timeframe of our stimulations.

We chose 40min and 60min for the duration of the stimulation and used high physiological (1.5nM) as well as supraphysiological (100nM) insulin doses. As there is evidence for an intracellular mechanism of EET action [244] we included an experimental condition were cells were pre-treated with the EET mix for 1h to allow the eicosanoids to accumulate in the cells. This was based on previous experiments that showed that 1h EET treatment led to measurable amounts of EETs in cell lysates (data not shown). The pre-treatment was conducted without phosphatase inhibitors in the medium to avoid false positive results.
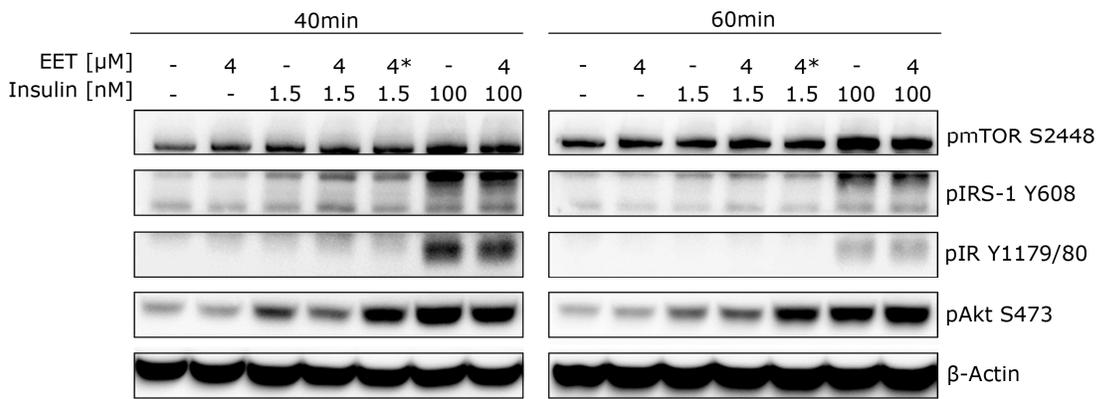
Figure 29. EETs enhance Akt activation through insulin in BNL Cl.2 cells.
Cells were seeded, serum starved and stimulated with insulin and/or an equimolar EET mix as described in 2.2.3.12. Irrespective of EET treatment, all wells contained DMSO at the same final concentration.10 µg lysate for each condition were separated by SDS-PAGE on 10% gels, blotted onto PVDF membranes and target proteins were visualized by immunodetection. Bands were recorded with a digital developer at exposure times of 20s to 1.5min. Representative example of two experiments. Asterisk (*) denoted cells pre-treated with 4µM EETs but without phosphatase inhibitors for 1h before the start of insulin stimulation.

We found that EET treatment alone did not result in Akt activation in the cell line after either 40 or 60min stimulation (Fig. 29, pAkt panels). However, EET treatment caused a marked increase in Akt phosphorylation at 1.5nM insulin when cells were pre-treated with EET (Fig. 29, pAkt panels, lanes marked with asterisk). This effect could not be observed when cells were not pre-treated or at supraphysiological insulin concentrations. In this regard, it is important to note that 100nM insulin caused maximal Akt activation in these cells (Fig. 28a, b). The boost in Akt phosphorylation at 1.5nM insulin through EET pre-treatment almost increased the phospho Akt signal to this maximal possible intensity at both 40min and 60min (Fig. 29, pAkt panels).

In contrast, we found no effect of EETs on insulin mediated IR activation at either concentration or time point (Fig. 29, pIR panels). However, we noted a small

increase in phospho IRS-1 at 1.5nM insulin though EETs at 40min (Fig. 29, pIRS-1 left panel). However, this small increase could not be reproduced in replicate experiments and was not visible after 60min of stimulation. EETs had not effect on IRS-1 phosphorylation at 100nM insulin (Fig. 29, pIRS-1 right panel). Additionally, we evaluated the effect of insulin and EETs on activation of mTOR, a second important kinase in the insulin signaling pathway. We found that 1.5nM was not sufficient to induce marked activation of mTOR phosphorylation over control levels. Stimulation with 100nM insulin was sufficient to induce mTOR phosphorylation but EET had not impact on this activation (Fig. 29, pmTOR panels).
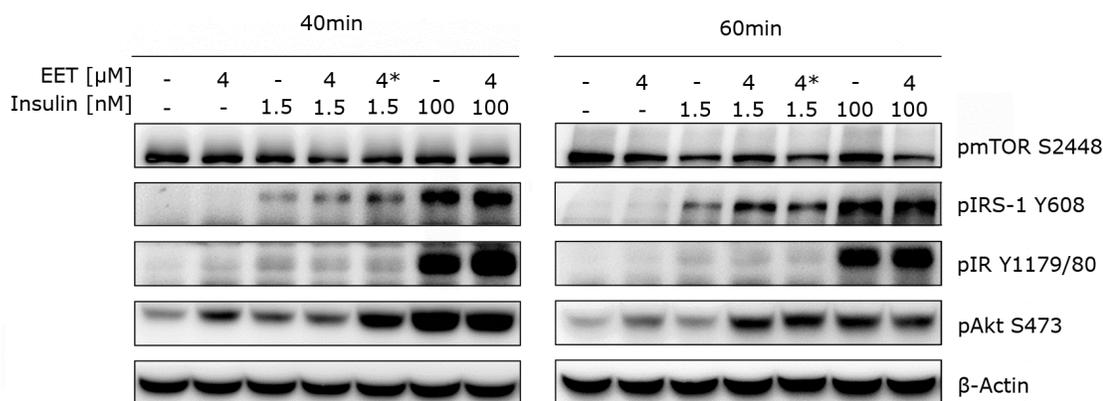
Figure 30. EETs enhance Akt activation through insulin in primary mouse hepatocytes.
Primary hepatocytes were seeded immediately after isolation, serum starved overnight and stimulated with insulin and/or an equimolar EET mix as described in 2.2.3.12. Irrespective of EET treatment, all wells contained DMSO at the same final concentration. 10 μg lysate for each condition were separated by SDS-PAGE on 10% gels and blotted onto PVDF membranes and target proteins were visualized by immunodetection. Bands were recorded with a digital developer at exposure times of 15s to 5min. Representative example of two experiments. Asterisk (*) denoted cells pre-treated with 4μM EETs but without phosphatase inhibitors for 1h before the start of insulin stimulation.

Next, we attempted to transfer these results to freshly isolated primary hepatocytes from normal diet fed C3H/FeJ mice. In this way, we could assess the effect of EETs on an experimental system, that was very close to the physiological situation in mouse liver. We used the same experimental conditions as described for the costimulation of the cell line.

We could confirm the strong increase in Akt phosphorylation at 1.5nM insulin through EETs (Fig. 30, pAkt panels). However, in contrast to the cell line, EETs alone could already induce Akt phosphorylation, and the boost in Akt phosphorylation at 1.5nM insulin was not restricted to pre-treated samples. The boost could also be observed after 60min treatment with both EET and 1.5nM insulin even without pre-treatment (Fig. 30, right pAkt panel). As in the cell line, EETs had no effect on IR or mTOR phosphorylation (Fig. 30, pIR and pmTOR

panels). However, in analogy to the results from BNL Cl.2 we noted a small increase in pIRS band intensity through EET costimulation at 1.5nM insulin (Fig. 30, pIRS panels). As in the cell lines this effect proved difficult to reproduce. We suspect that the effect size may be too small to be reliably quantified using western blots.

3.3.3 EET enzymes themselves have no impact on insulin signaling

Based on these results we concluded that EETs are indeed positive regulators of insulin signaling in hepatocytes, taking effect at the level of Akt, thereby proving our working hypothesis. As the initial results implicating EETs were based on observations of alterations of EET pathway enzymes, we next asked the question whether these enzymes themselves had an impact on insulin signaling. Ephx2 in particular could influence the phosphorylation cascade in cells as it has phosphatase in addition to epoxide hydrolase activity, with the different catalytic activities residing in the N- and C-terminal domains, respectively [268].

To address this question, we used an EET and arachidonic acid free cell system that allowed overexpression of EET pathway enzymes. As primary hepatocytes are very hard to transfect or transduce we used Hepa 1-6 cells. Insulin/EET costimulation of Hepa 1-6 showed that they were also susceptible to the boost of Akt phosphorylation at 1.5nM insulin (data not shown).

Arachidonic acid is an essential fatty acid (EFA) for mammals because it can only be synthesized from the EFA precursor linoleic acid through the PUFA synthesis pathway (see chapter 3.2) [269]. Therefore, it should be absent from cultured cells if they are deprived of EFAs. We used standard cell culture medium that did not contain any essential fatty acids. However, fetal calf serum is a potential source of EFAs. When cells were starved overnight, we were unable to detect arachidonic acid in their lysates (Fig. 31a, middle panel). For comparison 25fmol pure arachidonic acid gave a clear signal in this assay (Fig. 31a, left panel) demonstrating its high sensitivity. When free arachidonic acid was added to the medium of starved cells it could be readily detected again in lysates (Fig. 31a, right panel). In addition, no EETs or DHETs were detectable in starved cell lysates. Considering the fmol sensitivity of the LC-SRM assay we conclude that starved cells can be considered an arachidonic acid and EET free system.

Hepa 1-6 cells could be transfected with very high efficiency shown by a reporter construct driving GFP expression (Fig. 31b). We cloned the EET pathway

enzymes mEphx2a (murine Ephx2, long isoform a), Cyp2C29, Cyp2C50a (long isoform a), Cyp2C70 and Cyp2J5 from C3H/FeJ mouse liver into expression constructs using the Gateway system. Coding sequences were verified by restriction fragment analysis and complete sequencing of the open reading frames. Sequencing primers are enclosed in annex table A9. Endogenous Ephx2 was expressed at very low levels in Hepa 1-6 and a band of the right MW (60kDa) was readily detected using an Ephx2 antibody after transfection (Fig. 31c). As there was a lack of specific antibodies for individual Cyps, we generated N-terminal strep-flag (SF) tagged Cyp constructs and detected those with an anti-Flag antibody. We found that bands of the correct MW (55 kDa) could be detected after transfection of these constructs but not in empty vector transfected cells (Fig. 31d). We note that Cyp2C50a and Cyp2J5 were much stronger expressed than Cyp2C29 and Cyp2C70. This was surprising given that all Cyp constructs had been cloned to be expressed under the control of the strong CMV immediate early promotor and had the same translation promoting Kozak sequences fused to their translation start point. Interestingly, we noted double bands for the three Cyp2C enzymes. As the epitope was contained in the first amino acids of the N-terminus this would implicate either C-terminal processing or posttranslational modification of these enzymes. Note that the Flag western blot does not give information about endogenous Cyp2 expression. However, in parallel experiments we could not identify any of the Cyp2 enzymes using LC-MS/MS after membrane protein enrichment of a whole flask of Hepa 1-6 cells (data not shown).

Expression controls (Fig. 31 c, d) show the state 24h after transfection. We found that expression levels only marginally increased from 24h to 48h after transfection and decided that 24h were already sufficient in terms of transfection efficiency (Fig. 31b) and overexpression of target proteins (Fig. 31c, d). We tried to show the enzymatic activity of the transfected Cyps towards arachidonic acid but failed in doing so due to high levels of non-enzymatic oxidation of free arachidonic in the medium (data not shown). However, EET synthase activity has been shown for Cyp2C29, Cyp2C50 and Cyp2J5 from recombinant sources [270-272]. The results up to this point showed that the Hepa 1-6 cell system was ideal to isolate and study the effect of EET enzymes on insulin signaling. It could be depleted of arachidonic acid as well as EETs and overexpression was very successful considering that the great majority of cell was transfected and a sharp contrast in the levels of EET enzymes within cells could be induced.

Results
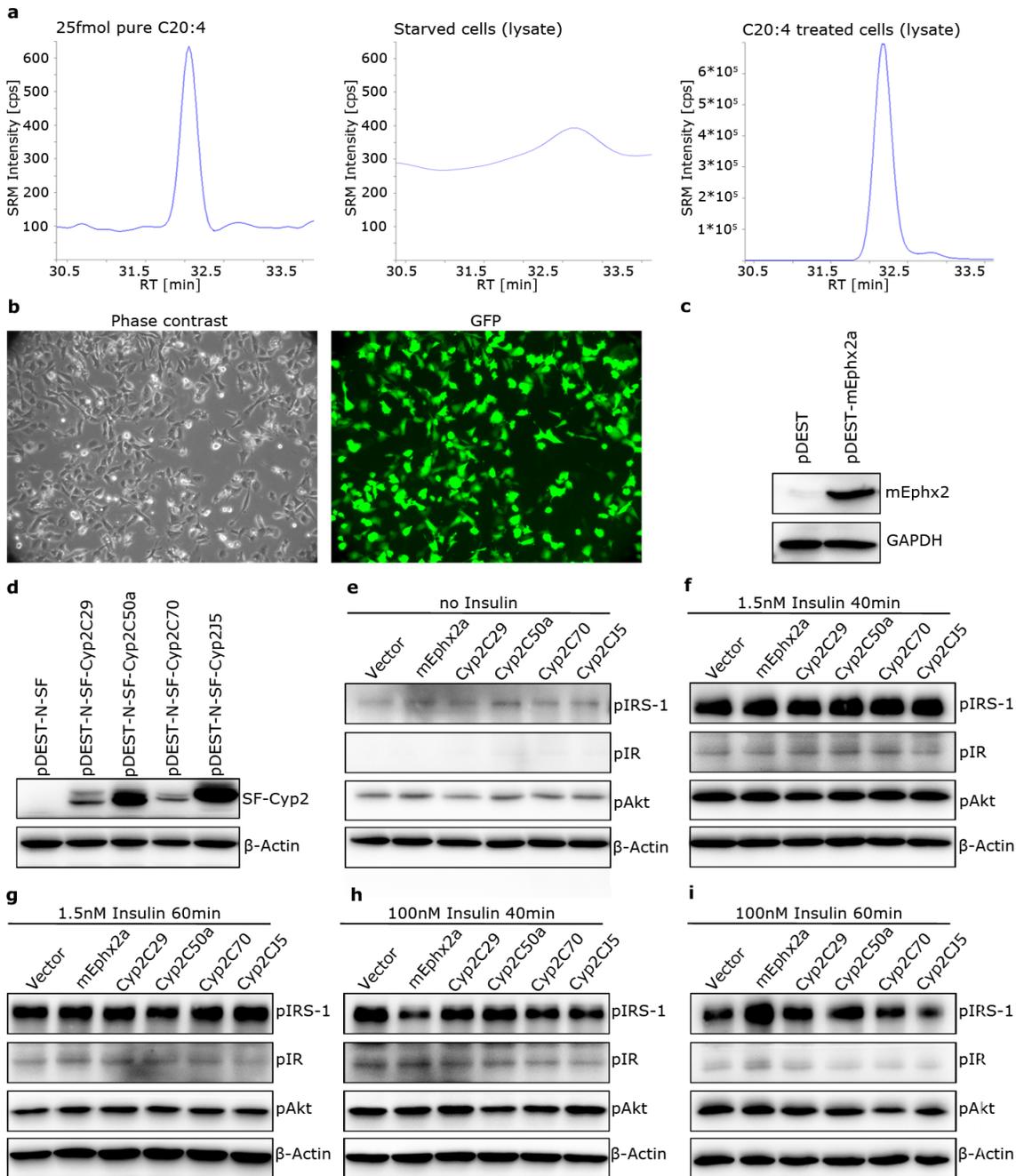
Figure 31. EET enzymes do not influence insulin signaling.
(**a**) Measurement of arachidonic acid (C20:4) content in Hepa 1-6 cells by LC-SRM. From left to right: 25fmol pure arachidonic acid, lipid extract of serum starved Hepa 1-6 cells, lipid extract of starved Hepa 1-6 cells treated with 150µM arachidonic acid for 1h. (**b**) Transfection efficiency. Hepa 1-6 cell were transfected using Lipofektamine with the reporter plasmid pCMV-GFP. Pictures were taken 24h after transfection. (**c**) Expression control of Ephx2. Hepa 1-6 cells were transfected with empty vector or the mEphx2a construct, harvested after 24h and Ephx2 protein detected by western blot with an Ephx2 specific antibody. (**d**) Hepa 1-6 cells were transfected with empty vector or constructs encoding N-terminal strep-flag (SF) tagged Cyp enzymes. Cells were lysed after 24h and SF constructs detected with an anti-Flag antibody (M2). (**e-i**) Hepa 1-6 were transfected with the empty vector or the indicated constructs, serum starved and stimulated with insulin 24h after transfection. Stimulation conditions are indicated above each panel. 10 µg lysate for each condition were separated by SDS-PAGE on 10% gels and blotted onto PVDF membranes and target proteins were visualized by immunodetection. Bands were recorded with a digital developer at exposure times of 15s to 8min. Representative example of two experiments.

We proceeded to conduct insulin stimulation of transfected, starved cells using the same conditions under which the effect of synthetic EETs was observed. We found no impact of any of the five studied EET enzymes in comparison to empty vector transfected cells on IRS-1, IR or Akt phosphorylation at baseline levels without insulin (Fig. 31e) at 1.5nM insulin after 40min (Fig. 31f) or 60min (Fig. 31g) as well as at 100nM insulin after 40min (Fig. 31h) or 60min (Fig.31i).

We conclude that even with exhaustive measures taken, no impact of the EET enzymes mEphx2a, Cyp2C29, Cyp2C50a, Cyp2C70 or Cyp2J5 could be observed. These results show that the impact of the EET pathway on insulin signaling is conferred by the eicosanoids themselves and imply that the role of the EET enzymes lies in regulating the levels of the eicosanoids rather than a direct influence on signaling.

3.3.4 Glycogen synthesis in cell culture enables the study of the effect of insulin on glucose homeostasis

Finally, we wanted to explore whether EETs would have a functional impact on glucose metabolism of hepatocytes. This aim proved difficult to achieve, hence only the setup of an experimental system to study this question will be presented.

Insulin induces a metabolic state in hepatocytes that is characterized by the activation of all pathways leading to reduction of intracellular glucose levels. This comprises activation of glycolysis and glycogen synthesis as well as inhibition of gluconeogenesis and glycogen breakdown [27]. This reduction in intracellular glucose (more precisely glucose 6-phosphate) levels leads to increased influx of glucose. In contrast to muscle and adipose tissue there is no translocation of the glucose transporter GLUT4 [273] (hepatocytes express GLUT2 instead) and change in transport capacity of the membrane.

Attempts to measure the disappearance of glucose from customized culture medium or uptake of 2-deoxyglucose, which is a measure of transport capacity of the membrane, failed because they could not be stimulated by insulin treatment (data not shown).

Assays to dissect individual pathways were needed. Measurement of glycolysis and gluconeogenesis involve very complicated or hazardous assay [274]. We opted for the measurement of glycogen synthesis. For this purpose we used the enzymatic amyloglucosidase (AG) assay [202].

Results

Initial tests showed that our implementation of the assay could accurately quantify glycogen amounts up to 400µg per sample, even in the background of a cellular lysate (Fig. 32a), which is more than sufficient for the ng glycogen/µg protein amounts usually present in hepatocytes [275]. Moreover, we could show that intracellular glycogen content in Hepa 1-6 cells could be slightly repressed by glucagon and markedly increased by insulin (Fig. 32b). The high physiological dose of 1.5nM insulin was already sufficient to induce a marked effect.

Application of this assay to study the impact of EET/Insulin costimulation on hepatic glucose homeostasis is pending.
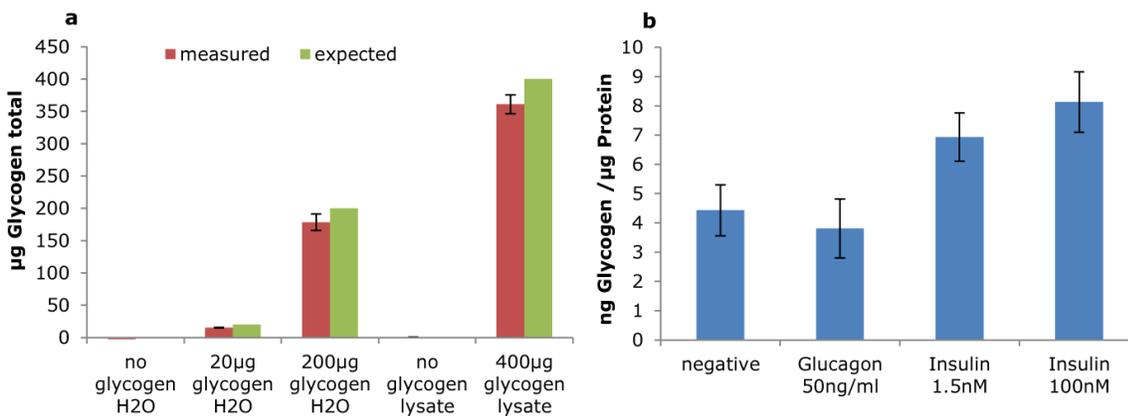
Figure 32. Insulin induced glycogen synthesis can be measured using the AG assay. (**a**) Glycogen assay development. 0, 20 and 200µg glycogen were digested and quantified using the amyloglucosidase assay. Glycogen content in a Hepa 1-6 cell lysate was determined with or without spiking 400µg glycogen. (**b**) Hepa 1-6 cells were seeded on six well plates starved overnight and treated with either 50ng/ml glucagon, 1.5nM insulin or 100nM insulin for 5h. Glycogen content was normalized to protein concentration. Bars show mean±SD for three biological replicates. Representative example of three independent experiments.

4. Discussion

4.1 Improvement of existing non-targeted and targeted proteomic strategies

4.1.1 Conceptual refinement of the application of discovery proteomics to T2D and its technical implementation

A variety of different proteomic studies of primary organs involved in T2D from mouse models or patient samples have been published (Table 8). In the present work, discovery proteomics was used with the aim of finding a new pathway associated with insulin resistance and with a functional impact on the physiological effect of insulin in a diet induced T2D mouse model. In order to achieve this goal the discovery strategy of earlier works was refined in three substantial points, contrasting it to previous proteomic studies of T2D. First, the mouse model used in this study was subjected to thorough phenotypic characterization. Development of insulin resistance was monitored using the state of the art hyperinsulinemic-euglycemic clamp technique by our collaboration partners Dr. Susanne Neschen and Melanie Kahle. In this way, the onset of insulin resistance in relation to the development of obesity could be determined. Moreover, insulin induced peripheral glucose utilization (muscle and WAT) could be evaluated separately from inhibition of endogenous glucose production (liver). Second, proteomic changes in liver could be determined in a time resolved manner, including changes before onset of hepatic insulin resistance, as well as correlation of expression changes with the severity of insulin resistance. Almost all other studies (with the exception of [276] and [277]) have been snapshots at one time only, with the timing mostly determined by glucose tolerance test, which gives only superficial information about the dynamic of glucose homeostasis and insulin action compared to clamp experiments [278].

Third, most studies have relied on a relatively small sample size, mostly four versus four comparison of diabetic and control subjects (Table 8). This stems from the fact that 2D-gel studies are difficult to conduct with many replicates due to reproducibility problems and LC-MS/MS based proteomic analyses often strive to maximize proteome coverage through fractionation at the cost of throughput of biological replicates. The issue of sample size for discovery analyses was

investigated for RNA microarray studies which used statistics similar to discovery proteomics [279]. The authors compared 16 microarray studies with up to 50 replicates with a resampling procedure forming smaller datasets to evaluate apparent statistical power and recovery of results when replicates were removed. They showed that the increase in apparent statistical power in relation to the number of biological replicates is most prominent between five and ten replicates and that five replicates is the minimum requirement for stable datasets [279]. At least six and, if possible, up to eight animals per group were used in this study for each time point. While this is still not a satisfactory group sizes for accurate statistics it is more appropriate for a dietary mouse model. In fact, this study led to the generation of the largest proteomics dataset for a T2D model in terms of mice included in the study. We used 68 mice in total, with the next largest study in this regard being Sabido et al [277] with 36 mice.

These conceptual considerations led to requirements for the discovery proteomics workflow in terms of accuracy and reproducibility as well as consistency of generated datasets. In the first part of this thesis a label-free workflow without fractionation was compared to an ICPL workflow with fractionation for this purpose. Both workflows delivered comparable proteome coverage, accuracy and reproducibility. The ICPL workflow generated slightly better results concerning these three characteristics but a large discrepancy concerning the consistency of datasets was found. While label-free proteomics generated highly consistent datasets, the consistency of datasets for the ICPL approach decreased with increasing number of biological replicates. Moreover, the proteome coverage of the label-free datasets increased with increasing number of replicates through matching and pooling of MS/MS spectra. Up to now most LC-MS/MS proteomics studies of T2D have used the iTRAQ isotopic labeling strategy although two recent studies also employed label-free quantification [280, 281]. In summary, the label-free concept without fractionation was found to be a superior analysis strategy for this study considering 68 mice needed to be analyzed.

The unsatisfactory performance of the isotopic labeling strategy at high numbers of replicates in this study was most likely due to the process of generating overlaps of identified proteins from randomly sampled LC-MS/MS runs for each replicate. These overlaps get progressively smaller with increasing numbers of replicates. Theoretically, the same problem should have arisen with any other type of isotopic labeling strategy, also for instance with SuperSILAC [282]. This

outcome has important implications for the upcoming field of clinical proteomics [148]. The inherent flaw of isotopic labeling designs, which manifests with increasing numbers of biological replicates needs to be considered for higher throughput human or mouse studies. Strategies to overcome this problem for isotopic labeling shotgun proteomics could implement the concept of matching LC-MS/MS runs and gathering MS/MS spectra based identifications in a cumulative manner, which is an inherent feature of label-free analysis. Our own attempts to implement this in the flexible OpenMS environment [283] have so far been unsuccessful. In this context it is should be pointed out that this would not affect SRM based targeted proteomics strategies and is unlikely to be a problem for SWATH [284] approaches.

4.1.2 Increased sensitivity of targeted proteomics

In the present study we adapted the concept of SRM based targeted proteomics by assaying proteins already implicated in T2D through other lines of evidence (Table 5). A T2D liver SRM panel was successfully developed and it could be shown that our assay development was state of the art in comparison to recently published works with similar instrumentation, e.g. [226].

As the targeted proteins were selected without consideration for their abundance in liver tissue, the sensitivity of standard workflows was not sufficient to quantify all proteins of interest. This problem could be solved completely through the use of peptide fractionation, a technical solution that fits very well to the use of isotope labeled peptide standards [167, 180], which have become the gold standard for quantification for SRM assays. In addition, OGE was found to be the method of choice for the peptide fractionation in combination with SRM. This could be attributed to its very high resolution, good loading capacity, predictability of fractionation results and ease of coupling to the LC-MS system.

The necessity for fractionation of plasma samples in order to access low abundance proteins by SRM had already been recognized [227]. In contrast, results from single cell organisms like, yeast [171] and bacteria [285, 286] have shown convincingly that quantification of proteins of all abundance levels in these cells can be achieved using SRM without fractionation. Because these studies were carried out with LC systems very similar to the one used here, in terms of column dimensions and bead size, it is surprising that the need to fractionate mammalian tissue samples was found.

Discussion

An explanation for these results may be connected to the fact that while liver samples do not have the extreme dynamic range (10^{10}) found in plasma [136], they contain a much higher number of different proteins. Specifically, more than 6700 proteins and more than 10.000 transcripts have been found in human liver up to now [203]. In contrast, only 4399 proteins have been found in yeast [153], which may explain why fractionation prior to SRM is beneficial for robust quantification in mammalian tissue.

As the SRM technology matures, improvements in MS performance, ionization efficiency and ion transfer from the source to the instrument may extend the capabilities of the SRM approach in this respect. By the same token, improvements in the resolution of the reverse-phase chromatographic separation may provide an additional boost to achieve the required sensitivity. This could be achieved, for instance, by increasing the efficiency of the analytical column (longer column, smaller beads) or working without a trapping column. However, these improvements will take time and usually come at a substantial price for new generation equipment. In the present work, it could be shown that extension of the separation-space of the SRM approach by an additional dimension of peptide separation is an effective and reliable way to achieve the same result with OGE being the method of choice.

4.2 Saff-diet feeding influences known as well as novel HFD influenced pathways

The investigation of the saff-diet model led to the description of regulated pathways before and after the onset of hepatic insulin resistance. In the following section, the regulated pathways (Table 6) will be discussed and compared to the results of previous studies (Table 8). Comparison of different proteomic studies is complicated by the use of different models, techniques and criteria for identifying regulated proteins. For comparison of different studies, regulated pathways are reported rather than individual regulated proteins. Priority was given to pathways the authors themselves deduced from their datasets and if this was not the case a pathway is listed as regulated if at least four proteins belonging to it were regulated in the same direction (i.e. up- or downregulated). The majority of studies were conducted in mice with either HFD feeding or genetic models. It is important to keep in mind that HFDs used in different studies are not the same but differ in their individual compositions. The genetic models utilized the most are *lep/lep* and *db/db*.

120

Ref	n	#Proteins	Technique	Model	Tissue	Regulated Proteins/Pathways
[287]	4	25/25	2D Gel (Silver)	lep/lep mice	Liver WAT Muscle	Anxa2 (WAT), **TCA** (M), Cps1, Aldh1L1, Aldh2, Ahcy Fabp1, Gnmt, Dct (L)
[288]	4	6/20	2D Gel (Silver)	HFD in BL6 mice	Liver WAT Muscle	Selenbp1 (L), Atp5a1(M), Uqcrc1 (WAT)
[289]	4 vs. 5	41/58	2D Gel (Sypro)	lep/lep mice	Liver	**β-oxidation, FFA synthesis, Glycolysis, Amino acid degradation**
[290]	3	12/12	2D Gel (DIGE)	HFD in BL6 mice	Liver	Khk, Hmgcs2, Mat1a, ApoE, Selenbp2, Mup1, Stfa3
[280]	5	95/698	LC-MS/MS (label-free)	db/db mice	Liver	**Ribosome, ER stress**
[277]	3*	n.a./144	LC-SRM (AQUA)	HFD in BL6 mice	Liver	**β Oxidation, Ketogenesis, FFA synthesis, Glycolysis, Glycogen synthesis**
[291]	3	92/913	LC-MS/MS (iTRAQ)	HFD in BL6 mice	Liver	**Oxphos, TCA, Amino acid degradation, FFA metabolism, Retinol metabolism**
[276]	3*	4/4	2D Gel (Sypro)	HFD in BL6 mice	Pancreas	Reg1, Reg2
[292]	2**	159/590	LC-MS/MS (iTRAQ)	MKR mice	Pancreas	**Protein biosynthesis, ER stress, Insulin secretion, Oxphos**
[293]	6 vs. 9	11/11	2D Gel (Silver)	T2D patients	Muscle	Pgm1, Myl2, Atp5B, CKB, Col6a1
[294]	10	44/107	2D Gel (Sypro)	T2D patients	Muscle	**Glycolysis, Oxphos, TCA**
[281]	8	15/400	LC-MS/MS (label-free)	T2D patients	Muscle	**Proteasome, Protein folding, Oxphos, Actin cytoskeleton**
[295]	3**	12/2832	LC-MS/MS (iTRAQ)	T2D patients	Myotubes	ApoA1 Ada Aldh1b, Myh2,3&8, Tnc, eIF-4a, Capg, Fabp3
[296]	4	9/21	2D Gel (Sypro)	HFD in HSD$^{-/-}$	WAT	Clic1, Capg, Fth1, Aldh2, Acads, Ivs, Ppa1

Table 8. T2D discovery proteomics studies.
Listed for each study from left to right are: sample group size (n), regulated proteins/identified proteins, technical approach, T2D model, investigated tissues and regulated pathways. Pathways are indicated by boldface. Up- and downregulation are indicated by green and red font, respectively. * time course data ** each sample was a pool of 8-10 biological samples. Studies on end organ damage like diabetic nephropathy are not included.

4.2.1 Oxidative phosphorylation

The earliest change we could find was repression of enzymes of oxidative phosphorylation (Oxphos), which could be observed already after two days of saff diet feeding and was associated with ultrastructural changes of mitochondria

after two and three weeks of saff-diet feeding [173]. All subunits of the five Oxphos complexes were found downregulated. Strikingly, none of these changes were found at the transcript level (personal communication Dr. Susanne Neschen, IEG; concerning the transcriptomics dataset from [233]). Oxphos is the pathway most often found regulated in T2D proteomic studies. Downregulation of Oxphos has been found in three proteomic studies of skeletal muscle biopsies from T2D patients [281, 293, 294]. A fourth study found no changes in Oxphos enzymes, which may be attributed to the fact that cultured myotubes instead of biopsies were used [295]. Interestingly, Oxphos downregulation was also found in a proteomic study of pancreatic islets from MKR mice [292]. These mice have a dominant negative IGF-1 receptor mutation in skeletal muscle and are insulin resistant without a primary pancreas defect. Upon ultrastructural investigation of these islets, similar structural changes to the saff-diet were found [297]. Proteomic studies of WAT have only been conducted with 2D-gel based approaches and are thus limited in the number of proteins identified. Nonetheless, one out of three proteomic 2D-gel studies of WAT [287, 288, 296] found Uqcrc1, a subunit of complex III, downregulation through HFD [288]. In the case of liver, only one of seven studies [277, 280, 287-291] found alterations of Oxphos [291]. Interestingly, these authors found Oxphos upregulation, contrasting this finding to the results from all studies in different organs mentioned above which described downregulation of Oxphos. A possible explanation may be that in this particular study isolated liver mitochondria instead of tissue homogenates were used.

Impaired mitochondrial substrate oxidation is being discussed in the context of HFD mediated hepatic insulin resistance but currently there is no consensus as to its role and significance [298]. Studies on substrate oxidation of HFD modified mitochondria in the safflower oil diet model showed no differences to control mitochondria (personal communication Dr. Susanne Neschen, IEG). In addition, the finding of altered mitochondrial structure through HFD by our collaboration partners and others raises the question whether downregulation of Oxphos may be an indicator of a remodeling process and may be secondary to presently unknown changes happening on the subcellular level. In light of this speculation it is interesting that the one study that used isolated mitochondria instead of liver homogenates [291] found up- rather than downregulation of Oxphos. Further investigation of the influence of HFD on mitochondrial structure,

respiratory activity and protein expression will be needed in the future to more clearly define which processes intrinsic to mitochondria are affected by HFD.

4.2.2 Fatty acid metabolism

Fatty acid anabolic and catabolic pathways are of major interest in the context of the metabolic syndrome and T2D. In the present study an induction of mitochondrial as well as peroxisomal β-oxidation enzymes was found. As shown in Results this induction affected enzymes involved in the breakdown of long unsaturated fatty acids most prominently. Other proteomic studies of liver tissue also found induction of β-oxidation through HFD or in *lep/lep* mice [277, 289, 291]. A surprising outcome of our study was the observation of increased synthesis of a subgroup of unsaturated fatty acids - PUFAs. Interestingly, fatty acid anabolic processes were also found upregulated together with β-oxidation in the above mentioned studies. Alterations of fatty acid synthesis or breakdown were not found by any proteomic study of pancreas, muscle or WAT.

4.2.3 Ribosomes

After one week of saff-diet a rather pronounced induction of ribosomal proteins was observed in the saff-diet study. However, this was transient and many of the ribosomal proteins returned to baseline levels after three weeks of saff-diet. While ribosomal changes seem to play a minor role in the saff-diet model and are not correlated with insulin resistance, downregulation of ribosomes has also been observed in the livers of HFD-fed mice in a different proteomic study [280] and upregulation was found in pancreatic islets of MKR mice [292]. Insulin has an established role in stimulating ribosome activity and translation through phosphorylation by the bifurcated pathway downstream of mTORC1 shown in 1.2.2. This effect is mediated by activation of p70S6 kinase [52] and inactivation of the translation initiation inhibitor 4E-BP1 [53]. Moreover, insulin plays a role in regulating whole body protein content as well as regulation of ribosome biogenesis [299]. However, a tracer study on the effect of short-term insulin withdrawal on ribosome biogenesis in rats found only very small effects on synthesis and degradation of ribosomal proteins in liver. In contrast, a substantial reduction in ribosomal content could be induced in muscle in the same study, which was mainly attributed to increased degradation [300]. Effects of ribosomes on hepatic insulin resistance seem unlikely and may be a side product of disturbed insulin signaling.

4.2.4 Ascorbate and retinol metabolism

Pathway enrichment analysis also outlined changes in the metabolism of vitamin A (retinol) and C (ascorbate). Closer examination of affected enzymes showed downregulation of different pathways of retinoic acid biotransformation, while for ascorbate the synthesizing pathway from UDP-glucose was downregulated (in contrast to primates, rodents are able to synthesize ascorbate [301]). One additional proteomic study of HFD induced alterations in liver also identified repression of retinol metabolism [291]. The common function of both vitamins is their ability to scavenge reactive oxygen species and work as antioxidants. Oxidative stress has long been a suspect in the pathogenesis of T2D [302]. This is based on observations from multiple mouse studies showing that the administration of the diabetes inducing drugs streptozotocin (STZ) and alloxan as well as hyperglycemia reduces the concentration of antioxidants like ascorbate or glutathione and increases markers of oxidative stress like lipid peroxidation degradation products [303]. Both STZ and alloxan are β-cell toxins that specifically destroy insulin producing cells. Therefore, STZ or alloxan treated rodents resemble T1D rather than T2D. Besides, STZ and alloxan themselves produce ROS to damage β-cells [304]. Despite a clear association of reactive oxygen species and T2D, no clear evidence of their functional impact on glucose metabolism or a causative relationship to the disease could be discovered [302, 303]. Translation of these findings to T2D patients showed reduced ascorbate levels [305] in patients but ambiguous results concerning alterations in retinol levels [306, 307]. Attempts to use ascorbate in the treatment of T2D have not been successful. Ascorbate supplementation rescued the diabetes induced decrease in ascorbate plasma levels in STZ mice but did not reduce the generation of malondialdehyde, a marker for membrane lipid peroxidation [308]. Similarly, ascorbate supplementation normalized ascorbate plasma levels in T2D patients, but had no beneficial effect on glucose levels [305]. Follow-up on alterations in antioxidant homeostasis in T2D do not seem promising.

In contrast to ascorbate, retinoids (retinol and its oxidation products retinal and retinoic acid) have a variety of additional functions in addition to its antioxidant properties, the most prominent being its function in the vision cascade. Retinoids are ligands of the nuclear retinoic acid receptors (RAR) and retinoid X receptors (RXR) and influence gene expression in a variety of different tissues during development and during adulthood [309], when its known functions include modulation of the immune system and cell differentiation [310]. Interestingly,

RXR is also an important coactivator for PPAR transcription factors regulating lipid metabolism [309]. As stated above, differences in plasma levels of retinol were only found in some studies of T2D patients. Dietary retinoids are primarily stored in dedicated stellate cells in the liver (also called Ito cells). The availability of retinoids in the organism is regulated by their export from the liver by specific retinoid binding proteins (RBPs) [310]. An impressive discovery study found upregulation of RBP4 in adipose tissue of mice with secondary muscle and liver insulin resistance through WAT specific GLUT4 knock-out [311]. The authors could show that HFD induced diabetes in wild type mice was associated with increased RBP4 plasma levels, which could be normalized by a retinoid antagonist. Injection of RBP4 into mice could influence insulin signaling in muscle negatively, while knock-out of RBP4 had the opposite effect [311]. Furthermore, transgenic expression of RBP4 from muscle could cause insulin resistance in muscle and influence gluconeogenesis in hepatocytes [311]. Moreover, they found a similar increase in RPB4 plasma levels in human T2D patients [311]. A more detailed study in a human cohort of T2D patients showed that RBP4 levels correlated closely with the extent of insulin resistance as well as BMI and serum TG levels [312]. The mechanism of these effects is not known but it raises the question whether they are mediated the influence of RBP4 on the distribution of retinoids between liver, muscle and WAT or a different, unknown function of RBP4. Taken together possible effects of retinoids on hepatic insulin sensitivity seem an interesting alternative angle for future follow up studies.

4.2.5 Primary bile acid synthesis

The primary bile acids cholic acid and chenodeoxycholic acid are synthesized from cholesterol through the parallel classical and alternative pathways in hepatocytes. Following conjugation with amino acids they are secreted into the intestinal lumen via the bile ducts [313]. Bile acid synthesis is regulated at the first enzymatic step in both pathways. Both rate-limiting enzymes Cyp7A1 (classical pathway) and Cyp27A1 (alternative pathway) as well as other synthesis enzymes were found downregulated through saff-diet feeding in this study, which points to a disturbance in bile acid homeostasis. This seems counterintuitive as an increased bile acid pool may be necessary to properly digest the HFD.

After digestion, bile acids are reabsorbed by the intestine and extracted from portal vein blood by the liver. This mechanism of synthesis and reabsorption has

two consequences. First, the bile acid pool is subject to enterohepatic circulation, i.e. continuously circulating between liver and intestine [313]. Second, a small proportion of bile acids escapes extraction from portal vein blood and enters systemic circulation. Therefore, bile acid concentrations in human serum are fluctuating between 5 and 15 µM during the day [314]. It was recognized recently that bile acids are not only crucial for lipid digestion but also exert multiple hormonal functions. The first evidence that bile acids may have an effect on glucose homeostasis came from T2D patient studies in which sequestration of bile acids in the intestine lowered blood glucose. This effect could be confirmed in multiple clinical studies [315]. While the underlying mechanism is not understood, modulation of signaling and gene expression through bile acids at multiple levels has been discovered. Bile acids activate the nuclear farnesoid X receptor α (FXR-α) as well as the transmembrane G-protein coupled receptor (GPCR) TGR5 [315]. Both receptors are prominently expressed in liver and intestine [316]. FXR-α mediates the feedback inhibition of bile acid synthesis through Cyp7A1 repression but also influences plasma TG content and lipoprotein composition by lowering LDL and increasing HDL through multiple mechanisms [315]. TGR5 has been shown to modulate cellular signaling at the stage of AC [317], MAPKs (ERK, JNK, p38) and epidermal growth factor receptor (EGFR) activation [316].

Increasing evidence characterizes bile acids as potent modulators of glucose and energy homeostasis. They were shown to increase energy expenditure in muscle and brown adipose tissue by increasing thyroid hormone activation through activation of deiodinase D2 [317]. Furthermore, they stimulate secretion of the incretin GLP-1 [318] and improve hepatic insulin signaling and glucose tolerance in *lep/lep* mice [319]. This could be attributed to improved hepatic insulin sensitivity using hyperinsulinemic-euglycemic clamps [320]. The FXR-α knock-out mouse is insulin resistant and an FXR-α agonist could improve insulin signaling in 3T3-L1 adipocytes [320]. Interestingly, FXR-α knock-out mice have normal hepatic insulin sensitivity, implying the TGR5 dependent pathway in improved hepatic insulin sensitivity though bile acids. This is surprising, given that TGR5 increases cAMP, thus mimicking glucagon or catecholamine stimulation. Bile acids were shown to reduce the expression of SREBP-1c and its target genes through FXR-α activation in mouse liver [321]. This could cause an insulin sensitizing effect, as increased nuclear SREBP-1c has been demonstrated to cause insulin resistance [72]. Multiple studies have investigated the effect of

bile acids on hepatic gluconeogenesis, but the results have been ambiguous [316].

The observed repression of both rate-limiting enzymes Cyp7A1 and Cyp27A1 may be attributed to different affected pathways in our model. Cyp7A1 expression is suppressed by insulin [322], bile acids themselves [316] as well as PPAR-α [323]. The concerted repression of the PPAR-α target genes Cyp7B1, Cyp27A1 and Cyp8B1 [323], all involved in bile acid synthesis indicates that PPAR-α may be the determining factor. On the other hand, a study on liver-specific disruption of the insulin receptor in mice found downregulation of the same four Cyps, partly mediated by the insulin regulated transcription factor FOXO1 [324]. In this model the insulin signaling defect alone was sufficient to downregulate bile acid synthesis and predisposed the mice for gallstone formation. Given the strong association of bile acids with glucose and lipid metabolism as well as basal metabolic rate this pathway seems another prime candidate for further investigation. Bile acid sequestrants are used to treat dyslipidemia and have the additional beneficial effect of lowering blood glucose [315]. It would be highly interesting to evaluate the bile acid pool in saff-diet fed mice, which would unfortunately be complicated by their enterohepatic circulation. In addition, targeting bile acids in future investigation will have the drawback that endogenous synthesis is tightly regulated through a feedback inhibition mechanism [313].

4.2.6 Steroid hormone metabolism

The identification of steroid hormone metabolism as enriched pathway is problematic. This stems from the fact that KEGG integrates multiple synthesis and degradation pathway (sex hormones, gluco- and mineralocorticoids) from different tissues (gonads, adrenals, liver) in one scheme. The overall effect would appear to be repression of sex hormone degradation, but on closer examination even this conclusion is difficult. Hsd3b5 is exclusively expressed in male liver and has been shown to inactive dihydroandrostendione, although the physiological relevance of this is not known [325]. Hsd3b5 is repressed by PPAR-α [326], which is in line with PPAR-α activation in the saff-diet model. Similarly, Hsd17b2 inactivates 17β-estradiol *in vitro* [327] but a Hsd17b2 transgenic mouse did not display signs of estrogen deficiency and had dysfunctional testicles [328]. This phenotype could be partly rescued by a retinoic acid receptor agonist, strongly implying Hsd17b2 in retinoic acid metabolism rather than sex hormones [328].

Discussion

Hsd17b7 was shown to have an essential role in cholesterol synthesis by a yeast complementation study [329] and the severe phenotype of the Hsd17b7$^{-/-}$ mouse makes it very likely that this is its primary function [330]. Interestingly, Hsd17b7 is upregulated by SREBP-1 [331], indicating SREBP-1 activation in the saff-diet model. The Ugt isoforms and Comt are biotransformation enzymes which such broad substrate specificity that they are not indicative of changes in steroid metabolism. In summary, it is not possible to make conclusions about steroid hormone metabolism as a pathway, but the regulation of individual enzymes through the saff-diet showed interesting connections to retinoid metabolism and the transcription factors PPAR-α and SREBP (see 4.3.1).

4.3 Saff-diet feeding induces a biphasic disturbance of the PUFA and EET pathways

One of the reasons the EET pathway was chosen for functional validation was its connection with the PUFA synthesis pathway, which itself was regulated. However, PUFA synthesis pathway alterations preceded EET pathway changes and insulin resistance. Therefore, the biphasic response of these two pathways is highly interesting, as it connects the causative agent to the disease relevant outcome. While observational studies, like the proteomic survey presented here, cannot determine causality by definition, it is nevertheless interesting to discuss how these two pathways may connect saff-diet feeding to hepatic insulin resistance. It should be noted however, that this is by no means an attempt to explain the whole phenotype of this T2D mouse model, but should rather be seen as a novel mosaic piece in the challenging investigation of diet induced insulin resistance.

4.3.1 PUFAs influence lipid and carbohydrate metabolism through modulation of transcriptional master regulators

The upregulated enzymes of the PUFA synthesis pathway regulated after one week of saff-diet were Fads1 and 2 as well as Elovl2 and 5. They are responsible for the synthesis of essential long unsaturated fatty acids of the ω-6 and ω-3 series [238]. For each fatty acid the carbon (C_1) of the carboxyl group is designated α and the one at the end of the aliphatic chain ω (C_n). The distance of the last double bond from the ω-carbon is used to indicate the configuration of unsaturated fatty acids. Animal cells are limited in the distance from the ω atom they can introduce double bonds in. ω-7 and -9 fatty acids but not ω-6 and ω-3

fatty acids can be synthesized *de novo* [269]. This is due to the elongation and desaturation mechanism. Elovl enzymes introduce two carbons at the α-carbon and Fads enzymes introduce double bonds at carbons 5, 6 and 8 only. Therefore longer fatty acids with more than two double bonds can only be synthesized from appropriate precursors, mostly from C18:2 ω-6 and C18:3 ω-3 for the ω-6 and ω-3 series, respectively [238]. Lipids in the safflower oil diet are composed to more than 60% of linoleic acid, the ω-6 precursor. However, the diet contains only trace amounts of α-linolenic acid (C18:3 ω-3), the ω-3 precursor or its derivates [73, 332]. Note that the essential precursors are PUFAs themselves.

PUFAs are the natural ligands of one of the master regulators of lipid metabolism – PPAR-α. In contrast to synthetic agonists used to treat dyslipidemia, particularly fibrates, they mediate only low grade activation of PPAR-α [333]. Although ω-3 PUFAs have been shown to activate PPAR-α stronger than ω-6 PUFAs [333], linoleic acid (C18:2 ω-6) and arachidonic acid (C20:4 ω-6) both can activate PPAR-α reporter constructs [334]. In contrast to PPAR-γ in WAT, PPAR-α in liver does not mediate fatty acid storage as TG but rather directs them towards breakdown in β-oxidation [83]. Surprisingly, PPAR-α induces Fads enzymes [239, 335], thereby generating a positive feedback loop for PUFA synthesis (Fig. 33). This feedback loop is modulated by PPAR-α downregulation through food intake [239] and increase in blood glucose levels [333] as well as a second master regulator of lipid metabolism – SREBP-1c. SREBP-1c is a transcription factor with a complex maturation process which is modulated by metabolic inputs (food intake, hyperglycemia, saturated fatty acids and insulin) at multiple levels [51] (Fig. 33). Although SREBP-1c also induces Fads expression, the levels of active nuclear SREBP-1c is negatively regulated by PUFAs [336], generating a negative feedback loop. PPAR-α and SREBP-1c are the two main regulators responsible for the PUFA elongation and desaturation activity [83, 333]. Although both induce the pathway, they can be considered antagonists in lipogenesis as they also mediate opposing effects on the synthesis of unsaturated and monounsaturated fatty acids, with SREBP-1c inducing lipogenesis [83].

The importance of the SREBP-1c inhibitory input was demonstrated using PUFA rich diets, which inhibited Fads1 and 2 expression in mouse liver. This effect was abolished in SREBP-1 transgenic mice [239]. Elovl5$^{-/-}$ mice are an instructive example of the potency of the PPAR-SREBP-PUFA circuit. In addition to increased linoleic acid and reduced arachidonic acid levels these mice developed

Discussion

hepatosteatosis, which was shown to be caused by unchecked SREBP-1c activation [240]. Paradoxically, the knock-out of a lipid synthetic gene caused fatty liver due to excessive lipid synthesis induced by SREBP-1c, which could be rescued by administration of arachidonic acid (C20:4 ω-6) or C22:6 ω-3 [240].
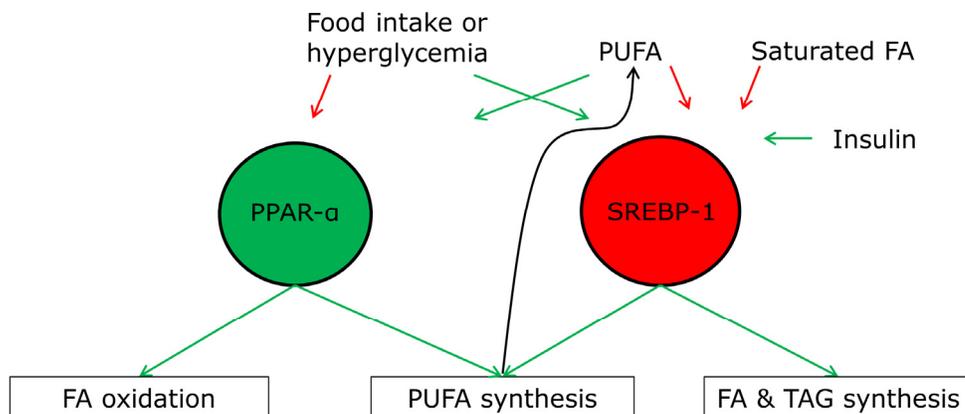
Figure 33. The transcriptional regulators PPAR-α and SREBP-1 regulate PUFA synthesis. Activation and inhibition is shown as green and red arrow, respectively. Redrawn after [333] including additional information from [51, 72, 83].

In addition to their role in lipid metabolism, multiple studies have implicated PUFAs in carbohydrate metabolism and T2D. Early work showed that STZ treatment of rats could reduce the overall levels of PUFA in heart, liver, kidney, and aorta. This was accompanied by a change in lipid composition, reducing ω-6 PUFAs stronger than ω-3 PUFAs, and depletion of arachidonic acid [337]. It was later shown that STZ treatment reduced Fads2 activity in rat liver, which could be rescued by insulin administration [338]. A possible explanation for this finding is the positive influence of insulin on SREBP-1 activity (Fig. 33). Different PUFA rich diets could ameliorate hyperglycemia and hyperinsulinemia in *lep/lep* mice and were associated with reduced nuclear SREBP-1c levels in liver [339]. Adenoviral based gene transfer of Elovl5 to the livers of HFD challenged mice could improve glucose tolerance and lower expression of the gluconeogenetic enzyme PEPCK. Moreover, these mice showed increased phosphorylation and nuclear exclusion of FOXO1, indicating enhanced insulin signaling. These beneficial changes were accompanied by an increase in the PUFAs C20:3 ω-6 and C24:4 ω-6 [241]. These results seem to indicate a beneficial or protective function for PUFAs in T2D. Unfortunately, the situation is complicated by the presence of two series of PUFAs between which no clear distinction was made in these studies.

The finding that ω-3 PUFA can inhibit proinflammatory eicosanoid production, which originates from the ω-6 PUFA arachidonic acid, gave rise to the notion that

130

these two substance classes may antagonize each other [340]. The generalization of this idea to different organ systems has since been criticized, as ω-3 and ω-6 PUFA levels do not always correlate negatively [341] and both have beneficial effects in hyperlipidemia [342]. The issue of a general antagonism remains undecided. Convincing evidence from a supplementation study with fish oil by Storlien et al. pointed to a similar antagonism in the context of T2D. When mice were fed an ω-6 rich diet, they developed hepatic and peripheral insulin resistance. Substituting 6% of the ω-6 PUFA rich diet by ω-3 PUFA rich fish oil protected mice from both types of insulin resistance [343]. Subsequently, these results were transferred to the saff-diet model. Substituting 8% of safflower oil with fish oil ameliorated hepatic insulin resistance [344]. This protective effect was lost in PPAR-α$^{-/-}$ mice [344]. These results underscore the participation and importance of PPAR-α for the saff-diet model, but they also show that it is not the only pathway affected, as fish oil supplementation did not complete reverse the phenotype and PPAR-α$^{-/-}$ mice were still amenable to induction of hepatic insulin resistance. Transfer of the results of Storlien et al. [343] to T2D patients has shown a mild beneficial effect of ω-3 supplements on glucose tolerance which could only be observed in a subset of clinical studies [345].

In summary, PUFA seem to exert a protective effect in T2D, but alterations in the complex PUFA profile through dietary changes complicates and confounds the interpretations of their role. In the present study a transient upregulation before the onset of hepatic insulin resistance was found. As no further investigation concerning this pathway was conducted, e.g. monitoring changes in the hepatic PUFA profile, only speculations are possible. Upregulation of the pathway would appear to be a compensatory mechanism to protect the liver, but it is also possible that changes in the PPAR-SREBP-PUFA circuit through massive influx of linoleic acid are part of the pathomechanism. In this regard it is interesting that estimation of Fads1 and 2 activity in T2D patients showed that high Fads1 activity was protective while high Fads2 activity was a risk factor for T2D [346]. PPAR-α is clearly activated in the saff-diet model, as shown through pathway enrichment analysis of the proteomic data (Table 6). Furthermore, predicting activated transcription factors from the transcriptomics dataset for our model (from [233]) using the tool Ingenuity yielded activation of PPAR-α and modulation of SREBP-1 target genes at d7, 14 and 21 (Table 9). Interestingly, the highest number of affected genes for both transcription factors was found at d7. This indicates that an alteration of the PPAR-SREBP-PUFA circuit occurs in the

compensated stadium of the model, before transition to hepatic insulin resistance.

	d2	d7	d14	d21	Predicted state
PPAR-α	37 ($1*10^{-29}$)	107 ($1*10^{-77}$)	82 ($1*10^{-76}$)	67 ($7*10^{-67}$)	Activated
SREBP1	4 ($8*10^{-6}$)	10 ($1*10^{-9}$	5 ($6*10^{-6}$)	3 ($3*10^{-4}$)	Ambiguous

Table 9. Prediction of activated transcription factors in the saff-diet mode (selection).
The number of regulated genes and p-value of the prediction in brackets is given for each time point and transcription factor. Regulated proteins from transcriptomics data from [233] were analyzed for consensus transcription factors using Ingenuity (cutoff for regulation was BH 10% FDR).

Consistent with this notion is that expression of Ephx2 itself has been shown to be upregulated by PPAR-α [248, 323] but significant induction in the saff-diet model is first seen at d14. By the same token, PPAR agonists-α have been shown to repress the transcription of a Cyp2C isoform in rat liver [347]. The results from the insulin signaling assays show clearly that EETs would be positive modulators of insulin action. The downregulation of the Cyps and upregulation of Ephx2 therefore appears to be an alteration contributing to hepatic insulin resistance rather than a defense mechanism against it. It is tempting to speculate that flooding the liver with dietary lipids perturbs the PPAR-SREBP-PUFA circuit in an unknown way which leads to the pathological changes in EET pathway activity.

4.3.2 The EET pathway enhances hepatic insulin signaling and is repressed in HFD induced hepatic insulin resistance

EETs are presently mostly known for being prime candidates for the elusive endothelium derived hyperpolarizing factor (EDHF). Endothelial cells release NO and prostaglandin I2 (prostacyclin, PGI_2) which relaxes smooth muscle cells and causes vasodilation. However, blocking NO and PGI_2 production does not completely abolish this effect, which has led to the hypothesis, that it is caused by an unknown factor, the EDHF [348]. Characterization of EETs as EDHFs has driven research into their function in the vasculature. Their synthesis has already been outlined in Results. EETs are nonpolar molecules that are able to enter cells by crossing membranes [349], enabling them to function in a para- and autocine manner [244]. Their function as EDHF mainly relies on their ability to modulate ion channels, specifically their ability to activate K^+ channels in smooth muscle cells [348, 350]. Investigation of the functions of EETs in the cardiovascular system have shown that they lower the tone of arteries and also exert protective

effects in ischemia models of heart, kidney and brain [351]. In contrast to most eicosanoids, they display anti-inflammatory activity by inhibiting NF-kB activation [352] and beneficial effects on atherosclerosis have been found [351]. Pharmacological inhibition of Ephx2 has proven an effective strategy to increase EET levels and phase II clinical trials of these inhibitors for the indications hypertension and cardiovascular disease are ongoing [351]. Enthusiasm for these drugs has recently been tempered by the finding that EET pathway activation promotes tumor growth and metastasis by enhancing angiogenesis [353].

In contrast to hepatocytes, the autocrine signaling function of EETs in endothelial cells has been extensively studied. EETs have been shown to activate the kinase Akt [264] as well as the MAP kinase p42/44 ERK [354] and inhibit the transcription factors FOXO1 and FOXO3 [265]. In this manner they drive proliferation [265] and migration [264] of endothelial cells and induce angiogenesis [355]. Interestingly, these signaling molecules are also affected by insulin in hepatocytes [27]. Moreover the type of effect of EETs in endothelial cells and insulin in hepatocytes on signaling proteins is the same, e.g. both active the kinases. Conversely, EETs were found to increase cAMP levels and activate PKA in endothelial cells [356]. Physiological antagonists of insulin, most notably glucagon and catecholamines, also employ PKA activation to inhibit the physiological effects of insulin (see 1.2.2). Therefore EETs have been shown to affect a fourth signaling target connected to insulin signaling, but in an antagonistic manner. In this regard it is interesting to note that EETs can also induce secretion of glucagon as well as insulin from rat pancreatic islets [357].

The mechanism of the influence of EETs on intracellular signaling is not known. The current opinion is that they bind to a receptor, but it is unclear whether this putative receptor is a transmembrane protein, reacting to extracellular ligands, or an intracellular receptor. Evidence for an extracellular mechanism is that stable bead immobilized 14(15)-EET can induce the same degree of aromatase repression as free 14(15)-EET [358], the necessity of heterotrimeric G-proteins in EET mediated cAMP increase [356] and the presence of specific EET binding activity in membrane fractions of certain cells [244]. Conversely, EETs were shown to interfere with the binding of ATP to its intracellular binding site in outside-out patch clamp isolated potassium channels, indicating an at least partially intracellular mode of action [350].

Discussion

Beyond their direct function in signaling, EETs have been shown to enhance activation of growth factors and modulate gene expression. Specifically, they cause EGFR phosphorylation by enhancing EGF processing [355]. While DHETs were initially considered inert degradation products, they have been shown to activate PPAR-α [349]. Hydroxylation of DHETs at the ω-carbon, mediated by Cyp4A isoforms, was subsequently shown to turn them into potent PPAR-α agonists [246]. In this way, the EET pathway very likely provides a feedback input to the PPAR-SREBP-PUFA circuit.

The extensive role of EETs in blood vessels raises the question if hepatocytes are the cell type affected in the saff-diet model. Histochemical expression analysis of a human tissue microarray has shown that hepatocytes are the main cells expressing Ephx2, Cyp2C isoform and Cyp2J2 (ortholog of Cyp2J5) in liver [359]. Unfortunately, the authors did not comment on the expression of these enzymes in larger afferent or efferent vessels. Nevertheless, but it would appear that expression of these enzymes in the main endothelial cells population of the liver lobule microcirculation is lower than in hepatocytes [359]. Given the ability of EETs to diffuse through cells and act in an autocrine or paracrine manner, the results obtained in the validation experiments concerning enhanced insulin signaling are still valid as they show unequivocally that EETs can enhance insulin signaling at the level of Akt specifically in hepatocytes. Using overexpression of EET pathway enzymes in hepatocytes, these enzymes themselves were shown to have no effect on insulin signaling. This finding may not be as relevant if EET enzyme induction or repression did happen in a different cell type. Nevertheless, the predominant expression of these enzymes in hepatocytes, the fact that most of the mass of the liver is made up of hepatocytes and the comparatively high regulation factors of these enzymes are all indications that make it very likely that EET enzyme expression changes in liver are a reflection of expression changes in hepatocytes.

The bifunctional enzyme Ephx2 has received the most attention among EET pathway enzymes to date, as pharmacological inhibition of its hydrolase activity has proven an effective strategy for modulating EET levels through drugs. However, Ephx2 is also a phosphatase [268] and its known substrates are lysophosphatidic acids and fatty acid phosphates [360]. As it was not known whether the phosphatase may also affect protein phosphorylation, the overexpression experiments were very valuable for this enzyme in particular. These experiments showed that Ephx2 did not affect insulin signaling at the

levels or IR, IRS-1 or Akt phosphorylation. Moreover, a novel acetylation site on Ephx2 could be described and it was found that the degree of acetylation of Ephx2 was increased through the saff-diet in addition to the general induction of Ephx2. Acetylation of non-nuclear proteins has been found to impact different cellular processes and there are examples of this type of modification having a functional impact on signaling and metabolism [251]. Therefore, modification of Ephx2 function through this acetylation site seems entirely possible. This would be of interest in its emerging role in metabolic disorders as well as in the context of its role as a pharmacological target in hypertension and cardiovascular disease.

This study was not the first to implicate Ephx2 and the EET pathway in T2D and metabolic disorders. The first evidence goes back more than 25 years, when Thomas et al showed that cytoplasmic epoxide hydrolase activity was impacted by experimental diabetes and re-feeding of rats. STZ or alloxan induced diabetes and fasting increased hydrolase activity, which could be normalized by insulin administration of re-feeding, respectively [361]. Intriguingly, an unrelated study found that EET mediated relaxation of mesenteric arteries was completely lost in HFD fed insulin resistant rats. Patch clamp experiments on smooth muscle cell showed that this was not due to alterations of the ion channels themselves but was caused by intracellular factors [362]. Genetic evidence for a mutation of Ephx2 (Arg287Glu) showed that Japanese T2D patients bearing the mutation had lower insulin sensitivity as determined by hyperinsulinemic-euglycemic clamps. This difference was not found in healthy subjects [363]. The Arg287Glu mutation was also found to modify dyslipidemia in patients with an LDL receptor defect (familial hypercholesterolemia). Patients bearing the mutation had lower plasma TG and cholesterol levels [364]. Four different studies have recently shown different beneficial effects of the EET pathway in rodent models of T2D while work for this thesis was ongoing. Cyp2J3 (ortholog of Cyp2J5) gene delivery in fructose treated rats and *db/db* mice improved glucose tolerance as determined by ipGTT and lowered blood pressure of rats [365]. Ephx2$^{-/-}$ mice were found to have higher basal insulin and lower basal glucose levels when diabetes was induced by a low dose of STZ [256]. Moreover, they had improved glucose tolerance in ipGTT. The pancreatic islets of these mice displayed improved insulin secretion in response to glucose, which could be attributed to enhanced Ca^{2+} influx [256]. When insulin resistance was induced in Ephx2$^{-/-}$ mice with a HFD they also showed improved glucose tolerance as determined by ipGTT and faster

plasma glucose decrease in ITT [366]. Interestingly, $Ephx2^{-/-}$ mice had enlarged pancreatic islets, a phenotype that could also be induced by 5 months treatment with an Ephx2 inhibitor and was therefore not a developmental abnormality [366]. Finally, the authors showed increased IR, IRS-1 and Akt phosphorylation in livers of $Ephx2^{-/-}$ mice, but this finding was confounded by elevated insulin levels of these mice [366]. Hence it was not possible for them to separate the effect of higher levels of insulin and putative changes in liver EET concentrations on hepatic insulin signaling. While Ephx2 inhibitor treatment failed to improve glucose tolerance in this study, an improvement of glucose tolerance, determined by ipGTT, could be shown in another study using 16 weeks treatment of rats on HFD with a different Ephx2 inhibitor [367]. In these rats, Ephx2 inhibition also lowered blood pressure and reduced plasma free fatty acids but increased plasma TG [367]. Collectively, these studies clearly show a role of the EET pathway in T2D and outlined the therapeutic potential of Ephx2 inhibitors. However, the beneficial effects in these studies were assumed to be mainly caused by enhanced pancreatic insulin secretion.

A major flaw in the argument for a role of EETs in hepatic insulin resistance is that eicosanoids are usually only produced in response to a stimulus, a feature common to all classes of eicosanoids [368]. The most widely known examples are prostaglandins, which are inflammation mediators synthesized in bursts in response to ligand-mediated activation of phospholipase A2 (PLA_2). PLA_2 regulates the availability of the precursor free arachidonic acid, by releasing it from membrane phospholipids, regulating eicosanoid production accordingly.

In this regard, it is interesting to contrast the stimulated synthesis of prostaglandins to the synthesis of PGI_2, which shares many similarities with EETs. Both are eicosanoids produced in the endothelium and affect vascular tone by relaxing the neighboring smooth muscle cells [348, 369]. In contrast to EETs, PGI_2 also inhibits platelet aggregation and coagulation. The propensity for blood clotting is strongly affected by the balance of PGI_2 and the prothrombotic eicosanoid thromboxane A2 (TXA_2). In homeostasis, there has to be a basal production of PGI_2 to prevent blood clotting [369, 370]. In contrast, isolated endothelial cells produce practically no measureable PGI_2 [371]. While pulsatile production can be induced, for example by bradykinin [370], PGI_2 production is also induced in endothelial cells by the physical forces of shear stress from blood flow [371] or inhibited by hypoxia [370]. As a consequence, intact bovine arteries show a constant, basal PGI_2 production. The example of PGI_2 shows that

eicosanoid synthesis is not always exclusive to scenarios with acute stimulation. Interestingly, EET production in endothelial cells has been shown to be induced by hypoxia mediated induction of Cy2C enzymes [372] and may also be regulated by sheer stress [373].

4.4 Perspectives

This study could successfully describe alterations in different metabolic pathways through saff-diet feeding. Due to the nature of a proteomic study only changes in enzyme levels could be evaluated. Follow up experiments should address changes in enzymatic activity as well as metabolite levels for the affected pathways. In addition to the PUFA and EET pathways, bile acid synthesis and retinoid metabolism were affected by the saff-diet. In light of the background of these pathways in regard to T2D and glucose homeostasis they seem promising candidates for future validation projects.

The evidence presented in this thesis shows that the EET pathway is repressed though HFD feeding and that EET themselves are mediators that affect signaling in hepatocytes. Specifically, they cooperate with insulin in activating Akt, the most important kinase for the metabolic effects of insulin. However, new questions arise from this finding. How do the actual arachidonic acid, EET and PUFA levels change in the liver upon high fat diet feeding? This question required a new assay which has been developed by our collaboration partners in GAC at HMGU and whose application to mouse liver samples is pending. We also plan to investigate whether the Ephx2 knock-out mouse or Ephx2 inhibitor treated mice may be protected from HFD induced hepatic insulin resistance.

Moreover, the current state of this project offers the attractive opportunity to attempt translation of results from the mouse study to T2D patients. To this end the application of the eicosanoid assay will be extended to plasma samples. If successful, EET levels in plasma and if possible liver samples will be determined for T2D patients in order to investigate if a similar deregulation can be found for those patients. As Ephx2 inhibitors are currently being evaluated in advanced stages of clinical trials for the treatment of cardiovascular disease this could reveal an application of these already partly verified new drugs for an additional indication in the context of T2D, possibly hepatic insulin resistance.

In light of the medical interest in the EET signaling pathway, currently mostly in regard to cardiovascular disease but possibly also for T2D, there is considerable merit in further elucidation of the molecular mechanisms of EET signaling in

Discussion

hepatocytes. Currently three different subprojects are ongoing. First, in spite of multiple studies, the actual EET receptor has remained elusive until now. Considering that none of these were LC-MS/MS based, that one of the main fields in proteomics is determination of protein-protein interactions and that there are immobilized EETs available [358], interaction proteomics based identification of this receptor seems a realistic possibility.

Second, studies on the functional relevance of the newly discovered Ephx2 Lys176 acetylation are in preparation. To this end it is planned to use the cloned Ephx2 construct, mutate Lys176 to Arg and determined a possible impact on subcellular localization, catalytic activity and interactome. Experimental systems and established assays to assess all these functional readouts are already available with collaboration partners contributing additional expertise.

Finally, we are interested in determining the intersection of the insulin and EET signaling pathways. For this purpose, SRM based quantification of phosphosites on key proteins of the insulin signaling pathway is currently being developed. With a high accuracy assay of this kind, attempts to determine the intersection by a computational modeling approach may be feasible. A very similar study has already determined Gab1 to be a major point of crosstalk between insulin and EGF signaling [374].

5. References

1.   Alberti, K.G.M.M. and P. Zimmet, *Definition, diagnosis and classification of diabetes mellitus and its complications. Part 1: diagnosis and classification of diabetes mellitus. Provisional report of a WHO consultation.* Diabet. Med., 1998. **15**(7): p. 539-553.
2.   Srinivasan, B.T., et al., *Recent advances in the management of type 2 diabetes mellitus: a review.* Postgrad. Med. J., 2008. **84**(996): p. 524-31.
3.   Stumvoll, M., B.J. Goldstein, and T.W. van Haeften, *Type 2 diabetes: principles of pathogenesis and therapy.* The Lancet, 2005. **365**(9467): p. 1333-1346.
4.   Scully, T., *Diabetes in numbers.* Nature, 2012. **485**(7398): p. S2-3.
5.   Consultation, W., *Definition, diagnosis and classification of diabetes mellitus and its complications.* Geneva, Switzerland: World Health Organization, 1999. **31**(3): p. 1-59.
6.   DeFronzo, R.A., *Pathogenesis of type 2 diabetes mellitus.* Med. Clin. North Am., 2004. **88**(4): p. 787-835, ix.
7.   Samuel, V.T. and G.I. Shulman, *Mechanisms for insulin resistance: common threads and missing links.* Cell, 2012. **148**(5): p. 852-71.
8.   DeFronzo, R.A., E. Ferrannini, and D.C. Simonson, *Fasting hyperglycemia in non-insulin-dependent diabetes mellitus: contributions of excessive hepatic glucose production and impaired tissue glucose uptake.* Metabolism, 1989. **38**(4): p. 387-395.
9.   Gastaldelli, A., et al., *Influence of obesity and type 2 diabetes on gluconeogenesis and glucose output in humans: a quantitative study.* Diabetes, 2000. **49**(8): p. 1367-1373.
10.   Magnusson, I., et al., *Increased rate of gluconeogenesis in type II diabetes mellitus. A 13C nuclear magnetic resonance study.* J. Clin. Invest., 1992. **90**(4): p. 1323.
11.   Clore, J.N., J. Stillman, and H. Sugerman, *Glucose-6-phosphatase flux in vitro is increased in type 2 diabetes.* Diabetes, 2000. **49**(6): p. 969-974.
12.   DeFronzo, R.A., *The triumvirate: β-cell, muscle, liver. A collusion responsible for NIDDM.* Diabetes, 1988. **37**(6): p. 667-687.
13.   Mitrakou, A., et al., *Contribution of abnormal muscle and liver glucose metabolism to postprandial hyperglycemia in NIDDM.* Diabetes, 1990. **39**(11): p. 1381-1390.
14.   Diamond, M.P., et al., *Reciprocal variations in insulin-stimulated glucose uptake and pancreatic insulin secretion in women with normal glucose tolerance.* J. Soc. Gynecol. Investig., 1995. **2**(5): p. 708-715.
15.   van Haeften, T.W., et al., *Disturbances in β-cell function in impaired fasting glycemia.* Diabetes, 2002. **51**(suppl 1): p. S265-S270.
16.   Banerji, M.A. and H.E. Lebovitz, *Insulin action in black Americans with NIDDM.* Diabetes Care, 1992. **15**(10): p. 1295-1302.
17.   Kulkarni, R.N., et al., *Tissue-Specific Knockout of the Insulin Receptor in Pancreatic< i> β</i> Cells Creates an Insulin Secretory Defect Similar to that in Type 2 Diabetes.* Cell, 1999. **96**(3): p. 329-339.
18.   Michael, M.D., et al., *Loss of insulin signaling in hepatocytes leads to severe insulin resistance and progressive hepatic dysfunction.* Mol. Cell, 2000. **6**(1): p. 87-97.
19.   Brüning, J.C., et al., *A muscle-specific insulin receptor knockout exhibits features of the metabolic syndrome of NIDDM without altering glucose tolerance.* Mol. Cell, 1998. **2**(5): p. 559-569.
20.   Blüher, M., B.B. Kahn, and C.R. Kahn, *Extended longevity in mice lacking the insulin receptor in adipose tissue.* Science, 2003. **299**(5606): p. 572-574.
21.   DeFronzo, R.A., J.D. Tobin, and R. Andres, *Glucose clamp technique: a method for quantifying insulin secretion and resistance.* Am. J. Physiol. Endocrinol. Metab., 1979. **237**(3): p. E214.
22.   Myers, M.G., M.A. Cowley, and H. Munzberg, *Mechanisms of leptin action and leptin resistance.* Annu. Rev. Physiol., 2008. **70**: p. 537-56.
23.   Kahn, C., *The molecular mechanism of insulin action.* Annu. Rev. Med., 1985. **36**(1): p. 429-451.

References

24. Cheatham, B. and C.R. Kahn, *Insulin action and the insulin signaling network.* Endocr. Rev., 1995. **16**(2): p. 117-142.
25. Sawka-Verhelle, D., et al., *Insulin Receptor Substrate-2 Binds to the Insulin Receptor through Its Phosphotyrosine-binding Domain and through a Newly Identified Domain Comprising Amino Acids 591786.* J. Biol. Chem., 1996. **271**(11): p. 5980-5983.
26. Taniguchi, C.M., B. Emanuelli, and C.R. Kahn, *Critical nodes in signalling pathways: insights into insulin action.* Nat. Rev. Mol. Cell Biol., 2006. **7**(2): p. 85-96.
27. Saltiel, A.R. and C.R. Kahn, *Insulin signalling and the regulation of glucose and lipid metabolism.* Nature, 2001. **414**(6865): p. 799-806.
28. Tsuruzoe, K., et al., *Insulin receptor substrate 3 (IRS-3) and IRS-4 impair IRS-1-and IRS-2-mediated signaling.* Mol. Cell. Biol., 2001. **21**(1): p. 26-38.
29. Fritsche, L., et al., *How insulin receptor substrate proteins regulate the metabolic capacity of the liver-implications for health and disease.* Curr. Med. Chem., 2008. **15**(13): p. 1316-1329.
30. Ragolia, L. and N. Begum, *Protein phosphatase-1 and insulin action*, in *Insulin Action*. 1998, Springer. p. 49-58.
31. Löffler, G., *Stoffwechsel von Glucose und Glycogen*, in *Biochemie und Pathobiochemie*, G. Löffler and P.E. Petrides, Editors. 2003, Springer. p. 395-432.
32. Löffler, G., M. Kellerer, and H.-U. Häring, *Endokrine Funktionen III: Die schnelle Stoffwechselregulation*, in *Biochemie und Pathobiochemie*, G. Löffler and P.E. Petrides, Editors. 2003, Springer. p. 838-864.
33. Löffler, G. and P.E. Petrides, *Koordinierung des Stoffwechsels*, in *Biochemie und Pathobiochemie*, G. Löffler and P.E. Petrides, Editors. 2003, Springer. p. 558-578.
34. Alessi, D.R., et al., *Mechanism of activation of protein kinase B by insulin and IGF-1.* EMBO J., 1996. **15**(23): p. 6541.
35. Toker, A. and A.C. Newton, *Akt/protein kinase B is regulated by autophosphorylation at the hypothetical PDK-2 site.* J. Biol. Chem., 2000. **275**(12): p. 8271-8274.
36. Hagiwara, A., et al., *Hepatic mTORC2 activates glycolysis and lipogenesis through Akt, glucokinase, and SREBP1c.* Cell metabolism, 2012. **15**(5): p. 725-38.
37. Cho, H., et al., *Insulin resistance and a diabetes mellitus-like syndrome in mice lacking the protein kinase Akt2 (PKBβ).* Science, 2001. **292**(5522): p. 1728-1731.
38. Boura-Halfon, S. and Y. Zick, *Phosphorylation of IRS proteins, insulin action, and insulin resistance.* Am. J. Physiol. Endocrinol. Metab., 2009. **296**(4): p. E581-E591.
39. Tamemoto, H., et al., *Insulin resistance and growth retardation in mice lacking insulin receptor substrate-1.* Nature, 1994. **372**(182-186).
40. Araki, E., et al., *Alternative pathway of insulin signalling in mice with targeted disruption of the IRS-1 gene.* Nature, 1994. **372**(6502): p. 186-190.
41. Withers, D.J., et al., *Disruption of IRS-2 causes type 2 diabetes in mice.* Nature, 1998. **391**(6670): p. 900-904.
42. Simmgen, M., et al., *Liver-specific deletion of insulin receptor substrate 2 does not impair hepatic glucose and lipid metabolism in mice.* Diabetologia, 2006. **49**(3): p. 552-561.
43. Kido, Y., et al., *Tissue-specific insulin resistance in mice with mutations in the insulin receptor, IRS-1, and IRS-2.* J. Clin. Invest., 2000. **105**(2): p. 199-205.
44. Taniguchi, C.M., K. Ueki, and C.R. Kahn, *Complementary roles of IRS-1 and IRS-2 in the hepatic regulation of metabolism.* J. Clin. Invest., 2005. **115**(3): p. 718-727.
45. Huang, C., et al., *Differential contribution of insulin receptor substrates 1 versus 2 to insulin signaling and glucose uptake in l6 myotubes.* J. Biol. Chem., 2005. **280**(19): p. 19426-19435.
46. Watson, R.T. and J.E. Pessin, *GLUT4 translocation: the last 200 nanometers.* Cell. Signal., 2007. **19**(11): p. 2209-2217.
47. Holm, C., *Molecular mechanisms regulating hormone-sensitive lipase and lipolysis.* Biochem. Soc. Trans., 2003. **31**(6): p. 1120-1124.
48. Wijkander, J., et al., *Insulin-induced phosphorylation and activation of phosphodiesterase 3B in rat adipocytes: possible role for protein kinase B but not mitogen-activated protein kinase or p70 S6 kinase.* Endocrinology, 1998. **139**(1): p. 219-227.

49. Rider, M., et al., *6-phosphofructo-2-kinase/fructose-2, 6-bisphosphatase: head-to-head with a bifunctional enzyme that controls glycolysis.* Biochem. J., 2004. **381**: p. 561-579.

50. Deprez, J., et al., *Phosphorylation and activation of heart 6-phosphofructo-2-kinase by protein kinase B and other protein kinases of the insulin signaling cascades.* J. Biol. Chem., 1997. **272**(28): p. 17269-17275.

51. Horton, J.D., J.L. Goldstein, and M.S. Brown, *SREBPs: activators of the complete program of cholesterol and fatty acid synthesis in the liver.* J. Clin. Invest., 2002. **109**(9): p. 1125-1131.

52. Von Manteuffel, S.R., et al., *4E-BP1 phosphorylation is mediated by the FRAP-p70s6k pathway and is independent of mitogen-activated protein kinase.* Proceedings of the National Academy of Sciences, 1996. **93**(9): p. 4076-4080.

53. Beretta, L., et al., *Rapamycin blocks the phosphorylation of 4E-BP1 and inhibits cap-dependent initiation of translation.* EMBO J., 1996. **15**(3): p. 658.

54. De León, D.D. and C.A. Stanley, *Mechanisms of disease: advances in diagnosis and treatment of hyperinsulinism in neonates.* Nature Clinical Practice Endocrinology & Metabolism, 2007. **3**(1): p. 57-68.

55. Tahrani, A.A., et al., *Management of type 2 diabetes: new and future developments in treatment.* The Lancet, 2011. **378**(9786): p. 182-197.

56. Scharfmann, R., et al., *Beta cells within single human islets originate from multiple progenitors.* PLoS One, 2008. **3**(10): p. e3559.

57. Bonner-Weir, S., *beta-cell turnover: its assessment and implications.* Diabetes, 2001. **50**(suppl 1): p. S20.

58. Butler, A.E., et al., *β-Cell deficit and increased β-cell apoptosis in humans with type 2 diabetes.* Diabetes, 2003. **52**(1): p. 102-110.

59. Dobbins, R.L., et al., *Circulating fatty acids are essential for efficient glucose-stimulated insulin secretion after prolonged fasting in humans.* Diabetes, 1998. **47**(10): p. 1613-1618.

60. Rossetti, L., et al., *Effect of chronic hyperglycemia on in vivo insulin secretion in partially pancreatectomized rats.* J. Clin. Invest., 1987. **80**(4): p. 1037.

61. Del Prato, S., *Role of glucotoxicity and lipotoxicity in the pathophysiology of Type 2 diabetes mellitus and emerging treatment strategies.* Diabet. Med., 2009. **26**(12): p. 1185-1192.

62. Löffler, G., *Stoffwechsel von Phosphoglyceriden, Sphingolipiden und Cholesterin*, in *Biochemie und Pathobiochemie*, G. Löffler and P.E. Petrides, Editors. 2003, Springer. p. 600-627.

63. Utzschneider, K.M. and S.E. Kahn, *The role of insulin resistance in nonalcoholic fatty liver disease.* J. Clin. Endocrinol. Metab., 2006. **91**(12): p. 4753-4761.

64. Samuel, V.T., et al., *Mechanism of hepatic insulin resistance in non-alcoholic fatty liver disease.* J. Biol. Chem., 2004. **279**(31): p. 32345-53.

65. Marchesini, G., et al., *Nonalcoholic fatty liver disease a feature of the metabolic syndrome.* Diabetes, 2001. **50**(8): p. 1844-1850.

66. Kelley, D.E., et al., *Fatty liver in type 2 diabetes mellitus: relation to regional adiposity, fatty acids, and insulin resistance.* Am. J. Physiol. Endocrinol. Metab., 2003. **285**(4): p. E906-E916.

67. Kim, J.K., et al., *Mechanism of insulin resistance in A-ZIP/F-1 fatless mice.* J. Biol. Chem., 2000. **275**(12): p. 8456-8460.

68. Seip, M. and O. Trygstad, *Generalized lipodystrophy, congenital and acquired (lipoatrophy).* Acta Paediatr., 1996. **85**(s413): p. 2-28.

69. Aragno, M., et al., *SREBP-1c in nonalcoholic fatty liver disease induced by Western-type high-fat diet plus fructose in rats.* Free Radic. Biol. Med., 2009. **47**(7): p. 1067-1074.

70. Iizuka, K., et al., *Deficiency of carbohydrate response element-binding protein (ChREBP) reduces lipogenesis as well as glycolysis.* Proceedings of the National Academy of Sciences, 2004. **101**(19): p. 7281-7286.

71. Shimomura, I., et al., *Decreased IRS-2 and Increased SREBP-1c Lead to Mixed Insulin Resistance and Sensitivity in Livers of Lipodystrophic and< i> ob/ob</i> Mice.* Mol. Cell, 2000. **6**(1): p. 77-86.

72. Ide, T., et al., *SREBPs suppress IRS-2-mediated insulin signalling in the liver.* Nat. Cell Biol., 2004. **6**(4): p. 351-7.

References

73. Neschen, S., et al., *Contrasting effects of fish oil and safflower oil on hepatic peroxisomal and tissue lipid content.* Am. J. Physiol. Endocrinol. Metab., 2002. **282**(2): p. E395-401.

74. Zhou, G., et al., *Role of AMP-activated protein kinase in mechanism of metformin action.* J. Clin. Invest., 2001. **108**(8): p. 1167-1174.

75. DeFronzo, R., et al., *The effect of insulin on the disposal of intravenous glucose: results from indirect calorimetry and hepatic and femoral venous catheterization.* Diabetes, 1981. **30**(12): p. 1000-1007.

76. Thiebaud, D., et al., *The effect of graded doses of insulin on total glucose uptake, glucose oxidation, and glucose storage in man.* Diabetes, 1982. **31**(11): p. 957-963.

77. Shulman, G.I., et al., *Quantitation of muscle glycogen synthesis in normal subjects and subjects with non-insulin-dependent diabetes by 13C nuclear magnetic resonance spectroscopy.* N. Engl. J. Med., 1990. **322**(4): p. 223-228.

78. Shulman, G.I., *Cellular mechanisms of insulin resistance.* J. Clin. Invest., 2000. **106**(2): p. 171-176.

79. Brechtel, K., et al., *Fast elevation of the intramyocellular lipid content in the presence of circulating free fatty acids and hyperinsulinemia: A dynamic 1H-MRS study.* Magn. Reson. Med., 2001. **45**(2): p. 179-183.

80. Dresner, A., et al., *Effects of free fatty acids on glucose transport and IRS-1–associated phosphatidylinositol 3-kinase activity.* J. Clin. Invest., 1999. **103**(2): p. 253-259.

81. Griffin, M.E., et al., *Free fatty acid-induced insulin resistance is associated with activation of protein kinase C theta and alterations in the insulin signaling cascade.* Diabetes, 1999. **48**(6): p. 1270-1274.

82. Mackay, H.J. and C.J. Twelves, *Targeting the protein kinase C family: are we there yet?* Nat. Rev. Cancer, 2007. **7**(7): p. 554-562.

83. Jump, D.B., et al., *Fatty acid regulation of hepatic gene transcription.* J. Nutr., 2005. **135**(11): p. 2503-2506.

84. Yu, C., et al., *Mechanism by which fatty acids inhibit insulin activation of insulin receptor substrate-1 (IRS-1)-associated phosphatidylinositol 3-kinase activity in muscle.* J. Biol. Chem., 2002. **277**(52): p. 50230-50236.

85. Liu, L., et al., *Upregulation of myocellular DGAT1 augments triglyceride synthesis in skeletal muscle and protects against fat-induced insulin resistance.* J. Clin. Invest., 2007. **117**(6): p. 1679-1689.

86. Kim, J.K., et al., *PKC-ϑ knockout mice are protected from fat-induced insulin resistance.* J. Clin. Invest., 2004. **114**(6): p. 823-827.

87. Morino, K., et al., *Muscle-specific IRS-1 Ser→ Ala transgenic mice are protected from fat-induced insulin resistance in skeletal muscle.* Diabetes, 2008. **57**(10): p. 2644-2651.

88. Itani, S.I., et al., *Increased protein kinase C theta in skeletal muscle of diabetic patients.* Metabolism, 2001. **50**(5): p. 553-557.

89. Samuel, V.T., K.F. Petersen, and G.I. Shulman, *Lipid-induced insulin resistance: unravelling the mechanism.* The Lancet, 2010. **375**(9733): p. 2267-2277.

90. Nagle, C.A., et al., *Hepatic overexpression of glycerol-sn-3-phosphate acyltransferase 1 in rats causes insulin resistance.* J. Biol. Chem., 2007. **282**(20): p. 14807-14815.

91. Wajchenberg, B.L., *Subcutaneous and visceral adipose tissue: their relation to the metabolic syndrome.* Endocr. Rev., 2000. **21**(6): p. 697-738.

92. Cnop, M., et al., *The concurrent accumulation of intra-abdominal and subcutaneous fat explains the association between insulin resistance and plasma leptin concentrations distinct metabolic effects of two fat compartments.* Diabetes, 2002. **51**(4): p. 1005-1015.

93. Miyazaki, Y., et al., *Abdominal fat distribution and peripheral and hepatic insulin resistance in type 2 diabetes mellitus.* Am. J. Physiol. Endocrinol. Metab., 2002. **283**(6): p. E1135-E1143.

94. Hayashi, T., et al., *Visceral Adiposity and the Risk of Impaired Glucose Tolerance A prospective study among Japanese Americans.* Diabetes Care, 2003. **26**(3): p. 650-655.

95. Xu, H., et al., *Chronic inflammation in fat plays a crucial role in the development of obesity-related insulin resistance.* J. Clin. Invest., 2003. **112**(12): p. 1821-1830.

96.   Bruun, J.M., et al., *Monocyte chemoattractant protein-1 release is higher in visceral than subcutaneous human adipose tissue (AT): implication of macrophages resident in the AT.* J. Clin. Endocrinol. Metab., 2005. **90**(4): p. 2282-2289.

97.   Cancello, R., et al., *Increased infiltration of macrophages in omental adipose tissue is associated with marked hepatic lesions in morbid human obesity.* Diabetes, 2006. **55**(6): p. 1554-1561.

98.   Curat, C.A., et al., *From blood monocytes to adipose tissue-resident macrophages induction of diapedesis by human mature adipocytes.* Diabetes, 2004. **53**(5): p. 1285-1292.

99.   Kershaw, E.E. and J.S. Flier, *Adipose tissue as an endocrine organ.* J. Clin. Endocrinol. Metab., 2004. **89**(6): p. 2548-2556.

100.   Feinstein, R., et al., *Tumor necrosis factor-alpha suppresses insulin-induced tyrosine phosphorylation of insulin receptor and its substrates.* J. Biol. Chem., 1993. **268**(35): p. 26055-26058.

101.   Torti, F.M., et al., *A macrophage factor inhibits adipocyte gene expression: an in vitro model of cachexia.* Science, 1985. **229**(4716): p. 867-869.

102.   Hotamisligil, G.S., N.S. Shargill, and B.M. Spiegelman, *Adipose expression of tumor necrosis factor-alpha: direct role in obesity-linked insulin resistance.* Science, 1993. **259**(5091): p. 87-91.

103.   Hotamisligil, G.S., et al., *Reduced tyrosine kinase activity of the insulin receptor in obesity-diabetes. Central role of tumor necrosis factor-alpha.* J. Clin. Invest., 1994. **94**(4): p. 1543.

104.   Hotamisligil, G.S., et al., *Increased adipose tissue expression of tumor necrosis factor-alpha in human obesity and insulin resistance.* J. Clin. Invest., 1995. **95**(5): p. 2409.

105.   Lang, C., C. Dobrescu, and G. Bagby, *Tumor necrosis factor impairs insulin action on peripheral glucose disposal and hepatic glucose output.* Endocrinology, 1992. **130**(1): p. 43-52.

106.   Fürnsinn, C., et al., *Acute and chronic exposure to tumor necrosis factor-α fails to affect insulin-stimulated glucose metabolism of isolated rat soleus muscle.* Endocrinology, 1997. **138**(7): p. 2674-2679.

107.   Uysal, K.T., et al., *Protection from obesity-induced insulin resistance in mice lacking TNF-α function.* Nature, 1997. **389**(6651): p. 610-614.

108.   Ventre, J., et al., *Targeted disruption of the tumor necrosis factor-α gene: metabolic consequences in obese and nonobese mice.* Diabetes, 1997. **46**(9): p. 1526-1531.

109.   Engelman, J.A., et al., *Tumor necrosis factor α-mediated insulin resistance, but not dedifferentiation, is abrogated by MEK1/2 inhibitors in 3T3-L1 adipocytes.* Mol. Endocrinol., 2000. **14**(10): p. 1557-1569.

110.   Aguirre, V., et al., *The c-Jun NH2-terminal kinase promotes insulin resistance during association with insulin receptor substrate-1 and phosphorylation of Ser307.* J. Biol. Chem., 2000. **275**(12): p. 9047-9054.

111.   Hotamisligil, G.S., et al., *IRS-1-Mediated Inhibition of Insulin Receptor Tyrosine Kinase Activity in TNF- -and Obesity-Induced Insulin Resistance.* Science, 1996. **271**(5249): p. 665-670.

112.   Müller, G., et al., *Regulation of Raf-1 kinase by TNF via its second messenger ceramide and cross-talk with mitogenic signalling.* EMBO J., 1998. **17**(3): p. 732-742.

113.   Kanety, H., et al., *Sphingomyelinase and ceramide suppress insulin-induced tyrosine phosphorylation of the insulin receptor substrate-1.* J. Biol. Chem., 1996. **271**(17): p. 9895-9897.

114.   Moller, D.E., *Potential role of TNF-α in the pathogenesis of insulin resistance and type 2 diabetes.* Trends Endocrinol. Metab., 2000. **11**(6): p. 212-217.

115.   Zhang, B., et al., *Negative regulation of peroxisome proliferator-activated receptor-gamma gene expression contributes to the antiadipogenic effects of tumor necrosis factor-alpha.* Mol. Endocrinol., 1996. **10**(11): p. 1457-1466.

116.   Emanuelli, B., et al., *SOCS-3 inhibits insulin signaling and is up-regulated in response to tumor necrosis factor-α in the adipose tissue of obese mice.* J. Biol. Chem., 2001. **276**(51): p. 47944-47949.

References

117. Scherer, P.E., et al., *A novel serum protein similar to C1q, produced exclusively in adipocytes.* J. Biol. Chem., 1995. **270**(45): p. 26746-26749.

118. Wannamethee, S.G., et al., *Adipokines and risk of type 2 diabetes in older men.* Diabetes Care, 2007. **30**(5): p. 1200-1205.

119. Kadowaki, T. and T. Yamauchi, *Adiponectin and adiponectin receptors.* Endocr. Rev., 2005. **26**(3): p. 439-451.

120. Yamauchi, T., et al., *The fat-derived hormone adiponectin reverses insulin resistance associated with both lipoatrophy and obesity.* Nature Methods, 2001. **7**(8): p. 941-946.

121. Yamauchi, T., et al., *Adiponectin stimulates glucose utilization and fatty-acid oxidation by activating AMP-activated protein kinase.* Nat. Med., 2002. **8**(11): p. 1288-1295.

122. Fain, J.N., et al., *Comparison of the release of adipokines by adipose tissue, adipose tissue matrix, and adipocytes from visceral and subcutaneous abdominal adipose tissues of obese humans.* Endocrinology, 2004. **145**(5): p. 2273-2282.

123. Senn, J.J., et al., *Interleukin-6 induces cellular insulin resistance in hepatocytes.* Diabetes, 2002. **51**(12): p. 3391-3399.

124. Senn, J.J., et al., *Suppressor of cytokine signaling-3 (SOCS-3), a potential mediator of interleukin-6-dependent insulin resistance in hepatocytes.* J. Biol. Chem., 2003. **278**(16): p. 13740-13746.

125. Rui, L., et al., *SOCS-1 and SOCS-3 block insulin signaling by ubiquitin-mediated degradation of IRS1 and IRS2.* J. Biol. Chem., 2002. **277**(44): p. 42394-42398.

126. Klover, P.J., et al., *Chronic exposure to interleukin-6 causes hepatic insulin resistance in mice.* Diabetes, 2003. **52**(11): p. 2784-2789.

127. Klover, P.J., A.H. Clementi, and R.A. Mooney, *Interleukin-6 depletion selectively improves hepatic insulin action in obesity.* Endocrinology, 2005. **146**(8): p. 3417-3427.

128. Wallenius, V., et al., *Interleukin-6-deficient mice develop mature-onset obesity.* Nat. Med., 2002. **8**(1): p. 75-79.

129. Tsigos, C., et al., *Dose-dependent effects of recombinant human interleukin-6 on glucose regulation.* J. Clin. Endocrinol. Metab., 1997. **82**(12): p. 4167-4170.

130. Carey, A.L., et al., *Interleukin-6 increases insulin-stimulated glucose disposal in humans and glucose uptake and fatty acid oxidation in vitro via AMP-activated protein kinase.* Diabetes, 2006. **55**(10): p. 2688-2697.

131. Brownlee, M., *The pathobiology of diabetic complications a unifying mechanism.* Diabetes, 2005. **54**(6): p. 1615-1625.

132. Lottspeich, F., *Proteome analysis: a pathway to the functional analysis of proteins.* Angewandte Chemie International Edition, 1999. **38**(17): p. 2476-2492.

133. Tian, Q., et al., *Integrated genomic and proteomic analyses of gene expression in mammalian cells.* Mol. Cell. Proteomics, 2004. **3**(10): p. 960-969.

134. Aebersold, R. and M. Mann, *Mass spectrometry-based proteomics.* Nature, 2003. **422**(6928): p. 198-207.

135. Lottspeich, F. and J.W. Engels, *Proteomanalyse*, in *Bioanalytik*, D.D.F.L.P.D. Engels, Editor. 2012, Spektrum Akademischer Verlag: München. p. 995-1015.

136. Anderson, N.L., *The Human Plasma Proteome: History, Character, and Diagnostic Prospects.* Mol. Cell. Proteomics, 2002. **1**(11): p. 845-867.

137. Klose, J., *Protein mapping by combined isoelectric focusing and electrophoresis of mouse tissues.* Humangenetik, 1975. **26**(3): p. 231-243.

138. O'Farrell, P.Z., H.M. Goodman, and P.H. O'Farrell, *High resolution two-dimensional electrophoresis of basic as well as acidic proteins.* Cell, 1977. **12**(4): p. 1133-1142.

139. Westermeier, R., et al., *High-resolution two-dimensional electrophoresis with isoelectric focusing in immobilized pH gradients.* J. Biochem. Biophys. Methods, 1983. **8**(4): p. 321-330.

140. Lilley, K.S. and D.B. Friedman, *All about DIGE: quantification technology for differential-display 2D-gel proteomics.* Expert Review of Proteomics, 2004. **1**(4): p. 401-409.

141. Hillenkamp, F., et al., *Matrix-assisted laser desorption/ionization mass spectrometry of biopolymers.* Anal. Chem., 1991. **63**(24): p. 1193A-1203A.

142. Patterson, S.D. and R. Aebersold, *Mass spectrometric approaches for the identification of gel-separated proteins.* Electrophoresis, 1995. **16**(1): p. 1791-1814.

143. Patterson, S.D. and R.H. Aebersold, *Proteomics: the first decade and beyond.* Nat. Genet., 2003. **33**: p. 311-323.

144. Fenn, J.B., et al., *Electrospray ionization for mass spectrometry of large biomolecules.* Science, 1989. **246**(4926): p. 64-71.

145. Mann, M., R.C. Hendrickson, and A. Pandey, *Analysis of proteins and proteomes by mass spectrometry.* Annu. Rev. Biochem., 2001. **70**(1): p. 437-473.

146. Yates, J.R., C.I. Ruse, and A. Nakorchevsky, *Proteomics by mass spectrometry: approaches, advances, and applications.* Annual review of biomedical engineering, 2009. **11**: p. 49-79.

147. Nesvizhskii, A.I. and R. Aebersold, *Interpretation of shotgun proteomic data the protein inference problem.* Mol. Cell. Proteomics, 2005. **4**(10): p. 1419-1440.

148. Nilsson, T., et al., *Mass spectrometry in high-throughput proteomics: ready for the big time.* Nature Methods, 2010. **7**(9): p. 681-5.

149. Wilm, M., et al., *Femtomole sequencing of proteins from polyacrylamide gels by nano-electrospray mass spectrometry.* Nature, 1996. **379**(6564): p. 466-9.

150. Mann, M. and N.L. Kelleher, *Precision proteomics: the case for high resolution and high mass accuracy.* Proceedings of the National Academy of Sciences, 2008. **105**(47): p. 18132-8.

151. Marshall, A.G. and C.L. Hendrickson, *High-resolution mass spectrometers.* Annu. Rev. Anal. Chem. (Palo Alto Calif.), 2008. **1**: p. 579-99.

152. Domon, B. and R. Aebersold, *Mass spectrometry and protein analysis.* Science, 2006. **312**(5771): p. 212-7.

153. de Godoy, L.M., et al., *Comprehensive mass-spectrometry-based proteome quantification of haploid versus diploid yeast.* Nature, 2008. **455**(7217): p. 1251-4.

154. Mueller, L.N., et al., *An assessment of software solutions for the analysis of mass spectrometry based quantitative proteomics data.* J. Proteome Res., 2008. **7**(01): p. 51-61.

155. Bantscheff, M., et al., *Quantitative mass spectrometry in proteomics: critical review update from 2007 to the present.* Anal. Bioanal. Chem., 2012. **404**(4): p. 939-65.

156. Ong, S.-E., et al., *Stable isotope labeling by amino acids in cell culture, SILAC, as a simple and accurate approach to expression proteomics.* Mol. Cell. Proteomics, 2002. **1**(5): p. 376-386.

157. Schmidt, A., J. Kellermann, and F. Lottspeich, *A novel strategy for quantitative proteomics using isotope-coded protein labels.* Proteomics, 2005. **5**(1): p. 4-15.

158. Gygi, S.P., et al., *Quantitative analysis of complex protein mixtures using isotope-coded affinity tags.* Nat. Biotechnol., 1999. **17**(10): p. 994-999.

159. Ross, P.L., et al., *Multiplexed protein quantitation in Saccharomyces cerevisiae using amine-reactive isobaric tagging reagents.* Mol. Cell. Proteomics, 2004. **3**(12): p. 1154-1169.

160. Thompson, A., et al., *Tandem mass tags: a novel quantification strategy for comparative analysis of complex protein mixtures by MS/MS.* Anal. Chem., 2003. **75**(8): p. 1895-1904.

161. Bantscheff, M., et al., *Quantitative mass spectrometry in proteomics: a critical review.* Anal. Bioanal. Chem., 2007. **389**(4): p. 1017-31.

162. Kruger, M., et al., *SILAC mouse for quantitative proteomics uncovers kindlin-3 as an essential factor for red blood cell function.* Cell, 2008. **134**(2): p. 353-64.

163. Vogt, A., et al., *ICPL-IP: A novel approach for quantitative protein complex analysis from native tissue.* Mol. Cell. Proteomics, 2012.

164. Barnidge, D.R., et al., *Absolute quantification of the G protein-coupled receptor rhodopsin by LC/MS/MS using proteolysis product peptides and synthetic peptide standards.* Anal. Chem., 2003. **75**(3): p. 445-451.

165. Picotti, P. and R. Aebersold, *Selected reaction monitoring-based proteomics: workflows, potential, pitfalls and future directions.* Nature Methods, 2012. **9**(6): p. 555-66.

166. Picotti, P., et al., *High-throughput generation of selected reaction-monitoring assays for proteins and proteomes.* Nature Methods, 2010. **7**(1): p. 43-6.

167. Gerber, S.A., et al., *Absolute quantification of proteins and phosphoproteins from cell lysates by tandem MS.* Proceedings of the National Academy of Sciences, 2003. **100**(12): p. 6940-5.

References

168. Gillette, M.A. and S.A. Carr, *Quantitative analysis of peptides and proteins in biomedicine by targeted mass spectrometry.* Nature Methods, 2013. **10**(1): p. 28-34.

169. Lange, V., et al., *Selected reaction monitoring for quantitative proteomics: a tutorial.* Mol. Syst. Biol., 2008. **4**: p. 222.

170. Mallick, P., et al., *Computational prediction of proteotypic peptides for quantitative proteomics.* Nat. Biotechnol., 2007. **25**(1): p. 125-31.

171. Picotti, P., et al., *Full dynamic range proteome analysis of S. cerevisiae by targeted proteomics.* Cell, 2009. **138**(4): p. 795-806.

172. Gloeckner, C.J., K. Boldt, and M. Ueffing, *Strep/FLAG tandem affinity purification (SF-TAP) to study protein interactions.* Current Protocols in Protein Science, 2009. **Chapter 19**: p. Unit19 20.

173. Kahle, M., et al., *High fat diet-induced modifications in membrane lipid and mitochondrial-membrane protein signatures precede the development of hepatic insulin resistance in mice.* Molecular Metabolism, 2015. **4**(1): p. 39-50.

174. Nagaraj, N., et al., *Detergent-based but gel-free method allows identification of several hundred membrane proteins in single LC-MS runs.* J. Proteome Res., 2008. **7**(11): p. 5028-32.

175. Smith, P.K., et al., *Measurement of protein using bicinchoninic acid.* Anal. Biochem., 1985. **150**(1): p. 76-85.

176. Laemmli, U.K., *Cleavage of structural proteins during the assembly of the head of bacteriophage T4.* Nature, 1970. **227**(5259): p. 680-5.

177. Neuhoff, V., et al., *Improved staining of proteins in polyacrylamide gels including isoelectric focusing gels with clear background at nanogram sensitivity using Coomassie Brilliant Blue G-250 and R-250.* Electrophoresis, 1988. **9**(6): p. 255-62.

178. Towbin, H., T. Staehelin, and J. Gordon, *Electrophoretic transfer of proteins from polyacrylamide gels to nitrocellulose sheets: procedure and some applications.* Proceedings of the National Academy of Sciences, 1979. **76**(9): p. 4350-4.

179. Schäfer, A., et al., *Two-Dimensional Peptide Separation Improving Sensitivity of Selected Reaction Monitoring-Based Quantitative Proteomics in Mouse Liver Tissue: Comparing Off-Gel Electrophoresis and Strong Cation Exchange Chromatography.* Anal. Chem., 2012. **84**(20): p. 8853-8862.

180. Beynon, R.J., et al., *Multiplexed absolute quantification in proteomics using artificial QCAT proteins of concatenated signature peptides.* Nature Methods, 2005. **2**(8): p. 587-9.

181. Gelfi, C. and P.G. Righetti, *Preparative isoelectric focusing in immobilized pH gradients. II. A case report.* J. Biochem. Biophys. Methods, 1983. **8**(2): p. 157-172.

182. Wessel, D. and U.I. Flugge, *A method for the quantitative recovery of protein in dilute solution in the presence of detergents and lipids.* Anal. Biochem., 1984. **138**(1): p. 141-3.

183. Alpert, A.J. and P. Andrews, *Cation-exchange chromatography of peptides on poly (2-sulfoethyl aspartamide)-silica.* J. Chromatogr. A, 1988. **443**: p. 85-96.

184. Ros, A., et al., *Protein purification by Off-Gel electrophoresis.* Proteomics, 2002. **2**(2): p. 151-6.

185. Horth, P., et al., *Efficient fractionation and improved protein identification by peptide OFFGEL electrophoresis.* Mol. Cell. Proteomics, 2006. **5**(10): p. 1968-74.

186. Apffel, A., et al., *Enhanced sensitivity for peptide mapping with electrospray liquid chromatography-mass spectrometry in the presence of signal suppression due to trifluoroacetic acid-containing mobile phases.* J. Chromatogr. A, 1995. **712**(1): p. 177-190.

187. Makarov, A., et al., *Performance evaluation of a hybrid linear ion trap/orbitrap mass spectrometer.* Anal. Chem., 2006. **78**(7): p. 2113-20.

188. Makarov, A., *Electrostatic axially harmonic orbital trapping: a high-performance technique of mass analysis.* Anal. Chem., 2000. **72**(6): p. 1156-62.

189. Olsen, J.V., et al., *Parts per million mass accuracy on an Orbitrap mass spectrometer via lock mass injection into a C-trap.* Mol. Cell. Proteomics, 2005. **4**(12): p. 2010-21.

190. Benjamini, Y. and Y. Hochberg, *Controlling the false discovery rate: a practical and powerful approach to multiple testing.* J. R. Stat. Soc., 1995: p. 289-300.

191. Käll, L., et al., *Semi-supervised learning for peptide identification from shotgun proteomics datasets.* Nature Methods, 2007. **4**(11): p. 923-925.

192. Le Blanc, J.C., et al., *Unique scanning capabilities of a new hybrid linear ion trap mass spectrometer (Q TRAP) used for high sensitivity proteomics applications.* Proteomics, 2003. **3**(6): p. 859-69.

193. Stahl-Zeng, J., et al., *High sensitivity detection of plasma proteins by multiple reaction monitoring of N-glycosites.* Mol. Cell. Proteomics, 2007. **6**(10): p. 1809-1817.

194. Hager, J.W., *Q TRAP™ mass spectrometer technology for proteomics applications.* Drug Discovery Today: Targets, 2004. **3**(2): p. 31-36.

195. Sambrook, J. and D.W. Russell, *The Hanahan Method for Preparation and Transformation of Competent E. coli: High-efficiency Transformation.* Cold Spring Harbor Protocols, 2006. **2006**(1): p. pdb. prot3942.

196. Chomczynski, P. and N. Sacchi, *Single-step method of RNA isolation by acid guanidinium thiocyanate-phenol-chloroform extraction.* Anal. Biochem., 1987. **162**(1): p. 156-9.

197. Hartley, J.L., G.F. Temple, and M.A. Brasch, *DNA cloning using in vitro site-specific recombination.* Genome Res., 2000. **10**(11): p. 1788-1795.

198. Mullis, K., et al., *Specific enzymatic amplification of DNA in vitro: the polymerase chain reaction.* Cold Spring Harb. Symp. Quant. Biol., 1986. **51 Pt 1**: p. 263-73.

199. Smith, L.M., et al., *Fluorescence detection in automated DNA sequence analysis.* Nature, 1986. **6071**(321): p. 674-9.

200. Klingmüller, U., et al., *Primary mouse hepatocytes for systems biology approaches: a standardized in vitro system for modelling of signal transduction pathways.* IEE Proceedings - Systems Biology, 2006. **153**(6): p. 433.

201. Keston, A. *Specific colorimetric enzymatic analytical reagents for glucose*. in *129th. Meeting ASC Dallas, Texas*. 1956.

202. Roehrig, K.L. and J.B. Allred, *Direct enzymatic procedure for the determination of liver glycogen.* Anal. Biochem., 1974. **58**(2): p. 414-421.

203. Lai, K.K., D. Kolippakkam, and L. Beretta, *Comprehensive and quantitative proteome profiling of the mouse liver and plasma.* Hepatology, 2008. **47**(3): p. 1043-51.

204. Sun, A., et al., *Liverbase: a comprehensive view of human liver biology.* J. Proteome Res., 2010. **9**(1): p. 50-8.

205. Barjaktarovic, Z., et al., *Radiation-induced signaling results in mitochondrial impairment in mouse heart at 4 weeks after exposure to X-rays.* PLoS One, 2011. **6**(12): p. e27811.

206. Hauck, S.M., et al., *Deciphering membrane-associated molecular processes in target tissue of autoimmune uveitis by label-free quantitative mass spectrometry.* Mol. Cell. Proteomics, 2010. **9**(10): p. 2292-2305.

207. Helbig, A.O., A.J. Heck, and M. Slijper, *Exploring the membrane proteome--challenges and analytical strategies.* J. Proteome Res., 2010. **73**(5): p. 868-78.

208. Neville, D.M., Jr., *The isolation of a cell membrane fraction from rat liver.* The Journal of biophysical and biochemical cytology, 1960. **8**: p. 413-22.

209. Kall, L., A. Krogh, and E.L. Sonnhammer, *A combined transmembrane topology and signal peptide prediction method.* J. Mol. Biol., 2004. **338**(5): p. 1027-36.

210. Wallin, E. and G. von Heijne, *Genome-wide analysis of integral membrane proteins from eubacterial, archaean, and eukaryotic organisms.* Protein Sci., 1998. **7**(4): p. 1029-38.

211. Yoshinari, O. and K. Igarashi, *Anti-diabetic effect of pyroglutamic acid in type 2 diabetic Goto-Kakizaki rats and KK-A y mice.* Br. J. Nutr., 2011. **106**: p. 995-1004.

212. Yagui, K., et al., *A missense mutation in the CD38 gene, a novel factor for insulin secretion: association with Type II diabetes mellitus in Japanese subjects and evidence of abnormal function when expressed in vitro.* Diabetologia, 1998. **41**(9): p. 1024-8.

213. Illig, T., et al., *A genome-wide perspective of genetic variation in human metabolism.* Nat. Genet., 2010. **42**(2): p. 137-41.

214. Dupuis, J., et al., *New genetic loci implicated in fasting glucose homeostasis and their impact on type 2 diabetes risk.* Nat. Genet., 2010. **42**(2): p. 105-16.

References

215. Vionnet, N., et al., *Nonsense mutation in the glucokinase gene causes early-onset non-insulin-dependent diabetes mellitus.* Nature, 1992. **356**(6371): p. 721-2.

216. Saxena, R., et al., *Genome-wide association analysis identifies loci for type 2 diabetes and triglyceride levels.* Science, 2007. **316**(5829): p. 1331-6.

217. Scott, R.A., et al., *Large-scale association analyses identify new loci influencing glycemic traits and provide insight into the underlying biological pathways.* Nat. Genet., 2012. **44**(9): p. 991-1005.

218. Zhang, D., et al., *Mitochondrial dysfunction due to long-chain Acyl-CoA dehydrogenase deficiency causes hepatic steatosis and hepatic insulin resistance.* Proceedings of the National Academy of Sciences, 2007. **104**(43): p. 17075-80.

219. Porzio, O., et al., *Missense mutations in the TGM2 gene encoding transglutaminase 2 are found in patients with early-onset type 2 diabetes.* Hum. Mutat., 2007. **28**(11): p. 1150-1150.

220. Amano, S., et al., *Sorbitol dehydrogenase overexpression potentiates glucose toxicity to cultured retinal pericytes.* Biochem. Biophys. Res. Commun., 2002. **299**(2): p. 183-8.

221. Ioachimescu, A.G., et al., *Serum uric acid, mortality and glucose control in patients with Type 2 diabetes mellitus: a PreCIS database study.* Diabet. Med., 2007. **24**(12): p. 1369-74.

222. Deutsch, E.W., H. Lam, and R. Aebersold, *PeptideAtlas: a resource for target selection for emerging targeted proteomics workflows.* EMBO Rep., 2008. **9**(5): p. 429-34.

223. Mirzaei, H., et al., *Comparative evaluation of current peptide production platforms used in absolute quantification in proteomics.* Mol. Cell. Proteomics, 2008. **7**(4): p. 813-23.

224. Hanke, S., et al., *Absolute SILAC for accurate quantitation of proteins in complex mixtures down to the attomole level.* J. Proteome Res., 2008. **7**(3): p. 1118-30.

225. Maclean, B., et al., *Effect of collision energy optimization on the measurement of peptides by selected reaction monitoring (SRM) mass spectrometry.* Anal. Chem., 2010. **82**(24): p. 10116-24.

226. Addona, T.A., et al., *Multi-site assessment of the precision and reproducibility of multiple reaction monitoring-based measurements of proteins in plasma.* Nat. Biotechnol., 2009. **27**(7): p. 633-41.

227. Keshishian, H., et al., *Quantitative, multiplexed assays for low abundance proteins in plasma by targeted mass spectrometry and stable isotope dilution.* Mol. Cell. Proteomics, 2007. **6**(12): p. 2212-29.

228. Keshishian, H., et al., *Quantification of cardiovascular biomarkers in patient plasma by targeted mass spectrometry and stable isotope dilution.* Mol. Cell. Proteomics, 2009. **8**(10): p. 2339-49.

229. Anderson, N.L., et al., *SISCAPA peptide enrichment on magnetic beads using an in-line bead trap device.* Mol. Cell. Proteomics, 2009. **8**(5): p. 995-1005.

230. Rafalko, A., et al., *Development of a Chip/Chip/SRM platform using digital chip isoelectric focusing and LC-Chip mass spectrometry for enrichment and quantitation of low abundance protein biomarkers in human plasma.* J. Proteome Res., 2012. **11**(2): p. 808-17.

231. Hörth, P., et al., *Efficient peptide fractionation and improved protein identification with the Agilent 3100 OFFGEL Fractionator.* Application Note.

232. Bjellqvist, B., et al., *The focusing positions of polypeptides in immobilized pH gradients can be predicted from their amino acid sequences.* Electrophoresis, 1993. **14**(10): p. 1023-31.

233. Kahle, M., et al., *Phenotypic comparison of common mouse strains developing high-fat diet-induced hepatosteatosis.* Molecular Metabolism, 2013. **2**(4): p. 435-46.

234. Diz, A.P., A. Carvajal-Rodriguez, and D.O. Skibinski, *Multiple hypothesis testing in proteomics: a strategy for experimental work.* Mol. Cell. Proteomics, 2011. **10**(3): p. M110 004374.

235. Kanehisa, M. and S. Goto, *KEGG: kyoto encyclopedia of genes and genomes.* Nucleic Acids Res., 2000. **28**(1): p. 27-30.

236. Da Wei Huang, B.T.S. and R.A. Lempicki, *Systematic and integrative analysis of large gene lists using DAVID bioinformatics resources.* Nat. Protoc., 2008. **4**(1): p. 44-57.

237. Huyghe, S., et al., *Peroxisomal multifunctional protein-2: the enzyme, the patients and the knockout mouse model.* Biochim. Biophys. Acta, 2006. **1761**(9): p. 973-994.

238. Guillou, H., et al., *The key roles of elongases and desaturases in mammalian fatty acid metabolism: Insights from transgenic mice.* Prog. Lipid Res., 2010. **49**(2): p. 186-99.

239. Matsuzaka, T., et al., *Dual regulation of mouse Δ5-and Δ6-desaturase gene expression by SREBP-1 and PPARα.* J. Lipid Res., 2002. **43**(1): p. 107-114.

240. Moon, Y.A., R.E. Hammer, and J.D. Horton, *Deletion of ELOVL5 leads to fatty liver through activation of SREBP-1c in mice.* J. Lipid Res., 2009. **50**(3): p. 412-23.

241. Tripathy, S., M. Torres-Gonzalez, and D.B. Jump, *Elevated hepatic fatty acid elongase-5 activity corrects dietary fat-induced hyperglycemia in obese C57BL/6J mice.* J. Lipid Res., 2010. **51**(9): p. 2642-54.

242. Cinti, D.L., et al., *The fatty acid chain elongation system of mammalian endoplasmic reticulum.* Prog. Lipid Res., 1992. **31**(1): p. 1-51.

243. Park, W.J., et al., *A novel FADS1 isoform potentiates FADS2-mediated production of eicosanoid precursor fatty acids.* J. Lipid Res., 2012. **53**(8): p. 1502-12.

244. Spector, A.A. and A.W. Norris, *Action of epoxyeicosatrienoic acids on cellular function.* Am. J. Physiol. Cell Physiol., 2007. **292**(3): p. C996-C1012.

245. Arnold, C., et al., *Cytochrome P450-dependent metabolism of omega-6 and omega-3 long-chain polyunsaturated fatty acids.* Pharmacol. Rep., 2010. **62**(3): p. 536-47.

246. Cowart, L.A., et al., *The CYP4A isoforms hydroxylate epoxyeicosatrienoic acids to form high affinity peroxisome proliferator-activated receptor ligands.* J. Biol. Chem., 2002. **277**(38): p. 35105-35112.

247. Widstrom, R.L., A.W. Norris, and A.A. Spector, *Binding of cytochrome P450 monooxygenase and lipoxygenase pathway products by heart fatty acid-binding protein.* Biochemistry, 2001. **40**(4): p. 1070-1076.

248. Newman, J.W., C. Morisseau, and B.D. Hammock, *Epoxide hydrolases: their roles and interactions with lipid metabolism.* Prog. Lipid Res., 2005. **44**(1): p. 1-51.

249. Martinez-Jimenez, C.P., et al., *Transcriptional regulation and expression of CYP3A4 in hepatocytes.* Current drug metabolism, 2007. **8**(2): p. 185-94.

250. Shilov, I.V., et al., *The Paragon Algorithm, a next generation search engine that uses sequence temperature values and feature probabilities to identify peptides from tandem mass spectra.* Mol. Cell. Proteomics, 2007. **6**(9): p. 1638-1655.

251. Yang, X.J. and E. Seto, *Lysine acetylation: codified crosstalk with other posttranslational modifications.* Mol. Cell, 2008. **31**(4): p. 449-61.

252. Kendrick, A., et al., *Fatty liver is associated with reduced SIRT3 activity and mitochondrial protein hyperacetylation.* Biochem. J., 2011. **433**: p. 505-514.

253. Soupene, E. and F.A. Kuypers, *Mammalian long-chain acyl-CoA synthetases.* Exp. Biol. Med., 2008. **233**(5): p. 507-521.

254. Ghisla, S. and C. Thorpe, *Acyl-CoA dehydrogenases.* Eur. J. Biochem., 2004. **271**(3): p. 494-508.

255. Le, W., et al., *Long-chain acyl-CoA dehydrogenase is a key enzyme in the mitochondrial β-oxidation of unsaturated fatty acids.* Biochim. Biophys. Acta, 2000. **1485**(2): p. 121-128.

256. Luo, P., et al., *Inhibition or deletion of soluble epoxide hydrolase prevents hyperglycemia, promotes insulin secretion, and reduces islet apoptosis.* J. Pharmacol. Exp. Ther., 2010. **334**(2): p. 430-438.

257. Darlington, G.J., et al., *Expression of liver phenotypes in cultured mouse hepatoma cells.* J. Natl. Cancer Inst., 1980. **64**(4): p. 809-819.

258. Patek, P.Q., J.L. Collins, and M. Cohn, *Transformed cell lines susceptible or resistant to in vivo surveillance against tumorigenesis.* Nature, 1978. **276**(5687): p. 510-511.

259. Klaunig, J.E., et al., *Mouse liver cell culture.* In Vitro, 1981. **17**(10): p. 913-925.

260. Sun, X.J., et al., *Pleiotropic insulin signals are engaged by multisite phosphorylation of IRS-1.* Mol. Cell. Biol., 1993. **13**(12): p. 7418-7428.

261. Hers, I., E.E. Vincent, and J.M. Tavaré, *Akt signalling in health and disease.* Cell. Signal., 2011. **23**(10): p. 1515-1527.

262. Song, S.H., et al., *Direct measurement of pulsatile insulin secretion from the portal vein in human subjects.* J. Clin. Endocrinol. Metab., 2000. **85**(12): p. 4491-4499.

References

263. Marshall, S., *Kinetics of insulin receptor internalization and recycling in adipocytes. Shunting of receptors to a degradative pathway by inhibitors of recycling.* J. Biol. Chem., 1985. **260**(7): p. 4136-4144.

264. Pozzi, A., et al., *Characterization of 5, 6-and 8, 9-epoxyeicosatrienoic acids (5, 6-and 8, 9-EET) as potent in vivo angiogenic lipids.* J. Biol. Chem., 2005. **280**(29): p. 27138-27146.

265. Potente, M., et al., *11, 12-Epoxyeicosatrienoic acid-induced inhibition of FOXO factors promotes endothelial proliferation by down-regulating p27Kip1.* J. Biol. Chem., 2003. **278**(32): p. 29619-29625.

266. Arnold, C., et al., *Arachidonic acid-metabolizing cytochrome P450 enzymes are targets of ω-3 fatty acids.* J. Biol. Chem., 2010. **285**(43): p. 32720-32733.

267. Inch, W., et al., *Water content and proton spin relaxation time for neoplastic and non-neoplastic tissues from mice and humans.* J. Natl. Cancer Inst., 1974. **52**(2): p. 353-356.

268. Newman, J.W., et al., *The soluble epoxide hydrolase encoded by EPXH2 is a bifunctional enzyme with novel lipid phosphate phosphatase activity.* Proceedings of the National Academy of Sciences, 2003. **100**(4): p. 1558-1563.

269. Das, U.N., *Essential fatty acids: biochemistry, physiology and pathology.* Biotechnology Journal, 2006. **1**(4): p. 420-439.

270. Luo, G., et al., *Cloning and expression of murine CYP2Cs and their ability to metabolize arachidonic acid.* Arch. Biochem. Biophys., 1998. **357**(1): p. 45-57.

271. Ma, J., et al., *Molecular cloning, enzymatic characterization, developmental expression, and cellular localization of a mouse cytochrome P450 highly expressed in kidney.* J. Biol. Chem., 1999. **274**(25): p. 17777-17788.

272. Wang, H., et al., *Cloning, expression, and characterization of three new mouse cytochrome p450 enzymes and partial characterization of their fatty acid oxidation activities.* Mol. Pharmacol., 2004. **65**(5): p. 1148-1158.

273. Pessin, J.E. and G. Bell, *Mammalian facilitative glucose transporter family: structure and molecular regulation.* Annu. Rev. Physiol., 1992. **54**(1): p. 911-930.

274. Landau, B.R., et al., *Use of 2H2O for estimating rates of gluconeogenesis. Application to the fasted state.* J. Clin. Invest., 1995. **95**(1): p. 172.

275. Katz, J., S. Golden, and P. Wals, *Stimulation of hepatic glycogen synthesis by amino acids.* Proceedings of the National Academy of Sciences, 1976. **73**(10): p. 3433-3437.

276. Qiu, L., E.O. List, and J.J. Kopchick, *Differentially expressed proteins in the pancreas of diet-induced diabetic mice.* Mol. Cell. Proteomics, 2005. **4**(9): p. 1311-1318.

277. Sabido, E., et al., *Targeted proteomics reveals strain-specific changes in the mouse insulin and central metabolic pathways after a sustained high-fat diet.* Mol. Syst. Biol., 2013. **9**: p. 681.

278. Trout, K.K., C. Homko, and N.C. Tkacs, *Methods of measuring insulin sensitivity.* Biol. Res. Nurs., 2007. **8**(4): p. 305-318.

279. Pavlidis, P., Q. Li, and W.S. Noble, *The effect of replication on gene expression microarray experiments.* Bioinformatics, 2003. **19**(13): p. 1620-1627.

280. Kim, G.H., et al., *Proteomic and bioinformatic analysis of membrane proteome in type 2 diabetic mouse liver.* Proteomics, 2013. **13**(7): p. 1164-79.

281. Hwang, H., et al., *Proteomics analysis of human skeletal muscle reveals novel abnormalities in obesity and type 2 diabetes.* Diabetes, 2010. **59**(1): p. 33-42.

282. Geiger, T., et al., *Super-SILAC mix for quantitative proteomics of human tumor tissue.* Nature Methods, 2010. **7**(5): p. 383-385.

283. Sturm, M., et al., *OpenMS–an open-source software framework for mass spectrometry.* BMC Bioinformatics, 2008. **9**(1): p. 163.

284. Gillet, L.C., et al., *Targeted data extraction of the MS/MS spectra generated by data-independent acquisition: a new concept for consistent and accurate proteome analysis.* Mol. Cell. Proteomics, 2012. **11**(6): p. O111 016717.

285. Malmstrom, J., et al., *Proteome-wide cellular protein concentrations of the human pathogen Leptospira interrogans.* Nature, 2009. **460**(7256): p. 762-5.

286. Lange, V., et al., *Targeted quantitative analysis of Streptococcus pyogenes virulence factors by multiple reaction monitoring.* Mol. Cell. Proteomics, 2008. **7**(8): p. 1489-500.

287. Sanchez, J.C., et al., *Effect of rosiglitazone on the differential expression of obesity and insulin resistance associated proteins in lep/lep mice.* Proteomics, 2003. **3**(8): p. 1500-1520.

288. Schmid, G.M., et al., *Effect of high-fat diet on the expression of proteins in muscle, adipose tissues, and liver of C57BL/6 mice.* Proteomics, 2004. **4**(8): p. 2270-82.

289. Edvardsson, U., et al., *Hepatic protein expression of lean mice and obese diabetic mice treated with peroxisome proliferator-activated receptor activators.* Proteomics, 2003. **3**(4): p. 468-478.

290. Kirpich, I.A., et al., *Integrated hepatic transcriptome and proteome analysis of mice with high-fat diet-induced nonalcoholic fatty liver disease.* The Journal of Nutritional Biochemistry, 2011. **22**(1): p. 38-45.

291. Guo, Y., et al., *Quantitative Proteomic and Functional Analysis of Liver Mitochondria from High Fat Diet (HFD) Diabetic Mice.* Mol. Cell. Proteomics, 2013. **12**(12): p. 3744-3758.

292. Lu, H., et al., *The Identification of Potential Factors Associated with the Development of Type 2 Diabetes A Quantitative Proteomics Approach.* Mol. Cell. Proteomics, 2008. **7**(8): p. 1434-1451.

293. Hojlund, K., et al., *Proteome analysis reveals phosphorylation of ATP synthase beta -subunit in human skeletal muscle and proteins with potential roles in type 2 diabetes.* J. Biol. Chem., 2003. **278**(12): p. 10436-42.

294. Giebelstein, J., et al., *The proteomic signature of insulin-resistant human skeletal muscle reveals increased glycolytic and decreased mitochondrial enzymes.* Diabetologia, 2012. **55**(4): p. 1114-1127.

295. Thingholm, T.E., et al., *Characterization of human myotubes from type 2 diabetic and nondiabetic subjects using complementary quantitative mass spectrometric methods.* Mol. Cell. Proteomics, 2011. **10**(9).

296. Hansson, O., et al., *Inflammatory response in white adipose tissue in the non-obese hormone-sensitive lipase null mouse model.* J. Proteome Res., 2006. **5**(7): p. 1701-1710.

297. Lu, H., et al., *Molecular and metabolic evidence for mitochondrial defects associated with beta-cell dysfunction in a mouse model of type 2 diabetes.* Diabetes, 2010. **59**(2): p. 448-59.

298. Begriche, K., et al., *Mitochondrial dysfunction in NASH: causes, consequences and possible means to prevent it.* Mitochondrion, 2006. **6**(1): p. 1-28.

299. Kimball, S.R., T.C. Vary, and L.S. Jefferson, *Regulation of protein synthesis by insulin.* Annu. Rev. Physiol., 1994. **56**(1): p. 321-348.

300. Ashford, A.J. and V.M. Pain, *Effect of diabetes on the rates of synthesis and degradation of ribosomes in rat muscle and liver in vivo.* J. Biol. Chem., 1986. **261**(9): p. 4059-4065.

301. Ha, M.N., et al., *Functional rescue of vitamin C synthesis deficiency in human cells using adenoviral-based expression of murine l-gulono-γ-lactone oxidase.* Genomics, 2004. **83**(3): p. 482-492.

302. West, I., *Radicals and oxidative stress in diabetes.* Diabet. Med., 2000. **17**(3): p. 171-180.

303. Maritim, A., R. Sanders, and r.J. Watkins, *Diabetes, oxidative stress, and antioxidants: a review.* J. Biochem. Mol. Toxicol., 2003. **17**(1): p. 24-38.

304. Szkudelski, T., *The mechanism of alloxan and streptozotocin action in B cells of the rat pancreas.* Physiol. Res., 2001. **50**(6): p. 537-546.

305. Som, S., et al., *Ascorbic acid metabolism in diabetes mellitus.* Metabolism, 1981. **30**(6): p. 572-577.

306. Abahusain, M., et al., *Retinol, alpha-tocopherol and carotenoids in diabetes.* Eur. J. Clin. Nutr., 1999. **53**(8): p. 630.

307. Sasaki, H., et al., *High retinol/retinol-binding protein ratio in noninsulin-dependent diabetes mellitus.* Am. J. Med. Sci., 1995. **310**(5): p. 177.

308. Young, I.S., J.J. Torney, and E.R. Trimble, *The effect of ascorbate supplementation on oxidative stress in the streptozotocin diabetic rat.* Free Radic. Biol. Med., 1992. **13**(1): p. 41-46.

309. Pfahl, M. and F. Chytil, *Regulation of metabolism by retinoic acid and its nuclear receptors.* Annu. Rev. Nutr., 1996. **16**(1): p. 257-283.

References

310. Gerster, H., *Vitamin A-functions, dietary requirements and safety in humans.* Int. J. Vitam. Nutr. Res., 1997. **67**(2): p. 71-90.

311. Yang, Q., et al., *Serum retinol binding protein 4 contributes to insulin resistance in obesity and type 2 diabetes.* Nature, 2005. **436**(7049): p. 356-362.

312. Graham, T.E., et al., *Retinol-binding protein 4 and insulin resistance in lean, obese, and diabetic subjects.* N. Engl. J. Med., 2006. **354**(24): p. 2552-2563.

313. Hofmann, A.F., *Bile acids: the good, the bad, and the ugly.* Physiology, 1999. **14**(1): p. 24-29.

314. Everson, G.T., *Steady-state kinetics of serum bile acids in healthy human subjects: single and dual isotope techniques using stable isotopes and mass spectrometry.* J. Lipid Res., 1987. **28**(3): p. 238-252.

315. Staels, B. and V.A. Fonseca, *Bile Acids and Metabolic Regulation Mechanisms and clinical responses to bile acid sequestration.* Diabetes Care, 2009. **32**(suppl 2): p. S237-S245.

316. Thomas, C., et al., *Targeting bile-acid signalling for metabolic diseases.* Nat. Rev. Drug Discov., 2008. **7**(8): p. 678-93.

317. Watanabe, M., et al., *Bile acids induce energy expenditure by promoting intracellular thyroid hormone activation.* Nature, 2006. **439**(7075): p. 484-489.

318. Katsuma, S., A. Hirasawa, and G. Tsujimoto, *Bile acids promote glucagon-like peptide-1 secretion through TGR5 in a murine enteroendocrine cell line STC-1.* Biochem. Biophys. Res. Commun., 2005. **329**(1): p. 386-390.

319. Özcan, U., et al., *Chemical chaperones reduce ER stress and restore glucose homeostasis in a mouse model of type 2 diabetes.* Science, 2006. **313**(5790): p. 1137-1140.

320. Cariou, B., et al., *The farnesoid X receptor modulates adiposity and peripheral insulin sensitivity in mice.* J. Biol. Chem., 2006. **281**(16): p. 11039-11049.

321. Watanabe, M., et al., *Bile acids lower triglyceride levels via a pathway involving FXR, SHP, and SREBP-1c.* J. Clin. Invest., 2004. **113**(10): p. 1408-1418.

322. Ishida, H., et al., *Insulin is a dominant suppressor of sterol 12α-hydroxylase P450 (CYP8B) expression in rat liver: possible role of insulin in circadian rhythm of CYP8B.* J. Biochem., 2000. **127**(1): p. 57-64.

323. Rakhshandehroo, M., et al., *Peroxisome proliferator-activated receptor alpha target genes.* PPAR Research, 2010. **2010**.

324. Biddinger, S.B., et al., *Hepatic insulin resistance directly promotes formation of cholesterol gallstones.* Nat. Med., 2008. **14**(7): p. 778-782.

325. Payne, A.H., et al., *The multiple murine 3β-hydroxysteroid dehydrogenase isoforms: structure, function, and tissue-and developmentally specific expression.* Steroids, 1997. **62**(1): p. 169-175.

326. Wong, J.S., et al., *Effect of a peroxisome proliferator on 3β-hydroxysteroid dehydrogenase.* Biochem. Biophys. Res. Commun., 2002. **293**(1): p. 549-553.

327. Wu, L., et al., *Expression cloning and characterization of human 17 beta-hydroxysteroid dehydrogenase type 2, a microsomal enzyme possessing 20 alpha-hydroxysteroid dehydrogenase activity.* J. Biol. Chem., 1993. **268**(17): p. 12964-12969.

328. Zhongyi, S., et al., *Transgenic male mice expressing human hydroxysteroid dehydrogenase 2 indicate a role for the enzyme independent of its action on sex steroids.* Endocrinology, 2007. **148**(8): p. 3827-3836.

329. Marijanovic, Z., et al., *Closing the gap: identification of human 3-ketosteroid reductase, the last unknown enzyme of mammalian cholesterol biosynthesis.* Mol. Endocrinol., 2003. **17**(9): p. 1715-1725.

330. Moeller, G. and J. Adamski, *Integrated view on 17beta-hydroxysteroid dehydrogenases.* Mol. Cell. Endocrinol., 2009. **301**(1): p. 7-19.

331. Ohnesorg, T., et al., *Transcriptional regulation of human and murine 17β-hydroxysteroid dehydrogenase type-7 confers its participation in cholesterol biosynthesis.* J. Mol. Endocrinol., 2006. **37**(1): p. 185-197.

332. Garg, M., et al., *Differential effects of dietary linoleic and α-linolenic acid on lipid metabolism in rat tissues.* Lipids, 1988. **23**(9): p. 847-852.

333. Clarke, S.D., *Polyunsaturated fatty acid regulation of gene transcription: a molecular mechanism to improve the metabolic syndrome.* J. Nutr., 2001. **131**(4): p. 1129-1132.

334. Göttlicher, M., et al., *Fatty acids activate a chimera of the clofibric acid-activated receptor and the glucocorticoid receptor.* Proceedings of the National Academy of Sciences, 1992. **89**(10): p. 4653-4657.

335. Guillou, H., et al., *Comparative effect of fenofibrate on hepatic desaturases in wild-type and peroxisome proliferator-activated receptor α-deficient mice.* Lipids, 2002. **37**(10): p. 981-989.

336. Xu, J., et al., *Sterol Regulatory Element Binding Protein-1 Expression Is Suppressed by Dietary Polyunsaturated Fatty Acids: A Mechanism for the coordinate suppression of lipogenic genes by polyunsaturated fats.* J. Biol. Chem., 1999. **274**(33): p. 23577-23583.

337. Holman, R.T., et al., *Arachidonic acid deficiency in streptozotocin-induced diabetes.* Proceedings of the National Academy of Sciences, 1983. **80**(8): p. 2375-2379.

338. Rimoldi, O.J., G.S. Finarelli, and R.R. Brenner, *Effects of diabetes and insulin on hepatic Δ6 desaturase gene expression.* Biochem. Biophys. Res. Commun., 2001. **283**(2): p. 323-326.

339. Sekiya, M., et al., *Polyunsaturated fatty acids ameliorate hepatic steatosis in obese mice by SREBP-1 suppression.* Hepatology, 2003. **38**(6): p. 1529-1539.

340. Jump, D.B., *The biochemistry of n-3 polyunsaturated fatty acids.* J. Biol. Chem., 2002. **277**(11): p. 8755-8758.

341. Horrobin, D., et al., *Eicosapentaenoic acid and arachidonic acid: collaboration and not antagonism is the key to biological understanding.* Prostaglandins, Leukotrienes and Essential Fatty Acids, 2002. **66**(1): p. 83-90.

342. Rustan, A., M. Nenseter, and C. Drevon, *Omega-3 and Omega-6 Fatty Acids in the Insulin Resistance Syndrome.* Ann. N. Y. Acad. Sci., 1997. **827**(1): p. 310-326.

343. Storlien, L.H., et al., *Fish oil prevents insulin resistance induced by high-fat feeding in rats.* Science, 1987. **237**(4817): p. 885-888.

344. Neschen, S., et al., *n-3 Fatty acids preserve insulin sensitivity in vivo in a peroxisome proliferator-activated receptor-alpha-dependent manner.* Diabetes, 2007. **56**(4): p. 1034-41.

345. Nettleton, J.A. and R. Katz, *n-3 long-chain polyunsaturated fatty acids in type 2 diabetes: a review.* J. Am. Diet. Assoc., 2005. **105**(3): p. 428-440.

346. Warensjö, E., U. Risérus, and B. Vessby, *Fatty acid composition of serum lipids predicts the development of the metabolic syndrome in men.* Diabetologia, 2005. **48**(10): p. 1999-2005.

347. Ripp, S.L., et al., *Regulation of CYP2C11 by dehydroepiandrosterone and peroxisome proliferators: identification of the negative regulatory region of the gene.* Mol. Pharmacol., 2003. **64**(1): p. 113-122.

348. Busse, R., et al., *EDHF: bringing the concepts together.* Trends Pharmacol. Sci., 2002. **23**(8): p. 374-380.

349. Fang, X., et al., *14, 15-Dihydroxyeicosatrienoic acid activates peroxisome proliferator-activated receptor-α.* Am. J. Physiol. Heart Circ. Physiol., 2006. **290**(1): p. H55-H63.

350. Lu, T., et al., *Activation of ATP-sensitive K+ channels by epoxyeicosatrienoic acids in rat cardiac ventricular myocytes.* J. Physiol., 2001. **537**(3): p. 811-827.

351. Imig, J.D. and B.D. Hammock, *Soluble epoxide hydrolase as a therapeutic target for cardiovascular diseases.* Nat. Rev. Drug Discov., 2009. **8**(10): p. 794-805.

352. Node, K., et al., *Anti-inflammatory properties of cytochrome P450 epoxygenase-derived eicosanoids.* Science, 1999. **285**(5431): p. 1276-1279.

353. Panigrahy, D., et al., *Epoxyeicosanoids stimulate multiorgan metastasis and tumor dormancy escape in mice.* J. Clin. Invest., 2012. **122**(1): p. 178.

354. Wang, Y., et al., *Arachidonic acid epoxygenase metabolites stimulate endothelial cell growth and angiogenesis via mitogen-activated protein kinase and phosphatidylinositol 3-kinase/Akt signaling pathways.* J. Pharmacol. Exp. Ther., 2005. **314**(2): p. 522-532.

355. Michaelis, U.R., et al., *Cytochrome P450 2C9-derived epoxyeicosatrienoic acids induce angiogenesis via cross-talk with the epidermal growth factor receptor (EGFR).* FASEB J., 2003. **17**(6): p. 770-772.

References

356. Node, K., et al., *Activation of Galpha s mediates induction of tissue-type plasminogen activator gene transcription by epoxyeicosatrienoic acids.* J. Biol. Chem., 2001. **276**(19): p. 15983-9.

357. Falck, J., et al., *Epoxyeicosatrienoic acids stimulate glucagon and insulin release from isolated rat pancreatic islets.* Biochem. Biophys. Res. Commun., 1983. **114**(2): p. 743-749.

358. Snyder, G.D., et al., *Evidence for a membrane site of action for 14,15-EET on expression of aromatase in vascular smooth muscle.* Am. J. Physiol. Heart Circ. Physiol., 2002. **283**(5): p. H1936-42.

359. Enayetallah, A.E., et al., *Distribution of soluble epoxide hydrolase and of cytochrome P450 2C8, 2C9, and 2J2 in human tissues.* J. Histochem. Cytochem., 2004. **52**(4): p. 447-454.

360. Morisseau, C., et al., *Role of soluble epoxide hydrolase phosphatase activity in the metabolism of lysophosphatidic acids.* Biochem. Biophys. Res. Commun., 2012. **419**(4): p. 796-800.

361. Thomas, H., et al., *Effect of diabetes and starvation on the activity of rat liver epoxide hydrolases, glutathione S-transferases and peroxisomal β-oxidation.* Biochem. Pharmacol., 1989. **38**(23): p. 4291-4297.

362. Miller, A.W., et al., *Epoxyeicosatrienoic acid-induced relaxation is impaired in insulin resistance.* Am. J. Physiol. Heart Circ. Physiol., 2001. **281**(4): p. H1524-H1531.

363. Ohtoshi, K., et al., *Association of soluble epoxide hydrolase gene polymorphism with insulin resistance in type 2 diabetic patients.* Biochem. Biophys. Res. Commun., 2005. **331**(1): p. 347-350.

364. Sato, K., et al., *Soluble epoxide hydrolase variant (Glu287Arg) modifies plasma total cholesterol and triglyceride phenotype in familial hypercholesterolemia: intrafamilial association study in an eight-generation hyperlipidemic kindred.* J. Hum. Genet., 2004. **49**(1): p. 29-34.

365. Xu, X., et al., *Increased CYP2J3 expression reduces insulin resistance in fructose-treated rats and db/db mice.* Diabetes, 2010. **59**(4): p. 997-1005.

366. Luria, A., et al., *Soluble epoxide hydrolase deficiency alters pancreatic islet size and improves glucose homeostasis in a model of insulin resistance.* Proceedings of the National Academy of Sciences, 2011. **108**(22): p. 9038-9043.

367. Iyer, A., et al., *Pharmacological inhibition of soluble epoxide hydrolase ameliorates diet-induced metabolic syndrome in rats.* Exp. Diab. Res., 2012. **2012**: p. 758614.

368. Smith, W.L., *The eicosanoids and their biochemical mechanisms of action.* Biochem. J., 1989. **259**(2): p. 315.

369. Kawabe, J.-i., F. Ushikubi, and N. Hasebe, *Prostacyclin in vascular diseases.-Recent insights and future perspectives.* Circ. J., 2010. **74**(5): p. 836.

370. Shaul, P.W., et al., *Oxygen modulates prostacyclin synthesis in ovine fetal pulmonary arteries by an effect on cyclooxygenase.* J. Clin. Invest., 1992. **90**(6): p. 2147.

371. Frangos, J.A., et al., *Flow effects on prostacyclin production by cultured human endothelial cells.* Science, 1985. **227**(4693): p. 1477-1479.

372. Michaelis, U.R., et al., *Cytochrome P450 epoxygenases 2C8 and 2C9 are implicated in hypoxia-induced endothelial cell migration and angiogenesis.* J. Cell Sci., 2005. **118**(Pt 23): p. 5489-98.

373. Liu, Y., et al., *Laminar flow activates peroxisome proliferator-activated receptor-gamma in vascular endothelial cells.* Circulation, 2004. **110**(9): p. 1128-33.

374. Borisov, N., et al., *Systems-level interactions between insulin-EGF networks amplify mitogenic signaling.* Mol. Syst. Biol., 2009. **5**: p. 256.

6. Abbreviations

AC	Adenylate cyclase	DTT	Dithiothreitol
ACN	Acetonitrile	ECL	Enhanced chemoluminescence solution
AMP	Ampicillin		
AMP	Adenosine monophosphate	EDHF	Endothelium derived hyperpolarizing factor
AMPK	AMP activated kinase		
APS	Ammonium persulphate	EDTA	Ethylenediaminetetraacetic acid
AQUA	Absolute quantification	eGFP	Enhanced green fluorescent protein
AS160	Akt substrate of 160kDa		
BH	Benjamini Hochberg	EGFR	Epidermal growth factor receptor
BHT	3,5-Di-tert-4-butylhydroxytoluene	EGTA	Ethylene glycol tetraacetic acid
BMI	body mass index	ELISA	Enzyme linked immunosorbent assay
cAMP	Cyclic AMP	EPI	Enhanced product ion scan
CE	Collision energy	ERK	Extracellular-signal-regulated kinase
CHAPS	3-[(3-Cholamidopropyl) dimethylammonio]-1-propanesulfonate		
		ESI	Electrospray ionization
		FA	Formic acid
CHO	Carbohydrates	FCS	Fetal calf serum
Chow	Standard chow diet fed	FFA	Free fatty acids
ChREBP	Carbohydrate response element binding protein	FOX	Forkhead box
		Frc-1,6-Pase	Fructose-1,6-bisphosphatase
CMV	Cytomegalovirus		
CNS	Central nervous system	Frc-2,6-P	Fructose-2.6-bisphosphate
CV	Coefficient of variation	FT-ICR	Fourier transform ion cyclotron resonance
Da	Dalton		
DAG	Diacylglycerol	FWHM	Full width at half maximum
ddNTP	Dideoxyribonucleotide triphosphates	G-6-Pase	Glucose-6 phosphatase
		GEF	GTP exchange factor
DEPC	Diethylpyrocarbonat	GFP	Green fluorescent protein
DGAT	DAG-acyltransferase	GIST	Global integral standard
DH	Dehydrogenase	GK	Glucokinase
DIGE	Difference gel electrophoresis	GP	Glycogen Phosphorylase
DMEM	Dulbecco's Modified Eagle Medium		Acyl-CoA-glycerol-sn-3-phosphate acyltransferase 1
DMSO	Dimethyl sulfoxide	GPAT	
DNA	Deoxyribonucleic acid	GS	Glycogen synthase
dNTP	Deoxyribonucleotide triphosphates	GSK3	Glycogen synthase kinase 3
		gsp	Gene specific primer

Abbreviations

HBS	HEPES buffered solution	m/z	Mass to charge ratio
HEPES	4-(2-Hydroxyethyl)piperazine-1-ethanesulfonic acid	MALDI	Matrix-assisted laser desorption ionization
HFD	High fat diet	MAPK	Mitogen activated kinase
HPLC	High performance liquid chromatography	MHC	Major histocompatibility complex
h	Hour	min	Minute
HRP	Horseradish peroxidase	MODY	Maturity onset diabetes of the young
HSL	Hormone sensitive lipase	MS	Mass spectrometry
IAA	Iodoacetamide	mTOR	mammalian target of rapamycin
ICAT	Isotope coded affinity tag	mTORC	mTOR complex
ICPL	Isotope coded protein label	MW	Molecular weight
IDDM	Insulin dependent diabetes mellitus	NAFLD	Non-alcoholic fatty liver disease
IEF	Isoelectric focusing	NASH	Non-alcoholic steatohepatitis
IEG	Institute of Experimental Genetics	Nic-NHS	N-nicotinoyloxy-succinimide
IKK	IκB kinase	NIDDM	Non-insulin dependent diabetes mellitus
IL-6	Interleukin 6	OD	Optical density
IMAC	Immobilized metal affinity chromatography	OGE	Off-gel electrophoresis
IMCL	Intramyocellular lipid	oGTT	Oral glucose tolerance test
ipGTT	Intraperitoneal glucose tolerance test	Oxphos	Oxidative phosphorylation
IR	Insulin receptor	p.a.	pro analysi
IRS	Insulin receptor substrate	PLA$_2$	Phospholipase A2
ITT	Insulin tolerance test	PAGE	Polyacrylamide gel electrophoresis
ivGTT	Intravenous glucose tolerance test	PBS	Phosphate buffered saline
JNK	c-Jun N-terminal kinase	PC	PepClean
KAN	Kanamycin	PCR	Polymerase chain reaction
KEGG	Kyoto Encyclopedia of Genes and Genomes	PDE	Phosphodiesterase
LB	Lysogeny broth	PDK1	3-phosphoinositide-dependent-kinase 1
LC	Liquid chromatography	PepFDR	Peptide false discovery rate
LDL	Lipoprotein lipase	PFK1	Phosphofructokinase 1
LFD	Low fat diet	PFKBP	6-Phosphofructo-2-kinase
LOQ	Limit of quantification	PGI$_2$	Prostacyclin
LPA	Lysophosphatidic acid	PH	pleckstrin homology
		PhosK	Phosphorylase kinase
		pI	Isoelectric point
		PI3K	phosphatidylinositol-3-kinase

PIP2	phosphatidylinositol-(4,5)-bisphosphate
PIP3	phosphatidylinositol-(3,4,5)-trisphosphate
PK	Pyruvate kinase
PKA	Protein kinase A
PKC	Protein kinase C
PP1	Protein phosphatase 1
PTB	phosphotyrosine binding
PTM	Posttranslational modification
PTP	Proteotypic peptide
PVDF	Polyvinylidene fluoride
QconCAT	Quantification concatemer
RAR	Retinoic acid receptor
RIPA	Radioimmuno precipitation assay
ROK	Rho-associated protein kinase
RT	Room temperature
RXR	Retinoid X receptor
S/N	Signal-to-noise
Saff	Safflower oil diet fed
SCX	Strong cation exchange
SD	Standard deviation
SDS	Sodium dodecylsulphate
SILAC	Stable isotope labeling by amino acids in cell culture
SIK2	Serine/threonine-protein kinase
SISCAPA	Stable isotope standards and capture by anti-peptide antibodies
SOCS-3	Suppressor of cytokine signaling 3
SOS	Son-of-sevenless
SPE	Solid phase extraction
SREBP	Sterol response element binding protein
SRM	Selected reaction monitoring
STZ	Streptozotocin
T1D	Type 1 Diabetes mellitus
T2D	Type 2 diabetes mellitus
TBE	Tris-borate-EDTA

TBS	Tris buffered saline
TBS-T	Tris buffered saline-tween 20
TCA	Tricarboxylic acid cycle
TCEP	Tris(2-carboxyethyl)phosphine)
TEMED	Tetramethylethylenediamine
TOF	Time of flight
TFA	Trifluoroacetic acid
TG	Triacylglycerol
TNF-α	Tumor necrosis factor α
Tris	Tris(hydroxymethyl)amino methane
Tsc1	Tuberin
Tsc2	Hamartin
TxA$_2$	Thromboxane A2
U	Unit
UV	Ultra violet
WAT	White adipose tissue
WHO	World health organization

7. Annex

7.1. Figure index

7.2 Table index

7.3 Publications and presentations

7.3.1 Peer reviewed publications

- Schäfer A, Neschen S, Kahle M, Sarioglu H, Gaisbauer T, Imhof A, Adamski J, Hauck SM, Ueffing M (2014). "The epoxyeicosatrienoic acid pathway enhances hepatic insulin signaling and is repressed in insulin resistant mouse liver." In revision in *Molecular and Cellular Proteomics.*

- Kahle M, Schäfer A, Seelig A, Schultheiß J, Wu M, Leonhardt J, Rathkolb B, Rozman J, Sarioglu H, Hauck SM, Ueffing M, Wolf E, Kastenmueller G, Adamski J, Walch A, Hrabe de Angelis M, Neschen S (2014). "High fat diet-induced modifications in membrane lipid and mitochondrial-membrane protein signatures precede the development of hepatic insulin resistance in mice." *Molecular Metabolism* 4(1): 39-50.

- Haep L, Britzen-Laurent N, Weber TG, Naschberger E, Schaefer A, Kremmer E, Foersch S, Vieth M, Scheuer W, Wirtz S, Waldner M, Stürzl M (2014). "IFN-γ counteracts the angiogenic switch and induces vascular permeability in DSS colitis in mice." Accepted by *Inflammatory Bowel Diseases.*

- Ly-Verdu S, Schaefer A, Kahle M, Groeger T, Neschen S, Arteaga-Salas JM, Ueffing M, Hrabe de Angelis M, Zimmermann R (2014). "The impact of blood on liver metabolite profiling - a combined metabolomic and proteomic approach." *Biomed. Chromatogr*. 28(2): 231-240.

- von Toerne C, Kahle M, Schäfer A, Ispiryan R, Blindert M, Hrabe De Angelis M, Neschen S, Ueffing M, Hauck SM (2013). "Apoe, Mbl2, and Psp plasma protein levels correlate with diabetic phenotype in NZO mice-an optimized rapid workflow for SRM-based quantification." *J. Proteome Res*. 12(3): 1331-1343.

- <u>Schäfer A</u>, von Toerne C, Becker S, Sarioglu H, Neschen S, Kahle M, Hauck SM, Ueffing M (2012). "Two-Dimensional Peptide Separation Improving Sensitivity of Selected Reaction Monitoring-Based Quantitative Proteomics in Mouse Liver Tissue: Comparing Off-Gel Electrophoresis and Strong Cation Exchange Chromatography." *Anal. Chem.* 84(20): 8853-8862.

- Meding S, Balluff B, Elsner M, Schöne C, Rauser S, Nitsche U, Maak M, <u>Schäfer A</u>, Hauck SM, Ueffing M, Langer R, Höfler H, Friess H, Rosenberg R, Walch A (2012). "Tissue-based proteomics reveals FXYD3, S100A11 and GSTM3 as novel markers for regional lymph node metastasis in colon cancer." *J. Pathol.* 228(4): 459-470.

- Barjaktarovic Z, Schmaltz D, Shyla A, Azimzadeh O, Schulz S, Haagen J, Dorr W, Sarioglu H, <u>Schäfer A</u>, Atkinson MJ, Zischka H, Tapio S (2011). "Radiation-induced signaling results in mitochondrial impairment in mouse heart at 4 weeks after exposure to X-rays." *PLoS One* 6(12): e27811.

7.3.2 Poster presentations

- DZD workshop, Helmholtz Center Munich, Munich, Germany: "Targeted and non-targeted quantitative proteomic profiling of liver tissue in type 2 diabetes mouse models". November 2012.

- Proteomic forum 2011, Berlin, Germany: "Targeted and non-targeted quantitative proteomic profiling of liver tissue in type 2 diabetes mouse models". April 2011.

7.3.3 Oral presentations

- DZD meeting 2010, Helmholtz Center Munich, Munich, Germany: "Phenotypic-Proteomic-Metabolomic Approach to Re-investigate the Role of the Liver in Type 2 Diabetes". Oktober 2010.

- HDC Project Meeting Diabetes, Helmholtz Center Munich, Munich, Germany: "The Epoxyeicosatrienoic acid pathway enhances hepatic insulin signalling and is repressed in high fat diet induced hepatic insulin resistance - A proteomic study". November 2013.

7.4 Danksagung

Zum Abschluss dieser Arbeit möchte ich den vielen Personen danken, die mich in den letzten fünf Jahren unterstützt, gefördert und diese Dissertation überhaupt erst ermöglicht haben.

Zunächst möchte ich mich bei Prof. Dr. Marius Ueffing bedanken. Er hat mir während meiner Arbeit stets mit hochwertiger wissenschaftlicher Diskussion und Aufmunterung zur Seite gestanden. Ich schätze sein ehrliches Interesse daran, dass mein weiterer beruflicher Weg in der Wissenschaft erfolgreich und erfüllt sein wird. Unsere Zusammenarbeit wurde für ihn leider durch seine Tätigkeit an der Universitätsklinik Tübingen und langwieriges Pendeln zwischen München und Tübingen erschwert und ich wünsche ihm für die Zukunft weiterhin viel Erfolg für seine Forschung in Tübingen.

Meine Doktorarbeit wurde an der LMU begonnen und an der TUM fertiggestellt. Daher möchte ich mich bei Prof. Dr. Axel Imhof bedanken, der mich an der LMU betreut hat und in den ersten vier Jahren regelmäßig mit sehr hilfreichen wissenschaftlichen Diskussionen und Anleitung zum weiteren Verlauf meiner Arbeit wesentlich zum Erfolg dieses Projekts beigetragen hat.

Besonderer Dank gebührt Prof. Dr. Jerzy Adamski. Durch seine Initiative und unter Mithilfe der Dekanin Frau Prof. Dr. Schnieke wurde es mir ermöglicht diese Dissertation bei der TUM einzureichen. Neben dieser entscheidenden Unterstützung hat außerdem seine Expertise zu Lipidmetabolismus und Analytik sehr günstig auf den Verlauf meiner Arbeit gewirkt und durch ihn wurden weitere Möglichkeiten für die Erforschung der Rolle der EETs in T2D ermöglicht.

Bei Dr. Stefanie Hauck möchte ich für die Aufrechterhaltung der Abteilung Proteinanalytik bedanken, sowie dafür, dass sie mir ermöglicht hat in dieser Zeit meine Ideen für dem Projekt frei und mit den nötigen Mitteln umzusetzen. Des Weiteren auch für Einblicke wie Forschung auf der administrativen Ebene funktioniert und meine Einbindung in diese Prozesse. In diesem Zusammenhang darf natürlich Saskia Hanf nicht vergessen werden, die für die Organisation der Abteilung Proteinanalytik unerlässlich ist und die mir, worüber ich mich jedes Mal ganz besonders gefreut habe, die Verwaltungsangelegenheiten soweit möglich aus dem Kreuz gehalten hat.

Besonderer Dank gebührt an dieser Stelle Dr. Hakan Sarioglu. Direkt nach meinem Studium kam ich mit Kenntnis von Molekularbiologie und Biochemie, hatte aber keine Ahnung von Analytik. Besonders im ersten Jahr der Promotion, aber auch danach habe ich von ihm, der mich am Anfang sehr eng betreut hat

Annex

(bzw. nicht entkommen konnte, da er mir gegenüber saß), alle Grundlagen der Analytik gelernt, die das Fundament dieser Arbeit bilden. Während er für den reibungslosen Ablauf der Core Facility Proteomics verantwortlich war, ermöglichte er mir dennoch die LC-MS Systeme so nah und gründlich kennenzulernen wie nötig um meine Neugier zu stillen. Ohne ihn wäre auch meine erste, rein analytische, Publikation nicht zustande gekommen und er hat sich stets bemüht mich durch den zähen Ablauf meiner Dissertation zu motivieren.

Eigentlich ist das Fundament des Projektes, wenn auch nicht exklusiv meiner Arbeit, durch die hochwertige und unermüdliche Arbeit von Dr. Susanne Neschen und ihrer Doktorandin Melanie Kahle entstanden. Daher möchte ich mich für die Bereitstellung der Proben des exzellenten Dieselöl Modells bedanken, sowie für die anregenden Diskussionen die mir die Krankheit T2D näher gebracht haben.

Jeder der mit LC-MS Systemen gearbeitet hat, weiß wie wichtig das detaillierte Verständnis dieser komplizierten Apparate und sorgfältige Pflege und Qualitätskontrolle sind. Damit sind in der Core Facility Proteomics seit Jahren Silke Becker und Sandra Helm in gewissenhafter und kompetenter Weise beschäftigt. Daher will ich mich an dieser Stelle herzlich für die herausragende und weit über die üblichen Pflichten herausgehende technische Assistenz dieser beiden bedanken. Neben moralischer Unterstützung habe ich von ihnen auch vieles über die Funktion und Pflege von LC-MS Systemen gelernt.

Für die Funktion der Core Facility Proteomics ist auch unser Informatiker Marcel Blindert unerlässlich, und ich möchte mich für die tausend Kleinigkeiten bedanken mit denen er mir über die Jahre geholfen hat und dafür, dass er mich fürs Schreiben bei sich im Container aufgenommen hat und wünsche ihm und seiner jungen Familie alles Gute für die Zukunft.

Weiterhin bedanke ich mich bei meinen Leidensgenossen Joanna Kucharska, Matteo Gorza, Dr. Andrea Meixner, Jörn Leonhardt und Dr. Yves Texier, die mich in verschiedenen Phasen und mit unterschiedlichen Hintergründen fachlich, jedoch auch stets moralisch unterstützt haben. Da die Kooperation zwischen den Doktoranden hier sehr ausgeprägt war, hoffe ich auch an der ein- oder anderen Stelle geholfen zu haben. Es freut mich besonders, dass einige den Titel schon geschafft haben und die anderen ausnahmslos sehr nahe dran sind.

Für exzellente technische Assistenz in den späteren Stadien meiner Dissertation, besonders in der Zellkultur, möchte ich mich bei Jennifer Behler und Nicole

162

Senninger bedanken. Bei Jen, Matteo und natürlich Joanna will ich mich auch noch für die netten und lustigen Abende gegen Ende der Dissertation bedanken.

Einige der Kollegen aus der Abteilung Proteinanalytik zogen in meinem ersten Jahr in München nach Tübingen. Daher habe ich leider mit Dr. Andreas Vogt, Dr. Karsten Boldt, Dr. Norbert Kinkl und Dr. Johannes Glöckner weniger zusammengearbeitet als ich gehofft hatte. Trotzdem haben wir über die Zeit, wenn auch meist telefonisch, Kontakt gehalten, und sie haben mit vielen guten Ratschlägen und ihrer freundlichen und offen Art mehrmals geholfen.

Als nächstes möchte ich noch Dr. Gabriele Möller und Tobias Gaisbauer aus dem GAC von Prof. Adamski danken. Gabi für ihre aufbauenden Worte zu unterschiedlichen Zeiten, zahlreiche Hilfestellungen bei verschiedensten Versuchen und die gastfreundliche Art in der ich bei der Benutzung der Labors des GACs stets empfangen wurde. Tobi für die Mühe die er sich für die Messung der EETs bei einigen meiner Versuche gemacht hat, die aber bis jetzt leider erst teilweise erfolgreich waren.

Um die Isolation und Kultivierung von primären Hepatozyten zu lernen besuchte ich das DKFZ in Heidelberg. Daher möchte ich noch Dr. Lorenza D'Alessandro aus der Gruppe von Prof. Dr. Ursula Klingmüller für ihre Zeit und das Teilen ihrer Expertise danken.

Schließlich möchte ich besonderen Lehrern in meinem Leben danken, ohne die ich wahrscheinlich keine Promotion angestrebt hätte - Mein Onkel Dr. Reinhold Kovacs, mein Gymnasiallehrer Walter Noll sowie Prof. Dr. Cord-Michael Becker von der Universität Erlangen-Nürnberg.

Am wichtigsten ist aber der Dank an meine Familie, meine Eltern Norbert und Marita, meine Schwester Susanne, meine Freundin Joanna und meine treuen Freunde Peter, Steffi, Hannes, Kuba und Martin, ohne die all das Andere keinen Sinn machen würde.